december 1960
the
institute
of
radio
engineers

Proceedings of the IRE

in this issue

CAVITY COUPLER FOR TW PARAMETRIC AMPLIFIER: PAGE 1973

SPECIAL FILTERS

TO YOUR REQUIREMENTS

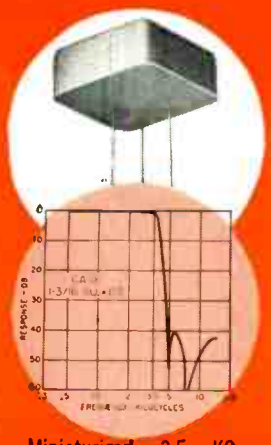

Miniaturized 3.5 KC low pass filter. 10K ohms to 10K ohms. Within 1 db up to 3500 cycles. Greater than 40 db beyond 4800 cycles.

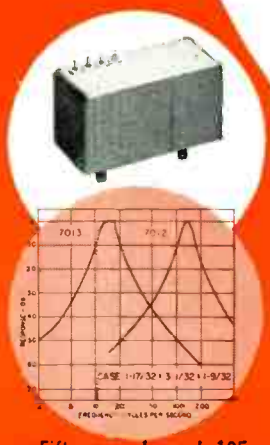

Fifteen cycle and 135 cycle filters for Tacan. 600 ohms to high impedance. Extreme stability —55°C. to + 100°C.

Almost thirty years of experience in the design and production of special filters have resulted in UTC being a first source for difficult units. Present designs incorporate a wide variety of core structures, winding methods, and capacitors to provide maximum performance, stability, and reliability. The units illustrated show a few of the thousands of specials produced by UTC, to customers' requirements, and only slightly indicate the possibilities in present special filter design. Range of frequencies on special units is from .1 cycles to 400 MC.

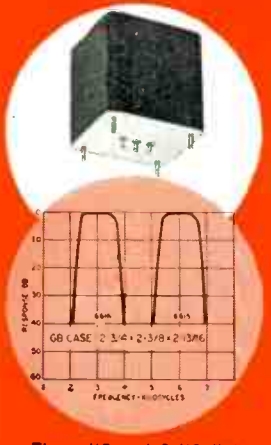

Three KC and 6 KC flat top band pass filters. 400 ohms to 20K ohms. MIL-T-27A each filter 1.7 lbs.

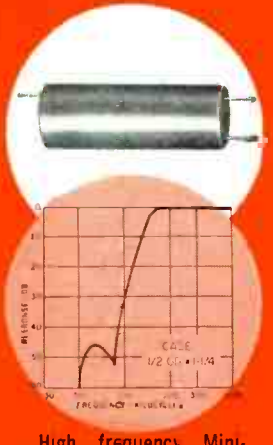

High frequency Mini-filters, .33 oz. MIL-T-27A Grace 5 150 KC High Pass 3 db to 150 KC, down 45 db below 85 KC. 7500 ohms.

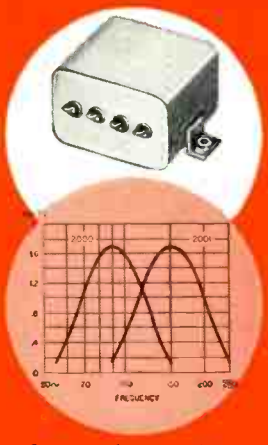

Curves of our miniaturized 90 and 150 cycle filters for glide path systems. 1¼" x 1¼" x 1⅝".

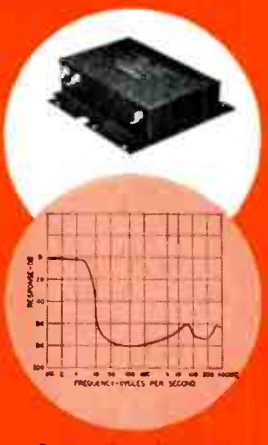

Power line filter from sources of 50 to 400 cycles . . . attenuation from 14 KC to 400 MC . . . 29 cubic inches.

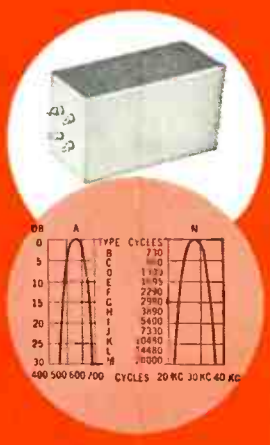

Multi-channel telemetering band pass filters for 400 cycle to 40 KC. Miniaturized units for many applications.

Plus over 1,000 STOCK ITEMS with UTC High Reliability from your local distributor

→ *write for catalog*

UNITED TRANSFORMER CORP.

150 VARICK STREET, NEW YORK 13, N. Y.

PACIFIC MFG. DIVISION: 4008 W. JEFFERSON BLVD., LOS ANGELES 16, CALIF.
EXPORT DIVISION: 13 EAST 40th STREET, NEW YORK 16, N. Y. CABLES: "ARLAB"

VOLUME 48, NUMBER 12

December, 1960

published monthly by The Institute of Radio Engineers, Inc.

Proceedings of the IRE®

contents

COVER

Unlikely as it may seem, the structure on the cover is part of a circuit for a traveling-wave parametric amplifier. The amplifier, developed at Hughes Research Laboratories and described on page 1973, consists of a series of diode-loaded cavities which are coupled to each other by means of the ferrite-loaded iris and magnetic circuit shown here.

DECEMBER

published monthly by The Institute of Radio Engineers, Inc.

Proceedings of the IRE®

continued

PROCEEDINGS OF THE IRE, published monthly by The Institute of Radio Engineers, Inc. at 1 East 79 Street, New York 21, N. Y. Manuscripts should be submitted in triplicate to the Editorial Department. Responsibility for contents of papers published rests upon the authors, and not the IRE or its members. All republication rights, including translations, are reserved by the IRE and granted only on request. Abstracting is permitted with mention of source.

Thirty days advance notice is required for change of address. Price per copy: members of the Institute of Radio Engineers, one additional copy $1.25; non-members $2.25. Yearly subscription price: to members $9.00, one additional subscription $13.50; to non-members in United States, Canada, and U. S. Possessions $18.00; to non-members in foreign countries $19.00. Second-class postage paid at Menasha, Wisconsin under the act of March 3, 1879. Acceptance for mailing at a special rate of postage is provided for in the act of February 28, 1925, embodied in Paragraph 4, Section 412, P. L. and R., authorized October 26, 1927. Printed in U.S.A.

DECEMBER

1949

December, 1960
Vol. 48 No. 12

Proceedings of the IRE

Poles and Zeros

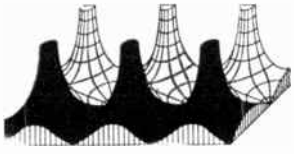

Collaboration. The two professional societies, IRE and AIEE, representing the broad areas of electrical engineering, have many fields of overlapping and mutual interest. From time to time the two societies have cooperatively conducted joint ventures, as exemplified by joint student branches, and joint symposia and meetings. Recognition of the importance of combined endeavor has been increasingly evident. During the past several years this recognition has led to the appointment of a number of Ad Hoc Committees charged with specific tasks. The most recent action was the appointment of a Task Group comprised of IRE and AIEE members, and charged with the responsibility of exploring areas of potential cooperation. IRE was represented by D. G. Fink, serving as chairman, J. D. Ryder, and Haraden Pratt; AIEE was represented by W. Scott Hill, as chairman, G. H. Brown, E. I. Green, and L. C. Holmes. Two specific recommendations evolved, and both of these have been approved by the Board of Directors of both societies.

As a result, an AIEE-IRE Joint Standards Committee will function in standard's areas of common interest. The approved Task Group resolution stated that, "where it is desirable that a single standard be submitted to the American Standards Association in fields covered by the two societies, . . . the Joint Standards Committee be empowered to approve, jointly in the names of the societies, such standards as the Joint Committee determines, on its own cognizance, are suitable for joint promulgation." The existing Ad Hoc Committee on AIEE-IRE Cooperation on Standards has established an approved modus operandi for the Joint Standards Committee.

The second recommendation of the Task Group, approved by both Boards, deals with the question of admission to the several grades in the two societies. The resolution as approved, to take effect January 1, 1961, makes it possible for a member of one society, based solely on the qualifications submitted to that society, to join the other society at an equivalent grade of membership without the payment of an entrance fee. This action applies *only* to the three grades of membership for which the equivalences are shown below.

AIEE	IRE
Member	Senior Member
Associate Member	Member
Affiliate	Associate

The Task Group recommended the appointment of a separate committee to devote itself to the question of increased cooperative effort with regard to student affairs. For this joint effort J. D. Ryder will chair the IRE contingent comprising Messrs. J. F. Reintjes, T. F. Jones, and R. E. Nolte. The AIEE representatives are chairman, D. E. Garr, W. R. Grogan, S. R. Warren, Jr., and D. G. Wilson. Each member of this committee is both a member of IRE and of AIEE. May their deliberations be successful.

USASC 1860–1960. June 21, 1960 marked the first one hundred years of service to the Army and the Nation of the U. S. Army Signal Corps. IRE extends congratulations in this centennial year.

Albert James Myer was appointed the first Signal Officer of the U. S. Army following his invention of a system of flag telegraphy in 1856. This appointment in 1860 marked the origin of the USASC and the beginning of its remarkable history. Tactical electric telegraph lines were first used by USASC in 1862; then followed the initiation of the first weather bureau, the participation in the first polar year (1881); the use of telephony, of field radio, of aircraft radio, of fire control systems, of teletype, the superheterodyne, radar, and frequency modulation. In recent years the Signal Corps has continued to maintain its high position in the art of communications. It has provided the electronic support for guided missiles and participated in electronic warfare and countermeasures efforts, and in space communications. The magnitude and scope of this work is amply demonstrated by the October issue of the IRE TRANSACTIONS ON MILITARY ELECTRONICS, a special Centennial Issue describing current Signal Corps programs in nearly three dozen areas of communications and electronics.

In any one hundred year history many individuals will have made outstanding contributions to any art. In such a brief comment as this, only a few contributors to Signal Corps accomplishments can be mentioned. Logically, some of the IRE members who contributed are selected for mention. Major General George O. Squier, a Chief Signal Officer from 1917–1923, was Director of IRE in 1918–1922. Edwin H. Armstrong as a Major in the Signal Corps developed the superheterodyne circuit during his overseas services in World War I. He was a Fellow of IRE, the first recipient of the Medal of Honor in 1917, and a Director in 1916–1922 and 1936–1938. The Signal Corps honored him when it dedicated Armstrong Hall, the Signal Corps Museum, in 1955. Major General H. C. Ingles, Chief Signal Officer from 1943–1947, is a Senior Member of IRE. Lt. General J. D. O'Connell, the Chief Signal Officer from 1955–1959, became an IRE Fellow in 1957.

Unquestionably the next hundred years will add still more illustrious pages to Signal Corps history, and IRE and its members should continue to contribute to signal progress through the USASC.

Section 108—Student Branch 193. The Executive Committee, at its October meeting, approved the formation of the Mobile Section, Number 108. Welcome is extended to this newest Section in Alabama, and in Region 3. Approval was also granted for Student Branch Number 193 at the University of Buenos Aires, Argentina, the first Student Branch established outside of the United States and Canada.—F. H., Jr.

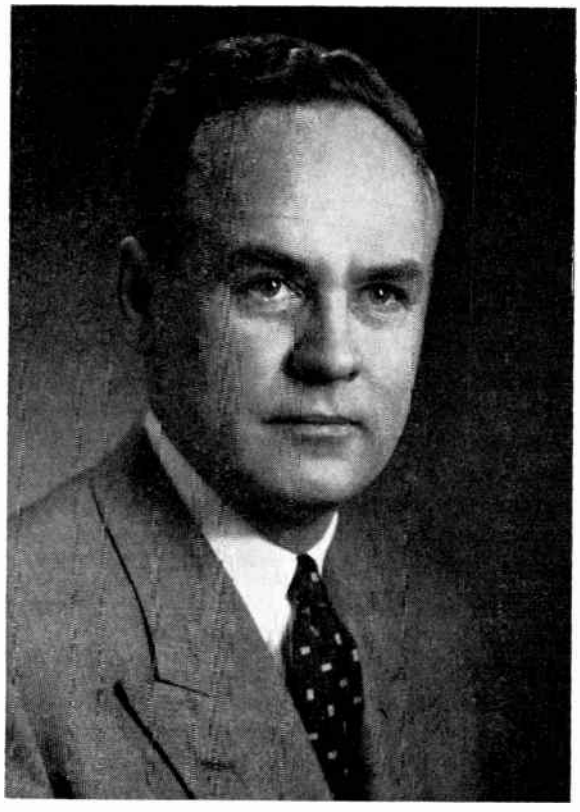

G. Sinclair

Director, 1960–1962

Dr. George Sinclair (A'37–SM'46–F'54) is Professor of Electrical Engineering at the University of Toronto, Ontario, Canada, and President of Sinclair Radio Laboratories Limited, Toronto. He was born in Hamilton, Ontario, on November 5, 1912. He attended public and high schools in Edmonton, Alberta, Canada, and entered the University of Alberta in 1929, receiving the B.Sc. degree in Electrical Engineering in 1933, and the M.Sc. degree in 1935. He received the Ph.D. degree from The Ohio State University, Columbus, in 1946.

He was largely responsible for the organization of the Antenna Laboratory of The Ohio State University Research Foundation during World War II, and was its Director until 1947. Many of the techniques for model measurement of aircraft antennas, now widely used by antenna laboratories, were developed under his direction. He also did some of the early work on the theory of slot antennas and arrays of slots on cylinders, and experimental and theoretical studies of radar echoes from targets. In 1947 he became associated with the University of Toronto, where he established the Antenna Laboratory of the University. Here he has continued his work on various aspects of antenna theory.

He has served on many IRE committees, including Antennas and Propagation, and Papers Review. He has been an Editorial Reviewer since 1954. He was Chairman of the Professional Group on Antennas and Propagation in 1951 when this Group published its first TRANSACTIONS, and he has been a member of the Administrative Committee of the Professional Group on Microwave Theory and Techniques since 1957.

Dr. Sinclair has been very active in Canadian IRE affairs, particularly the IRE Canadian Convention. He was General Chairman of this Convention in 1958, Chairman of its Technical Program Committee for 1956 and 1957, and Chairman of the Toronto Section in 1951.

In URSI affairs, he has been Chairman of Canadian Commission VI since 1953, and was International Chairman of Sub-Commission VI-3 from 1954 to 1960. He organized the URSI International Symposium on Electromagnetic Theory, which was held at the University of Toronto in 1959.

Dr. Sinclair was awarded a Certificate of Appreciation by the U. S. War and Navy Departments in 1948. In 1958 he received a Guggenheim Fellowship. He is a member of Sigma Xi, and is a licensed engineer in the State of Ohio and the Province of Ontario.

Scanning the Issue

Electron-Optical Properties of a Flat Television Picture Tube (Ramberg, p. 1952)—Visitors to the 1956 WESCON show were startled to see an experimental television receiver which incorporated a flat picture tube only a few inches thick. The tube owed its radically thin look to the fact that the electron gun, instead of pointing directly at the face of the tube, was placed off to one side and aimed parallel to the bottom edge. The electron beam was then bent up and into the tube face by means of two sets of deflection plates. Another interesting feature was that the device could be made completely transparent by employing transparent phosphors and conducting materials on the tube face and deflection plates. It has been suggested, for example, that this arrangement might be incorporated in an aircraft windshield for displaying on it flight information in bad weather without impairing the pilot's vision in good weather. The first published description of the tube in the December, 1957 PROCEEDINGS evoked widespread interest because, whether or not the tube eventually proved suitable for television, it represented the first major breakaway from conventional display tubes and involved new techniques which might find important applications in other fields. The present paper digs into the question of how to achieve linear deflection and sharp focusing over the entire picture area. It is noteworthy in that it is the first quantitative discussion of the tube that has been published. Moreover, it answers questions raised by the earlier paper and clarifies some of the problems of a type of tube which is of considerable current interest to all investigators of display devices.

Coupled-Cavity Traveling-Wave Parametric Amplifiers: Part I—Analysis (Currie and Gould, p. 1960)—The term "parametric amplifier" has been in common use for only three years. Yet in this brief span it has become one of the most widely discussed topics in the literature of our field. Some, if not most, of this popularity stems from the fact that "parametric amplifier" is not a specific device but rather refers to a broad principle of operation, one which can result in many different forms of devices. One of the early forms suggested was a ferromagnetic amplifier which employed traveling waves. This was followed by proposals for other traveling-wave types using nonlinear capacitive diodes. Interest has grown to the point where today a great deal of attention is being given to employing traveling-wave techniques in parametric amplifiers in order to increase their bandwidth capabilities. This paper proposes a new form of traveling-wave circuit for a parametric amplifier. The circuit consists of a chain of inductively coupled cavities loaded by diodes in the capacitive region. This structure leads to a number of advantages over earlier types which make it particularly attractive for operation at microwave frequencies. Among these advantages is the increase in interaction impedance which results. In other words, by the use of cavities the field strength in the vicinity of the diodes has been increased and this increases the gain that can be obtained per diode. The authors analyze their amplifier and, with the aid of a computer, provide detailed information on its operating characteristics. How well this theoretical investigation agrees with experiment is disclosed in the companion paper which follows.

Coupled-Cavity Traveling-Wave Parametric Amplifiers: Part II—Experiments (Grabowski and Weglein, p. 1973)—This paper reports experimental results obtained with the new amplifier which was analyzed theoretically in the preceding companion paper. The results represent more than a verification of predicted behavior, however, for the authors have added and experimentally explored several interesting features not incorporated in the basic model of the previous paper, including the use of ferrite-loaded coupling irises and an upper passband to improve stability. This experimental program demonstrates that low-noise broadband amplification is now a practical possibility well beyond the centimeter wavelength region.

Regenerative Fractional Frequency Generators (Plotkin and Lumpkin, p. 1988)—An interesting modification has been made to a class of frequency dividers which offers several noteworthy advantages over its predecessors. In addition to the simplicity of the circuit, the new frequency divider boasts an ability to track the input signal over much wider frequency ranges than heretofore possible and still remain locked to an exact submultiple. Since frequency dividers are so widely used, these and other attributes of the circuit will interest a large group of practical designers, including those concerned with transmitters, receivers, television circuits, frequency standards, measuring equipment and computers.

An Improved Decision Technique for Frequency-Shift Communications Systems (Thomas, p. 1998)—The transmission of binary information by frequency-shift keying is accomplished by transmitting "marks" on one frequency and "spaces" on an adjacent frequency. The process of deciding whether a mark or a space has been received normally consists of determining which frequency channel produces the greater output, a procedure which can result in errors when deep fading occurs on one of the channels. The author reasoned that since the mark and space transmissions are exactly complementary to one another the entire message could still be determined from one channel alone. He therefore developed a new decision circuit which operates on each channel independently and has found that it results in a 10 to 30 fold reduction in error rates, an advance of substantial significance to the radio telegraph field.

Generalized Padé Approximation (Stewart, p. 2003)—Approximation problems, although especially familiar to network theorists and practitioners, arise in all areas of engineering analysis. The problem may be one of reducing the difficulties of analysis by replacing a complicated function with a less complicated one, or it may be that of finding a function which is a valid model for a physical system. As the examples in this paper show, applications may arise in the study of such varied matters as RC transmission lines, transistor alpha, and Z transforms. The approach presented here of minimizing the error between the approximation and that which it approximates provides interesting insight into this basic analytical tool.

A Study of Surface Roughness and Its Effect on the Backscattering Cross Section of Spheres (Hiatt, *et al.*, p. 2008)—This study was undertaken to settle a growing difference of opinion among authorities regarding the influence of surface imperfections in model scattering experiments. Such effects, if as serious as some believe, would seriously affect an entire class of antenna and radar experiments. Important evidence is presented which, fortunately, shows that a reasonable amount of roughness can be tolerated.

Annual Indexes (follows page 2070)—During 1960 the IRE published nearly 500 technical papers and letters in the PROCEEDINGS and another 400 papers in the Convention Records for the International and Wescon Conventions. The 1960 annual indexes for these three publications, containing listings by subject and by author, appear at the end of the editorial section of this issue. An annual index for TRANSACTIONS will be published in the PROCEEDINGS in the spring of 1961. Readers are reminded that cumulative indexes for the periods 1913–1942, 1943–1947, 1948–1953, and 1954–1958 may be purchased from IRE Headquarters.

Scanning the Transactions appears on page 2048.

Electron-Optical Properties of a Flat Television Picture Tube*

E. G. RAMBERG†, FELLOW, IRE

Summary—Ray paths and focusing properties are calculated for the deflection and acceleration fields of a flat picture tube with lateral beam injection such as has been introduced to the art by W. R. Aiken. The results give insight into the measures which must be taken to achieve linearity of deflection and to assure sharp spot focus over the picture area. Specifically, it is found that linear deflection can be obtained by the application of voltage variations to the deflection electrodes which do not depart greatly from linear variations between the prescribed maximum and minimum values. Horizontal focus is determined almost entirely by the focusing action of the gun and the horizontal deflection plates. The focusing action of the latter is such that the beam incident on the deflection field must be, in general, divergent. The point of divergence required shifts with the horizontal scan, resulting in the need for some kind of dynamic control of gun focus. The horizontal deflection fields, the fields between the accelerating electrodes, and the vertical deflection fields all contribute to vertical focusing. If the separation of the side plates of the horizontal deflection system is of the same order as or less than the height of the deflection structure, the first focus formed by the horizontal deflection field is re-imaged at the screen by the remaining focusing elements. The vertical deflection field alone will not focus a parallel incident pencil in the plane of the screen.

Introduction

A FLAT television picture tube was announced by W. Ross Aiken of the Kaiser Aircraft and Electronics Corporation early in 1955, and has been described in greater detail in a U. S. Patent issued to him since then.[1] Since this tube incorporated several unusual electron-optical features, a theoretical examination giving better insight into the operation of the tube was undertaken several years ago. The results of this analysis are presented here.

The operation of the tube may be envisaged with the aid of the schematic diagram shown in Fig. 1. A conventional electron gun injects a beam from the upper left into a sequence of U-shaped channels, the horizontal deflection plates. If the channels close to the gun are maintained at gun-anode potential and the more remote channels are maintained at gun-cathode potential, the beam will be bent downward close to the transition point. After passing through a sequence (*B* and *C*) of plane parallel accelerating electrodes, the beam enters the viewing space, bounded by a flat phosphor screen (*D*) and a succession of vertical deflection plates in the form of parallel conducting strips. Again, if the vertical deflection plates close to the point of entry of the beam are maintained at screen potential while the more remote deflection plates are at a potential close to cathode potential, the beam is bent toward the screen near the transition point, forming a luminous scanning spot. By modulating the voltages of the horizontal deflection plates, the scanning spot is shifted horizontally, and by modulating the voltage of the vertical deflection plates, it is shifted vertically.

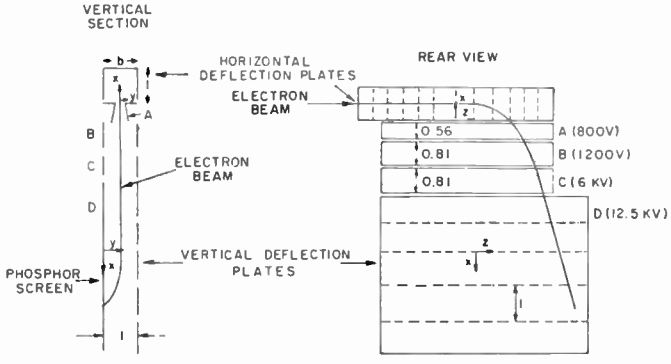

Fig. 1—Schematic projections of electrode structure of flat kinescope.

The electron-optical characteristics of this system, or the action of the electrostatic fields within it on the electron paths, affect its operation in two ways:

1) They determine the voltage variations which must be applied to the horizontal and the vertical deflection electrodes to achieve linearity of scan in both directions.
2) They determine the conditions under which sharp spot focus can be obtained in both the horizontal and the vertical directions.

In both respects, the horizontal and vertical deflection fields play a dominant role and, consequently, received major attention. The potential distribution in either case can be expressed in the form of integrals or infinite sums, which, along with the differential equations for the electron paths, are given in the Appendix. Numerical methods were employed to integrate the path equations in both instances. For the simpler vertical deflection fields an IBM Card Programmed Calculator located at the David Sarnoff Research Center in Princeton, N. J. was employed. The path integration for the more complex horizontal deflection fields demanded the use of the much larger IBM 701 calculator located at the IBM World Headquarters in New York.

* Received by the IRE, June 3, 1960; revised manuscript received, August 31, 1960.

† Institut für theoretische Physik, Technische Hochschule, Darmstadt, Hochschulstr. 1, Ger. (on leave from RCA Labs., Princeton, N. J., where the work reported here was carried out).

[1] See W. R. Aiken, U. S. Patent No. 2,795,731; issued June 11, 1957. Also, "A thin cathode-ray tube," PROC. IRE, vol. 45, pp. 1599–1604; December, 1957.

Linearity of Deflection

A straightforward method of applying deflection voltages to a set of deflection plates is indicated in Fig. 2. The exponential shape of the sawtooth applied to the grid resistances and the exponential variation of the grid resistance with distance, x, of the plate in question from the end of the chain causes the sawtooth to progress with uniform speed L/T, corresponding to the ratio of the length of the deflection range to the time of scan, from one end of the system of plates to the other. As long as the potential applied to the deflection tube grid for a particular deflection plate is less than $(V_b + V_c)$, where V_c is the cutoff voltage of the tube and V_b is the cathode bias, the plate remains fixed at the high-voltage potential. As the grid potential rises above $(V_c + V_b)$, the plate voltage drops toward V_b, the steepness and shape of the drop being determined by the tube characteristics, the coupling impedance Z, and the bias V_b. These factors must be manipulated to give linearity of scan within the subperiod corresponding to the width of a single deflection plate.

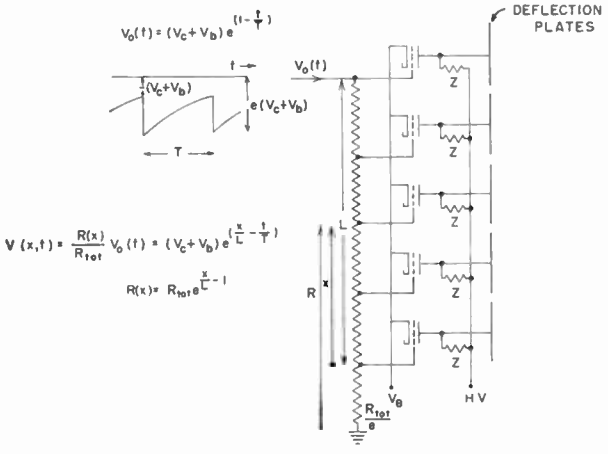

Fig. 2—Principle of scanning system in flat kinescope.

Calculations of the variation of the point of beam impact on the screen with the voltages applied to the deflection plates have been carried out for the vertical deflection system only. The required variation of plate potential is readily determined from ray plots if the potential of only one plate is varied at a time, *i.e.*, if the plate potential drops from the high-voltage value substantially to ground in a subperiod T/n, where n is the number of plates. Thus, Fig. 3 shows the variation in the point of incidence on the screen $(y=0)$ with the voltage of the modulated electrode for rays incident in the x direction at various heights y_0 above the screen.[2] If the unit of abscissas is put equal to a subperiod T/n, the same curve gives the voltage variation on the modulated electrode required to give a perfectly linear scan for rays incident at the indicated heights y_0. It is seen that the required voltage variation is fairly close to linear for heights of incidence ranging approximately from 0.2 to 0.6 of the separation between deflection plates and screens.

If the potential is varied on more than one electrode at a time, corresponding to a more gradual potential variation and a reduced maximum voltage difference between adjoining deflection plates, it is no longer possible to deduce the voltage variation required for linearity from a single set of ray paths. Instead the voltage variation must be assumed and the departure from linearity for this variation utilized, in order to guess a more favorable voltage variation. Fig. 4 shows the scan obtained for a straight linear sawtooth with a length equal to two subperiods T/n. Again, the departures from linearity, for heights of incidence $y_0 = 0.4, 0.5, 0.6$, are moderate. Thus it appears that the voltage variation required for any one electrode is nearly linear, increasing slightly in steepness with time. The voltage variation requirements for the horizontal deflection system can be expected to be essentially similar to those for the vertical deflection system.

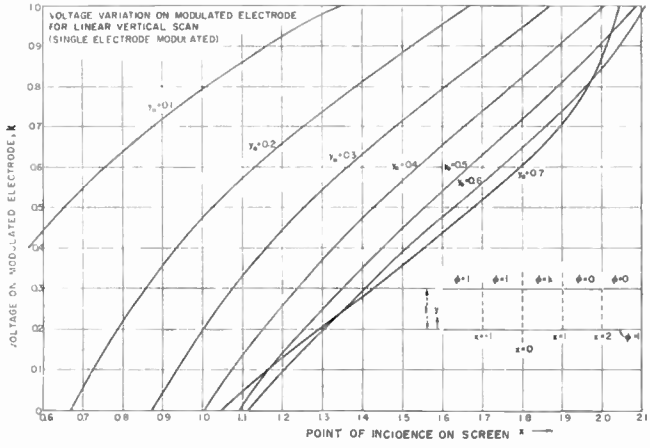

Fig. 3.

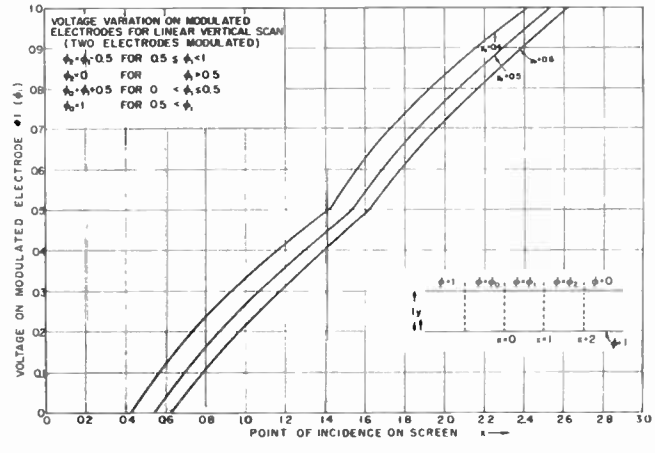

Fig. 4.

[2] The inserts on Figs. 3 and 4 and 6 through 10 represent the geometrical structure of the deflection system and the potentials applied to the several electrodes in relative units. For a more detailed discussion see the Appendix.

Focusing Effects of the Deflection Systems

General Description

It is convenient to consider the focusing effects of the horizontal and vertical deflection systems together, since, electron-optically, the vertical deflection system may be regarded as a limiting case (for $2b \rightarrow \infty$) of the horizontal deflection system.

Fig. 5 indicates the role which the deflection systems play in focusing in the horizontal and vertical direction, respectively.

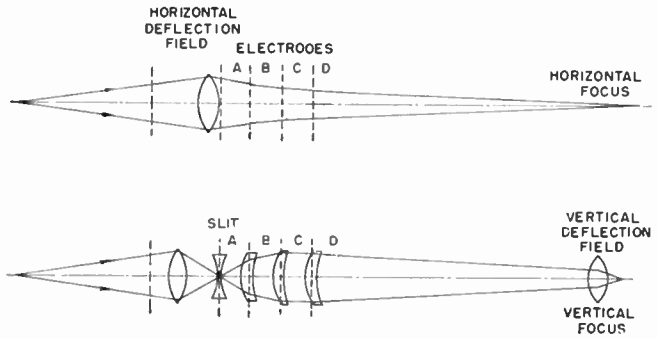

Fig. 5—Schematic presentation of focusing action of electrode structure in flat kinescope.

In the horizontal direction, the only focusing action is exercised by the horizontal deflection field. Thus, for optimum horizontal focus on the screen, the gun focus must be adjusted so that the lens action of the horizontal deflection field in the xz plane produces an image of the crossover in the effective plane of the screen.

In the vertical direction, on the other hand, focus is determined by:

1) the focusing action of the horizontal deflection field in the y direction;
2) the lens action of the slit in the bottom electrode of the horizontal deflection system;
3) the cylinder lenses formed between electrodes A, B, C, and D in Fig. 1; and
4) the lens action of the vertical deflection system. All of these, with the exception of the slit lens, are converging lenses.

The Focusing Action of the Deflection Fields in the xz Plane (Horizontal Focusing)

Figs. 6–9 (opposite) show the ray paths of electrons incident parallel to the z direction in the horizontal deflection system for an abrupt transition in potential from anode potential to zero between successive field electrodes, for ratios of the width to the height of the U-shaped electrodes $2b = \infty$, 1.5, and 1.0. $2b = \infty$ corresponds to the electrode configuration of the vertical deflection plates.

Circles on the curves indicate the point of convergence of a narrow pencil of electrons.[3]

A comparison of the results for different values of b indicates, in general, a slight decrease in the focusing action of the deflection field as b becomes smaller or the sidewalls of the U-electrode are brought closer together. It is seen, furthermore, that the focusing action varies little over a range of x_0 from 0.3 to 0.5 and remains reasonable for a range from 0.2 to 0.6. Fig. 10 shows, furthermore, that for a more gradual decrease in voltage along the field electrode structure, the ray slopes are slightly smaller and the effective focal length of the deflection field is increased somewhat.

The focusing action in the xz plane of the deflection field is modified by the accelerating fields beyond the deflection field. Two examples of such fields are treated very readily: the example of a uniform accelerating field and that of an accelerating field concentrated on a very short distance. Quite generally, the effect of an accelerating field is to increase the distance D, measured in the direction of the field, of the point of convergence from the point of incidence on the accelerating field. The ratio of the distance D to the distance D_0, representing the initial separation of the point of convergence and the point of incidence measured in the direction of the field (x direction), is given for some specific cases as follows:[4]

Angle of Incidence	D/D_0 for Uniform Field		D/D_0 for Concentrated Field	
	$V/V_0=10$	$V/V_0=5$	$V/V_0=10$	$V/V_0=5$
0	2.08	1.62	3.16	2.24
45°	4.39	3.0	8.28	5.4
60°	9.56	5.9	22.8	14.0

V_0 is here the initial beam potential; V, that after acceleration.

[3] If (x_c, z_c) denotes the point of convergence, $(0, z_i)$ the point-of-incidence on the plane $x=0$, and x_i' the slope of the ray at the point of incidence,

$$z_c = z_i + x_i'(dz_i/dx_0)/(dx_i'/dx_0); \; x_c = x_i'(z_c - z_i).$$

[The functions $z_i(x_0)$ and $x_i'(x_0)$ were obtained by fitting a polynomial in x_0 to the points and slopes of incidence obtained from the electronic computer.]

[4] With $a = V/V_0$ and $x' = \cot\theta$ (θ = angle of incidence) we have, for a uniform field:

$$\frac{D}{D_0} = \frac{\sqrt{a(1+x'^2)} - 1(\sqrt{a(1+x'^2)} - 1 + x')^2}{2x'^2(\sqrt{a(1+x'^2)} - 1 + ax')}$$

and for a concentrated field:

$$\frac{D}{D_0} = \frac{\{a(1+x'^2) - 1\}^{3/2}}{ax'^3}.$$

These expressions follow directly from the requirement that the initial horizontal displacement of two converging rays be equal to the difference in the product of the horizontal velocity component, and the transit time to the point of convergence for the two rays.

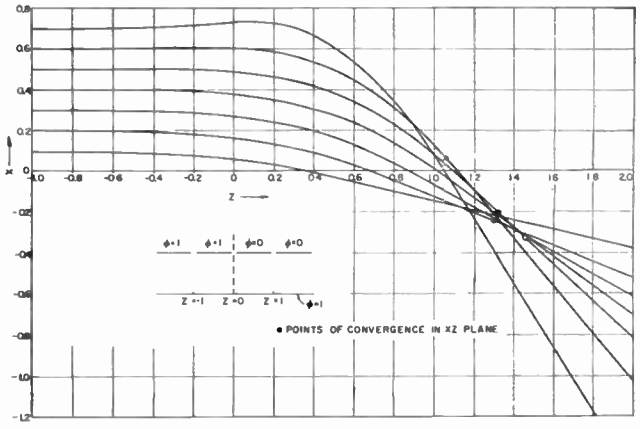

Fig. 6—Ray paths of electrons when $2b = \infty$.

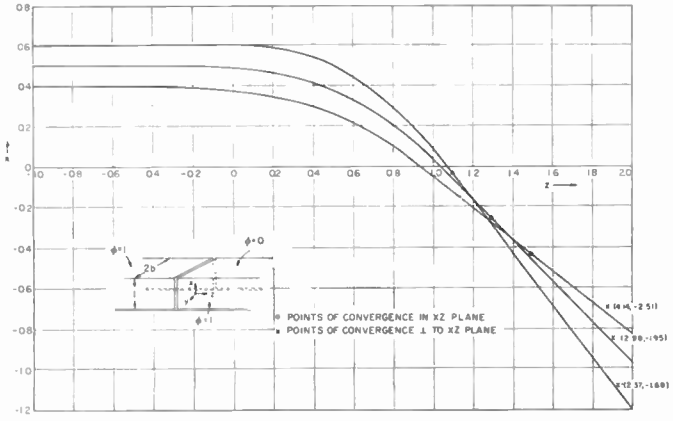

Fig. 7—Ray paths of electrons when $2b = 2$.

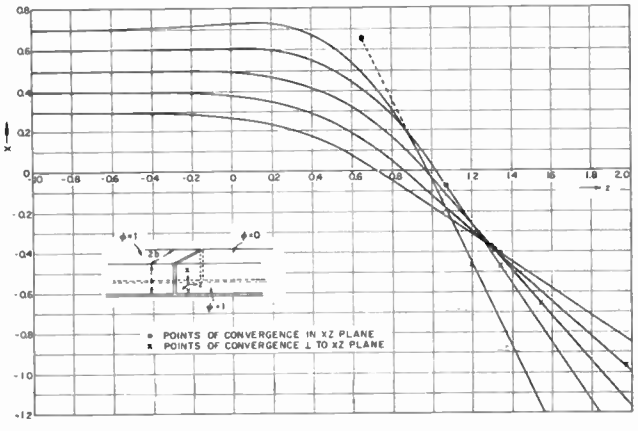

Fig. 8—Ray paths of electrons when $2b = 1.5$.

An examination of the structure in Fig. 1 indicates that most of the accelerating action, between electrodes B and C, is concentrated at a point well beyond the region where initially parallel beams are focused by the deflection fields. Under these circumstances, the effect of the accelerating field is simply to reduce the divergence of the electron beam and to translate the effective

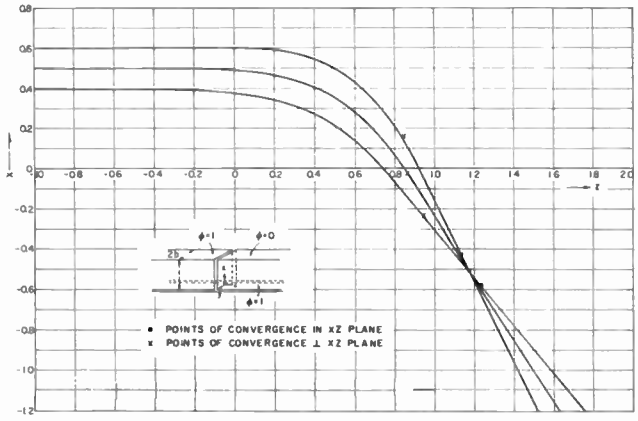

Fig. 9—Ray paths of electrons when $2b = 1.0$.

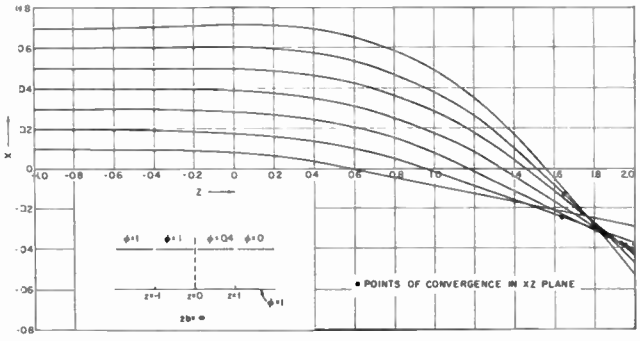

Fig. 10—Ray paths for a more gradual decrease in voltage along the field electrode structure.

source to a greater distance from the final point of incidence on the screen. In order to obtain focusing on the screen, the beams falling on the horizontal deflection fields must be divergent, so that the point of divergence is imaged (for pencils in the xz plane) some distance beyond the point of principal acceleration.

The Focusing Action at Right Angles to the xz Plane (Vertical Focusing)

Fig. 11 shows the focusing action of the horizontal deflection fields for rays deviating by a small distance Δy from the principal rays in the plane of symmetry for several different values of the width $2b$ of the U-shaped electrodes and several heights of incidence of the principal ray x_0. The individual rays are terminated at the point of intersection with the plane $x = 0$ (which, for purposes of the calculation, was considered as unipotential) and then continued by dotted lines to their point of convergence. The points of convergence for narrow pencils in the xz plane are indicated by circles and crosses in Figs. 8–10. Finally, the refractive powers of the horizontal deflecting field in the two directions, defined by

$$\frac{1}{f_x} = \frac{d\theta}{dx_0} = \frac{1}{1 + x_i'^2} \frac{dx_i'}{dx_0} \qquad \frac{1}{f_y} = \frac{d\theta}{dy_0} = \frac{1}{\sqrt{1 + x_i'^2}} \frac{y_i'}{v_0},$$

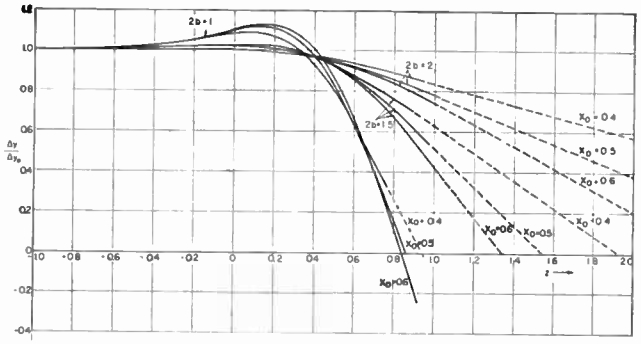

Fig. 11—Focusing action of the horizontal deflection fields for rays deviating by a small distance Δy from the principal rays.

are plotted in Fig. 12. In the formulas, $d\theta$ represents the angle formed with the principal ray after passage through the field, and x_i' the slope of the principal ray at $x=0$.

The data show that the focusing in the y direction depends strongly on the width of the U-shaped electrodes, as is to be expected, whereas the focusing in the x direction is relatively little affected thereby. For $2b=1$ the focusing in the y direction is actually stronger than in the x direction. Attention was concentrated on the dimension $2b=1.5$ since here the focal points for the two pencils came most nearly together. It is true that this is relatively unimportant in view of the strong unilateral focusing action of the cylindrical fields in the remainder of the structure.

Fig. 13 shows the trace of an initially round parallel pencil in the plane $x=0$ for a horizontal deflection-field structure with $2b=1$. It was obtained by extrapolating the focusing action along the principal rays for $x_0=0.3$ and 0.7, and assuming displacements to vary linearly with the initial value y_0 for the range in y covered by the beam. Even though this assumption may not be fulfilled, Fig. 13 should give a qualitatively correct picture of the beam cross section in the plane $x=0$ (the bottom plane of the horizontal deflection structure).

A diverging lens is formed at the slit in the base plate of the horizontal deflection structure. For a principal ray incident with a slope x_i', the effective focal point of this lens lies a distance D_s above the bottom plate, with[5]

$$D_s = 2\phi_i\left[\frac{\partial\phi_i}{\partial x}(1+x_i'^2)\right]^{-1} \cong (1+x_i'^2)^{-1} \quad \text{for} \quad 2b=1.$$

Here the height of the horizontal deflection structure is taken as unit of length. ϕ_i and $\partial\phi_i/\partial x$ are the potential and potential gradient at the bottom plate of the structure. If the position of the initial point of convergence

[5] This is the Davisson-Calbick formula for the focal distance of a slit lens generalized for oblique incidence. See C. J. Davisson and C. J. Calbick, "Electron lenses," *Phys. Rev.*, vol. 38, p. 585, August, 1931; vol. 42, p. 580, November, 1932.

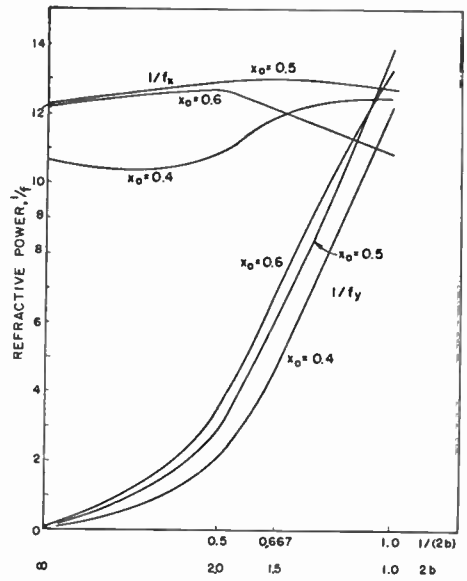

Fig. 12—Variation of refractive power with separation $2b$ of sidewalls of field electrode (detailed shape of curves uncertain because of extrapolations.)

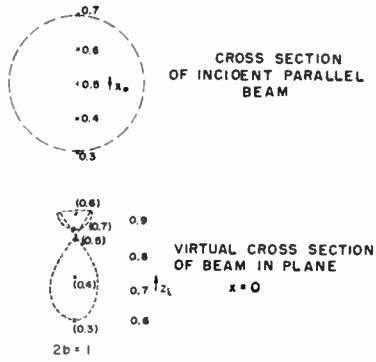

Fig. 13—Effect of horizontal deflection field on beam cross section.

is given by $D_0=-x_i'y_i/y_i'$, it is shifted by the negative slit lens to

$$D = \frac{-x_i'}{-x_i'(1+x_i'^2)+y_i'/y_i}.$$

For $2b=1$ the term y_i'/y_i is very large numerically and the shift produced by the slit lens correspondingly unimportant. For $2b=1.5$, on the other hand, the two terms in the denominator are of the same order, with the divergence produced by the slit lens outbalancing the convergence produced by the deflection field for small heights of incidence.

Additional, converging, cylindrical lenses are formed between the several strip electrodes interposed between the horizontal deflection structure and the image field. Fig. 14 shows the focal properties of these lenses as a function of the voltages V_1 and V_2 applied to the electrodes; the detailed equations for the potential distribution and for the weak-lens behavior of these fields are given in the Appendix.

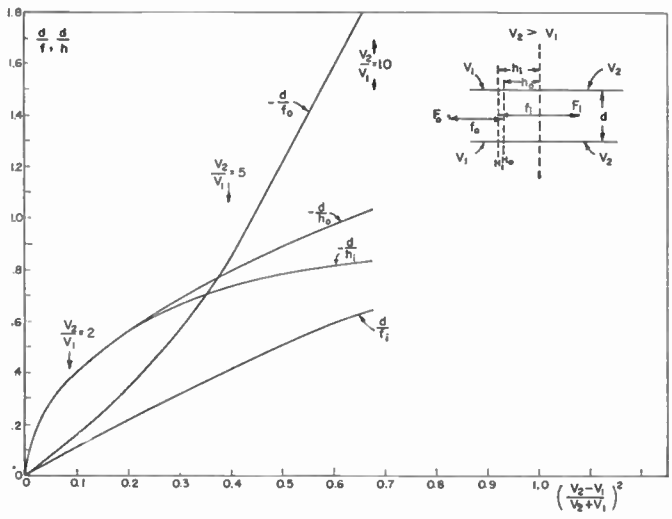

Fig. 14—Cylindrical-lens properties of two coplanar pairs of plates at different potentials.

Finally, for the focusing action of the vertical deflection field, we must refer back to Figs. 6, 10, and 12. These figures show immediately that a parallel beam occupying a reasonable fraction of the space between field electrodes and screen does not yield a sharp vertical focus on the screen. If the screen were replaced by an electron-permeable conducting membrane, sharp focus would be obtained at a distance beyond the screen of the order of 0.4 of the separation between deflection plates and screen.

Sharp vertical focus thus requires that the beam incident on the vertical deflection fields be converged to a point in the vicinity of the spot. Now a point at the bottom of the structure in Fig. 1 is approximately at the image side focus of the cylindrical lens between electrodes C and D since, by Fig. 14, the focal point on the high-voltage side of the lens, for $V_2/V_1=2$, is at $5.66d$ from the junction between electrodes; d signifies the separation of the electrodes. Consequently, the object point corresponding to an image point at the bottom of the structure lies at the low-voltage focal point of the combined lenses between electrodes A and B, and B and C. In determining the position of this focal point it is necessary to note that the effective potentials of the electrodes, V_1 and V_2, are less than the applied potentials by $V_0/(1+x_i'^2)$, if V_0 is the potential applied to the bottom electrode of the horizontal structure. Thus, for a ray slope $x_i'=1$, the potentials for the lens between electrodes A and B are $V_1=400$ and $V_2=800$ volts, or $V_2/V_1=2$, whereas for the lens between electrodes B and C, $V_2/V_1=7$. The low-voltage focal point for the combined lens system lies about half the height of the horizontal deflection structure above the bottom plate of the latter; for a slightly different potential distribution (*e.g.*, connecting electrodes B and A together) the effective object point moves down practically to the plane of the bottom plate. In either case, the beam cross section which is imaged by the cylindrical lens fields at the bottom of the structure is similar to that shown in Fig. 13. The magnification factor for the extent of the figure in the y direction may be computed to be about 2.5. This may be further reduced by a factor of 2 by the vertical deflection fields. The extent of the figure in the horizontal direction is determined, of course, by the degree of divergence of the beam prior to incidence on the horizontal deflection fields.

Conclusion

In summary, the results of the computations indicate:

1) Linear deflection can be obtained by the application of voltage variations to the deflection electrodes which do not depart greatly from linear variations between the prescribed maximum and minimum values.

2) Horizontal focus is determined almost entirely by the focusing action of the gun and the horizontal deflection plates. The focusing action of the latter is such that the beam incident on the deflection field must be, in general, divergent. The point of divergence requires shifts with the horizontal scan, resulting in the requirement of some form of dynamic control of the gun focus.

3) The horizontal deflection fields, the fields between the accelerating electrodes, and the vertical deflection fields all contribute to vertical focusing. If the separation of the side plates in the horizontal deflection system is of the same order as or less than the height of the deflection structure, the first focus formed by the horizontal deflection field is re-imaged at the screen by the remaining focusing elements. The vertical deflection field alone will not focus a parallel incident pencil in the plane of the screen.

Appendix

Horizontal Deflection Field

The geometry of the structure for which ray calculations were carried out is shown in Fig. 15. The base plate ($x=0$), which in the physical realization is split into two sections by a relatively wide longitudinal slit, is regarded as a continuous conducting plane. Rays are calculated which are incident from the left, parallel to the base plate, in the plane of symmetry $y=0$. They obey the equation[6]

$$\frac{d^2x}{dz^2}=\frac{1+\left(\frac{dx}{dz}\right)^2}{2\phi}\left[\frac{\partial\phi}{\partial x}-\frac{dx}{dz}\frac{\partial\phi}{\partial z}\right].$$

In addition, rays are computed which, for large nega-

[6] See, *e.g.*, V. K. Zworykin, G. A. Morton, E. G. Ramberg, J. Hiller, and A. W. Vance, "Electron Optics and the Electronic Microscope," John Wiley and Sons, Inc., New York, N. Y., p. 401; 1945.

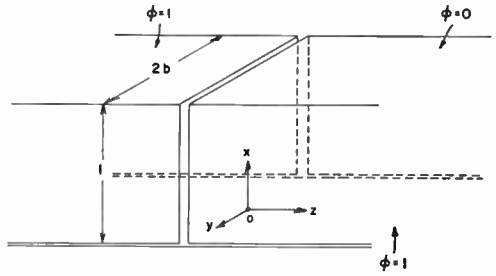

Fig. 15—Assumed structure of horizontal deflection system.

tive z, depart from the above "principal rays" by a small constant displacement y_0 in the y direction. The departure from the principal rays is given by

$$\frac{d^2\Delta y}{dz^2} = \frac{1+\left(\frac{dx}{dz}\right)^2}{2\phi}\left\{\left[\frac{1}{y}\frac{\partial\phi}{\partial y}\right]_{y\to 0}\Delta y - \frac{\partial\phi}{\partial z}\frac{d\Delta y}{dz}\right\}.$$

The solution of these two equations indicates the deflection experienced by the principal rays as well as the convergence along these rays, both in the xz plane and for small deviations in the y direction.

The general expression for the potential distribution in the structure is, in the form most convenient for calculation,

$$\phi = \frac{1}{2} - \frac{4}{\pi^2}\int_0^\infty \frac{\sin(lz)}{l}\,dl \sum_{n=0}^{\infty}\left\{\frac{\sin[(2n+1)\pi x]}{2n+1}\,\frac{\cosh\{y\sqrt{l^2+([2n+1]\pi)^2}\}}{\cosh\{b\sqrt{l^2+([2n+1]\pi)^2}\}}\right.$$
$$\left. + \frac{(-1)^n}{2n+1}\cos\frac{(2n+1)\pi y}{2b}\,\frac{\sinh\left\{x\sqrt{l^2+\left(\frac{2n+1}{2b}\pi\right)^2}\right\}}{\sinh\sqrt{l^2+\left(\frac{2n+1}{2b}\pi\right)^2}}\right\}$$
$$+ \frac{1}{\pi}\arctan\frac{\theta_1'\sqrt{(\theta^2-k\theta_1^2)(k\theta^2-\theta_1^2)(k'\theta'^2-\theta_1'^2)}}{k'\theta\theta'\theta_1\sqrt{\theta'^2-k'\theta_1'^2}}$$

with

$$\theta = 1 - 2g\cos(\pi x) + 2g^4\cos(2\pi x)\cdots$$

$$\theta_1 = 2\sqrt[4]{g}\left\{\sin\frac{\pi x}{2} - g^2\sin\frac{3\pi x}{2} + g^6\sin\frac{5\pi x}{2}\cdots\right\}$$

$$\theta' = 1 - 2g'\sin\frac{\pi y}{2b} - 2g'^4\cos\frac{\pi y}{b}\cdots$$

$$\theta_1' = \sqrt{2}\sqrt[4]{g'}\left\{\cos\frac{\pi y}{4b} - \sin\frac{\pi y}{4b} - g'^2\left(\cos\frac{3\pi y}{4b} + \sin\frac{3\pi y}{4b}\right)\right.$$
$$\left. + g'^6\left(\cos\frac{5\pi y}{4b} - \sin\frac{5\pi y}{4b}\right)\cdots\right\}$$

$$g = \frac{1}{2}\,\frac{1-\sqrt{k'}}{1+\sqrt{k'}} + \frac{1}{16}\left(\frac{1-\sqrt{k'}}{1+\sqrt{k'}}\right)^5 + \frac{15}{512}\left(\frac{1-\sqrt{k'}}{1+\sqrt{k'}}\right)^9\cdots$$

$$g' = \frac{1}{2}\,\frac{1-\sqrt{k}}{1+\sqrt{k}} + \frac{1}{16}\left(\frac{1-\sqrt{k}}{1+\sqrt{k}}\right)^5 + \frac{15}{512}\left(\frac{1-\sqrt{k}}{1+\sqrt{k}}\right)^9\cdots$$

and the moduli k and $k'=(1-k^2)^{1/2}$ determined by

$$K'/K = 2b.$$

Here K is the complete elliptic integral $F(\pi/2, k)$ of the first kind and, similarly, $K'=F(\pi/2, k')$.

The formula for the potential is obtained with the aid of the superposition principle by computing the potential distribution within the given geometrical structure for the following four sets of boundary conditions and adding the four results:

1) Potential of all the four bounding surfaces equal to $\frac{1}{2}$.
2) Potential of base electrode ($x=0$) and top panel of U-shaped channel ($x=1$) equal to zero; potential of two side panels ($|y|=b$) equal to $\mp\frac{1}{2}$ for $z\gtrless 0$.
3) Potential of base electrode ($x=0$) and side panels of U-shaped channel ($|y|=b$) equal to zero; potential of top panel ($x=1$) equal to $\mp\frac{1}{2}$ for $z\gtrless 0$.
4) Potential of base electrode ($x=0$) equal to $\frac{1}{2}$; potential of U-shaped channel ($x=1$ or $|y|=b$) equal to zero.

The potentials for these boundary conditions are represented by the four terms in the expression. The first, obviously, leads to the constant $\frac{1}{2}$. The second and third are the special solutions

$$\sum_m \int_0^\infty a_m(l)\sin(lz)\sin(m\pi x)\cosh(\sqrt{l^2+(m\pi)^2}\,y)\,dl$$

and

$$\sum_n \int_0^\infty b_n(l) \sin(lz) \cos\frac{(2n+1)\pi y}{2b} \cdot \sinh\left(\sqrt{l^2+\left[\frac{(2n+1)\pi}{2b}\right]^2}\, x\right) dl$$

of Laplace's equation in Cartesian coordinates which satisfy the prescribed boundary conditions; the choice of the trigonometric and hyperbolic functions is dictated by the requirement that the potentials by antisymmetric with respect to the planes $x=0$ and $z=0$ and symmetric with respect to the plane $y=0$.

The last term, representing the potential within the U-shaped channel at potential zero closed off by a base plate at potential $\frac{1}{2}$, is obtained by evaluating the two conformal transformations

$$x+iy = \int \frac{k\,dw}{\sqrt{(w^2-1)(w^2-c^2)}} \quad \text{and} \quad w = \exp\{\pi(\psi+i\phi)\}$$

for ϕ in terms of x and y. The first transformation is a Schwarz-Christoffel transformation,[7] transforming the U-shaped channel and its mirror image with respect to $x=0$ into the positive and negative real axis, respectively, of the complex w plane. The second transformation transforms these two half-axes in the w plane into the lines $\phi=0$ and $\phi=1$ in the $(\psi+i\phi)$ plane.

Vertical Deflection Field

Fig. 16 represents the basic building block of the vertical deflection field, with the potential distribution ϕ_0:

$$\phi_0(x,y) = \frac{2}{\pi}\int_0^\infty \frac{\sinh ky}{\sinh k}\frac{\sin kx}{k}\,dk = \pm\left\{y+\frac{2}{\pi}\sum_{n=1}^{\infty}(-1)^n\frac{\sin n\pi y}{n}e^{\mp n\pi x}\right\}, \qquad x \gtrless 0.$$

The first representation is suitable for small values of $|x|$, the second for large values of $|x|$.

The integral form follows directly from the general solution of the two-dimensional Cartesian Laplace equation; the series expression may be derived from it by expressing sin (kx) as a sum of exponential terms and carrying out the integration over k as a contour integration in the complex k plane, around the half-plane above or below the real axis;[8] the selection of the half-plane is dictated by the requirement that the real part of the term exp $(\pm ikx)$ remains less than unity. Fig. 17 shows how the potential distribution for a structure with different potentials applied to different field electrodes can be derived from the basic solution $\phi_0(x, y)$.

The differential equation for the ray paths has the same form as for the horizontal deflection field, with (y, x) replacing (x, z).

Cylindrical Lens Formed Between Two Symmetrically Placed Coplanar Pairs of Plates

The potential distribution in the plane of symmetry of the structure shown in Fig. 18 is given by

$$\Phi(x) = V_1 + \frac{2(V_2-V_1)}{\pi}\arctan e^{\pi x/d},$$

$$\Phi'(x) = \frac{V_2-V_1}{d}\operatorname{sech}(\pi x/d)$$

$$\Phi''(x) = -\pi\frac{V_2-V_1}{d^2}\operatorname{sech}(\pi x/d)\tanh(\pi x/d).$$

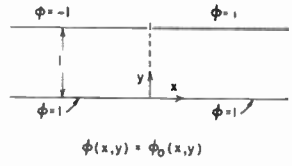

Fig. 16—Basic building block of the vertical deflection field.

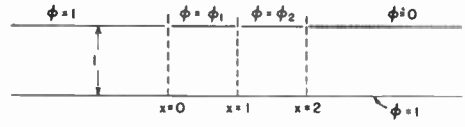

$$\phi(x,y) = \frac{1}{2} + \frac{1-\phi_1}{2}\phi_0(-x,y) + \frac{\phi_1-\phi_2}{2}\phi_0(1-x,y) + \frac{\phi_2}{2}\phi_0(2-x,y)$$

Fig. 17—Determination of potential distribution for a structure with different potentials applied to different field electrodes.

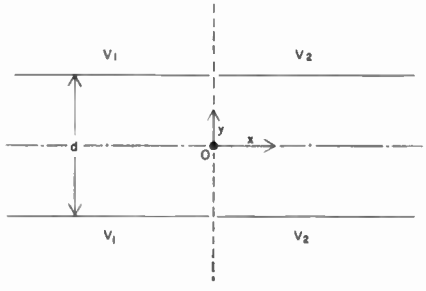

Fig. 18—Effect of horizontal deflection field on beam cross section.

[7] See, *e.g.*, L. P. Smith, "Mathematical Methods for Scientists and Engineers," Prentice-Hall, Inc., New York, N. Y., p. 225; 1953.
[8] *Ibid.*, p. 164.

Thus, the series expression for the potential on the axis ($y=0$), derived in the same manner as the series expression for the potential of the vertical deflection field, leads to

$$\Phi' = \frac{2}{d}(V_2 - V_1)\sum_{n=0}^{\infty}(-1)^n \exp\{\mp(2n+1)\pi x/d\} \quad x \gtrless 0$$

$$= \frac{2}{d}(V_2 - V_1)e^{\pi x/d}/(1 + e^{2\pi x/d})$$

$$= (1/d)(V_2 - V_1)\operatorname{sech}(\pi x/d).$$

The focusing properties of this lens are obtained by integrating the paraxial equation[9]

$$y'' = -\frac{\Phi' y + \Phi'' y}{2\Phi}.$$

[9] Zworykin, *et al.*, *op. cit.*, see (12.12) on p. 402. The expressions for the focal lengths and principal plane positions of a weak lens are obtained by integrating the path equation first with $y=$const and then integrating it again, treating the deviation of y from its initial value as a small quantity, found in the first integration.

For weak lenses $[(V_2-V_1)/(V_2+V_1)\ll 1]$ the image- and object-side focal lengths f_i and f_0 and the distance h of the principal plane from the junction plane (image- and object-side principal planes coincide approximately) are given by

$$f_i = \left(\frac{V_2+V_1}{V_2-V_1}\right)^2\left(\frac{2V_2}{V_2+V_1}\right)^{1/2}\frac{\pi d}{4}$$

$$f_0 = \left(\frac{V_2+V_1}{V_2-V_1}\right)^2\left(\frac{2V_1}{V_2+V_1}\right)^{1/2}\frac{\pi d}{4}$$

$$h = -\frac{V_2+V_1}{V_2-V_1}\frac{\pi d}{4}.$$

Acknowledgment

The author gratefully acknowledges the encouragement received from Dr. D. W. Epstein, at whose suggestion the analysis was carried out, as well as the invaluable assistance of Dr. F. Edelman, who programmed the numerical problems and supervised the machine computation required.

Coupled-Cavity Traveling-Wave Parametric Amplifiers: Part I—Analysis*

M. R. CURRIE†, SENIOR MEMBER, IRE, AND R. W. GOULD‡, MEMBER, IRE

Summary—**A general class of traveling-wave parametric amplifiers based on coupled-cavity filter circuits is described. This type of amplifier is particularly suited to microwave frequencies and incorporates new features that overcome some severe difficulties associated with other circuit structures. Traveling-wave diode-type amplifiers having relatively wide bandwidths and great simplicity at *S* band have already resulted from this approach (details of experiments will be described in Part II).**

An analysis is presented which provides detailed information on operating characteristics, including the effects of terminal impedances, reflected waves, circuit loss, etc., and also leads to a simple physical picture of the cumulative interaction mechanism in terms of coupled-mode concepts. This physical picture is emphasized throughout this paper. Gain bandwidth considerations are discussed in terms of a fundamental "interaction-impedance" parameter.

Representative calculated curves show that unilateral gains of 12 to 15 db over relatively wide bandwidths are attainable with as few as 4 to 6 diodes. Methods of increasing the gain through use of ferrites and special circuit techniques are proposed.

* Received by the IRE, May 3, 1960; revised manuscript received, August 19, 1960. This work was presented at the Seventeenth Annual Conf. on Electron Device Res., Mexico City, Mexico; June, 1959.

† Hughes Res. Labs., A Division of Hughes Aircraft Co., Malibu, Calif.

‡ Calif. Inst. Tech., Pasadena, Calif.

Introduction

A GREAT deal of attention currently is being given to increasing the bandwidth capabilities of solid-state parametric amplifiers by application of traveling-wave circuit techniques. In many respects, this situation is reminiscent of the evolution of broadband traveling-wave tubes from klystron amplifiers employing resonant cavity circuits. As will be shown in this paper, this analogy not only provides much useful conceptual information but also suggests a specific analytical and experimental approach which already has resulted in traveling-wave diode-type parametric amplifiers having relatively wide bandwidths and great simplicity at microwave frequencies.

Following the analysis of Tien and Suhl[1,2] of parametric amplification in a uniformly distributed non-

[1] P. K. Tien, "Parametric amplification and frequency mixing in propagating circuits," *J. Appl. Phys.*, vol. 29, pp. 1347–1357; September, 1958.

[2] P. K. Tien and H. Suhl, "A traveling wave ferromagnetic amplifier," PROC. IRE, vol. 46, pp. 700–706; April, 1958.

dispersive medium, Engelbrecht demonstrated an experimental amplifier in the UHF region which approximated Tien's model and resulted in excellent bandwidth performance.[3] This amplifier was based on a uniform transmission line (coaxial TEM mode) in which the nonlinear capacitive diodes were placed very close together with respect to wavelength so as to approximate a uniform nonlinear medium. Although the diodes were individually tuned for optimum performance, the essential nondispersive nature of the TEM mode was not changed.

In attempting to extrapolate directly this uniform transmission line approach to the microwave frequency range (*S* band and above) difficulties have been encountered which probably can be attributed to several factors.

First, the relatively low "interaction impedance" of such structures (in terms of voltage developed across the diode per unit power flow) implies a low gain per diode. With a large number of diodes, any nonuniformity in their characteristics can seriously affect amplifier gain. The diode losses also attenuate the pump power as it propagates down the system, which further reduces the contribution to gain of successive diode stages.

Second, such circuits can propagate some of the higher-order frequency components generated by mixing of the signal and the pump. In such systems, as shown recently by Roe and Boyd,[4] exponential gain at the signal frequency may not occur; rather, energy conversion to the propagating cross-product frequencies can take place with very little gain at the signal frequency.

Finally, at microwave frequencies, the lead inductance associated with the diode, together with its stray capacitance, can establish a self-resonance at or below the operating frequency of the amplifier. In this case, the voltage that is developed across the capacitive *p-n* junction itself may be greatly reduced with consequent severe degradation of amplifier performance.

This paper is concerned with a class of iterative circuits for traveling-wave parametric amplifiers which overcomes the first two difficulties and alleviates the third. It permits the realization of simple high-gain, broad-band parametric amplifiers at microwave frequencies.

The basic model is shown schematically in Fig. 1. It consists of a chain of inductively coupled cavities; each cavity is loaded by a diode in the capacitive region, and the diodes are individually pumped from an external circuit with the pump phase arranged so as to simulate a traveling wave. Some of the advantages of this general type of circuit are as follows:

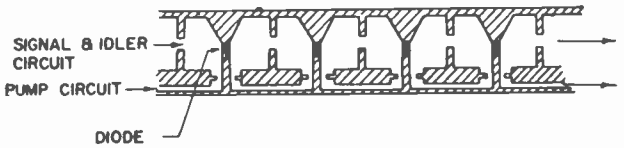

Fig. 1—Sketch of coupled-cavity type of traveling-wave parametric amplifier. Waves at the signal and idler frequencies propagate through a filter chain of inductively coupled cavities. Each cavity is loaded by a variable-capacitance diode at a position of maximum electric energy storage. Pump power is introduced from a parallel-feed system.

1) Since the structure constitutes a microwave bandpass filter circuit, the problems associated with the propagation of higher-frequency components are eliminated; these components can be made to fall in stop bands of the filter, where they cannot propagate and absorb energy.[5]

2) Unlike the case in which a uniform line is loaded by diodes, the diodes in this model are placed only in regions of concentrated electric energy storage. A higher voltage is developed across the nonlinear capacitance for a given power flow in the circuit. As a consequence, the gain per diode can be considerably higher than in the uniform case; the amplifier is greatly simplified by requiring fewer stages and lower pump power. As will be discussed, this situation can also be regarded from a more general viewpoint; a relation exists between gain per diode and bandwidth much like that between gain per unit length and bandwidth in traveling-wave tubes. By restricting the bandwidths to essentially the required value by means of a filter circuit, the gain per stage can be maximized.

3) The coupled-cavity circuit is particularly well adapted to microwave frequencies because it provides reasonably large diode spacings even at short wavelengths. For example, a direct scaling of Engelbrecht's amplifier, in which the diodes are spaced by $\frac{1}{8}$ wavelength at the signal frequency, would lead to prohibitively small spacings in the microwave region.

4) The circuit is a natural structure for incorporating ferrite elements as a possible means of improving stability by obtaining nonreciprocal attenuation. The regions of magnetic and electric energy storage are separated spatially so that elements sensitive to both electric and magnetic fields may be most effectively utilized in the amplifier design.

5) The use of parallel pumping permits efficient use of the available pump power and provides independent external adjustment of phase shift between sections so as to optimize gain, frequency response, and reverse attenuation.

6) The lead inductance of the diodes can be incorporated as part of the individual cavity circuits, thus

[3] R. S. Engelbrecht, "A low-noise nonlinear reactance traveling wave amplifier," PROC. IRE, vol. 46, p. 1655; September, 1958.

[4] G. M. Roe and M. R. Boyd, "Parametric energy conversion in distributed systems," PROC. IRE, vol. 47, pp. 1213–1218; July, 1959.

[5] When the pumping is not too strong, the diode elastance varies essentially sinusoidally with time. It is only necessary then to suppress the next highest idler (sum of signal and pump frequencies) to eliminate the effects of all other idlers.

alleviating some of the problems associated with self-resonance of the diode package.

The purpose of this paper is to describe the operation of filter-circuit traveling-wave parametric amplifiers of the type discussed above and to present an analysis that has proved very valuable in understanding some of their detailed characteristics. Certain aspects of this analysis are related to that of Bell and Wade[6] for the case of uniform transmission lines which are periodically loaded by diodes. A companion paper presents results of an experimental program in which these ideas have been demonstrated and extended by adding several features not incorporated in the basic model.

We shall first discuss the properties of coupled-cavity circuits and give a qualitative picture of the conditions under which an idler wave, which closely couples to the signal wave and leads to exponential growth, can be generated. The subsequent analysis is based on an equivalent circuit that closely represents the characteristics of its coupled-cavity microwave analog. The analytical approach has the advantage of taking into account the effects of terminal impedances and reflected waves and loss, all of which are of first-order importance in amplifier design. Detailed results of computer calculations clearly illustrate the essential characteristics of this type of amplifier and point up certain basic similarities with traveling-wave tubes. Finally, this approach is related to that of Tien in terms of a fundamental new interaction-impedance parameter.

Discussion of Model and Analysis

An equivalent-circuit representation of the coupled-cavity traveling-wave parametric amplifier is shown in Fig. 2. This particular circuit was chosen for analysis because it has been successfully applied in studying similar problems for traveling-wave-tube amplifiers.[7] In both cases, the basic cavity circuit elements are designed so as to concentrate the electric-energy storage at the point of active interaction (whether the interaction occurs with a time-varying capacitance or with an electron beam) and the cavities are inductively coupled. For fractional bandwidths less than about 25 per cent, this equivalent circuit can provide an accurate quantitative description of the characteristics of the actual distributed microwave circuit. This has been established by extensive measurements. For increasing bandwidths, the quantitative accuracy is not as good because of the use of frequency-independent elements in the equivalent circuit. However, the representation contains all the essentials of the physical problem, and the results of the analysis apply in a qualitative way to other possible iterated circuits of the general type indicated in Fig. 1.

In discussing the model, it is useful to define the following dimensionless parameters:

$$\lambda = \omega\sqrt{LC_o} \tag{1}$$

is frequency normalized to the midband frequency $(LC_o)^{-1/2}$ of the cold filter circuit;

$$k = M/L \tag{2}$$

is the coefficient of coupling between cavities;

$$q = R\sqrt{\frac{C_o}{L}} \tag{3}$$

is the reciprocal resonator Q and provides a measure of resistive circuit loss. (Note that $C_o = 1/S_o$.)

The general properties of the model are indicated in the Brillouin diagram of Fig. 3. We will use this representation throughout as a convenient means for studying the properties of amplifiers of the filter-circuit type. Here we have assumed that k is positive. For negative k, the fundamental branch would be a backward wave, but this would not alter the nature of the problem. The abscissa θ is the phase shift per resonator corresponding to a dependence

$$i_n = i_{n-1} \exp(-\alpha - j\theta), \tag{4}$$

where α is a measure of the circuit loss. The upper and

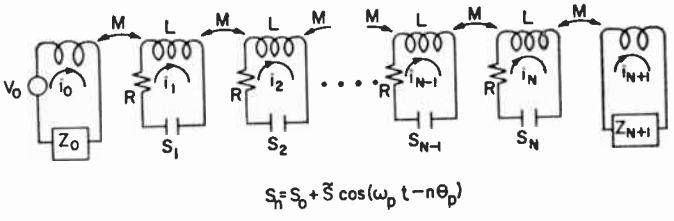

Fig. 2—Equivalent circuit of coupled-cavity traveling-wave parametric amplifier including arbitrary terminal impedances. The time variation of elastance of the nth cavity is indicated; $S_o = 1/C_o$, where C_o is the combined localized static capacitance of cavity and diode.

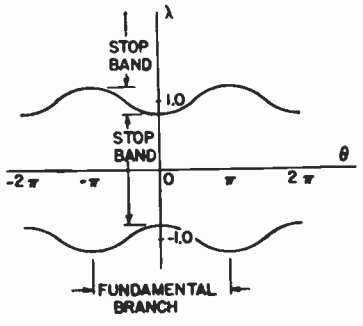

Fig. 3—Brillouin diagram of coupled-cavity filter circuit; λ is normalized frequency, θ is phase shift per section. Both the positive and negative frequency passbands are shown.

[6] C. V. Bell and G. Wade, "Circuit considerations in traveling wave parametric amplifiers," 1959 IRE WESCON Convention Record, pt. 2, pp. 75–82.

[7] R. W. Gould, "Characteristics of traveling wave tubes with periodic circuits," IRE Trans. on Electron Devices, vol. ED-5, pp. 186–195; July, 1958.

lower cutoff frequencies of the pass band are given by

$$\lambda_{\text{lower}}^{\text{upper}} = \frac{1}{\sqrt{1 \mp 2k}} \cong 1 \pm k \qquad (k \ll 1), \tag{5}$$

so that the fractional bandwidth is approximately equal to $2k$ for k small. The pass band shown in Fig. 3 represents only the principal pass band of the actual microwave filter circuit in which both the signal and idler waves propagate. Other higher-frequency bands will exist depending upon the specific geometry; these can be adjusted so that a frequency equal to the sum of the signal and pump frequencies falls in a stop band, thus eliminating the existence of all higher-frequency mixing components. (As discussed in Part II, the existence of a pass band at the sum frequency can even be used to advantage if it can be made to have a certain dispersion characteristic.) The filter characteristic as shown on the Brillouin diagram is periodic in θ with a period of 2π. In the case of a microwave filter circuit, this periodicity represents the space-harmonic structure due to spatial periodicity of the fields. In parametric amplifiers, however, only the fundamental branch ($-\pi < \theta < \pi$) is of importance.

In the case of no resonator loss ($q = 0$), there is no attenuation in the pass band. For nonzero q, the midband attenuation is

$$\alpha = \frac{q}{2k} \tag{6}$$

nepers per resonator. Outside of the pass band, of course, only evanescent waves can exist.

For any specific coupled-cavity circuit, the lumped parameters of the equivalent circuit can be determined directly from measurements of midband frequency, bandwidth, capacitance, and loss. The capacitance is obtained from an impedance measurement and, for reasonably high resonator and diode Q, is equal to the sum of diode and cavity capacitance.

We begin the analysis by writing Kirchhoff's voltage law for the nth resonant circuit of Fig. 2:

$$L\frac{d^2q_n}{dt^2} + M\frac{d^2q_{n-1}}{dt^2} + M\frac{d^2q_{n+1}}{dt^2} + R\frac{dq_n}{dt} + S_n q_n = 0, \tag{7}$$

where q_n is the charge on the nth capacitor. The current in the nth resonator is $i_n = dq_n/dt$. It will be assumed that the excitation at the pump frequency causes the elastance S_n to vary as[8]

$$\begin{aligned} S_n &= S_0 + 2\tilde{S}\cos(\omega_p t - n\theta_p) \\ &= S_0 + \tilde{S}\left[e^{j(\omega_p t - n\theta_p)} + e^{-j(\omega_p t - n\theta_p)}\right]. \end{aligned} \tag{8}$$

[8] In general, the time variation of elastance must be expressed as a Fourier series of terms varying at harmonics of the pump frequency ω_p. Assuming S_n to be of the form (8) does not restrict the analysis to situations in which these terms are of negligible magnitude. It merely implies that frequency components generated as a result of mixing between the signal and the harmonic pump terms cannot propagate in the filter circuit and enter in any significant way in the interaction process.

It is seen that a time-varying elastance of this form generates new frequencies $\omega_1 \pm \omega_p$ from a signal at frequency ω_1. Only if these new frequencies can propagate through the chain of coupled resonators with the proper phase velocity can the contributions from adjacent cavities be cumulative. We specify that the frequency $\omega_1 + \omega_p$ fall in a stop band, and thus we can neglect this frequency as well as all higher idlers. We retain only the frequency $\omega_2 = \omega_1 - \omega_p$, which, if ω_p is in the vicinity of twice the signal frequency, can propagate in the negative frequency pass band.[9]

Let

$$q_n = A_n e^{j\omega_1 t} + B_n e^{j\omega_2 t}. \tag{9}$$

Upon substituting (9) and (8) into (7) and requiring that coefficients of $e^{j\omega_1 t}$ and $e^{j\omega_2 t}$ vanish separately, we obtain

$$\begin{aligned} -\lambda_1^2\left[A_n + kA_{n-1} + kA_{n+1}\right] \\ + j\lambda_1 q A_n + A_n + \epsilon B_n e^{-jn\theta_p} = 0 \end{aligned} \tag{10}$$

and

$$\begin{aligned} -\lambda_2^2\left[B_n + kB_{n-1} + kB_{n+1}\right] \\ + j\lambda_2 q B_n + B_n + \epsilon A_n e^{jn\theta_p} = 0, \end{aligned} \tag{11}$$

where λ_1 and λ_2 are the normalized signal and idler frequencies, respectively, and ϵ is a pump parameter,

$$\epsilon = \tilde{S}/S_0. \tag{12}$$

Since amplitudes of other frequency components (higher idlers) are assumed to be vanishingly small in this model, we do not write their governing equations.

When there is no pump ($\epsilon = 0$), (10) and (11) reduce to separate characteristic equations for propagation of the signal frequency λ_1 and the idler frequency λ_2. For a dependence of the form (4), this characteristic equation is

$$-\lambda^2(1 + 2k\cos\theta) + 1 = 0, \tag{13}$$

and its solution is the Brillouin diagram in Fig. 3.

The effect of the additional terms in (10) and (11) arising from the pump is to couple the signal and idler equations and, in effect, to couple the modes propagating at the signal and idler frequencies. It should be kept in mind that the idler frequency λ_2 would not actually exist in the absence of the pump, although a disturbance at this frequency could propagate through the resonators, if excited. Because of the time-varying capacitance, a disturbance at frequency λ_2 has associated with it a disturbance at λ_1 and vice versa.

Eqs. (10) and (11) comprise a set of linear difference equations with nonconstant coefficients (the last coefficient in each equation depends on n). By making

[9] It is convenient in this analysis to employ the notion of negative frequency and thus avoid the necessity of using cumbersome complex conjugate quantities. Physical quantities are given by the real parts of the expressions thus obtained.

the substitution $B_n = B'_n e^{jn\theta_p}$, however, a set of constant coefficient equations is obtained:

$$-\lambda_1^2[A_n + kA_{n-1} + kA_{n+1}] + jq\lambda_1 A_n + A_n + \epsilon B'_n = 0 \quad (14)$$

$$-\lambda_2^2[B'_n + ke^{-j\theta_p}B'_{n-1} + ke^{+j\theta_p}B'_{n+1}] + jq\lambda_2 B'_n + B'_n + A_n = 0. \quad (15)$$

We interpret B'_n as follows. A signal at ω_2 would be described by $q_n = e^{j\omega_2 t}B_n$. The time-varying capacitor (8) generates a voltage at frequency ω_1 given by

$$\tilde{S}e^{j\omega_1 t}B_n e^{-jn\theta_p} = \tilde{S}e^{j\omega_1 t}B'_n.$$

Thus the variation of the phase of this converted signal is contained in the factor B'_n. In the limit of a very weak pump, $B'_n \sim e^{-jn(\theta_2+\theta_p)}$, where θ_2 is the phase shift of the circuit at ω_2.

To solve (14) and (15), we assume the solution to be of the form $A_n = A_0\mu^n$, $B'_n = B'_0\mu^n$, where μ is a complex constant. In the earlier discussion of the characteristics of the cold circuit, we let $\mu = e^{-(\alpha+j\theta)}$, where α and θ are the attenuation and phase shift per section, respectively. For a solution, μ must satisfy the determinantal equation

$$\left[-\lambda_1^2\left(1 + \frac{k}{\mu} + k\mu\right) + jq\lambda_1 + 1\right] \cdot \left[-\lambda_2^2\left(1 + \frac{k}{\mu e^{j\theta_p}} + k\mu e^{j\theta_p}\right) + jq\lambda_2 + 1\right] - \epsilon^2 = 0. \quad (16)$$

For each value of λ_1, this equation is satisfied by *four* different values of μ. The solutions for $q=0$, $\epsilon=0$ are particularly simple and have been previously discussed. The first factor in (16) leads to the usual dispersion curve, which is repeated as the solid curve in Fig. 4. The second factor has the same form as the first if we write $\mu = \mu' e^{j\theta_p}$. Thus, a curve of λ_2 vs θ' is identical in form to the solid curves of Fig. 4.

It is useful to express the latter solution in terms of λ_1 and θ. Noting that $\lambda_1 = \lambda_2 + \lambda_p$ and $\theta = \theta' + \theta_p$, we can construct the second set of solutions from the first by simply displacing the solid curve of Fig. 4 upward by an amount λ_p and to the right by an amount θ_p. This results in the dashed curves shown.

We are now in a position to give a simple physical picture of the traveling-wave interaction mechanism and an interpretation of this analysis. We may regard the dashed curves in Fig. 4 as giving the phase shift per section of a disturbance at λ_1, which would result from the conversion of a signal at λ_2 by a very weak pump (ϵ small). If this phase shift coincides with the *normal* phase of the circuit at λ_1 (as given by the solid curve), then the converted signal can propagate along the circuit in phase with the signal at λ_1 and a cumulative effect from section to section will exist. We expect this effect to be strongest and the gain to be maximum

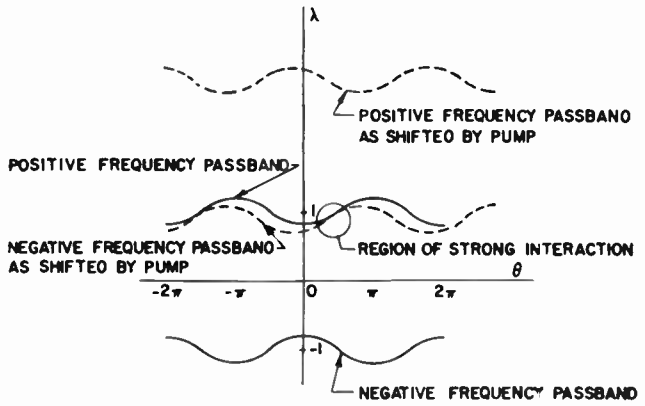

Fig. 4—Generation of the "idler curve," showing the phase shift per section of a wave at λ_1, which results from conversion of a wave at λ_2 (idler frequency) by mixing with a weak pump. The idler curve is generated by translating the negative frequency dispersion curve to the right by a distance θ_p and vertically upward by λ_p. A higher-order idler curve is also shown; it falls in a stop band of the filter circuit.

when the solid and dashed curves of Fig. 4 coincide. At this point

$$\theta(\lambda_2) + \theta_p = \theta(\lambda_1), \quad (17)$$

where $\lambda_2 = \lambda_1 - \lambda_p$. This is just the relation found by Tien[1] except for the change in the signs preceding λ_2 and $\theta(\lambda_2)$, which arises from our use of negative frequencies.

The range of frequency over which the solid and dashed lines of Fig. 4 nearly coincide determines the bandwidth over which traveling-wave parametric amplification can be obtained. The difference in phase shifts that can be tolerated and still have amplification increases as the pump parameter ϵ is increased. This will be illustrated in detail later.

The above description bears a close analogy to the theory of coupling of modes of propagation[10,11] and, as will be discussed in the next section, has proved to be very useful in understanding some of the detailed characteristics of iterated traveling-wave parametric amplifiers as they result from the present analysis.

A complete solution of the problem is given by a superposition of the four wave solutions; *i.e.*,

$$q_n = \sum_{r=1}^{4} A_{or}\mu_r^n e^{j\omega_1 t} + \sum_{r=1}^{4} B'_{or} e^{jn\theta_p}\mu_r^n e^{j\omega_2 t} \quad (18)$$

gives the charge on the nth capacitor. The four complex roots of the determinantal equation are $\mu_1 \cdots \mu_4$, and $A_{01} \cdots A_{04}$ are arbitrary constants, which are determined by the boundary conditions of the model; B'_{0r} is related to A_{or} by means of (14). The current in the nth

[10] J. R. Pierce, "Coupling of modes of propagation," *J. Appl. Phys.*, vol. 25, p. 179; February, 1954.
[11] J. R. Pierce and P. K. Tien, "Coupling of modes in helices," PROC. IRE, vol. 42, p. 1389; September, 1954.

resonator circuit is therefore given by

$$i_n = \sum_{r=1}^{4} I_{or}\mu_r{}^n \left\{ e^{j\omega_1 t} - e^{j\omega_2 t}\frac{\lambda_2}{\epsilon\lambda_1} e^{jn\theta_p} \cdot \left[1 + jq\lambda_1 - \lambda_1{}^2\left(1 + \frac{k}{\mu_r} + k\mu_r\right)\right]\right\}, \quad (19)$$

where we have written $I_{or} = j\omega_1 A_{or}$. The arbitrary constants $I_{01} \cdots I_{04}$ are determined from the boundary conditions, which are written as separate equations for the input and output circuits:

$$M\frac{di_1}{dt} + i_o Z_o = V_o e^{j\omega_1 t}, \quad (20)$$

$$M\frac{di_N}{dt} + i_{N+1}Z_{N+1} = 0. \quad (21)$$

Substituting (19) into (20) and (21) and equating ω_1 terms and ω_2 terms separately, we obtain four equations in the four unknowns:

$$\sum_{r=1}^{4} I_{or}\left[j\lambda_1 k\mu_r + Z_o^o(\lambda_1)\right] = V_o^o, \quad (22)$$

$$\sum_{r=1}^{4} I_{or}\mu_r^N\left[j\lambda_1 k + \mu_r Z_{N+1}^o(\lambda_1)\right] = 0, \quad (23)$$

$$\sum_{r=1}^{4} I_{or}\left[1 + jq\lambda_1 - \lambda_1{}^2\left(1 + k\mu_r + \frac{k}{\mu_r}\right)\right] \cdot \left[j\lambda_2 k\mu_r e^{j\theta_p} + Z_o^o(\lambda_2)\right] = 0, \quad (24)$$

$$\sum_{r=1}^{4} I_{or}\mu_r^N\left[1 + jq\lambda_1 - \lambda_1{}^2\left(1 + k\mu_r + \frac{k}{\mu_r}\right)\right] \cdot \left[j\lambda_2 k + Z_{N+1}^o(\lambda_2)\mu_r e^{j\theta_p}\right] = 0, \quad (25)$$

where we have written the result directly in terms of normalized variables using the additional definitions

$$Z_o^o(\lambda) = \sqrt{\frac{C_o}{L}}\,Z_o(\omega), \quad Z_{N+1}^o(\lambda) = \sqrt{\frac{C_o}{L}}\,Z_{N+1}(\omega),$$

$$V_o^o = \sqrt{\frac{C_o}{L}}\,V_o. \quad (26)$$

Results, which are discussed in the next section, are obtained as follows. The constants k, q, and N are determined from the fractional bandwidth, midband attenuation, and number of elements of the particular filter circuit being considered; similarly, the frequency-dependent terminating impedances $Z_o^o(\lambda)$ and $Z_{N+1}^o(\lambda)$ are determined from the input and output matching configurations. The pump strength parameter ϵ defined by (12) is related to the total swing in capacitance approximately by

$$\epsilon = \frac{1}{4}\frac{\Delta S}{S_o} \cong \frac{1}{4}\frac{\Delta C}{C_o}, \quad (27)$$

where ΔC is a function of pump voltage, bias, and the particular capacitance-voltage characteristic of the diodes considered. λ_p and θ_p, the pump frequency and phase shift between sections, respectively, exert a major influence on the amplifier characteristics; the choice of these parameters will be discussed presently. With the above parameters established, the determinantal equation (16) is solved for the four values of μ and as a function of the signal frequency λ_1. Eqs. (22) through (25) are then solved for the wave amplitudes I_o, with $V_o^o = 1$ and the current in the input and output circuits computed from (19).

Computations were made on an IBM 704 digital computer. As a check on the accuracy of the results, it was verified that the terminal characteristics in each case (for zero circuit loss) are in agreement with the Manley-Rowe relations.[12] That is, it was determined that $P_1/\lambda_1 = P_2/\lambda_2$, where P_1 is the sum of the powers appearing in the input and output circuits at frequency λ_1, and P_2 is the total power at λ_2.

Results of Analysis

Since the gain, bandwidth, and stability depend sensitively upon λ_p and θ_p, let us first develop a qualitative picture of how these parameters affect amplifier performance. This has proved to be of considerable value in arriving at optimum adjustments of experimental models in the laboratory. In the foregoing section, we discussed the generation of a propagating wave at the idler frequency and how this idler response can be represented on a Brillouin diagram (Fig. 4). The advantage of constructing an "idler curve" in this manner is that it relates the cumulative traveling-wave parametric-amplification mechanism to familiar concepts of coupled modes. When the "signal" and "idler" curves of Fig. 4 are close together, the phase conditions are favorable for cumulative interaction; the modes, which carry power in the same direction, can couple to establish a pair of exponentially growing and decaying waves. Indeed, the condition for maximum coupling from this point of view has been shown to coincide with the optimum relation between phase velocities found by Tien. Extending this picture slightly, we can develop a feeling for how λ_p and θ_p affect gain-bandwidth, band-edge response, and stability and thus arrive at criteria for choosing and adjusting these parameters.

[12] J. M. Manley and H. E. Rowe, "Some general properties of nonlinear elements—Part I. General energy relations," Proc. IRE, vol. 44, pp. 904–913; 1956.

Consider several specific situations. First, let us assume that $\lambda_p=2$ (pump frequency equal to twice the midband frequency of the filter circuit) and $\theta_p=\pi$. In this case, the idler curve coincides with the signal curve, as indicated in Fig. 5(a). The condition for maximum gain (17) is satisfied here for every frequency within the pass band of the filter circuit. Notice, however, that this optimum condition is also fulfilled for waves traveling in the *reverse direction*, as indicated by the left-hand or negative phase-shift branch of the diagram where the group velocity ($v_g \sim d\lambda/d\theta$) is negative. Thus, the amplifier is bilateral and in the absence of perfect terminations would be unstable.

Now let λ_p become somewhat less than 2, but maintain $\theta_p=\pi$. As shown in Fig. 5(b), this results in a downward displacement of the idler curve. The gain, although reduced, is still bilateral; *i.e.*, for propagation in either the forward or backward direction, the horizontal spacing of the curves is identical. Notice also that the maximum bandwidth over which amplification can now take place (*i.e.*, the bandwidth in which waves can propagate at both the signal frequency λ_1 and idler frequency $|\lambda_2| = |\lambda_1 - \lambda_p|$) is measured by the vertical overlap of the signal and idler curves and is reduced below the bandwidth of the cold ($\epsilon=0$) filter circuit.

Finally, let $\lambda_p<2$, $\theta_p<\pi$, as shown in Fig. 5(c). Since the idler curve is thus displaced horizontally, the gain will be different in the forward and backward directions. For the case shown, almost unilateral gain in the forward direction is possible, hence stability. Exactly how close the curves can be brought together in Fig. 5(c) depends on still another factor, *viz.*, band-edge response. As will be shown later, the interaction impedance at the band edge is higher than that in the center of the band and severe reflections at the terminations occur here. Thus, in this qualitative picture, unless a certain departure from synchronism (*i.e.*, intercurve spacing) is maintained at the band edge, the amplifier may oscillate at that point. This minimum spacing (which is a function of pump strength) determines how much gain can be achieved at the band center.

We have thus illustrated the important factors which determine the choice of λ_p and θ_p and establish limits on the performance of this type of amplifier. We would like to achieve the objectives of high unilateral gain with maximum utilization of the filter's cold bandwidth. Unilaterality can be achieved by making $\theta_p<\pi$, $\lambda_p<2$, thus reducing the maximum possible bandwidth of amplification. Gain is limited by band-edge stability considerations. To optimize performance in the presence of these conflicting requirements, λ_p and θ_p must be carefully balanced. (Note that the condition $\theta_p<\pi$, $\lambda_p<2$ leads to utilization of the lower part of the filter pass band. It can be similarly shown that the condition $\theta_p>\pi$, $\lambda_p>2$ leads to utilization of the upper part of the pass band consistent with unilateral amplification; however, only the former mode of operation is discussed in this paper for convenience in the presentation of results.) The above discussion assumes a symmetrical dispersion curve; as will be shown in Part II, asymmetry in the dispersion curve can remove the condition on λ_p.

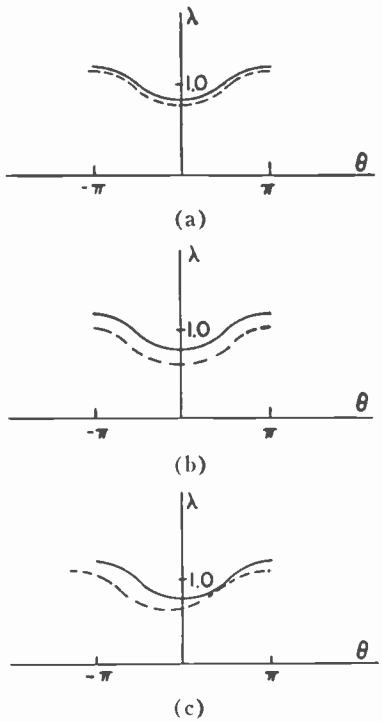

Fig. 5—With the use of coupled-mode ideas, these curves illustrate how pump frequency λ_p and pump phase θ_p affect amplifier performance. The gain (*i.e.*, coupling) decreases as the signal and idler curves are moved apart. (a) $\lambda_p=2$, $\theta_p=\pi$; (b) $\lambda_p<2$, $\theta_p=\pi$; (c) $\lambda_p<2$, $\theta_p<\pi$.

Fig. 6 illustrates the typical nature of the solutions of the characteristic equation (16). The uncoupled signal and idler curves are shown in Fig. 6(a) with the phase characteristics of the coupled system [*i.e.*, roots of (16)] plotted in Fig. 6(b). There are four waves at each frequency. A solid line indicates a wave of constant amplitude for which $\alpha=0$ where $|\mu| = e^{\alpha}$. It is thus seen that the waves in the reverse direction are virtually unaffected by the pump signal. On the other hand, the signal and idler waves in the forward direction are coupled strongly to form a pair of waves (at each frequency) that are growing and decaying; this is indicated by the dashed line for which the solutions have equal and opposite values of α. In traveling-wave parametric amplifiers, it is the exponentially growing wave in which we are interested.

The study of the normal modes of the system can provide valuable insight into the behavior of the traveling-wave amplifiers. However, it is also necessary to calculate the extent to which each of the normal modes is excited in order to compute the over-all amplifier gain. This is given by solution of (22) through (25) for the mode amplitudes, from which the current in the output circuit at the signal frequency can be obtained. The power gain is defined as

$$G = \frac{\text{power in load}}{\text{power available at input}} = \frac{|I_{N-1}|^2 R_{N+1}}{V_o^2/4R_o}, \quad (28)$$

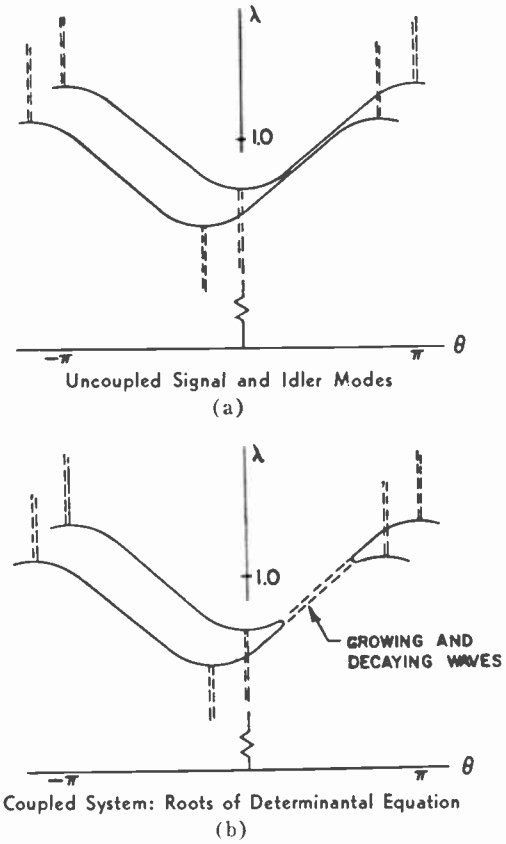

Fig. 6—Nature of the solutions of the determinantal equation. The signal and idler modes in the upper diagram are coupled by the pump as shown in the lower diagram. Solid lines indicate waves of constant amplitude; dashed lines indicate a conjugate pair of growing and decaying waves.

or, in terms of our normalized parameters,

$$G = 4\left| I_{N+1}\right|^2 R_o^o R_{N+1}^o, \tag{29}$$

with the input voltage V_o^o normalized to unity. In this formulation, the gain includes the effect of reflections from both input and output terminations.

In Figs. 7–9 (next page), we have presented calculated curves of gain vs frequency. These curves are not intended to represent optimized performance; rather, they have been chosen to illustrate typical effects of varying the principal parameters pump frequency λ_p, pump phase shift between sections θ_p, and pump strength ϵ. For convenience, the fractional bandwidth of the cold filter circuit has been chosen to be 10 per cent ($k = 0.05$). As shown in Appendix I, these results can be scaled to other bandwidths by simple scaling rules. The loss factor q is 0.002, corresponding to a cold insertion loss that is approximately 0.2 db at midband and rising to about 4 db per section in the neighborhood of the band edges. This corresponds roughly to the values measured in experimental models. The calculations are for a six-section amplifier; extensions to other numbers of active elements will be considered later.

Fig. 7 illustrates the effects of varying pump frequency λ_p while maintaining pump phase θ_p and amplitude ϵ constant at the values 2.85 radians and 0.033, respectively. The curves are seen to be approximately symmetrical about the degenerate frequency $\lambda_p/2$. As λ_p is reduced, several things occur: midband gain decreases, bandwidth decreases, and ripples in gain are smaller, particularly at the band edges.

This behavior follows immediately from our previous discussion. The present situation qualitatively resembles that shown in Fig. 5(c) or Fig. 6(a). As λ_p decreases, the idler curve is displaced vertically downward from the signal curve. The maximum bandwidth over which both signal and idler frequencies can propagate is thus reduced. In this case, a maximum utilization of about 80 per cent of the total bandwidth of the filter circuit is shown for $\lambda_p = 1.97$. Also, with decreasing λ_p, the separation between signal and idler curves increases; *i.e.*, the signal and idler wave velocities depart more and more from synchronism, resulting in smaller midband gain. Similarly, the gain ripples are reduced in magnitude, because of a reduced gain in the backward direction, which makes the amplifier less sensitive to reflections at the output termination, and because, at the lower cutoff frequency, the departure from the synchronous condition begins to exceed the value above which signal and idler waves are essentially uncoupled.

At reasonably high gains, the Manley-Rowe relations[12] show that in the absence of loss, the amount of output power at the signal and idler frequencies is about equal. Therefore, the signal and idler waves essentially interchange roles as the signal passes through the degenerate point and the response is more or less symmetrical about the half-pump frequency. Over-all bandwidth cannot exceed twice the difference between $\lambda_p/2$ and the nearer filter cutoff frequency.

Fig. 8 shows the effect of varying the pump phase shift. In terms of the Brillouin diagram, increasing θ_p corresponds to displacing the idler curve horizontally to the right. In this case, the bandwidth remains approximately constant (*i.e.*, the normalized degenerate frequency is fixed at 0.98). For smaller values of θ_p, in which midband synchronism is most nearly approached, the general gain level is the highest, although with large variations across the band in this particular case because of poor amplifier terminations.

Finally, in Fig. 9 it is seen that increased pump power results in larger gain, as expected, and also in a slightly enhanced bandwidth. The latter is due to the fact that the reduction in signal-idler coupling in the vicinity of the band edge, which results from departure from synchronism, is compensated by increased capacitance variation (*i.e.*, pump power).

Although the terminations can be greatly improved so as to smooth out the gain peaks (see below), the band edge poses a special problem. This can be seen by introducing the concept of an "interaction impedance," which measures the quality of a particular coupled-cavity circuit design. Letting P represent the average power flow associated with a peak voltage V_n across the localized capacitance of the nth cavity (loaded by a

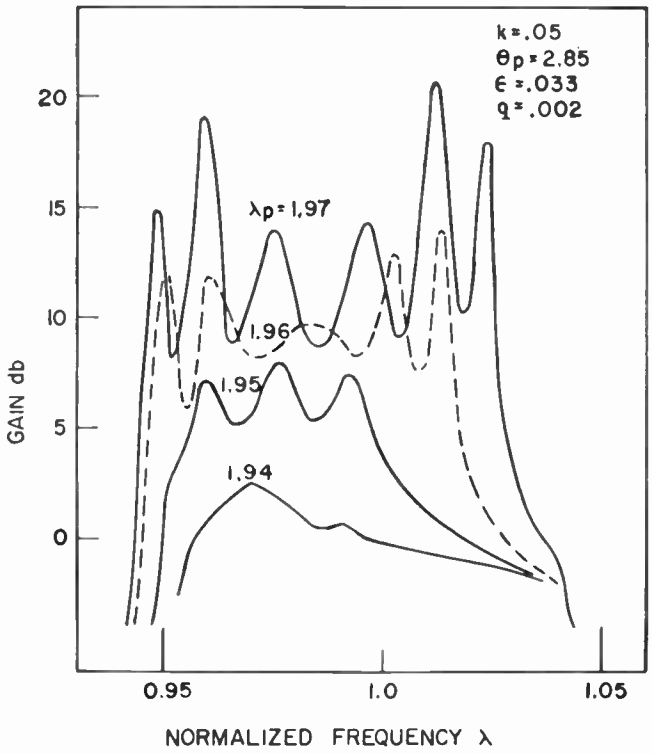

Fig. 7—Gain vs frequency for a six-section amplifier, showing the effect of varying pump frequency λ_p. A filter bandwidth of 10 per cent was chosen for convenience.

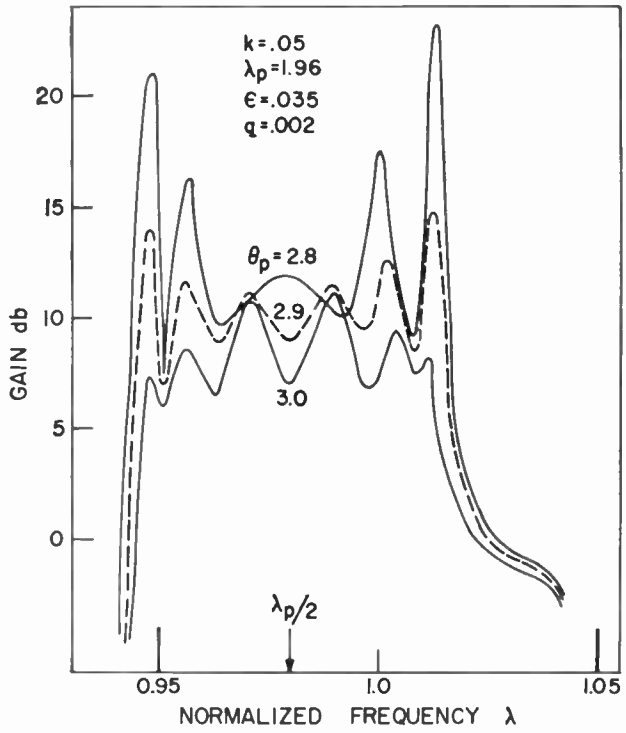

Fig. 8—Gain vs frequency for a six-section amplifier, showing the effect of varying pump phase θ_p.

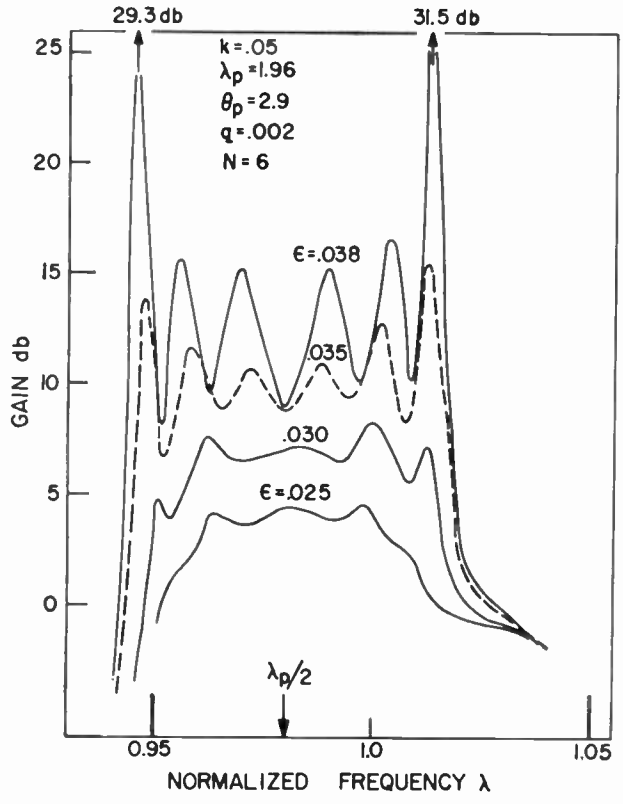

Fig. 9—Effect of increasing pump amplitude ϵ.

variable capacitance diode), we define the interaction impedance to be

$$K = \frac{|V_n|^2}{2P}. \tag{30}$$

It is shown in Appendix II that this interaction impedance is a fundamental parameter in all capacitively pumped, traveling-wave parametric amplifiers and should be maximized for strong coupling between the signal and pump frequencies at the diode junction. This also is in agreement with the intuitive idea that for a given power flow the signal voltage should be maximized across the variable capacitance. A similar parameter is important in the design of traveling-wave tubes. For the cold circuit ($\epsilon = 0$),

$$P = \tfrac{1}{2} \operatorname{Re} [j\omega M i_{n-1} i_n^*], \tag{31}$$

which can be expressed in terms of voltage as

$$P = \tfrac{1}{2}\omega^3 M C^2 |V_n|^2 \sin\theta \tag{32}$$

using $V_{n-1} = V_n e^{j\theta}$. Therefore, neglecting loss,

$$K = \frac{\sqrt{L/C_0}}{\lambda^3 k \sin\theta}. \tag{33}$$

Additional physical interpretation of interaction impedance can be obtained by expressing power flow in the form

$$P = W v_g, \tag{34}$$

where W is the total time average stored energy per cavity (half in the electric field, half in the magnetic) for a peak voltage V_n,

$$W = \tfrac{1}{2}C_0 |V_n|^2, \tag{35}$$

and v_g is the group velocity,

$$v_g = \frac{\partial\omega}{\partial\theta} = \frac{1}{\sqrt{LC_0}}\lambda^3 k \sin\theta \quad \text{cavities/second.} \tag{36}$$

Eq. (13) was employed in arriving at (36). Substituting (35) and (36) into the definition of interaction impedance, we again arrive at (33). High impedance results from minimizing electric-energy storage (*i.e.*, decreasing total capacitance C_0 or physically concentrating all of the electric field at the position of the variable capacitance) and by decreasing the group velocity. The former is a function of the basic cavity design, and the latter is controlled by adjusting the coupling between cavities.

In the vicinity of the lower and upper band-edge frequencies, θ approaches 0 and π, respectively, leading to extremely high values of interaction impedance. This results physically from extremely low group velocity. We then have a situation in which the cavities behave somewhat like individual single-cavity amplifiers with coupling predominantly by means of the idler wave. Thus, for example, the gain at midband, which can be attained by increasing the pump amplitude to higher and higher values, is ultimately limited by incipient band-edge instability.

Eq. (33) also indicates that at midband ($\lambda \cong 1$, $\sin\theta \cong 1$), the product of interaction impedance and bandwidth (k) is approximately constant. This is related to the bandwidth scaling considerations of Appendix I and is a fundamental result. Since interaction impedance is a measure of gain per section, a basic inverse relationship exists between bandwidth and gain per diode. An analogous impedance-bandwidth relationship obtains in the case of traveling-wave tubes.[13]

The philosophy that was used in determining the input and output impedance matches was to use a simple, physically realizable impedance function with only three adjustable constants. In particular, normalized generator and load impedance functions of the following form were employed:

$$Z_0^o = R_0^o + jX_0^o = C_1 + j\left(C_2\lambda + \frac{C_3}{\lambda}\right), \tag{37}$$

$$Z_{N+1}^o = R_{N+1}^o + jX_{N+1}^o = C_4 + j\left(C_5\lambda + \frac{C_6}{\lambda}\right), \tag{38}$$

corresponding to a series resistor, inductor, and capacitor.

[13] J. R. Pierce, "Traveling-Wave Tubes," D. Van Nostrand Co., Inc., New York, N. Y., Chap. V; 1950.

In all of the curves presented thus far, both Z_0^o and Z_{N+1}^o were chosen so as to constitute a match to the cold filter circuit at *midband only; i.e.*, the normalized input impedance of the coupled cavity circuit is

$$Z_{in}^o = \lambda k \sin\theta + j\lambda k \cos\theta, \tag{39}$$

where θ is the phase shift per section and circuit loss has been neglected. The resistive and reactive parts of (39) are shown by the solid lines in Fig. 10(a). In the calculations corresponding to Figs. 7 through 9, the constants $C_1 \cdots C_6$ were chosen so that the real part of the generator and load impedances exactly matched the resistive part of the cold-circuit impedance only at the center of the pass band ($\lambda = 1, \theta = \pi/2$). The reactive part was chosen to be zero at midband and to have an approximate conjugate slope to that of the reactance function in (39); *i.e.*, for Figs. 7 through 9, $C_1 \cdots C_6$ were adjusted so that

$$\begin{aligned} R_0^o &= R_{N+1}^o = k, \\ X_0^o &= X_{N+1}^o \cong -\lambda k \cos\theta. \end{aligned} \tag{40}$$

These relations are indicated by the dashed curves in Fig. 10(a). The approximate reactive compensation can be effected physically by simply placing a series resonant circuit in series with the transmission line.

The large fluctuations in the gain curves indicate that the above choice of generator and load impedances gives rise to large reflections. Indeed, it is intuitively evident that, at the output, we want to establish a match to the exponentially growing wave. The appropriate output

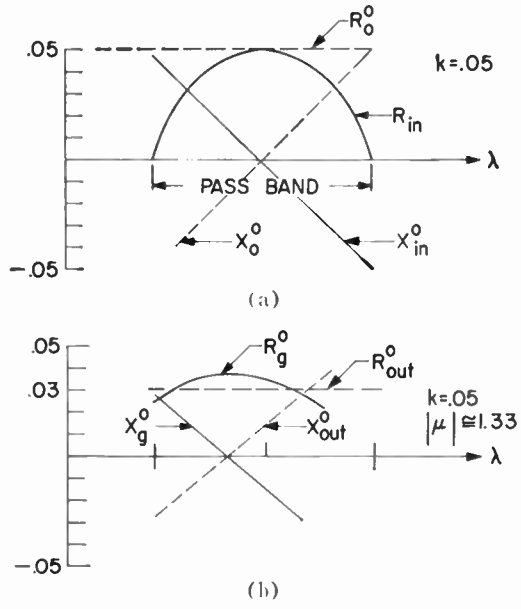

Fig. 10—The solid curves show the resistance and reactance of: (a) cold circuit input impedance $Z_{in}^o = \lambda k \sin\theta + j\lambda k \cos\theta$; (b) growing wave impedance $Z_g^o = j\lambda k/\mu_0$. In Figs. 7 through 9, the generator and load impedances were both chosen as indicated by the dashed curves in (a) above; in Fig. 11, the output was matched to the growing wave at two frequencies as indicated by the dashed curves in (b).

impedance is then

$$Z^{o}_{\text{out}} = \frac{j\lambda k}{\mu_{\theta}}, \tag{41}$$

where μ_{θ} is the particular root of the characteristic equation (16) associated with the growing wave. The impedance level at the output is thus reduced below the input level by essentially the voltage gain per cavity. A plot of (41) for a typical case is shown in Fig. 10(b).

The effect of matching to the growing wave at the output is shown in Fig. 11. With the generator and load impedances matched to the cold circuit [*i.e.*, as in (40)], the curve with large midband gain fluctuations and extremely high peaks at the band edge is obtained; this is the same as one of the curves in Fig. 9. With the output approximately matched to the growing wave [as indicated by the dashed curves in Fig. 10(b)] a greatly smoothed-out response curve results.

Thus, in the absence of stabilizing nonreciprocal attenuation the amplifier response is relatively sensitive to terminating impedances. It is, of course, possible to improve further the results of Fig. 11. Here, the resistive part of the output growing-wave impedance is matched exactly at only two frequencies, as indicated by the magnitude of R^{o}_{N+1} in Fig. 10(b). The use of more complicated impedance functions could make the curve of gain vs frequency almost flat. This has been demonstrated experimentally.

Included in Fig. 11 is a curve of reverse gain. Here, the input and output terminals of the amplifier were simply interchanged with the same matching conditions as those described above. It is seen that the reverse gain can be maintained at a value in the neighborhood of unity with 12- to 15-db gain in the forward direction; essentially unilateral amplification can therefore be achieved.

Midband gain is plotted in Fig. 12 as a function of the number of iterative cavity sections for a particular choice of parameters. The dashed curve represents the level of the exponentially increasing wave alone; this wave predominates after several cavity sections. Notice that an initial excitation loss of about 1 db can be associated with the growing wave for the case shown. In the case of perfect synchronism between the signal and idler waves [*i.e.*, if the phase relation in (17) is satisfied], the growing and decaying waves are excited in phase, each having associated with it $\frac{1}{2}$ the applied voltage. This would lead to an initial growing-wave loss of 6 db. With increased departure from synchronism, however, the initial amplitudes of the growing and decaying waves increase (they are no longer excited in phase),

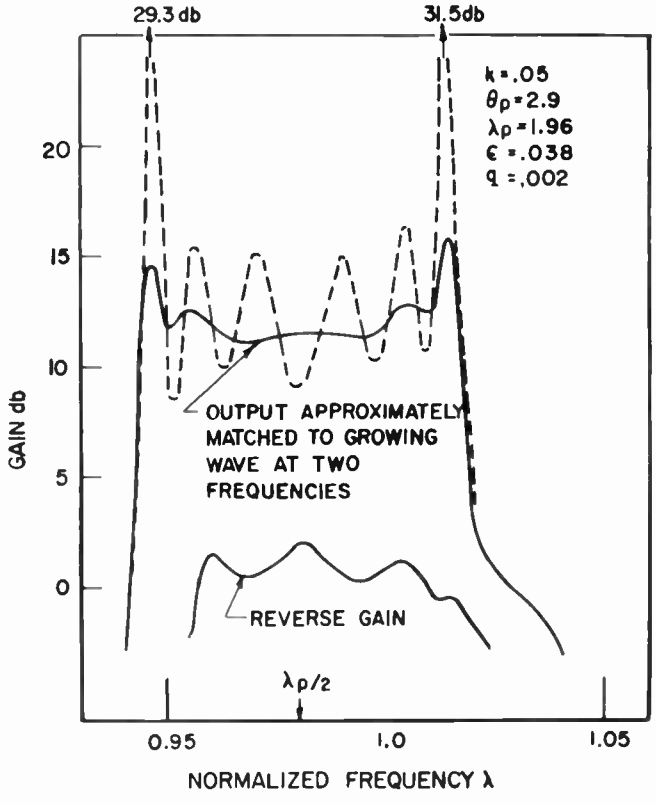

Fig. 11—Effect of matching to the growing wave. The solid gain curve was calculated for an output terminal impedance as shown in Fig. 10(b), which resulted in a smoothed-out frequency response and great reduction in band-edge gain spikes. The extremely low reverse gain shows that unilateral amplification is possible.

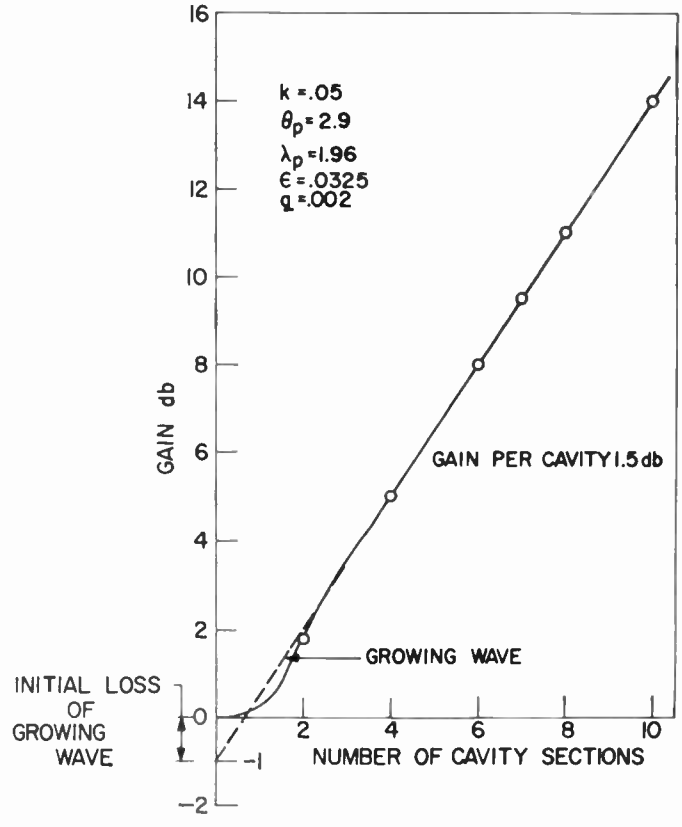

Fig. 12—Gain vs the number of iterated cavity sections as calculated for a particular case. The initial excitation loss of the exponentially growing wave is shown.

and the initial loss factor of the growing wave decreases, approaching 0 db.

The above behavior is, again, entirely analogous to that of traveling-wave tubes and is, in fact, basic to all active coupled-mode systems. In the traveling-wave-tube case, there are three characteristic waves (growing, decaying, and unattenuated). With exact synchronism between the electron beam waves and the unperturbed circuit wave, each of the characteristic waves is excited in phase with $\frac{1}{3}$ of the applied voltage, leading to an initial growing-wave loss of 9.54 db. This initial loss decreases with departure from synchronism of the unperturbed coupled modes.[14]

Parameter studies of the type described in this section show that the effect of increased circuit loss is twofold; the midband gain is decreased and the response curve is smoothed out, particularly at the band edges. The lowered gain can be made up simply by increasing the pump voltage. It should be noted that the maximum value of $\Delta C/C_o$ employed in the calculated results presented in this paper is less than 0.16, corresponding to a value of ϵ of 0.04 [see (27)]. Considerably larger capacitance swings are possible and have been achieved experimentally. The improved band-edge response results both from reducing the regenerative effects of reflections where the impedance mismatch is worst and from lowering the Q of the individual cavities in the narrow, band-edge mode of operation. Thus, the response curve of Fig. 11 can be smoothed out still further by the combination of better matching and slight additional circuit loss, although the latter would deteriorate the amplifier noise figure somewhat.

Conclusion

A class of traveling-wave parametric amplifiers based on coupled-cavity filter circuits has been described. This type of amplifier is particularly suited to microwave frequencies and incorporates new features that overcome some severe difficulties associated with other circuit structures. An analysis has been presented which not only provides detailed information on the operating characteristics of such amplifiers, including the effects of terminal impedances, reflected waves, circuit loss, etc., but also leads to a simple physical picture of the cumulative interaction mechanism based on the coupled-mode concept. This physical picture, presented in terms of a Brillouin diagram, has been emphasized throughout. Fundamental gain and bandwidth considerations have been discussed in terms of an interaction impedance parameter, which is basic to all amplifiers of the traveling-wave type.

Representative calculated curves of gain vs frequency have illustrated the general effects of the various parameters; these effects have been related to the qualitative description of the amplifier. The calculations have, of course, explored only a restricted range of parameters, but they indicate typical results and, more important, serve as a guide to experimental optimization of pump frequency and phase, terminal impedances, pump strength, etc.

From this investigation, we conclude that unilateral amplification can be obtained over an appreciable portion of the pass band of the coupled-cavity circuit. Stable gains of 12 to 15 db are possible with reasonably flat frequency response. With special stabilization, operation much closer to the ideal synchronous condition would be possible with resulting higher gain per stage. Such stabilization can be obtained, for example, by incorporating nonreciprocal ferrite elements in the coupled-cavity circuit itself or by cascading two or more amplifier sections separated by ferrite isolators and correctly phased with respect to pump voltage. Techniques such as staggered pass band edges and nonuniform phase shift between cavities, which have proved very important in solving various stability problems in traveling-wave tubes, can also be used to advantage; however, these possibilities are not provided in the present analytical approach.

It is not yet known how far bandwidth can be pushed with coupled-cavity amplifiers. Certainly fractional bandwidths of 20 to 30 per cent appear to be possible. As bandwidth increases (*i.e.*, for larger values of the coupling coefficient k), the Brillouin diagram becomes distorted appreciably from its approximately symmetrical shape at the low values of k, and the bandwidth scaling rules presented in Appendix I must be modified. This is an important area for further investigation, and can be most easily accomplished experimentally with the analysis serving as a general guide, as discussed in Part II.

Another area for further study consists of allowing the idler frequency to be several times larger than the signal frequency and to propagate in a separate coupled-cavity circuit (or perhaps in a higher pass band). This is important in reducing the noise contribution of the idler channel. With appropriate interpretation, the present theoretical approach can be made to include this situation.

Although noise considerations have not been included explicitly in this treatment, it is shown in Appendix II that over any small frequency region this analysis can be related in simple terms to analyses based on an idealized uniformly distributed model. Therefore, at least to first order, noise performance can be estimated by Tien's results as modified by Shafer[15] for the case of finite circuit loss.

[14] C. K. Birdsall and G. R. Brewer, "Traveling-wave tube characteristics for finite values of C," IRE Trans. on Electron Devices, vol. ED-1, pp. 1–11; August, 1954.

[15] C. G. Shafer, "Noise figure for a traveling wave parametric amplifier of the coupled-mode type," Proc. IRE, vol. 47, p. 217; December, 1959.

Appendix I

Bandwidth Scaling

Throughout the text we have, for convenience, taken $k=0.05$, leading to a 10 per cent cold bandwidth of the filter circuit. We show here that these results can be generalized to other values of k and hence to other bandwidths. The scaling considerations presented here assume k to be small compared with unity. For larger bandwidths, these scaling rules provide at least an approximate guide to the choice of parameters and to the expected performance.

To obtain the basic result, we introduce variables δ and δ_p, respectively:

$$\lambda_1 = 1 + k\delta, \qquad \lambda_p = 2 + k\delta_p; \tag{42}$$

δ varies from -1 to $+1$ as λ varies from the low-frequency cutoff

$$\lambda = \frac{1}{\sqrt{1+2|k|}} \cong 1 - |k|$$

to the high frequency cutoff

$$\lambda = \frac{1}{\sqrt{1+2|k|}} \cong 1 + |k|.$$

Substituting the above definitions into the determinantal equation (16), we may write

$$\left[2\delta + \mu + \frac{1}{\mu} - \frac{jq}{k}\right]\left[2(\delta - \delta_p) - \mu e^{j\theta_p} + \frac{1}{\mu e^{j\theta_p}} - \frac{jq}{k}\right] + \left(\frac{\epsilon}{k}\right)^2 = 0. \tag{43}$$

We see that the values of μ, and hence the gain per resonator, depend only upon the variables, δ, δ_p, θ_p, q/k, and ϵ/k. Thus, two amplifiers with different bandwidths (different k values) will have exactly the same gain vs reduced frequency $\delta=(\lambda_1-1)/k$ if they have the same values of δ_p, θ_p, q/k, and ϵ/k. In particular, the circuit with the larger bandwidth will require a larger value of the pump parameter ϵ, larger in the ratio of the bandwidths, for the same gain.

This result has been verified by computing gain vs frequency for circuits with different values of k but with identical δ_p, θ_p, q/k, and ϵ/k. The result is accurate in detail for small values of k; when k becomes as large as 0.1, some minor quantitative difference arises.

Appendix II

Relation to Tien's Result

We show here that when the gain per section is small and there is no circuit loss, (16) can be cast in the same form as Tien's result for a uniformly distributed transmission line. First we note that in the absence of the pump ($\epsilon=0$), each of the brackets of the determinantal equation (16) must vanish separately:

$$\lambda_1^2[1 + 2k\cos\theta_1] = 1,$$
$$\lambda_2^2[1 + 2k\cos(\theta_2 - \theta_p)] = 1. \tag{44}$$

Here we have taken $\mu=e^{-j\theta}$ and used the subscripts 1 and 2 for quantities pertaining to the signal and idler frequencies, respectively.

For optimum gain in the presence of the pump, we have shown that θ_1 and θ_2 should be approximately equal. We therefore write $\theta_2=\theta_1+\Delta\theta$, where $\Delta\theta$ is assumed to be small. Substituting $e^{-j\theta}$ for μ with $\theta=\theta_1+\Delta\theta/2+j\Gamma=\theta_2-\Delta\theta/2+j\Gamma$ (Γ small) into (16) and using the definitions of θ_1 and θ_2 in (44) above, we obtain an approximate equation for Γ the growth constant:

$$\Gamma^2 = \left(\frac{\xi}{2}\right)^2 - \left(\frac{\Delta\theta}{2}\right)^2, \tag{45}$$

where

$$\xi^2 = \frac{\epsilon^2}{k^2\lambda_1^2\lambda_2^2\sin\theta_1\sin(\theta_p - \theta_2)}. \tag{46}$$

This has the same form as Tien's equation (41), except that our quantities Γ, ξ, and $\Delta\theta$ are expressed on a per cavity basis and Tien's are referred to a unit length. From (45) and (46), the gain at midband for $\Delta\theta=0$ is essentially (ϵ/k) nepers per cavity, which again emphasizes the reciprocal relationship between gain and bandwidth (k).

To bring out further the analogy with Tien's result, we can rewrite our result in terms of the interaction impedance defined earlier [see (30)]. The interaction impedances at signal and idler frequencies are

$$K_1 = \frac{\sqrt{L/C_0}}{\lambda_1^3 k\sin\theta}, \qquad K_2 = \frac{\sqrt{L/C_0}}{\lambda_2^3 k\sin(\theta_p - \theta_2)}, \tag{47}$$

and are equal to the square of the voltage appearing across the pump element per unit power flow at signal and idler frequencies, respectively. Therefore, ξ^2 may be written

$$\xi^2 = K_1K_2\omega_1\tilde{C}\omega_2\tilde{C}, \tag{48}$$

where $\tilde{C}/C_0=\tilde{S}/S_0\ll 1$ is the fractional change in capacitance. We see that our result is the product of the interaction impedances K_1 and K_2 and the *variable* parts of the susceptances $\omega_1\tilde{C}$ and $\omega_2\tilde{C}$. The gain is clearly increased by increasing any of these quantities.

Tien's expression for ξ^2, applicable in the case of inductive pumping, can be expressed

$$\xi^2 = Y_{01}Y_{02}\omega_1L\omega_2L, \tag{49}$$

where Y_{01} and Y_{02} are the "interaction admittances" at the signal and idler frequencies, respectively, numerically equal to the square of the current flowing through the pump element per unit power flow ($Y_{01}=I_1^2/2P_1$), and ω_1L and ω_2L are the variable parts of the reactances added by the pump. In Tien's case, maximum gain is achieved by maximizing any of these quantities; in par-

ticular, the current flow through the pumped element should be a maximum. Note that for the uniform model considered by Tien, the interaction admittance and the circuit characteristic admittance are equal. The former, however, is a more fundamental parameter in traveling-wave parametric amplifiers. Tien's inductive pumping is the dual of our capacitive pumping, and this fact reflects itself in the dual nature of the expressions for ξ^2.

ACKNOWLEDGMENT

The authors gratefully acknowledge many fruitful discussions with R. D. Weglein and K. P. Grabowski of the Electron Dynamics Department, who contributed greatly to this investigation and carried out the associated experimental program. Thanks are also due B. Fik, who carried out the programming and numerical calculations on an IBM 704 digital computer.

Coupled-Cavity Traveling-Wave Parametric Amplifiers: Part II—Experiments*

K. P. GRABOWSKI†, MEMBER, IRE, AND R. D. WEGLEIN†, SENIOR MEMBER, IRE

Summary—**The filter-circuit approach to broadband traveling-wave parametric amplification at microwave frequencies is described from an experimental point of view. The experiment revolves around a series of inductively coupled microwave cavities, each loaded with one variable-capacitance semiconductor diode. Gain-bandwidth products of 2000 Mc with a 350-Mc bandwidth at *S* band have been obtained by using commercially available diodes. Noise temperatures of 130° K have been measured.**

Based on the analysis of the companion paper, a qualitative prediction of the gain-frequency behavior is given. The experimental arrangement is set forth in some detail. It consists of a series of these coupled cavities with separate pump power distribution at each diode. Through this flexibility in pump phase shift and amplitude, a variety of advantages is achieved. The effects of the many variables on the performance of the amplifier are described.

Several methods of achieving short-circuit stability of this amplifier are outlined. These are: 1) nonuniform pump phase shift between sections, 2) nonreciprocal loss with ferrites, and 3) nonreciprocal loss with upper pass bands. The experimental behavior of each method is shown, and the noise performance to date is briefly discussed.

INTRODUCTION

PARAMETRIC amplification is the result of constructive mixing of a small signal and a large signal (pump) in a nonlinear reactance. This principle was successfully demonstrated by Hines,[1] who first employed the voltage-dependent capacitance of a reverse-biased semiconductor diode for this purpose. Since then the principle has been much discussed and applied, and thus the familiar cavity parametric amplifier has evolved. Three frequencies, signal, idler, and pump, are generally of interest in this device, each of which is usually supported in a resonant circuit or cavity and all are coupled to each other through the nonlinear behavior of the diode capacitor. The high impedance of the resonant circuit at each frequency results in maximum utilization of the signal power to be amplified and in a minimum requirement of pump power for a given capacitance swing. Further consequences of the use of resonant circuits are restricted bandwidth and an approximately constant voltage gain-bandwidth product. Finally, because of its negative resistance character, a circulator is required in the amplifier to make it unilateral and stable.

When a series of these cavity-type amplifiers are properly cascaded, traveling-wave parametric amplification in a filter circuit results. The undesirable features of restricted bandwidth and regeneration largely give way to increased bandwidth and unilateral gain without the use of a circulator, while the advantages of low noise, high gain per diode, and low pump power are retained. The increase in bandwidth is a consequence of large coupling between individual cavities, resulting in a filter-circuit response. Unilateral gain is obtained by properly adjusting the relative phase shift between cavities at the pump frequency. High gain per stage (*i.e.*, per diode) and low pump power are intimately related to the high impedance level of the filter circuit. Additional advantages of this circuit at microwave frequencies are large physical separation of diodes, flexibility in control of higher pass bands, and the ease with which nonreciprocal loss may be incorporated to enhance unilateral gain stability.

It is the object of this paper to describe in detail the filter-circuit approach to traveling-wave parametric amplification, from the experimental point of view, and

* Received by the IRE, May 5, 1960; revised manuscript received August 19, 1960.

† Hughes Res. Labs., A Division of Hughes Aircraft Co., Malibu, Calif.

[1] M. E. Hines, "Amplification in Nonlinear Reactances Modulators," presented at the 15th Annual Conf. on Electron Tube Res., Berkeley, Calif.; June, 1957.

to compare the performance obtained experimentally with the results of calculations based on an approximate lumped-circuit analog. A companion paper[2] describes the theoretical behavior of this lumped-circuit model, which in many respects predicts the behavior of the fundamental mode pass band in the experimental version. Finally, a review of the over-all results leads to conclusions regarding the optimum design of circuits.

Traveling-Wave Parametric Interaction in a Filter Circuit

The physical picture of the cumulative interaction process through which parametric amplification in the filter circuit results is given by Currie and Gould,[2] who explain the mechanism in terms of the coupling modes. In this way, they give meaning to the optimum phase conditions of Tien,[3] who derived them for distributed propagating circuits. We discuss in this section the consequences of these conditions as they apply to the experimentally-determined filter circuit behavior because we wish to emphasize an important difference which tends to relax the bandwidth restriction imposed by the lumped-circuit model. However, the interpretation of the signal-idler wave interaction and the construction of the idler Brillouin diagram are in no way modified by this difference. In that connection it becomes necessary partially to reproduce that interpretation in order to explain the improved performance of the experimental circuit.

Frequency and Phase Requirements

The concept of the Brillouin diagram, as shown in Fig. 1, is helpful in studying the propagation of waves on a periodic circuit.[4] In particular, it is used here to describe qualitatively parametric amplification as a result of pumping. The nonlinear capacitance in each cavity is modulated by a pump voltage at frequency ω_p. The phase shift ϕ_p of this voltage between cavities

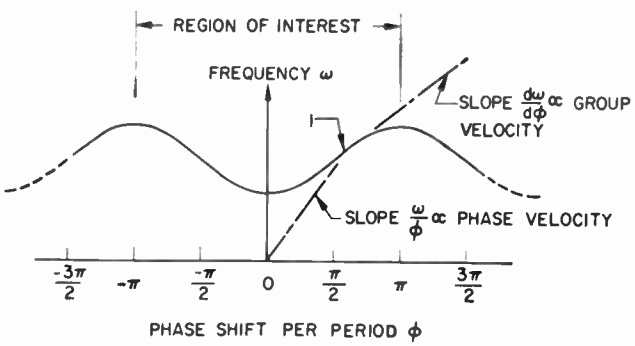

Fig. 1—Brillouin diagram illustrating phase and group velocity in the pass band of a filter circuit.

can be adjusted, while the phase shift of the signal wave ϕ_s at frequency ω_s is determined by the shape of the Brillouin diagram. An idler wave is produced at frequency ω_i in the process of pumping and satisfies the familiar relation

$$\omega_s + \omega_i = \omega_p. \tag{1}$$

All frequencies are positive quantities here, in contrast to the analysis in Part I, in which the normalized idler frequency λ_2 is a negative quantity.

It was shown by Tien[3] for the uniformly distributed transmission line, and by Currie and Gould[2] for the coupled-cavity circuit, that maximum gain results if, in addition to (1), the phase relation

$$\phi_s(\omega_s) + \phi_i(\omega_i) = \phi_p \tag{2}$$

is satisfied by the circuit. Here ϕ_i is the phase shift of the idler wave. In the diagrams of Fig. 2, we try to show the conditions under which cumulative interaction takes place in our experimentally determined Brillouin diagram (see Fig. 6 on page 1978).[5] It differs from that computed in Part I in that we find a larger-than-calculated departure from symmetry about a phase shift of $\pi/2$ radians.[6] It is apparent from the pertinent discussion of Part I, and from Fig. 2, that if the midband frequency occurs at a phase shift different from $\pi/2$ and the Brillouin diagram is approximately symmetrical about that point, nearly the entire cold pass band can be used for amplification. In fact, an inspection of Fig. 2 and the best experimentally-determined gain curves [Fig. 9(a) on page 1980, for example] shows that this has, indeed, been accomplished. The idler curve is found by rewriting (1) and (2) to yield

$$\omega_i = \omega_p - \omega_s \tag{1a}$$

and

$$\phi_i{}^+(\omega_p, \phi_p{}^+) = \phi_p{}^+ - \phi_s{}^+(\omega_s). \tag{2a}$$

The superscript + denotes the forward traveling wave. While the phase of the signal wave is determined by the Brillouin diagram, the desired phase of the idler wave as generated by (1a) and (2a) is a function of both pump coordinates, and these, fortunately, may be adjusted. When the indicated operations of (1a) and (2a) are plotted graphically, the dashed curve shown in Fig. 2(a) is obtained. Since a disturbance at the idler frequency must propagate as shown by the solid curve, cumulative interaction results to the extent that the two curves coincide. Thus, it is possible at a glance to

[2] M. R. Currie and R. W. Gould, "Coupled-cavity traveling-wave parametric amplifiers: Part I," this issue, p. 1960.

[3] P. K. Tien, "Parametric amplification and frequency mixing in propagating circuits," *J. Appl. Phys.*, vol. 29, pp. 1347–1357; September, 1958.

[4] L. Brillouin, "Wave Propagation in Periodic Structures," Dover Publications, Inc., New York, N. Y.; 1953.

[5] The discussion of the construction and meaning of the idler curve which follows has been treated by the authors of Part I, as shown in their Fig. 6, in a more elegant framework. Our discussion is based on the validity of this method, but invokes only the conditions (1) and (2) in constructing the idler curve in its relation to the experimentally determined shape of the Brillouin diagram.

[6] If the midband frequency of a pass band occurs at a given phase shift, symmetric means that the slope (group velocity) of the Brillouin diagram at frequencies equidistant above and below the midband frequency is the same.

predict qualitatively where gain may occur. In the reverse direction,

$$\left.\begin{aligned}\phi_s^- &= -\phi_s^+ \\ \phi_p^- &= \phi_p^+ - 2\pi\end{aligned}\right\}. \tag{3}$$

When (3) is substituted in (2), we obtain the phase-shift of the idler wave:

$$\phi_i^- = \phi_p^+ + \phi_s^+ - 2\pi. \tag{3a}$$

A comparison of (3a) and (2a) indicates the nonreciprocal nature of the interaction. Eq. (3a) is plotted as a continuation of the dashed curve in the left half plane of Fig. 2(a). The dashed curve is greatly displaced from the solid curve in the reverse direction, and consequently little gain should result. The pump coordinates (phase and frequency) have been properly positioned in Fig. 2(a) to achieve this unilateral behavior. If the pump phase is either advanced or retarded from this favorable position, the gain performance is degraded, while a change in the pump frequency will reduce the amplifying bandwidth. The effect of moving the pump phase to a position somewhat retarded from the optimum is shown in Fig. 2(b). Recalling the notions of the previous discussion, we see that the forward gain has been reduced severely and that the reverse gain has been increased. Further retarding of the pump phase (not shown) to the point $\phi_p^+ = \pi$ destroys the unilateral behavior completely, *i.e.*, the device has equally reduced gain in both directions. This follows if $\phi_p^+ = \pi$ is substituted into (3) and (3a). It is, of course, highly undesirable to have bilateral gain, and if stable unilateral broadband amplification is to be achieved, the shape of the pass band and the coordinates of the pump must be carefully chosen. The importance of this shape makes the filter circuit a desirable structure, because of its high degree of flexibility in shaping the pass band.

It has been assumed that the pump coordinates are somehow introduced to achieve optimum gain. If a second propagating circuit is chosen to support the pump wave, it is difficult continuously to adjust the pump phase in a flexible manner. A later section describes how this problem is circumvented and how the preceding considerations are put into practice.

Impedance Considerations

In addition to the properties considered in the previous section, the circuit should present high interaction impedance to the signal and idler waves as well as to the pumping source. Maximum utilization of the power at the respective frequencies is then obtained, and large gain per cavity and per diode results. In Part I, it is shown that for the capacitively pumped case this interaction impedance K is given by

$$K = \frac{\overline{V}^2}{2P} = \frac{\overline{V}^2}{2W_{st}v_g}, \tag{4}$$

where

V = peak voltage across the capacitor C_0,
P = power flow through the circuit,
W_{st} = peak stored electric energy per cavity,
v_g = group velocity.

Since the peak stored electric energy in the capacitor is given by

$$W_{st_c} = \tfrac{1}{2}C_o\overline{V}^2, \tag{5a}$$

and the peak stored electric energy in the remainder of the cavity can be put into the form

$$W_{st_c} = \tfrac{1}{2}C_c\alpha\overline{V}^2, \tag{5b}$$

where C_c is the equivalent cavity capacitance and α is a constant, the impedance takes on the form

$$K = \frac{1}{(C_o + \alpha C_c)v_g}. \tag{6}$$

Eq. (6) is the conservation principle (derived in Part I) between interaction impedance and bandwidth, the latter being intimately related to the group velocity

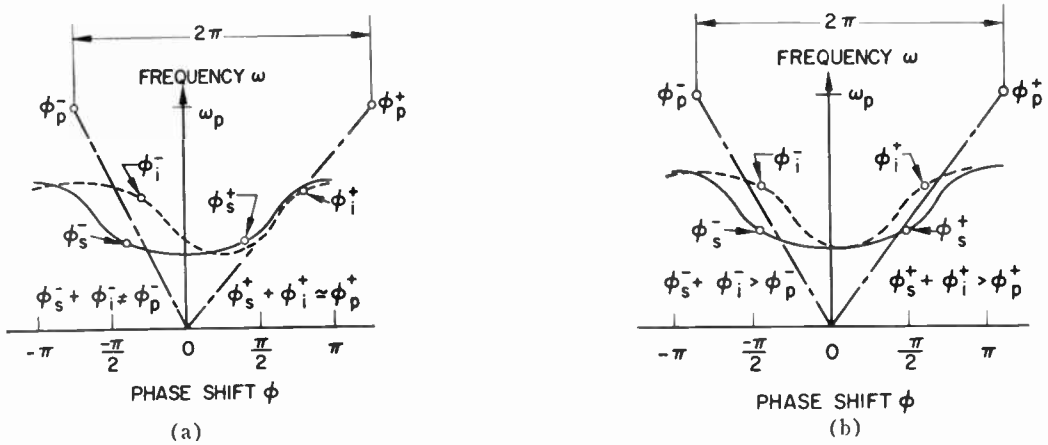

Fig. 2—Brillouin diagram showing the approximate experimental shape for two cases of pump phase shift. (a) Pump phase for optimum gain and best unilateral behavior. (b) Pump phase for less than optimum gain and inferior unilateral behavior.

[e.g., Part 1, (33) and (36)]. It is extended here to allow for more than one region of stored electric energy. In applying this conservation principle to the design of a practical amplifier, we find through (6) that it is necessary to minimize the total capacitance and hence the stored electric energy in each section and to concentrate the electric field in the vicinity of the diode capacitance. When this has been done and the desired bandwidth is known, the maximum interaction impedance is determined according to (6), with $C_c=0$ and C_o a minimum. The stored magnetic energy is also reduced, since the peak stored electric and magnetic energies are always equal in a cavity. Because the stored electric energy is concentrated in the vicinity of the diode capacitance, the stored magnetic energy serves exclusively to couple the cavities inductively with the desired bandwidth. Optimum design results from adherence to these considerations.

Additional Properties

There are several additional features of this approach which, at least at microwave frequencies, are decided advantages and deserve some mention here. First, because of the inherent mode structure in waveguides, which is only slightly perturbed by the presence of periodic loading, regions of circularly polarized fields exist where suitable nonreciprocal elements can be placed.[7] In this amplifying device, which in contrast with the traveling-wave tube has no built-in reverse loss mechanism, the specific inclusion of ferrites to achieve unilateral loss is very desirable if high gain is to be produced with a high degree of stability. If, on the other hand, no natural regions of circularly polarized fields exist, it is possible to use higher pass bands for the same effect. These pass bands must be designed so that nonreciprocal loss is introduced by conversion of power from the signal frequency to some higher frequency in the upper pass band. A later section is partially devoted to a detailed discussion of this effect.

Finally, in this filter-circuit approach, the allowable pump phase is not limited to any specific magnitude. In our experiments, the combination of high pump phase shifts (larger than π radians) and high phase velocities resulted in practical spacing between diodes. Spacing would remain reasonable in a filter-circuit amplifier if this design were scaled up to very high microwave frequencies. Usually one, or at most two, diodes are used per cavity, and the relatively large axial dimensions lead to a high degree of design flexibility.

Description of the Experimental Coupled-Cavity Circuit

The objective of this investigation was to determine the relative importance of all parameters on the gain, bandwidth, and the gain stability of the traveling-wave parametric amplifier. In order to measure the effects of each of these variables independently, flexibility was a primary objective. In addition to the analytical parameters, which are bandwidth, pump phase, pump frequency and amplitude, loss, and terminal impedances, there are the practical variables: diode capacitance, effects of parasitic inductance and capacitance, diode bias, internal reflections, and nonreciprocal loss. The necessary independence of adjustment of these variables was obtained to a large extent in the constructed model. A photograph of this model is shown in Fig. 3, while Figs. 4(a) and (b) are schematics of the amplifier and the separate pump distribution system, respectively. A compact amplifier incorporating the benefits of this investigation has since been built. Both amplifiers gave essentially the same results, but the data in this section were taken on the original model shown in the above figures; these figures show the arrangement of the combined amplifier and pumping system. Because of the objectives of this experiment and the encouraging results that were obtained, the flexibility proved to be a decided advantage. A variety of practical problems, which otherwise would probably have gone unnoticed, came to light and the interesting possibility of beneficial use of higher pass bands arose in the course of the program. A detailed description of the experiment itself as well as of these additional effects follows in subsequent sections.

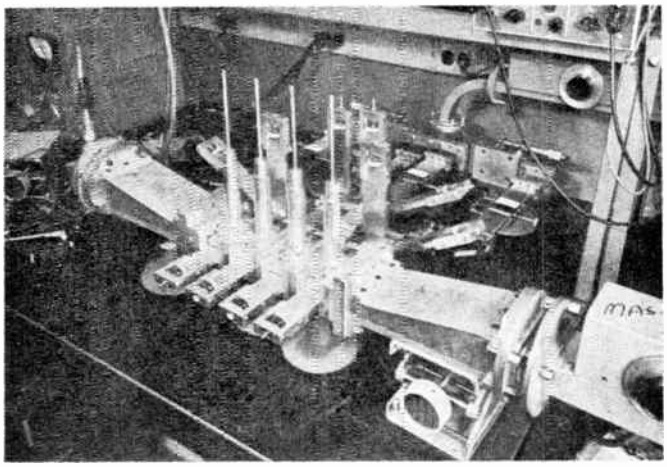

Fig. 3—Experimental arrangement of *S*-band amplifier.

Signal and Idler Circuit

The signal and idler waves both propagate along the four rectangular cavities which comprise the circuit. Each cavity is centrally loaded by a variable-capacitance diode and coupled to adjacent cavities through inductive irises. For the kind of operation described in this paper, the signal and idler belong to the lowest frequency pass band of the coupled-cavity structure. The field pattern of this pass band is such that the maximum electric field and hence the maximum voltage occur in the center of the cavity, this being the optimum location of the voltage-sensitive diode. Cavity loading by

[7] R. N. Carlile, "General properties of the propagation constant of a nonreciprocal iterated circuit," Proc. IRE, vol. 48, p. 1162; June, 1960.

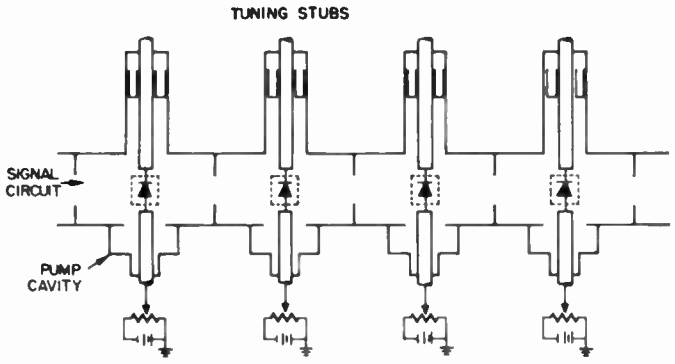

(a)

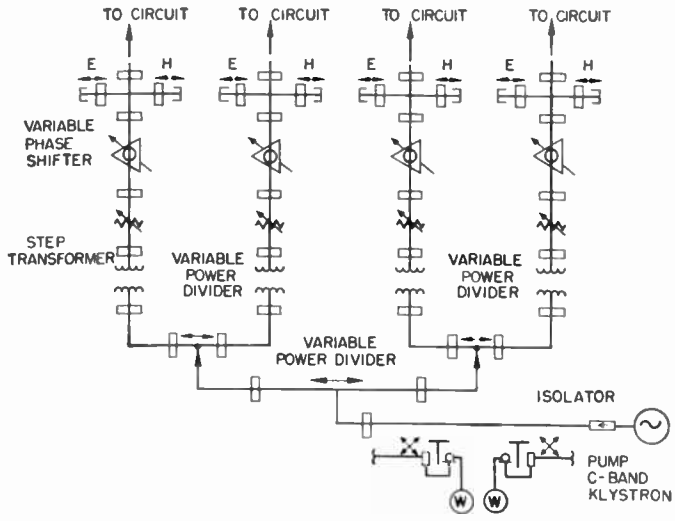

(b)

Fig. 4—Schematic of experimental layout. (a) Amplifier section. (b) Pump distribution system.

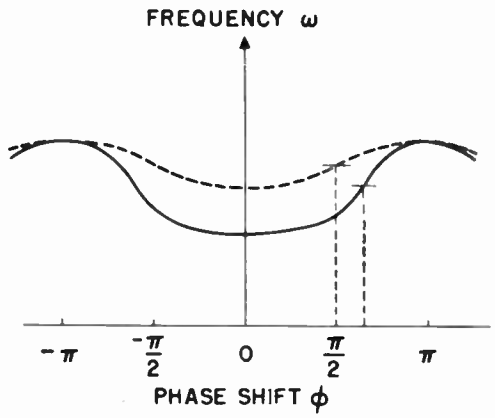

Fig. 5—The effect of coupling on the shape and bandwidth of the circuit. The dashed line is a Brillouin diagram for small coupling, where the phase shift at center frequency is $\pi/2$; the solid line is a Brillouin diagram for larger coupling, where the phase shift at center frequency is greater than $\pi/2$.

the diode further concentrates the central electric field.

The width of the pass band is determined by the strength of the mutual coupling of the cavities; larger coupling increases the bandwidth. Irises of various sizes can be substituted into the circuit to change bandwidth. Furthermore, the shape of the pass band depends on mutual coupling, as is illustrated in Fig. 5. For small coupling, the shape of the Brillouin diagram is approximately sinusoidal, but with increased coupling the midband frequency occurs at a phase greater than $\pi/2$. Fortunately, this distortion in the experimental circuit is more pronounced than that predicted from the analytical model presented in Part I. Thus, this effect can be used to obtain unilateral gain over essentially the entire cold bandwidth. The reason for this will be evident from the later discussion involving Fig. 2(a) and 2(b).

Pump Circuit

In the previous discussion of parametric interaction in a filter circuit, it was assumed that pump coordinates (frequency and phase) were somehow introduced to effect efficient mixing with the signal. In practice, at least, two alternatives suggest themselves. A pass band at the pump frequency with the proper Brillouin diagram with respect to the signal frequency must be provided or, alternatively, a pump voltage of equal amplitude and of the correct phase must be introduced separately in each cavity to simulate a traveling wave. Both methods properly carried out result in additive interaction, but the latter has the advantage of flexibility and was used in our experiment. Fig. 4(b) is a schematic illustration of this parallel feed system. The pump power originates in a *C*-band klystron and is channeled into four separate waveguide branches. Each branch contains a variable attenuator, a variable phase shifter, and matching elements. The branches terminate in rectangular cavities similar to but smaller than the signal cavities. The diodes, common to both pump and signal-idler circuit, provide the sole means of coupling between the two circuits. By careful adjustment of the variables in each branch of the pump circuit, any desired pump phase and amplitude distribution can be set up in the four channels. Since the signal-idler circuit presents a stopband at the chosen pump frequency, this pump amplitude and phase distribution is solely determined by the pump frequency circuit design.

The separate parallel pump feed provides an additional practical advantage. Unless the diodes are lossless (at present an unrealistic assumption at microwave frequencies), some pump power is absorbed by each diode. In a propagating pump circuit, the diodes gradually drain the pump power, and each successive diode has a correspondingly reduced capacitance swing. This gives rise to a gain limitation, which the parallel feed scheme completely overcomes.[8,9]

[8] At a lower signal frequency, where the diodes are essentially lossless, this factor is not important. Gain saturation due to a finite diode Q when the pump propagates along the circuit sets an upper bound to gain and the number of diodes.

[9] A. L. Cullen, "Theory of the traveling-wave parametric amplifier," IEE, Paper no. 2991; August, 1959.

Tuning Stubs

The tuning stubs, which can be seen either in Fig. 3 or Fig. 4(a), serve a twofold purpose. First, they are used to tune out the lead inductance of the diodes in the signal-idler frequency range. In our experiment, the series resonant frequency due to this inductance and the mean capacitance was considerably below the operating frequency. When stubs are not used, maximum voltage develops across the inductance rather than across the variable capacitance. Second, the tuning stubs permit favorable location of the diode in the cavity. As an integral part of the center conductor, the diode can be moved vertically and independently of the movable short. To find the desired position of the diode in each cavity, the center rod and the sliding coaxial short are simultaneously varied. The best position yields optimum mixing, as evidenced by a strong idler and low pump power.

Terminal Conditions

Because of the band-edge reflections and the absence of internal losses, the circuit, under amplifying conditions, should be well matched at both input and output terminals. For a particular set of parameters, the input and output admittances were measured and matched to a low VSWR by using simple susceptance elements. It was found that these simple matching elements could not always reduce the mismatch to the desired level when some circuit parameter was varied. Hence, rather than design and build new matching sections with each variation, the circuit was rematched by adjusting the bias voltage on the diodes. This proved to be a rapid and flexible matching method and had minor effects on the measured performance. It did, however, affect the pump-power level, which was raised substantially in many cases.

Variable-Capacitance Diodes

In all of the experiments reported here, commercially available gold-bonded germanium diodes were used exclusively. These diodes are characterized by a capacitance-voltage variation,

$$C(V) = C_o\left[1 + \left|\frac{V}{B}\right|\right]^{-1/2},$$

where C_o is the capacitance at zero bias voltage and B the diffusion potential = 0.4 volt. The zero bias capacitance was selected to be approximately 2.0 pf with a tolerance of ±15 per cent. The diodes, in their manufactured glass package, have a parasitic inductance resulting from the whisker of about 4 millimicrohenries. At a nominal bias voltage of 2 volts, the cutoff frequency is of the order of 30 to 40 kMc, which results in a diode Q of 10 to 15 at the signal frequency. Based on the above data, the self-resonant frequency of the diode at a nominal bias of 2 volts is approximately 2.8 kMc. In addition, while the maximum peak-to-peak normalized capacitance swing of these diodes is in excess of unity, the effective value of the swing depends on the particular transformation at a given position of the diode in each cavity.

The Experimental Performance of the Amplifier

With the above background the performance of the four-section amplifier can now be evaluated. An experimentally determined Brillouin diagram is shown in Fig. 6. It was taken for one set of coupling irises and a particular set of adjustments of the other variables which affect the signal frequency passband. The degenerate point, *i.e.*, the point at which the signal and idler frequencies cross over, is determined by the pump frequency, which was set at 6.32 kMc.

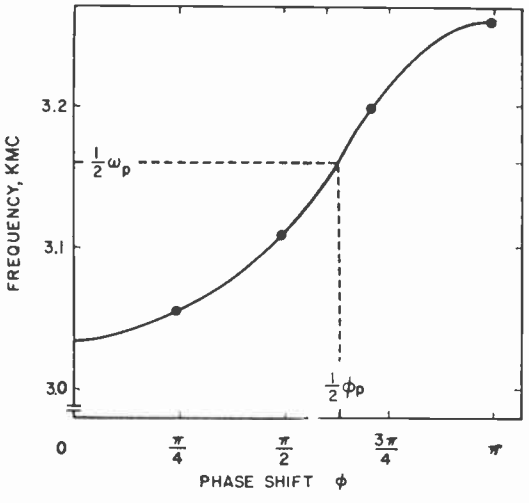

Fig. 6—Experimentally determined Brillouin diagram of the coupled-cavity circuit.

According to the previous discussion, the bandwidth over which gain is obtained and the magnitude of this gain are determined by the pump phase shift. As this phase shift is varied, the gain curves of Fig. 7(a) and 7(b) are obtained. "Gain" as used in this paper denotes insertion gain, *i.e.*, the ratio of power levels between two terminals with and without the amplifier inserted. Nominal "cold"-circuit loss of the amplifier in the signal frequency band with the pump power off was 2.5 db at the band center. Fig. 7(a) and 7(b) show the forward and reverse gain behavior, respectively. The curves correspond in such a way that when curve I of Fig. 7(a) gives the forward gain, curve I of Fig. 7(b) gives the corresponding reverse gain for the same pump phase shift.

Curve I of Fig. 7(a) is plotted for a pump phase shift of 180° per section; the corresponding pump phase shift in the reverse direction is also 180° and gain is, as expected, approximately the same in both directions. Gain is low because the 180° pump phase shift is quite far from the optimum. In curve II, the pump phase shift

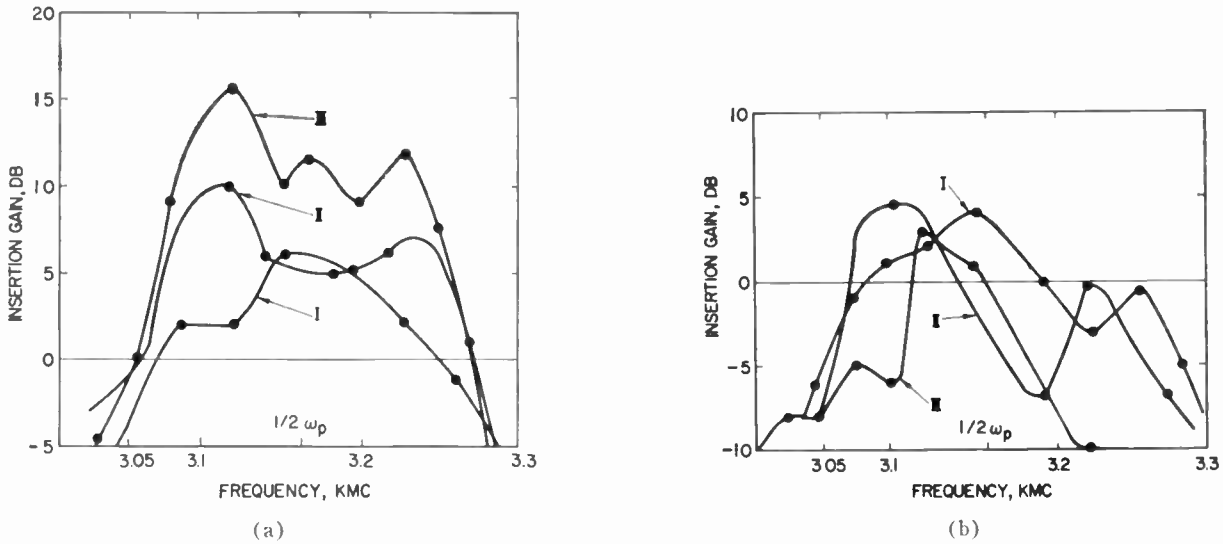

Fig. 7—(a) Forward insertion gain vs frequency; the parameter is pump phase shift per section. Curve I = 180°, II = 200°, and III = 230°. The pump power for I is 80 mw; for II and III it is 40 mw. (b) Reverse insertion gain vs frequency; the parameter is pump phase shift per section. Curve I = 180°, II = 160°, and III = 130°.

was adjusted to 200° in the forward direction and, correspondingly, to 160° in the reverse direction. The forward phase shift is closer to the optimum and the reverse phase shift is farther from the optimum than in curve I. The gain is accordingly nonreciprocal, as it has increased in the forward direction and decreased in the reverse direction. In curve III, the phase in the forward direction is adjusted to be optimum at the degenerate point, and since this is also the inflection point in the Brillouin diagram (see Fig. 6), a relatively wide pass band is obtained. In the reverse direction, the pump phase shift is still farther from optimum than that in curve II, and the gain is decreased.

It is interesting to note what happens when the gain is increased. If the diodes are not already at the point of incipient forward conduction or reverse breakdown, gain can be increased by increasing the pump power. If the diodes are saturated, then the gain can be increased by adding more sections. For the response of curve III in Fig. 7(a), however, the capacitance swing of the diodes is far from maximum, and the pump power can be increased. In Fig. 8, the pump-power input has been doubled, and the high regenerative gain peaks show the amplifier to be on the verge of oscillation. The resulting instability of this mode of operation can be traced to several compounding effects. Increasing the pump power results in a larger capacitance swing, which produces higher total gain. In the absence of correspondingly increased reverse loss, this gain increases feedback, particularly in the regions of the passband edge. In addition, the increased capacitance swing produces a change in the mean value of the effective capacitance. Thus, the input and output admittances, which are functions of this capacitance, will have changed correspondingly. The output admittance undergoes a further change caused by the increased gain per stage. The discussion pertaining to Fig. 11 of Part I makes plausible the concept of matching to the predominant (exponentially growing) wave and shows the effect of first-order improvement on the variation of gain with frequency when this matching condition has been achieved. Finally, the increase in mean capacitance causes a change in the effective bandwidth. In view of these remarks, it is not surprising to find that when the described effects have been minimized by carefully rematching and adjusting the parameters of the circuit, the increased gain and bandwidth performance of Fig. 9(a) results.

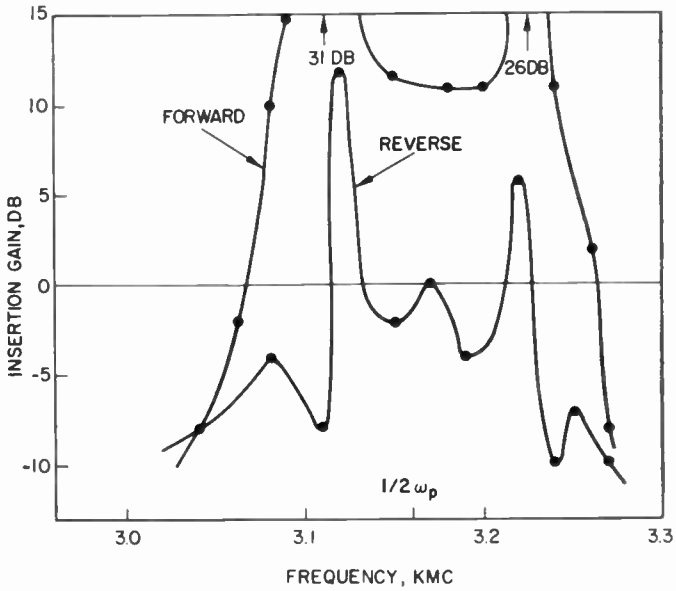

Fig. 8—The effect of increasing the pump power in each of the four sections. The pump phase shift is 230° per section in the forward direction and 130° backward; pump power is 80 mw.

While the effects of finite mismatch are still apparent, an average power insertion gain of greater than 12

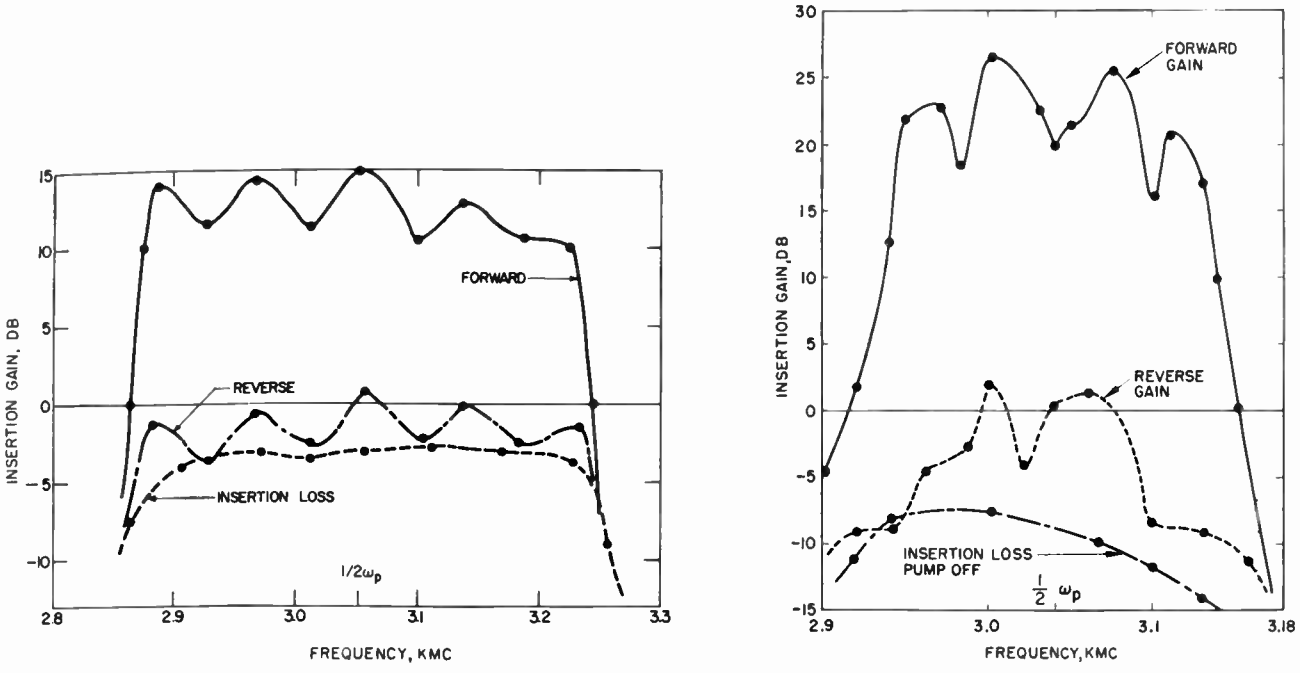

Fig. 9—(a) Gain vs frequency curves for the four-section amplifier; reverse gain and cold insertion loss are also shown. Pump phase shift per section and terminal matches have been optimized. Pump power is 100 mw. (b) Gain vs frequency curves for the six-section amplifier.

db over a 350-Mc band has been achieved with the four sections of the amplifier. The "hot" performance in the reverse direction, which vacillates between the "cold" insertion loss and unity gain, is also shown. While these numbers represent a gain-bandwidth product of about 1500 Mc (voltage-gain times bandwidth in megacycles), a variety of other combinations of bandwidth and gain have been achieved, some of which are mentioned to show the versatility and capability of this circuit. Nevertheless, there has been a trend toward achieving larger gain-bandwidth products at higher gains. For example, a bandwidth of 40 Mc at a gain-bandwidth product of 2000 Mc was obtained with a set of smaller coupling irises, while with a set of correspondingly larger irises, the bandwidth was 450 Mc and the gain-bandwidth product was only 600 Mc. In all of these cases, the four-section amplifier was adjusted for stable operation with relatively smooth gain-frequency response.

Several methods of increasing the gain-bandwidth product present themselves. We may, of course, simply add sections to enhance either the gain or the bandwidth. This method is limited to power gains of somewhat less than 20 db, because of the eventual onset of gain instabilities and the increasing sensitivity of the gain to terminal conditions. Two cavities were added to the initial four sections in order to explore the possibilities of this obvious approach. The gain-frequency performance of this six-cavity amplifier is shown in Fig. 9(b), where the insertion power gain is plotted vs frequency and the reverse gain and cold insertion loss have been included. The gain ripples are primarily caused by the terminal matches, which have a voltage-standing-wave-ratio of about 2 to 1 and the same frequency dependence as the power gain. The proportionately increased cold insertion loss resulting from internal diode losses is apparent. In spite of these relatively large power gains the amplifier remained stable. This performance (a gain-bandwidth product of 2000 Mc), while noteworthy, can be improved by a more careful matching procedure as well as by increasing the uniformity of the various sections. Even with the diodes used in these experiments, the combination of better matches and greater uniformity should increase the gain-bandwidth product of the six-cavity amplifier to an expected 2400 Mc.

The further increase of the gain-bandwidth product, particularly at larger bandwidths, depends upon a number of factors. As the number of stages increases, the matching admittances must become increasingly complex to maintain stability, particularly if spurious responses are associated with the active element in each cavity. One such response, for example, is the self-resonance of the diode, which results from its lead inductance. If the sensitivity of the amplifier to the terminal-admittance changes is to be eliminated, some form of nonreciprocal loss must become a part of the structure. Then the amplifier gain can be increased proportionally.

Various other factors are encountered as a further increase of bandwidth is attempted. In particular, the shape of the Brillouin diagram is important; for a very large bandwidth, a high degree of symmetry is required about some phase shift other than $\pi/2$. The diode losses

also become increasingly important not only because of noise, where these losses have a first-order effect, but also because they limit the gain-bandwidth product that can be obtained. In addition, the ratio of diode-to-circuit admittance becomes an important variable which, within the already outlined limitations resulting from the finite bandwidth-impedance product, probably has an optimum value.

In this section, the potentialities of the coupled-cavity traveling-wave parametric amplifier have been shown for applications in which broadband microwave amplification is desired. It has been pointed out, however, that as the gain per cavity and diode is increased, the regenerative effects which dominate the single-diode cavity amplifier performance become increasingly significant. Also, when greater amplifier gain and bandwidth are desired, the operation becomes more critically dependent upon terminal conditions. Several methods of reducing these regenerative effects appear feasible. A detailed discussion of these methods is presented in the following sections.

Elimination of Regenerative Effects

Three methods for increasing the stability of the amplifier have been investigated. These are 1) nonuniform pump phase shift between cavities, 2) nonreciprocal loss using ferrites, and 3) nonreciprocal loss using higher pass bands. Each method is separately discussed and some experimental evidence of the behavior of each of the three methods is presented. The choice of the particular method depends upon several aspects, not the least of which is the effect of its inclusion on the noise performance.

Nonuniform Pump Phase Shift Between Cavities

Theoretical investigation of traveling-wave parametric amplifiers has been concerned with a definite uniform value of pump phase shift between sections. Also, most experimental investigations have utilized a uniform pump phase shift, probably for the same reason, *viz.*, simplicity. The most important result of including independently variable pump phase was the discovery of the large effect that a nonuniform pump phase shift can have on the shape of the gain-response curve and on the stability of the amplifier.

Nonuniform pump phase shift provides a means by which signal and idler waves reflected at the output by some arbitrary mismatch can be made to cancel each other and cause the circuit to appear to be perfectly matched. To understand this, consider what would happen to an amplifier operating with optimum and uniform pump phase for N sections, but with the pump phase shift between the Nth and the $(N+1)$st section 180° from optimum. Two components then comprise the signal in the $(N+1)$st cavity: one component comes from propagation of the signal from the Nth cavity; the second component comes from the propagation of the idler from the Nth cavity mixed with the pump in the $(N+1)$st cavity to yield a voltage at the signal frequency. If the pump phase is optimum, the two components add; but if the pump phase is 180° from optimum, the two components cancel. Similarly, the idler in the $(N+1)$st cavity, which is caused by propagation from the Nth cavity, can be made to cancel the idler established in the $(N+1)$st cavity by the mixing of the signal and pump.

The example just given would cause cancellation in the forward direction. Obviously it is desirable to obtain cancellation in the reverse direction with little, if any, reduction in forward gain. This is accomplished by adjusting the pump phase between the cavities N and $N+1$ ($N+1$ is now the output cavity) such that the signal and idler, in a round trip from N to $N+1$ to N including an arbitrary phase shift at the output termination, experience an effective phase shift approximately 180° from optimum. The frequency band over which cancellation of the reflected waves occurs depends on the rapidity with which the relative phase shift for the round trip of the signal and idler waves varies as the frequency is changed. The forward gain is thereby reduced, since the phase for maximum gain has been changed.

The effectiveness of this procedure is illustrated in Figs. 10(a) and (b). We obtained the response of Fig. 10(a) from that shown in Fig. 8 by simply varying the phase shift in the last branch of the pump distribution system. Similar results can be obtained for a variety of pump phase-shift values if the other cavities are adjusted as well; *e.g.*, Fig. 10(a), where the criterion for adjustment was to obtain a flat response curve irrespective of required phase shift. It has also been found that this method is helpful in stabilizing the response at high gain over a narrow frequency range, which is shown by the curve in Fig. 11.

The preceding remarks may be summarized as follows: Nonuniform pump phase shift can be used effectively over a limited frequency range to minimize the effects of terminal mismatches and to smooth out the frequency response in a manner reminiscent of the staggering process used in low-frequency amplifiers. It has also been useful in stabilizing narrow-band high-gain responses. The method at the time of this writing is purely experimental. A recasting of the analytical framework is required in order to pursue a theoretical investigation of the effects of nonuniform pump phase shift.

Nonreciprocal Loss with Ferrites

Utilization of the nonreciprocal properties of ferrites is a second and possibly more promising approach to achieving short-circuit stability of the amplifier at any gain. With this approach, the attenuation in the reverse direction can be made larger than the forward gain, thus precluding a loop gain that is larger than unity. The application of ferrites to one-way loss in traveling-wave

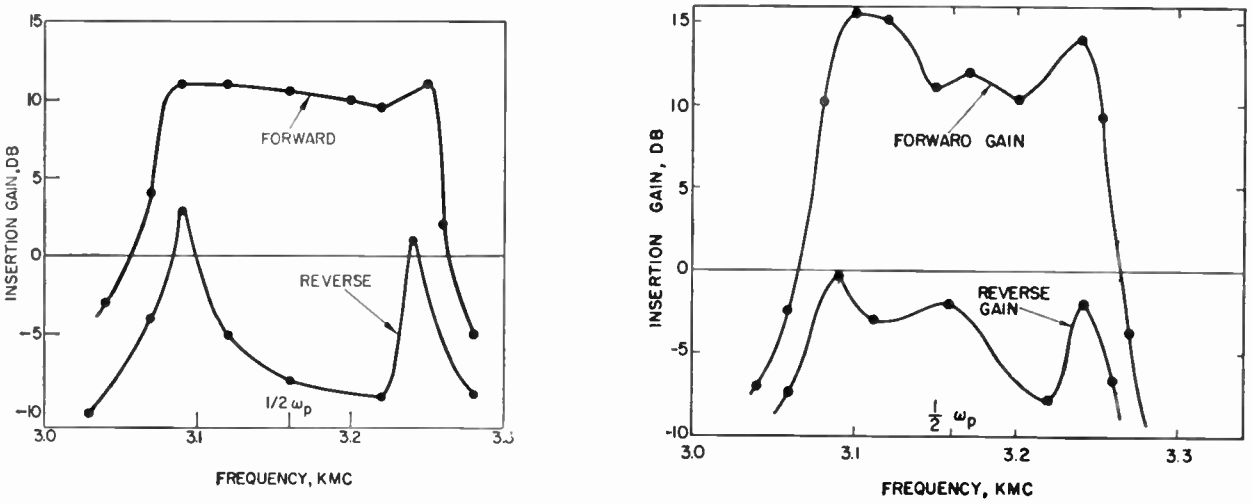

Fig. 10—(a) Gain vs frequency. This response was obtained from that of Fig. 8 by changing the pump phase shift in the output cavity alone. In the remaining three sections, the pump phase shift is 230° per section in the forward direction and 130° backward. Total pump power is 80 mw. (b) Gain vs frequency curves showing the effect of changing the pump phase shift in more than one cavity. Note that reverse gain is less than unity at all points.

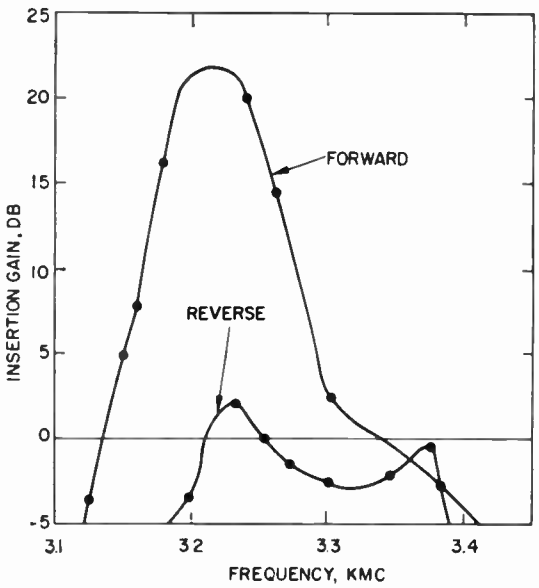

Fig. 11—High nonreciprocal gain through nonuniform pump phase shift per section.

structures has been discussed by Sensiper,[10] while the effect of ferrite properties on the Brillouin diagram, for the case of a lossless ideal structure, has been treated by Carlile.[7] Recently, ferrites have been used successfully to increase the stability of the traveling-wave maser.[11] In this section, the experimental behavior of the traveling-wave parametric amplifier with ferrite-loaded coupling irises will be discussed.

The unique feature of this type of amplifier is the possibility of including ferrites. The individual cavities of the amplifier are coupled through inductive irises; when ferrite bodies of the proper material and geometry are placed in such an iris, large nonreciprocal coupling results between cavities. It is clear, then, that such an iris behaves in many respects like an isolator. The ideal isolator offers infinite attenuation in the reverse direction and none in the forward direction. A practical isolator, however, need only provide a reverse attenuation somewhat larger than the largest expected forward gain. Its forward loss should be as small as possible since, in addition to reducing the available gain, the excess noise temperature of the amplifier increases in direct proportion to the forward attenuation of the circuit in the absence of pumping.[12] Refrigeration proportionately reduces this thermally generated noise and, in the case of the maser, almost completely obviates its importance. One additional point must be stressed. The large reverse attenuation gives rise to considerable thermal noise power. This noise, however, is only "matched" to the reverse direction and propagates along the circuit in that direction. It is absorbed by the input termination, if there are no reflections along the way.

It is apparent that the ferrite-loaded irises used in this experiment must be placed in regions of circularly polarized fields. These fields exist within the iris, just as they exist in the waveguide. The optimum position and shape of the ferrite body can be found empirically. One embodiment of this idea together with the magnetic circuit to bias the material is shown in Figs. 12(a)

[10] R. N. Carlile and S. Sensiper, "A nonreciprocal-loss traveling-wave-tube circuit," IRE TRANS. ON ELECTRON DEVICES, vol. ED-7, pp. 289–296; October, 1960.

[11] R. W. DeGrasse, E. O. Schultz-Dubois, and H. E. D. Scovil, "The three-level solid state traveling wave maser," *Bell Sys. Tech. J.*, vol. 38, p. 305; March, 1959.

[12] C. Shafer, "Noise figure for a traveling-wave parametric amplifier of the coupled-mode type," PROC. IRE, vol. 47, p. 2117; December, 1959.

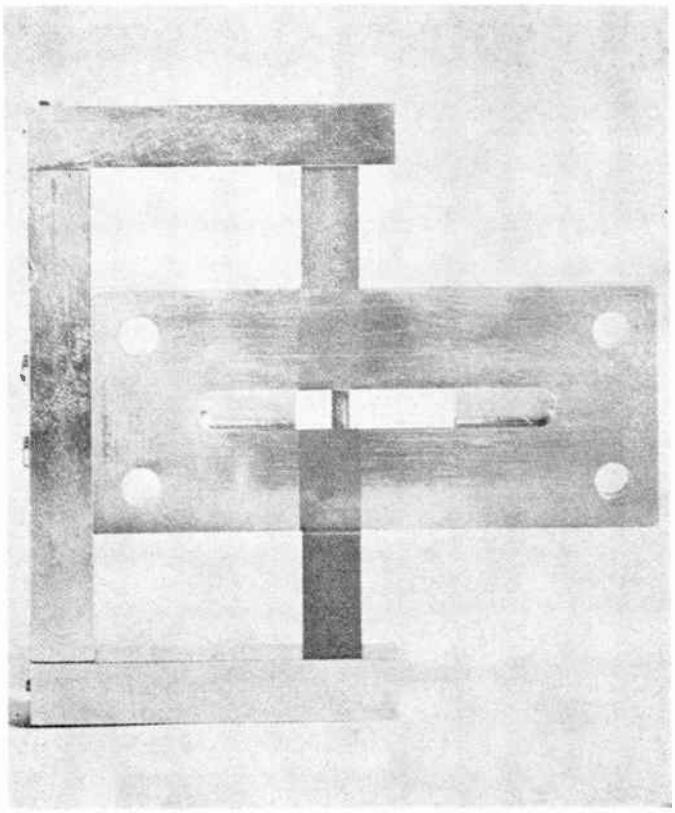

(a)

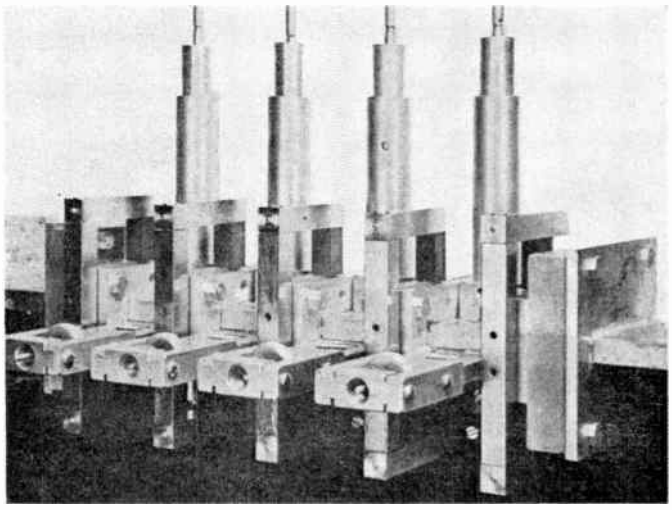

(b)

Fig. 12—(a) A ferrite-loaded coupling iris and its magnetic circuit. (b) Assembled four-cavity circuit with ferrite-loaded irises.

and (b). The ferrite (Transtech 414) is a circular rod 0.150 inch thick, a diameter which gave the best front-to-back ratio at the time. The typical behavior of this configuration is shown in Fig. 13. When incorporated into the filter circuit, a set of similarly loaded irises yielded the response shown in Fig. 14. The forward loss of the circuit with ferrite is about 5 db over the band of interest; however, most of this loss is caused by loading due to the diodes rather than due to the ferrite. The reverse loss is well in excess of 10 db.

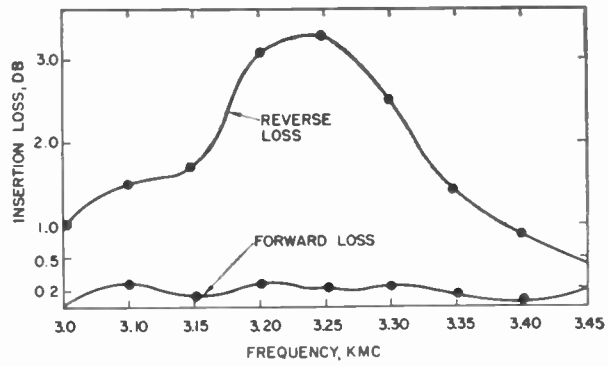

Fig. 13—Forward and reverse loss characteristic of the single-iris configuration shown in Fig. 12.

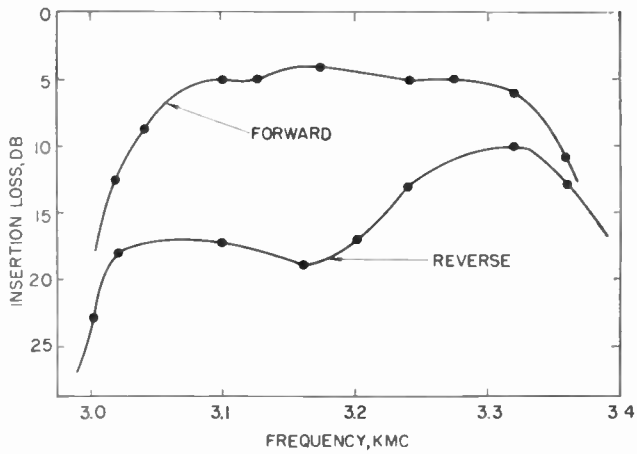

Fig. 14—Measured transmission behavior of the four-section circuit with ferrite-loaded irises in the absence of pumping.

A complete set of the nonreciprocal irises (a total of five to isolate the four cavities) when included in the filter circuit gave the amplifier performance shown in Fig. 15. The forward gain response is quite flat except for small peaks at the edges. The cause of these peaks is not understood in view of the reverse gain response, which has no band-edge peaks. They probably result from internal irregularities which become more pronounced at the passband edges rather than from the terminal matches. Hence, more careful placement and adjustment of the ferrites could eliminate this effect. It is also noted that relatively high pump power was necessary to attain this gain performance. While at the time of the experiment this behavior was attributed to the ferrites, it has since been demonstrated to be primarily a consequence of unfortunate diode placement with respect to the pump coupling elements. Responses equivalent to those shown in Fig. 15 have since been obtained with normal pump-power levels.

Nonreciprocal Loss with Sum-Frequency Passband

In addition to the previously discussed methods for increasing the gain stability of the traveling-wave parametric amplifier, it is possible to employ a pass band centered approximately at the sum-frequency. This is

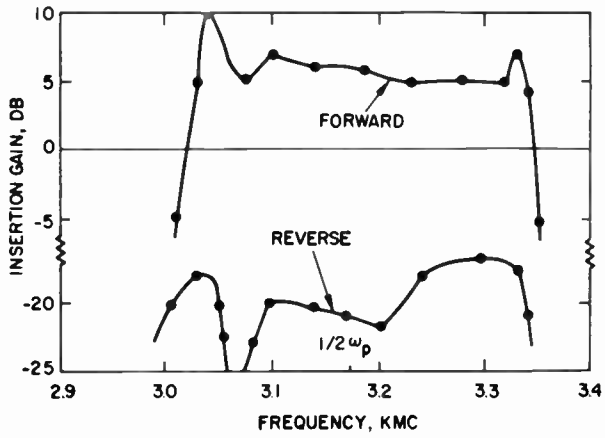

Fig. 15—Gain vs frequency curves for the ferrite-loaded amplifier circuit showing high nonreciprocal loss. Total pump power is 1 watt.

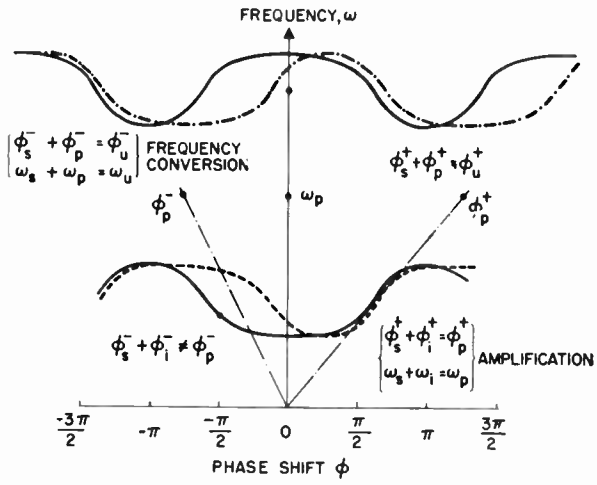

Fig. 16—Brillouin diagram, similar to Fig. 2, with upper sideband and pump phase shift properly placed to attain reverse attenuation and forward gain. In each case, near-coincidence produces coupling.

given by

$$\omega_s + \omega_p = \omega_u. \tag{7}$$

This band may be in the form of a higher mode of the filter circuit, or it may be a separate structure tailored to satisfy the fundamental, amplifying pass band and the following set of conditions:

For the pass band at ω_u,

$$\phi_s^- + \phi_p^- = \phi_u^-, \tag{8}$$

$$\phi_s^+ + \phi_p^+ \neq \phi_u^+; \tag{9}$$

for the fundamental, amplifying pass band,

$$\phi_s^+ + \phi_i^+ = \phi_p^+, \tag{10}$$

$$\phi_s^- + \phi_i^- \neq \phi_p^-. \tag{11}$$

These relations are illustrated in Fig. 16. Note that (10) and (11) pertain to the amplifying filter circuit and have already been discussed in connection with Fig. 2. They are repeated, however, to show the relative placement with respect to the upper pass band.

Roe and Boyd[13] have computed the effect on gain of mixing with higher frequencies in nondispersive propagating systems. They point out, in particular, that when the sum-frequency is an allowed mixing product, frequency conversion will take place between the lower and the higher pass bands. Thus, the power in the amplified signal wave is periodically converted into the sum-frequency wave, and to the extent that this conversion takes place no useful gain results. A further consequence of this reciprocal process is the conversion of noise from the sum-frequency to the signal-frequency band. This conversion does not take place unless certain phase relations are met. In a nondispersive propagating circuit, such as the lower frequency portion of a low-pass filter circuit, these relations once satisfied remain constant over a wide band of frequencies, while the phases in a filter circuit can be adjusted to almost any desired value. It is possible, therefore, to adjust the pass bands and the pump phase so that the signal pass band has gain in the forward direction only (lower right-hand portion of Fig. 16), and frequency conversion to the upper pass band takes place in the reverse direction only (upper left portion of Fig. 16). The upper pass band, just like the ferrites described previously, produces nonreciprocal loss. The upper pass band shown in Fig. 16 achieves this unilateral behavior over most of the useful amplifying frequency band. Selective absorption can be obtained, if it is desired, by employing a portion of a pass band which has opposite group and phase velocities. It should also be mentioned that this absorptive type of frequency-conversion process can be utilized for its own sake if it is desired to obtain nonreciprocal loss in a frequency range where ferrite devices are not possible, *e.g.*, at very low frequencies. Such an "isolator" can be very compact, but it must have a pump-power supply for its operation.

Experimental evidence of both broadband and selective reverse loss is shown in Figs. 17 and 18, where the reverse attenuation is seen to be considerably larger than the "cold" attenuation. In Fig. 17, the high reverse loss does not extend to the band edges, thus limiting the band-center gain to relatively low values because of band-edge oscillations. In Fig. 18, however, the narrow-band loss does occur near the band edge, and higher gain can be obtained; the limiting factor here is the regenerative effect near the band center. In both responses, the effect of imperfect matching conditions at the terminals is evident.

The achievement of nonreciprocal loss involving the methods described in the preceding two sections may now be summarized. We have demonstrated the com-

[13] G. M. Roe and M. R. Boyd, "Parametric energy conversion in distributed systems," presented at the 17th Conf. on Electron Tube Res., Mexico City, Mexico; June, 1959. Also, PROC. IRE, vol. 47, p. 1214; July, 1959.

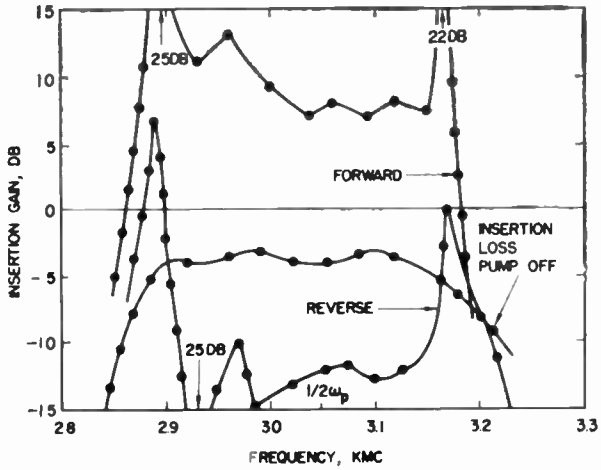

Fig. 17—Gain vs frequency curves showing nonreciprocal loss in reverse direction resulting from coupling to upper passband over broad frequency range.

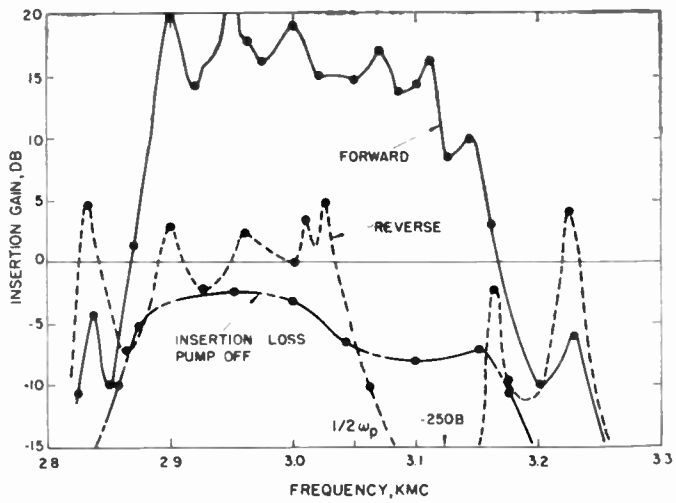

Fig. 18—Gain vs frequency curves, similar to Fig. 17, showing narrow-band coupling to upper sideband near 3.1 kMc, which results in the reduced band-edge peak evident in Fig. 17.

patibility of ferrite nonreciprocal elements in the coupled-cavity circuit. The high reverse loss which was achieved resulted in a first-order improvement in gain stability. As a result of the inclusion of the ferrite, which reduced the terminal reflections that cause regeneration, the frequency response improved. Although these exploratory studies have supported our qualitative understanding of the advantages of using ferrite in this device, further investigation appears warranted. Systematic studies of ferrite materials, their size, shape, and positioning, are needed to obtain uniformly high reverse loss and minimum forward loss, the latter of which directly affects the noise temperature of the amplifier.

It has been shown that the second method described, *i.e.*, the use of the sum-frequency band to obtain nonreciprocal frequency conversion, can indeed be realized. This method will very likely entail an additional complication in that precise phase conditions must be satisfied. The successful application of this method depends essentially on the ability to shape the upper pass band in a prescribed way.

The choice of the particular method to be used will depend upon the type of circuit considered. Further study is needed to determine the effect of various parameters on optimum one-way attenuation by frequency conversion. Both methods, ferrite and frequency conversion, can introduce additional noise contributions over the intrinsic forward loss, either through imperfect terminal matches or internal reflections. Finally, the frequency-conversion method can serve to make nonreciprocal attenuation possible at very low frequencies, where ferrites have, at least so far, made this impossible.

The Noise Performance

There has been little discussion thus far of the performance of this amplifier as a low-noise device, because the primary effort has been directed toward understanding the cumulative interaction process in the coupled-cavity parametric amplifier. During the program, however, the radiometer noise temperature was measured periodically at spot frequencies, with the usual precautions which must be considered in measuring devices of the negative resistance type. These measurements indicated double-channel noise temperatures of about 130°K, in close agreement with the predicted value based on the measured insertion loss of the amplifier without pumping.[14] No measurable increase in noise temperature was observed when ferrites were included in the amplifier. The insertion loss was found to be caused almost entirely by the losses associated with the diodes. On the other hand, the diodes were selected primarily for uniform zero-bias capacitance, and little attention was paid to the diode Q or the reverse breakdown voltage of the individual units. The diodes in these experiments, as mentioned earlier, were commercially available gold-bonded germanium alloy junctions.

These early measurements of the noise temperature of the coupled-cavity traveling-wave parametric amplifier suggest that diode and circuit losses affect the noise temperature approximately as these losses enter the performance of the distributed amplifier.[12] The effective noise temperature depends on the ratio of the total loss in the absence of pumping to the gain in the presence of pumping. There is also experimental evidence that noise temperature is sensitive to the terminal conditions. Detailed measurements of the noise behavior of this amplifier and its dependence on a variety of parameters are currently in progress and will be reported at some future time.

[14] It is assumed here that the noise temperature of this coupled-cavity amplifier is approximately the same as the equivalent distributed amplifier analyzed in footnote 12, which has the same loss and gain ratio.

Conclusions

The experimental behavior of the coupled-cavity traveling-wave parametric amplifier has been reported in detail. Starting with a qualitative discussion of the propagation of a signal wave in the phase plane of the Brillouin diagram, we have described the interaction process between the signal and the generated idler wave. This successfully led to a qualitative prediction of the gain-frequency behavior of the coupled-cavity circuit. The very general conclusions of the analysis in Part I have been substantiated by the experiments, insofar as the lumped-circuit model of that analysis bears resemblance to the actual microwave coupled-cavity structure. Some important differences have come to light, and these deserve a brief restatement as they bear on the conclusions of Part I. These are: 1) the existence of a bandwidth-impedance conservation principle through which a given gain and bandwidth results from a minimum number of diodes, 2) the practical interpretation of the interaction impedance parameter and its effective use in reducing the necessary pump power, 3) the advantages arising from an adjustable pump phase in determining the optimum unilateral amplifier response, and 4) the dependence of gain and gain variation with frequency on the terminal conditions.

For the lumped analog of the coupled-cavity circuit, the Brillouin diagram was shown to be approximately symmetrical about $\pi/2$ phase shift. Obtaining unilateral gain and reducing the effects of band-edge reflections required that the half-pump frequency be different from the midband frequency of the cold circuit. Although the choice was arbitrary, the analysis of Part I was carried out for a half-pump frequency that is less than the midband frequency of the circuit. The resulting computed bandwidth of the amplifier was curtailed, as is indicated by the statement that "the bandwidth cannot exceed twice the frequency separation between the half-pump frequency and the nearest cutoff frequency of the filter." In the microwave coupled-cavity circuit, however, it was found experimentally that the midband frequency of the cold circuit was significantly higher than the frequency at $\pi/2$ radians. (See Fig. 6.) As a direct consequence of this symmetry shift, it was possible to perform the experiments at a half-pump frequency approximately equal to the cold-circuit midband frequency, thereby realizing a "hot" bandwidth essentially equal to the "cold" bandwidth. Thus, unilateral gain was achieved over the entire pass band of the coupled-cavity circuit. As this shifting of the point of symmetry becomes more pronounced, the forward-to-reverse gain ratio increases. The precise shape of the pass band has, therefore, a direct bearing on the attainable gain and bandwidth of the amplifier. While an exact criterion for the optimum shape cannot be formulated at this stage, our experiments show that the symmetry property about the midband frequency of the filter and about a phase shift other than $\pi/2$ significantly influences the obtainable amplification band. Within the large family of microwave filter structures to which the coupled-cavity circuit belongs, there exists a variety of pass band shapes. Experience has shown that these circuits lend themselves readily to pass band shaping to enhance the desired symmetry properties.

While our experiments have demonstrated the performance of the coupled-cavity circuit in accordance with the previously stated conservation principle, the results were obtained only by carefully matching the terminal admittances. The early recognition of the sensitivity of the amplifier to these terminal conditions led to a search for practical schemes to circumvent this limitation and to render the amplifier immune to internal reflections. Two promising methods were found to be feasible, *viz.*, the incorporation of ferrites in regions of circularly polarized fields of the filter circuit, and alternatively, the judicious use of higher frequency pass bands. Experimental results were presented to support the feasibility of both methods. The advantages which can be gained by nonuniform pump phase shift per cavity were described in connection with obtaining uniform gain response.

There are a variety of aspects of this amplifier which have not been discussed and which deserve further study. The criterion of the optimum shape of the pass band for broadband amplification needs clarification and possibly may have to be modified under conditions other than those assumed here. The reported early results on the measurement of the noise temperature of the amplifier have been very encouraging, but the effect of the various circuit and diode parameters on the noise performance have not been considered. The effect of both diode parasitics (static capacitance, inductance, and loss), the effect of higher-order nonlinearities, and the effect of uniformity of the diodes and of the circuit on the achievement of true reflectionless traveling-wave amplification have not been treated and are sufficiently important to warrant further study.

Because of the strong interdependence of diode and circuit parameters and in view of the rapid progress which characterizes semiconductor-device development, it is almost impossible to predict even the near future. Whatever the trend may be, the new and original coupled-cavity-circuit approach to traveling-wave parametric amplification at microwave frequencies has been amply demonstrated in these experiments. Utilization of its advantages makes low-noise broadband amplifiers a practical possibility well beyond the centimeter-wavelength region.

Appendix

The Loaded Transmission Line

The previously described filter-circuit approach to traveling-wave parametric amplification is compared here with that using the periodically loaded, but other-

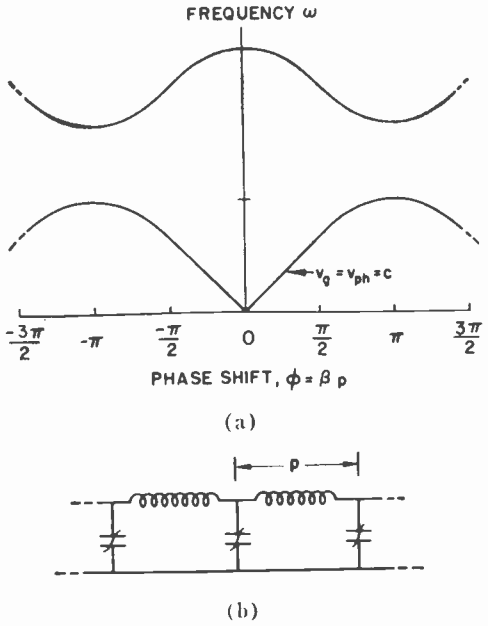

Fig. 19—(a) Brillouin diagram for loaded TEM transmission line. Bandwidth and group velocity are high and impedance is low. (b) Approximate equivalent circuit of loaded TEM line.

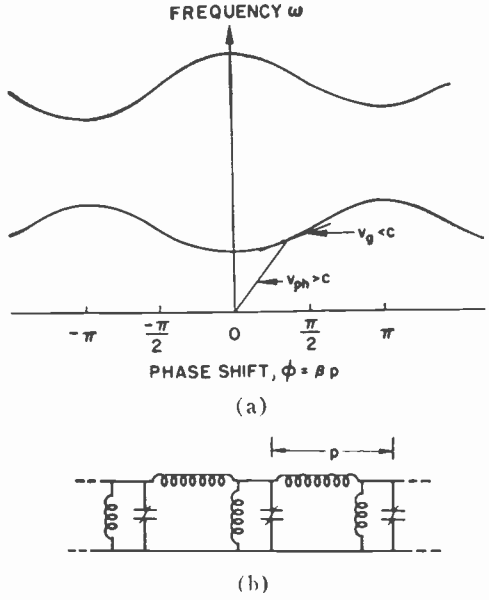

Fig. 20—(a) Effect of shunt inductance on Brillouin diagram; bandwidth and group velocity are reduced and impedance is increased. (b) Approximate equivalent circuit of inductance shunted, loaded TEM line.

wise uniform, transmission line. The Brillouin diagram and approximate equivalent circuit for such a line (in this case a TEM transmission line loaded periodically by the diodes themselves) are shown in Figs. 19(a) and (b). This model is similar to that treated by Tien[3] and others; for its detailed behavior, the reader is referred to the literature. As normally used in both theory and experiment, the diodes are separated by a distance p which is short compared with a wavelength at the signal frequency and no larger than one-quarter wavelength at the pump frequency. If the unloaded transmission line is lumped rather than distributed, Fig. 19(a) changes only in that all upper branches of the Brillouin diagram are missing. Since the group velocity in the region of low phase shift is high and in view of the previous discussion of the connection between impedance and group velocity, we would expect the impedance to be low. The bandwidth, on the other hand, is large, as can be seen from the nondispersive nature of the Brillouin diagram at low frequencies. Because of the small gain per diode to be expected from these considerations, it seems reasonable to decrease the effective mean capacitance of the line by inductances shunted across the diodes. This produces a transformation from a low-pass circuit to the band pass circuit shown in Fig. 20(b) with resulting Brillouin diagram shown in Fig. 20(a). Comparison of Figs. 19 and 20 shows that the group velocity of the latter circuit is lower, thereby increasing the impedance level and hence the gain per section or per diode. On the other hand, the bandwidth has been curtailed and the dispersive nature of the resulting filter circuit is again encountered with the associated band-edge problems already discussed. The choice of the approach to follow is usually settled by the frequency range. If the frequency is sufficiently low so that the available diodes have low loss, the use of many diodes closely spaced in a low-pass filter circuit may be the obvious choice, particularly if the high capacitance swing in the vicinity of zero bias can be employed. Remarkable results have been obtained by using this approach in the UHF range.[15] At higher frequencies and particularly well into the microwave range, where the diode Q and the effective capacitance swing are reduced, the maximum gain per diode becomes an important consideration from the standpoint of both impedance level of the circuit and the electrical length of the diode separation. The transition frequency between the loaded transmission line and filter circuit as described here is presently, and probably for some time to come, determined by the availability of high quality variable-capacitance diodes packaged with a minimum of parasitic reactance.

Acknowledgment

The degree of achievement in a novel experimental venture depends on a number of ingredients, not the least of which are analytical interpretation, continued interest, and appraisal. These were amply provided by M. R. Currie and R. W. Gould, to whom the authors express their sincere appreciation.

The authors further acknowledge the kind assistance of S. Sensiper in connection with the application of ferrites to the coupled-cavity circuit, and R. E. Johnson for his help in many measurements and mechanical design problems.

[15] R. S. Engelbrecht, "Non-Linear Reactance (Parametric) Traveling-Wave Amplifiers for UHF," presented at the Solid State Circuits Conf., Philadelphia, Pa.; February, 1959.

Regenerative Fractional Frequency Generators*

S. PLOTKIN†, MEMBER, IRE, AND O. LUMPKIN‡

Summary—**A new regenerative frequency divider circuit is presented which offers several advantages over other available circuits. These advantages are large lock-in or "stability" range, ability to produce either relatively constant output or amplitude modulated output, circuit simplicity and the fact that it is self-starting. An approximate nonlinear analysis is given which provides a reasonable prediction of the operation. This analysis is a quasi-linear, semigraphical technique which clearly shows the dependence upon diode characteristics and transistor input impedance. Results are also given for harmonic generation, in order to actually give a fractional frequency output and not merely a subharmonic.**

I. Introduction

THERE IS an increasing need at the present time for precise frequency dividers in a variety of specialized computers, precise time and frequency measuring instruments, and synchronized communication systems, to name a few applications. These dividers, or generators, must have the ability to produce an output frequency that is an exact submultiple, or fraction, of a source frequency. Of the different general types of generators that might be used, there is a particular class which is characterized by the fact that they must be excited in order to regenerate. This class was originally devised by Horton[1] in 1922, and received little attention until 1939 when Fortescue[2] discussed the class in general and Miller[3] devised a particular circuit configuration as well as a specific analysis. In recent years Hughes,[4] Tsejtlin,[5] and Butler[6] have presented further practical circuits for this class of devices, but mathematical analyses are lacking for the latter two. These latter two circuits are very similar to each other; they make use of semiconductor amplifiers and are somewhat simplified circuit-wise, as compared to the Miller generator. Hughes, on the other hand, makes use of special nonlinear resistive material to achieve harmonic generation and synthesizes his particular configuration from trigonometric identities.

The purpose of this paper is to present a further circuit simplification devised by Robuck.[7] His circuit uses only one semiconductor diode for harmonic generation and another for mixing. An analysis and experimental results are given which are in fair agreement, thus indicating the validity of using some very approximate techniques. There are several aspects to this circuit besides its simplicity which bear comment. The most important is its ability to track the input source frequency over a significant range and still remain locked to an exact submultiple. Ranges of 10 per cent are easily achieved, and with small fractional submultiple frequency generation much larger ranges of stability are possible. The general circuit configuration is the same as that of Miller; however, the specific circuit operation is different, which leads to a somewhat different analysis. The circuit presented has a small threshold level because of the inherent threshold of semiconductor diodes in the conducting region. Above that level, however, the circuit is self-starting and does not require transient or shock excitation to initiate regeneration. As the input increases in amplitude above the threshold, the output level follows almost linearly, thus allowing the possibility of amplitude modulated output. As the input increases above the point of overdriving the amplifier input, the output remains relatively constant. Thus, there is the possibility of generating a relatively constant output over a significant range of input amplitude variation; a range of 2:1 is easily achieved. Frequency modulation of the output without amplitude modulation at the same time is not possible because the output amplitude always changes with frequency.

The terms frequency divider and fractional frequency generator are almost synonymous but there is a slight difference. A frequency divider and a fractional frequency generator are identical if the fraction is of the form $1/n$, n being an integer. The two are different when the fraction is of the form p/n, where both p and n are different integers. Since it is a straightforward procedure to generate harmonics either before, after, or within a frequency divider, the resulting output frequency can always be a p/n fraction of some input frequency. Thus the divider itself is the main item of concern and the terms fractional frequency generator and frequency divider can be used interchangeably.

* Received by the IRE, April 14, 1960; revised manuscript received, August 29, 1960.

† Elec. Engrg. Dept., University of Southern California, Los Angeles, and consultant for Hoffman Electronics Corp., Los Angeles, Calif.

‡ Physics Dept., Columbia University, New York, N. Y. Formerly with Hoffman Electronic Corp., Los Angeles, Calif.

[1] J. W. Horton, U. S. Patent No. 1,690,299; 1922.

[2] R. L. Fortescue, "Quasi-stable frequency dividing circuits," *J. IEE*, vol. 84, pp. 693–698; 1939.

[3] R. L. Miller, "Fractional-frequency generator utilizing regenerative modulation," PROC. IRE, vol. 27, pp. 446–456; July, 1939.

[4] W. L. Hughes, "Analysis and performance of locked-oscillator frequency dividers employing nonlinear elements," PROC. IRE, vol. 27, pp. 241–245; February, 1953.

[5] M. Z. Tsejtlin, "Frequency dividers using semiconductor triodes," *Elektrosvyaz* (in Russian), p. 33; 1957.

[6] F. Butler, "A regenerative modulator frequency divider using transistors," *Electronic Engrg.*, vol. 31, pp. 72–75; February, 1959.

[7] E. R. Robuck, Hoffman Electronics Corp., Los Angeles, Calif., patent applied for.

II. Qualitative Circuit Operation

The general circuit configuration of Miller is given in Fig. 1. From this general configuration various specific circuits will use different elements and techniques for the different blocks. The specific circuit of Robuck is given in Fig. 2. Comparison with other circuits of this class reveals that the only difference is the method of generating harmonics and mixing.[3-6] The use of only two diodes makes for a very simple circuit; however, the nonlinear nature of the circuit operation makes analysis rather difficult. Another factor adding to the analytical difficulty is the interrelated action between different elements; in other words, the blocks of Fig. 1 are not independent.

The input, f_0, is from the "rock stable" frequency source and must also be a low impedance. Initially, the voltage amplitude of the input must be greater than the threshold of diode D_2, and as long as the gain of the amplifier is quite large there will be enough amplification to excite the output tank, f_0/n, at some frequency. Initially, there is no dc term biasing diode D_1, and if the amplification is large enough to overcome the zero biased threshold level some feedback will result which excites the idling tank,

$$\frac{(n \pm 1)}{(n)} f_0.$$

The nomenclature "idling tank" is borrowed from that of parametric amplifiers since the function here is the same. Once there is feedback, the circuit very quickly reaches steady state where diode D_1 generates an $(n \pm 1)$ harmonic from the output which appears across the idling tank. Diode D_2 mixes the idling frequency voltage with the input to give mixing products. One of the main mixing products is the difference between the idling frequency and the input frequency, which is the output frequency desired. Diode D_1 is capacitively coupled to the output tank and develops a dc voltage across R_1. This dc voltage is in a direction to back bias D_1 so that it is in a nonconducting state for most of the output cycle and the conduction of D_1 can be considered to be approximately a clipped sine wave (see Fig. 3). The harmonics generated by this clipped sine wave action are a function of the conduction angle, θ, and the conducting voltage, V. The resulting harmonic voltage across the idling tank is actually rather complicated. During conduction of D_1 a voltage builds up on the capacitor in the idling tank in a mathematically linear manner until the resulting voltage from point A to ground is greater than zero. At this time D_2 begins conducting somewhat and nonlinearly decreases the buildup of charge on the idling tank capacitor. During mixing action of D_2 the idling tank is being loaded down in a nonlinear manner. Thus the exact idling frequency voltage over an entire cycle of output is nonlinear and is not a straightforward calculation. The procedure used here is to calculate an effective value of idling frequency voltage; this is discussed later. One side of the mixing diode, D_2, is returned to ground through an RF choke so that there is no dc bias built up. The input to the amplifier is essentially a series of pulses which are then amplified to the output tank. The output will pick out the f_0/n component and the regenerative action is complete.

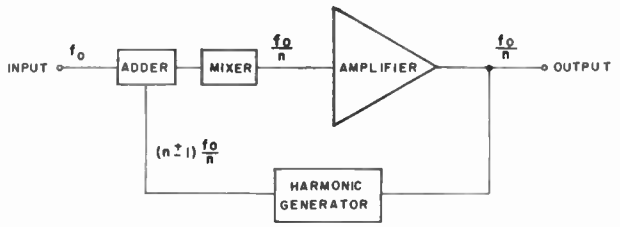

Fig. 1—Block diagram of regenerative fractional frequency generator.

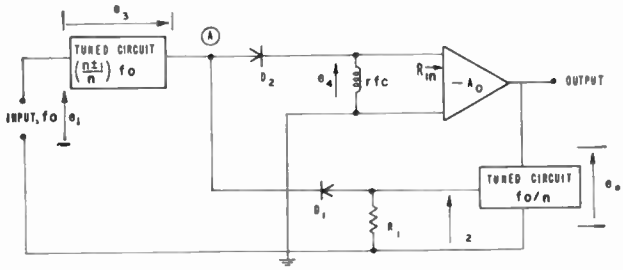

Fig. 2—Specific fractional frequency generator using simple diode harmonic generation and mixing.

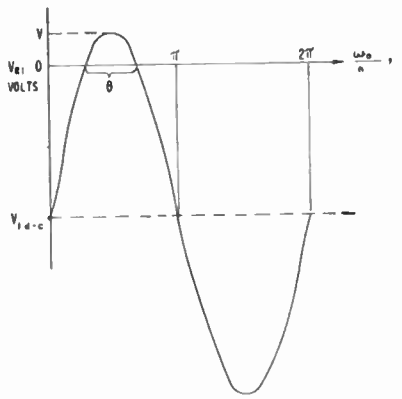

Fig. 3—Voltage across R_1.

It is noted that action of D_1 is not solely that of generating harmonics; there is also some mixing. Since the effect of dc bias on D_1 increases the higher order terms of a power series expansion while decreasing the first mixing coefficient, there is much less mixing action than with D_2 which has zero bias. However, there is some tendency to regenerate at a mixing frequency rather than at a subharmonic. It is easily seen that mixing of the output and input across D_1 will generate an idling frequency which, when mixed with the input across D_2, will support an output frequency based upon mixing

rather than harmonic generation. As long as the harmonic generation is large, the mixing across D_1 will be relatively suppressed, and the generator will lock on to the subharmonic. When the loop gain of the system is relatively large for a mixing frequency, a combination of the two frequencies results in the output. This output is then the subharmonic frequency amplitude modulated at the difference frequency between the subharmonic and the mixing frequency. The mixing frequency is a lower frequency than the natural resonant frequency of the output tank. In other words, the circuit in an excited state attempts to operate as a TGTP oscillator as well as a regenerative subharmonic oscillator.

Stability range can be considered in either of two ways. One can consider the ability of the circuit to regenerate at an exact submultiple frequency when the tuned circuits are detuned. Since there are two tuned circuits, the range of detuning can be expected to be different for each one. A second approach to the stability range is to consider the ability of the circuit to regenerate at an exact submultiple frequency when the input frequency is varied. This latter approach to stability is identical to the former approach if the tuned circuits are detuned simultaneously at a fixed rate depending upon the frequency division. Since the latter approach provides a very concise and meaningful result for measuring circuit stability, it will be used throughout this paper. It will be shown later that the two approaches are nearly identical anyway.

There must be sufficient loop gain for the output to be large enough to bias D_1 and generate a significant $(n \pm 1)$ harmonic for the idling tank. End points of the stability range are considered as the lower and upper end, and the input frequency is below and above f_0, respectively. The output tank is assumed tuned to f_0/n frequency. As the input frequency is decreased the output can go out of lock when the regenerative mixing frequency is not attenuated enough relative to the subharmonic frequency. To increase the stability range of the lower end, R_1 can be decreased. This lowers the gain of the amplifier but also reduces the dc bias on D_1, and thus generates proportionately more $(n \pm 1)$ harmonic while attenuating the regenerative mixing frequency. Another approach to increasing the lower end of the stability range is to increase the amplifier gain. This is accomplished by increasing the characteristic impedance of the output tank. Of course, a higher gain active element could also be used. The lower theoretical limit of this would be when the input frequency equals the tuned frequency of the idling tank. So far the explanation of circuit operation is quite satisfactory. The analysis of the upper end of the stability range presents some problems. The natural mixing frequency of the circuit is at some frequency close to but less than the natural resonant frequency of the output tank from TGTP oscillator considerations. The idling tank will always look inductive to the output frequency when $n > 2$. Thus, when the input frequency is greater than f_0, the output tank is on the capacitive side of resonance while the natural mixing frequency is on the inductive side of resonance. This situation leads to instability which is the condition when the output frequency is not locked precisely to the input. The only apparent explanation is that when the subharmonic is on the inductive side of resonance of the output tank, the subharmonic is in such a phase as to dominate the regenerative process. When the subharmonic is on the capacitive side of resonance of the output tank, the regenerative action is not completely dominated by the subharmonic and instability results. This explanation is qualitatively what happens, but a mathematical calculation showing the effect is lacking at the present time.

Since the upper end of the stability range is just on the high-frequency side of resonance of the output tank, the condition for maximum output voltage is very close to the upper end of this stability range. Maximum output occurs when there is maximum gain, which in turn is when the tuned circuits are operating at resonance. Also, significant frequency hysteresis is present at the upper end of the stability range.

Within the stability range of the frequency divider, the output voltage bears a near linear relationship to the input voltage as long as the amplifier is not overdriven. As the amplifier is overdriven there is a decrease in gain and the output decreases slightly, only to increase somewhat again as the input is increased. Since there is a dc term present in the mixing products of D_2, the effect is to shift the bias of the amplifier toward cutoff with the diode polarities shown in Fig. 2. The gain of the amplifier decreases as its bias approaches cutoff and, therefore, the product of the $(n \pm 1)$ harmonic and the amplifier gain tends to remain constant. This matter will be discussed in more detail later. It is sufficient to say here that the generator should work regardless of the polarity of the diodes as long as they are in the same direction in the feedback loop and the amplifier gives a 180° phase reversal. Theoretically, D_2 may be reversed if a high input impedance amplifier of positive gain is used. Any positive gain single-stage vacuum tube or transistor amplifier has a low input impedance and will not have sufficient over-all gain from point A to the output tank. Thus it would appear from the analysis presented here that a two-stage, high input impedance amplifier would work if D_2 were reversed. The input voltage and output voltage must be approximately 180° out of phase as the $(n \pm 1)$ harmonic is being generated. Otherwise D_1 would not conduct enough to generate the desired harmonic.

III. Quantitative Analysis

There are substantial difficulties which arise when attempts are made to analyze this circuit. First there is the nonlinear aspect of the components which actually

operate in their highly nonlinear regions. Secondly, there is the interaction between components because they are not isolated from each other. Attempts to change one element in general will affect the operating characteristics of one or more other elements. Several practical approaches may be used to incorporate the nonlinear elements in the analysis. All of these approaches involve linearization of one sort or another in order to use linear mathematics, except for graphical techniques. The approach used here is a piece-wise one with some graphical analysis. The diode characteristics may be expanded into a power series about the operating point. However, as the operating point or dc bias is increased into the nonconducting region, the number of significant terms in the power series increases rapidly. Therefore, only the power series expansion for D_2 will be used, and there the series is limited to only two terms in order to keep the algebra within bounds. Since only two terms are used, the coefficients will change value as the effective operating range is varied.

For determining the $(n\pm1)$ harmonic generation, an approach which attempts to evaluate the "effective" value is used. During the conduction period of D_1 in Fig. 2, the effective $(n\pm1)$ harmonic will be that component appearing from point A to ground. The input is considered to be a short circuit for this harmonic. Given the voltage fed back from the output tank and the dc bias on D_1, a clipped sine wave results, as shown in Fig. 3. As far as the $(n\pm1)$ harmonic is concerned, the idling tank itself looks like an open circuit and there is an impedance division between D_1 and (D_2+R_{in}). R_{in} is the effective ac input impedance of the amplifier. The various voltages in the circuit are defined as follows:

$$e_1 = A\cos(\omega_0 t + \phi_1) \tag{1}$$

$$e_2 = B\cos\left(\frac{\omega_0 t}{n} + \phi_2\right) \tag{2}$$

$$e_3 = C\cos\left(\frac{n\pm1}{n}\omega_0 t + \phi_3\right). \tag{3}$$

Cosine terms are used because the resulting mathematical manipulations are simplified. Appendix I shows the power series expansion as applied to the specific circuit used in the experimental confirmation of the analysis. The current through D_2 is given by

$$i_2 = a_2 e_{13} + b_2 e_{13}^2, \tag{4}$$

where e_{13} is the voltage from point A to ground or the instantaneous sum of e_1 and e_3. Of concern is the (f_0/n) component which appears at the input of the amplifier, e_4. The component is then amplified to give the output voltage, providing the amplifier operates in the linear region. The squared term of (4) gives the sum and difference frequencies as well as dc and second harmonic terms.

$$e_{13} = e_1 + e_3. \tag{5}$$

$$e_4\Big|_{\omega=\omega_0/n} = R_{in} i_2\Big|_{\omega=\omega_0/n} = b_2 \cdot 1 C R_{in}\cos\left(\frac{\omega_0}{n}t + \phi_1 \pm \phi_3\right). \tag{6}$$

The amplifier gives an additional 180° phase shift, plus ϕ_0 caused by the amplifier load impedance not being resistive. The output is therefore given by

$$e_0 = A_0 e_4 = |A_0| C \cdot 1 b_2 \cos\left(\frac{\omega_0}{n}t + \phi_1 \pm \phi_3 + \pi + \phi_0\right) \tag{7}$$

$$E_0 = |A_0| C \cdot 1 b_2, \tag{7a}$$

where the $\pm\phi_3$ is in accordance with the harmonic generated $(n\pm1)$.

The feedback voltage, e_2, is the same as the output except tapped down by the factor N.

$$e_2 = \frac{e_0}{N}. \tag{8}$$

Calculation of the idling frequency voltage is approximated for our purposes by considering the idling tank to be an open circuit during harmonic generation. A semigraphical approach is used at this point (see Appendix I and Fig. 4). During conduction of D_1, a clipped sine wave is considered to be impressed across D_2+R_{in} and the idling tank will pick out the $(n\pm1)$ harmonic. This "effective" value of idling frequency voltage is assumed to be constant over each cycle of the output. As explained in Section III, the idling frequency voltage is actually a damped wave. Thus the approach used to evaluate an "effective" quantity is only an approximate technique.

From Fig. 4 the total feedback voltage, $e_2+V_{1\,dc}$, is impressed across the diode characteristic $D_1+D_2+R_{in}$.

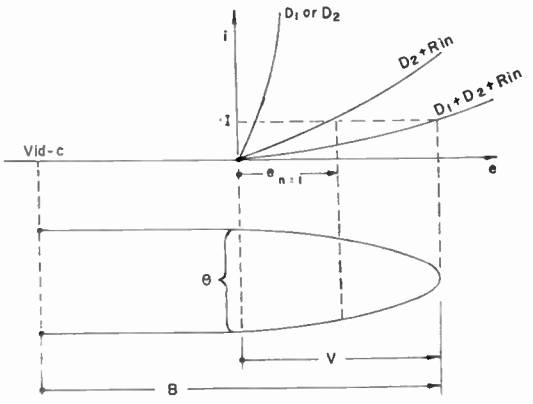

Fig. 4—Effective diode characteristic within the circuit.

This produces a clipped sine wave of peak conducting voltage V. The amount of "effective" peak voltage appearing across the idling tank is the voltage $e_{n\pm1}$ and the amount of $(n\pm1)$ harmonic present is given in Appendix II. Also given in Appendix II is the dc component in the current I. Thus the "effective" idling frequency voltage and dc bias on D_1 is given by

$$e_3 = \left(\frac{y_{n\pm1}}{y}\right)e_{n\pm1} \cdot \cos\left[\left(\frac{n\pm1}{n}\right)\omega_0 t + (n\pm1)\phi_2 + \phi_{30}\right] \quad (9)$$

$$V_{1\,dc} = \left(\frac{y_0}{y}\right)IR_1. \quad (10)$$

The additional phase shift, ϕ_{30}, is included to account for phase shifts introduced in generating the idling frequency besides the normal phase shift of the output. Since any reference may be chosen from which to measure phase shifts, it is convenient to use the output and let ϕ_2 equal zero. The harmonic generation is essentially of a cosine type, the choice of cosines in the first place therefore avoids adding a $\pi/2$ for ϕ_2.

$$\phi_2 = 0 \quad (11)$$

$$\phi_3 = (n\pm1)\phi_2 + \phi_{30} = \phi_{30} \quad (12)$$

$$C = \left(\frac{y_{n\pm1}}{y}\right)e_{n\pm1}. \quad (13)$$

It is pointed out that a change in R_1 produces a change in back bias on D_1 which in turn changes the $e_{n\pm1}$ quantity. For values of θ in the operating region, the value of $(y_{n\pm1}/y)$ changes only slightly and there is a negative feedback effect tending to make the "effective" idling frequency voltage constant. In actual practice there is an additional effect from the dc component of (D_2+R_{in}) mixing. This dc component provides a bias shift on the amplifier toward the cutoff region which reduces the amplifier gain, A_0, as the input is increased. This makes the product, A_0C, approximately constant. The constancy of this product is assumed in the analysis. From (2), (7), (8), (11), and (12) the feedback voltage and phase relations are determined.

$$B = \frac{|A_0|CAb_2}{N} \quad (14)$$

$$\phi_2 = \phi_1 \pm \phi_{30} + \pi + \phi_0 = 0. \quad (15)$$

One conclusion is immediately obvious from the above results, and that is the choice of idling frequency. Either $(n+1)$ or $(n-1)$ may be used and the circuit will function properly. However, it is apparent from Appendix II that the $(n+1)$ harmonic will have lower amplitude than the $(n-1)$ harmonic, and from (8) and (14) that the output will be proportionately lower with the $(n+1)$ harmonic idling frequency. In one reference[8] the comment is made that a regenerative divider of this class will not work with $(n+1)$ harmonic generation. This statement is not true and the argument used to support the statement only proves that with pure harmonic generation (no mixing in the feedback loop) regeneration can only occur at the f_0/n output frequency.

Eq. (15) shows that when the tuned circuits are at resonance and there is negligible phase shift in the coupling capacitors, the output will be 180° out of phase with the input. Also, the additional phase shifts ϕ_{30} and ϕ_0 are usually rather small so that the 180° phase between input and output is approximately maintained over the stability range.

Amplifier gain, A_0, cannot be calculated readily. This is caused by the nonlinear loading of D_1 conduction on the output tank. It appears that an experimental value of gain is the easiest approach to use. However, there is a linearized approach which can be used. Using the power series expansion coefficients of $(D_1+D_2+R_{in})$, the first term, a_1, is the effective admittance of the diodes during conduction. The effective linearized impedance, $(1/a_1)$, can then be divided by the fraction of a cycle that D_1 is conducting.

$$R_{11} = \frac{360°}{0} \times \frac{1}{a_1}. \quad (16)$$

This impedance is in parallel with R_1 and the parallel combination is reflected by the square of the step-up ratio from feedback to output across the output tank. Thus the total effective load impedance to the amplifier is the parallel combination of three parallel impedances reflected across the output tank.

$$R_L = \frac{Q_{f_0/n\ tank}\,R_0 \times N^2\,\dfrac{R_{11}R_1}{R_1+R_{11}}}{Q_{f_0/n\ tank}\,R_0 + N^2\,\dfrac{R_{11}R_1}{R_1+R_{11}}}. \quad (17)$$

In (17), R_0 is the characteristic impedance of the output tank, $\sqrt{L_0/C_0}$, and $Q_{f_0/n\ tank}$ is the effective Q of that tank when placed in the output circuit without feedback. Another expression for the same quantity is obtained by measuring an effective Q of the output tank with the feedback loop broken at the amplifier input and this broken end replaced with a resistance to ground equal to R_{in}.

$$R_L = Q_{eff\ (f_0/n)\ tank}R_0. \quad (18)$$

An effective value for the Q of the idling tank can be obtained which results in an expression similar to (16). D_2 conducts for one-half of the time so that the average impedance, R_2, shunting the idling tank is twice the lin-

[8] J. Millman and H. Taub, "Pulse and Digital Circuits," McGraw-Hill Book Co., Inc., New York, N. Y., pp. 382–384; 1956.

earized impedance of (D_2+R_{in}).

$$R_2 = \frac{2}{a_2} \tag{19}$$

$$Q_{(n\pm1/n)\text{ tank}} \approx \left(\frac{n \pm 1}{n}\right)\omega_0 C_{(n\pm1)/n} R_2 = \frac{R_2}{R_{0_{\text{idle}}}} \tag{20}$$

$R_{0_{\text{idle}}}$ is the characteristic impedance of the idling tank. Eq. (20) is based upon the effective parallel impedance of the idling tank at a resonance which is much greater than R_2. In the circuit of Fig. 2, $Q_{(n\pm1/n)\text{tank}}$ will always be rather low because R_2 is low.

As a consequence of (19) and (20) the two approaches to the stability range are essentially identical. Detuning the output tank is approximately the same as changing the input frequency, as long as the tuning of the idling tank has only a second-order effect. Since it is possible to use a relatively large characteristic impedance for the output tank and R_1 can be reduced to a relatively small value, there is a maximum theoretical stability range. The generator can theoretically be made to track the input frequency from the point where the output tank is tuned to $1/n$ times the input frequency to the point where the input frequency is equal to the idling tank frequency. When the input frequency is equal to the resonant frequency of the idling tank, no voltage appears at point A.

Per cent max theoretical stability range

$$= \frac{2 \times \dfrac{f_0}{n}}{f_0} \times 100 = \frac{200 \text{ per cent}}{n}. \tag{21}$$

In (21) f_0 is the center frequency of the stability range. Thus, if n equals 4, a stability range of 50 per cent might be possible. In practice a range of near 30 per cent was achieved. The major reason for not obtaining a larger range was that as one approaches the upper end the circuit began dividing by 5 rather than 4. However, ranges of 25 per cent are easily achieved for n equal to 4. Another circuit which used an n of 10 easily obtained a stability range of 13 per cent and no attempt was made to maximize it.

A further point of interest is the amount of idling frequency there is in the output circuit, so that an $(n-1/n)$ fractional frequency generator can be obtained. In this regard the additional tuned circuit that is placed in the output cannot present too large an impedance at the idling frequency because a TGTP oscillator would result. Therefore a small pick-off winding can be used with a high impedance tuned secondary. The output obtained from the $(n\pm1/n)$ component of amplifier input voltage is given by

$$C_{0(n\pm1/n)} = Ca_2 R_{in} \cdot A_{0(n\pm1/n)} \cdot N_{(n\pm1/n)}, \tag{22}$$

where $A_{0(n\pm1/n)}$ is the gain of the amplifier to the $(n\pm1/n)$ frequency and $N_{(n\pm1/n)}$ is the turns ratio or coupling from the output circuit to the secondary of the $(n\pm1/n)$ tuned circuit. For a transistor amplifier in the common emitter configuration a further relationship is given by

$$A_{0(n\pm1)/n} \cdot N_{(n-1)/n} \approx \frac{KR_{L(n-1)/n}}{N_{(n-1)/n}} \cdot \frac{f_{c0\beta}}{\sqrt{\left[f_0\left(\dfrac{n \pm 1}{n}\right)\right]^2 + f_{c0\beta}^2}}. \tag{23}$$

where K is a constant for the particular transistor used, $R_{L(n-1/n)}$ is the effective parallel impedance across the secondary winding, and $f_{c0\beta}$ is the β cutoff frequency of the transistor. A similar approach can be used for any of the mixing products available at the amplifier input. It is noted that if the product A_0C remains constant, the idling frequency output varies only as the power series coefficient, a_2. Since a_2 varies with voltage drive, the idling frequency output will vary with input voltage. If other mixing product outputs are used, more power series coefficients may be required in addition to the two obtained in Appendix I.

IV. Design Procedure and Experimental Results

A systematic design procedure can be outlined for the particular circuit configuration considered here, although some intuition is required in selecting starting points. A choice of diodes, amplifier and tap point, and characteristic impedance of the output tank is required. The diodes should be as nonlinear as possible, but are not critical. The amplifier should have as large a gain as possible, but this also is not critical as long as it is above some minimum value and maximum stability range is not required. Tap point, N, on the output tank is determined by the sensitivity of the over-all generator as well as the stability range. In the experimental work which has been done an N of 2:1 is approximately the optimum for the usual considerations. The approximate 0.1-volt threshold level of the diodes makes the sensitivity somewhat fixed and not too dependent upon N. When choosing the characteristic impedance of the output tank, the choice is between stability range and output waveform. With a small characteristic impedance the output waveform can be very nearly a pure sine wave with a somewhat decreased stability range.

Once a choice of components and voltage supply has been made, the procedure is to calculate the $(n-1)$ harmonic for an output at midrange. From (8) and (14) a plot of output vs input can be obtained, assuming A_0C to be a constant. Another approach might be to determine the gain, A_0, required for a given input and output desired. This gives a determination of output-tank characteristic impedance to be used, since R_{in} of the ampli-

fier must remain fixed. The driving voltage on (D_2+R_{in}) to evaluate the power series coefficients is taken to be $A+C/\sqrt{2}$.

For an example of the design procedure, the circuit of Fig. 5 will be used. The following data are assumed as a design point:

$E_0 = 8$ volts

$N = 2$

$B = 4$ volts

$\theta = 90°$ [from Appendix II, Fig. 13 for $(n-1)=3$]

$$R_{in|2N332\ transistor} = 600 \text{ ohms.}$$

For the value of C, Fig. 10 in Appendix I is used.

$$V_{1dc} = B\cos\frac{\theta}{2} = 2.8 \text{ volts}$$

$$V = B - V_{1dc} = 1.2 \text{ volts.}$$

From Fig. 10 the peak voltage across (D_2+R_{in}) can be determined for the particular diodes and amplifier chosen.

$$e_{n-1} = 0.8 \text{ volt}, \qquad I = 0.8 \text{ ma.}$$

From Fig. 13 the harmonic components are found.

$$\left(\frac{y_3}{y}\right)_{\theta=90°} = 0.18, \qquad \left(\frac{y_0}{y}\right)_{\theta=90°} = 0.165.$$

From (10) and (13)

$$R_1 = \frac{2.8}{0.8\times10^{-3}\times0.165} = 21.2K$$

$$C = 0.144 \text{ volt.}$$

The amplifier gain bears an approximate constant relationship with the output load impedance. Design center parameter values are assumed, frequency of operation is far below cutoff, and Z_L is the effective load impedance in the collector circuit.

$$A_{0|2N332} \approx 0.022Z_L.$$

Various approaches can be used to determine either A_0 directly or R_L, which would be Z_L when the output tank is tuned to resonance. Eq. (18) was used here.

$$R_L = Q_{eff}R_0 = 14\times650.$$

In this case an effective Q of the output tank was measured experimentally in the circuit with $R_1 = 21.2K$. R_0 is the characteristic impedance of the output tank, $\sqrt{L_0/C_0}$.

The amplifier gain is then determined.

$$A_0 = 0.022\times14\times650 = 201.$$

Assuming that A_0C is a constant over the linear range, from (2), (8), and (14)

$$e_0 = 201\times0.144\times600\times10^{-2}\left(\frac{b_2}{10^{-3}}\right)e_1$$

$$= 17.3\left(\frac{b_2}{10^{-3}}\right)e_1. \tag{24}$$

It is pointed out that the transistor used for this experimental verification had an input impedance, R_{in}, approximately in agreement with the value calculated from manufacturers, design center parameters. Additional 2N332 transistors checked later showed a considerably increased input impedance. A change in R_{in} seriously affects the diode characteristics in Appendix I and will therefore significantly affect the calculated results. Larger input impedances produce larger output voltages and smaller stability ranges. Vacuum tube amplifiers would not have this variation from one tube to another.

Eq. (24) is plotted in Fig. 6 which shows a fair agreement in the linear range and considerable deviation in the overdriven range where (A_0C) is not a constant. In the range of large input voltages the amplifier gain decreases very rapidly.

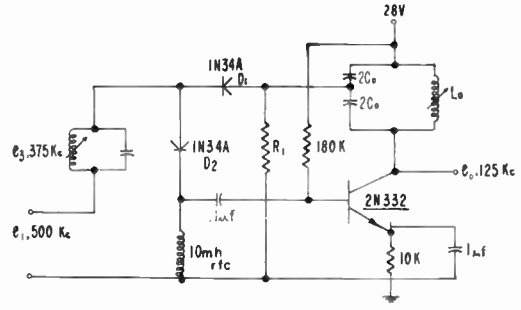

Fig. 5—Specific circuit for $n=4$.

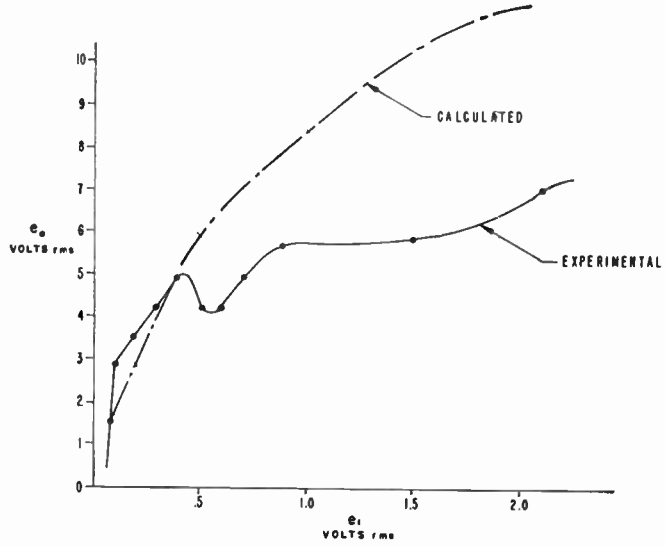

Fig. 6—Output at frequency ω_0/n vs input at frequency ω_0.

It is also possible to show the correlation between calculated and experimental values for an output of $(n-1/n)f_0$ frequency. Using (22) and (23), the value of the $(n-1)$ harmonic which is calculated above, and the load impedance across the tuned output circuit, the output for an $(n-1/n)$ fractional frequency generator can be determined (see Fig. 7).

$$R_{L(n-1/n)} = Q_{(n-1/n)}R_{0(n-1/n)} = 60 \times 800 = 48K$$

$$N_{(n-1/n)} = 3.$$

The Q of the $(n-1/n)$ output tank was measured and the characteristic impedance calculated.

In the particular circuit used here, the idling frequency is somewhat above the amplifier cutoff frequency so that (23) must be used as it stands.

$$f_{c0} = 280 \text{ kc}, \qquad C = 0.144 \text{ volt}$$

$$A_{0(n-1/n)}N_{(n-1/n)} \approx 0.022 \times \frac{48{,}000}{3} \times \frac{280}{\sqrt{375^2 + 280^2}} = 210$$

$$e_{0(n-1/n)\text{rms}} = \frac{0.144 \times 600 \times 210 \times 10^{-3}\left(\frac{a_2}{10^{-3}}\right)}{2} = 12.55\left(\frac{a_2}{10^{-3}}\right). \tag{25}$$

Eq. (25) is plotted in Fig. 8, and again the overdriven region shows a much smaller output compared with the calculated values, assuming A_0C to be constant.

V. Conclusions

A new circuit configuration for fractional frequency generation has been presented. Experimental confirmation of the theoretical analysis is reasonably good, indicating the validity of the analysis. The most important features of the generator are perhaps twofold. The simplicity of the circuit and the use of readily available components effect ease of fabrication. The stability range possible with this particular frequency divider is much greater than with any others presented to date. This stability range can be increased at the expense of sensitivity (output for a given input) and output waveform. To increase the stability range the characteristic impedance of the output tank may be increased and less bias can be developed across the harmonic generating diode. Both of these changes deteriorate the output waveform. Conversely, larger bias on the harmonic generating diode produces less loading of the output tank with larger output amplitude, better output waveform and less stability range resulting.

Further features of this new frequency divider include its ability to pick off additional mixing products in the output circuit. This aspect is a feature present in all the fractional frequency generators in this general class. Also, there is the ability to provide an amplitude modulated output at the subharmonic frequency which follows almost linearly the amplitude of the input. In addition, the input can be increased to the point where the amplifier is overdriven and resulting output will be somewhat constant over a wide range of input voltage levels.

Analysis of this new circuit configuration involves the use of some very approximate techniques, including the assumption that the product of idling frequency amplitude and amplifier gain remains constant. This assumption and the approximate technique appear to be reasonably valid over the linear range of amplifier operation but give errors of as much as 40 per cent in the overdriven region. Attainment of the maximum theoretical stability range is not achieved for small division ratios but becomes easier as the division ratio is increased. One difficulty of the analysis as presented is the necessity of knowing the diode characteristics in the region about zero voltage and current. Published manufacturers' data are not abundant and one is always plagued by the variations between diodes caused by manufacturing tolerances. Thus, significant errors can be introduced even though the approximate techniques and assumptions are valid.

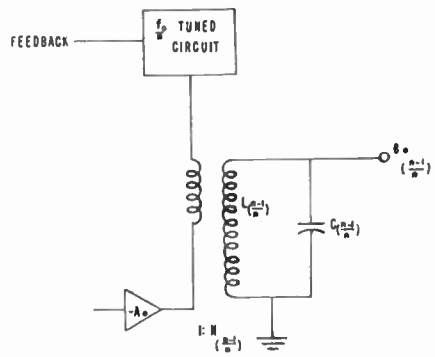

Fig. 7—Output for $(n-1)/n)$ fractional frequency generator.

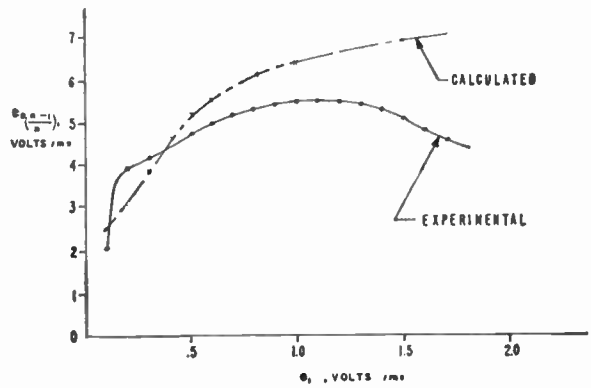

Fig. 8—Output at frequency $(n-1)/n)f_0$ vs input at frequency f_0.

Appendix I

Power Series Coefficients for Semiconductor Diodes with Loading

Several approaches can be used for mathematically representing the operation of a simple series diode configuration. These include an infinite power series expansion, piece-wise linearization, and graphical analysis. An infinite power series can be limited to several terms which can give a fairly good representation of the actual characteristic over a large range. If the diode is biased, however, the number of terms required for good representation increases appreciably and the resulting algebra becomes excessive. The use of piece-wise linearization for mixing when the mixer sources are close in both amplitude and frequency is rather complicated. Therefore, a two-term power series is used to calculate the mixer action and a combination of graphical analysis and piece-wise linearization is used to compute the effective harmonic generation. The piece-wise linearization is limited to two pieces and is treated in Appendix II for harmonic generation.

Because the power series for mixer action is limited to only two terms, the effective coefficients will change with the amplitude of the driving source. The diode characteristic with loading is represented by

$$i = ae + be^2. \tag{26}$$

As shown in Fig. 9, the diode characteristic is considered to be two straight lines over the effective voltage drive assumed. The assumed characteristic shows a finite resistance in the forward direction and an infinite resistance in the reverse direction. Various values of a and b can then be determined as a function of e. It is noted that within the effective range of $+e_1$ to $-e_1$, the accuracy of the power series as compared to the actual characteristic is better than the linearized characteristic.

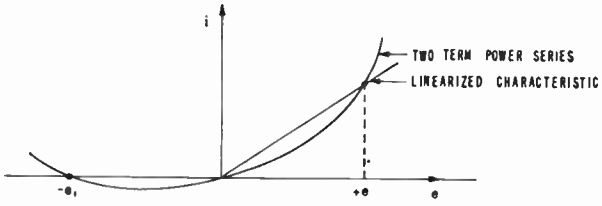

Fig. 9—Comparative accuracy of power series expansion with linearized characteristic over the effective driving angle, $+e$ to $-e$.

Figs. 10 and 11 are plotted for the actual components used in the circuit of Fig. 5. The coefficients a_1 and b_1 refer to the $(D_1+D_2+R_{in})$ characteristic and the coefficients a_2 and b_2 refer to the (D_2+R_{in}) characteristic. In the analysis b_1 is not used at all and a_1 only appears in (16) and (17), which are usually not used in favor of (18). In Fig. 10 the abscissa refers to the instantaneous voltage across the diode configuration, whereas in Fig. 11 the abscissa is the effective voltage or the voltage at which the coefficients were evaluated.

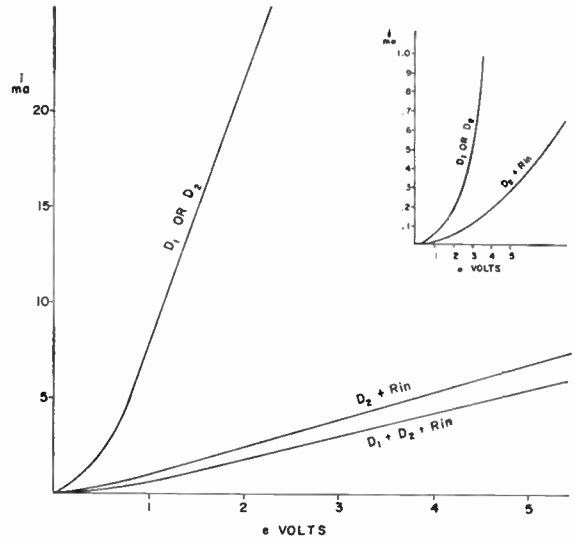

Fig. 10—1N34A characteristic at 29°C.

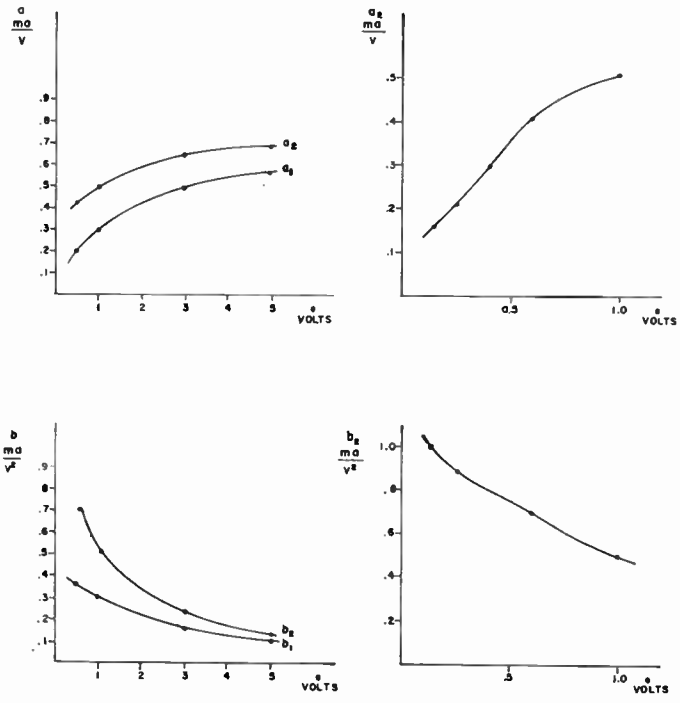

Fig. 11—Curves for particular 1N34A design.

Appendix II

Harmonic Components of a Clipped Sine Wave

Given a clipped sine wave as shown in Fig. 12, the harmonic components are readily calculated and plotted vs the conduction angle[9] (see Figs. 13 and 14).

The conducting part of the clipped wave is expressed by

$$y(t) = y_0 + \sum_{n=1}^{\infty} y_n \cos n\omega\,. \tag{27}$$

[9] F. E. Terman, "Radio Engineers Handbook," McGraw-Hill Book Co., Inc., New York, N. Y., pp. 20–22; 1943.

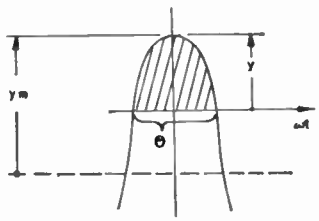

Fig. 12—Clipped sine wave.

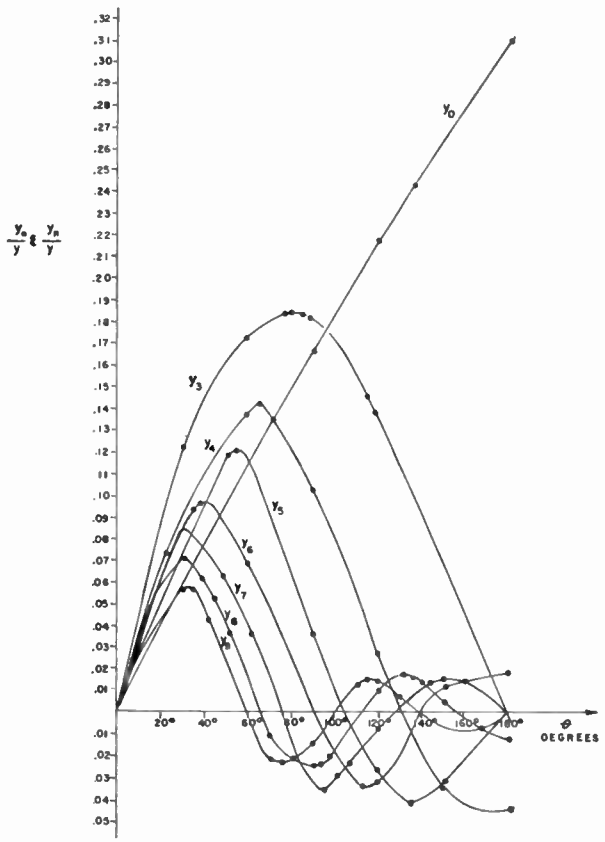

Fig. 13—Harmonic components of a clipped sine wave; fraction of conducting amplitude vs conducting angle.

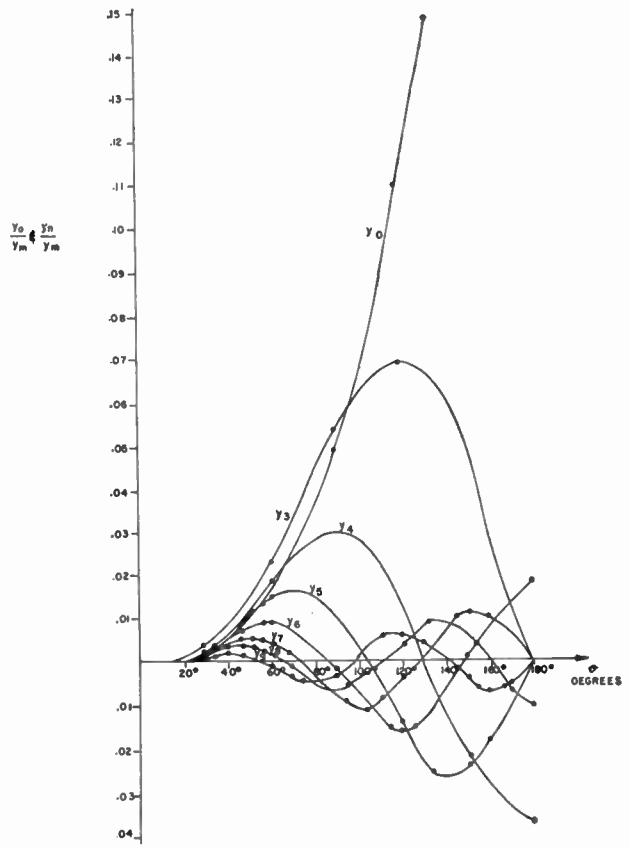

Fig. 14—Harmonic components of a clipped sine wave; fraction of sine wave peak vs conducting angle.

where the components are given as follows:

$$y_0 = \frac{y_m}{2\pi}\left[2\sin\frac{\theta}{2} - \theta\cos\frac{\theta}{2}\right] \tag{28}$$

$$y_n = \frac{y_m}{\pi}\left\{\frac{\sin\left[(n+1)\frac{\theta}{2}\right]}{n+1} + \frac{\sin\left[(n-1)\frac{\theta}{2}\right]}{n-1} - \frac{2\sin\left(\frac{n\theta}{2}\right)\cos\left(\frac{\theta}{2}\right)}{n}\right\} \tag{29}$$

$$y_m = \frac{y}{1-\cos\left(\frac{\partial}{2}\right)}. \tag{30}$$

The maximum value of y_n/y_m occurs when

$$f(\theta) = \frac{\cos(n+1)\frac{\theta}{2}}{2} + \frac{\cos(n-1)\frac{\theta}{2}}{2} - \cos\left(\frac{n\theta}{2}\right) + \frac{\sin\left(\frac{n\theta}{2}\right)\sin\left(\frac{\theta}{2}\right)}{n} = 0. \tag{31}$$

ACKNOWLEDGMENT

Helpful suggestions and illuminating discussions with E. R. Robuck, J. Raymond, R. Daniel, and R. McGaughey are gratefully acknowledged. Edith Rottersman typed the report and performed some of the calculations in Appendix II. E. W. Mehner, the section manager under whose direction this project was carried out, provided considerable encouragement.

An Improved Decision Technique for Frequency-Shift Communications Systems*

ELMER THOMAS†, MEMBER, IRE

Summary—This paper describes a new circuit technique called a decision threshold computer, which enables a frequency-shift-keyed receiver system to use information in mark and space channels independently, resulting in an improvement in circuit quality where fading exists between the mark and space frequencies.

Frequency selective fading observed on ionospheric-scatter circuits and on high-frequency communication circuits is discussed. The results of a correlation study are presented which show such fading to be relatively uncorrelated a large portion of the time.

Typical FSK demodulators, with a fixed decision level set halfway between the long-term average amplitudes of the received mark and space frequencies, are shown to result in a high error liability when deep fades occur on either the mark or space frequency. It is further shown that such errors are unnecessary since the complete message is available on either frequency.

The device discussed in this paper has been designed to make use of the normally deleterious effects of frequency selective fading, to provide up to a 30-fold reduction in teleprinter error rates over that which is theoretically possible when flat fading is assumed. Additional orders of diversity are shown to result where low correlation exists between the mark and space frequencies.

Theoretical error rate equations and resulting error rate curves for the new technique are compared with those resulting from a fixed threshold device of conventional design. Such comparison indicates a 6- to 15-db improvement for situations where dual-space diversity is not feasible, and from 2 to 5 db where the variable threshold technique is used in conjunction with dual-space diversity systems.

Design considerations for this variable decision threshold device are presented. Results of an extensive laboratory and field test program are given, which show good agreement with that predicted by theory. The application of this device to several ionospheric-scatter circuits is shown to have resulted in significant improvements in traffic quality, further verifying the theory and demonstrating the practicability of this technique. Additional data are supplied, illustrating the results of the variable decision threshold technique applicable to high-frequency radio communication circuits. Examples are given where application of this technique has resulted in error rate reduction of from 10 to 30 fold, corresponding to a 10- to 16-db improvement in signal detectability.

Introduction

THE purpose of this paper is to present a new circuit technique called a Decision Threshold Computer (DTC). The decision threshold computer is a device which automatically adjusts, according to predetermined criteria, the binary decision level on a signal perturbed by frequency-selective fading. Although this technique is adaptable to many types of data transmission systems, this paper shall deal in particular with its use on frequency-shift-keyed (FSK) systems.

In recent years, a number of papers have appeared on the optimum detection of FSK signals. This paper will review FSK signal characteristics and the conventional receiver design resulting from optimum detection studies. Differences between fading characteristics assumed in theory and those existing in practice will be explored and the effects of these differences will be presented. A new decision technique, based on the modified theory, will be described and data will be presented comparing a conventional system and the new system.

Statement of Problem

An FSK radio signal is a signal in which binary information is coded in a manner such that a "1" or a mark is transmitted on one frequency, and a "0" or space is transmitted on an adjacent frequency.

The optimum decision system, as determined by Middleton and Van Meter[1] for the detection of FSK signals in the presence of Gaussian noise and flat Rayleigh fading, computes the ratio of the probability of receiving a mark to the probability of receiving a space. The mark-space decision process, used in FSK demodulators, is frequently an approximation to the optimum criterion.

Fig. 1 illustrates a typical FSK receiving system.

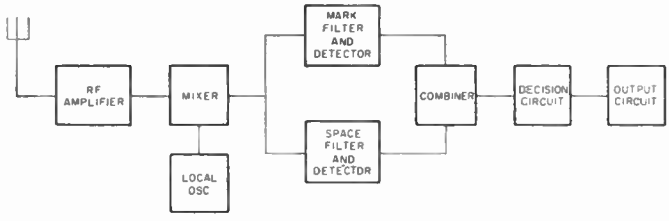

Fig. 1—Typical FSK linear receiver.

This receiver consists of dual filter channels, with one filter tuned to the mark frequency and the second filter tuned to the space frequency. The process of deciding whether a mark or space has been received normally consists of determining which filter has the greater output. Conventionally this is done simply by causing the mark filter to provide a positive output and the space filter to provide a negative output. The two outputs are then combined in such a manner that a decision or trigger circuit will provide a mark output if the combined signal is positive, and a space output if it is negative.

* Received by the IRE, May 16, 1960; revised manuscript received, September 2, 1960. The work reported in this paper was supported in part by the Signal Corps under contract DA 18-119-sc-449.

† Page Communications Engineers, Inc., Washington, D. C.

[1] D. Middleton and D. Van Meter, "Modern statistical approach to reception and communication theory," IRE TRANS. ON INFORMATION THEORY, vol. IT-4, pp. 119–146; September, 1954.

In determining the optimum FSK decision criteria, signal amplitudes and noise levels are generally assumed to be the same for the mark and space channels. The resulting system performs well where flat fading exists, but produces a high error liability when deep fades occur on either frequency. The entire message, however, is available on either frequency since in an FSK system the data transmitted on the mark frequency are exactly complementary to those transmitted on the space frequency. Decision ambiguity or failure, therefore, need not occur unless signals on both frequencies fade simultaneously. It seems obvious that if the fading of the two frequencies is relatively independent, a potential frequency diversity advantage is obtainable with existing FSK transmissions. The indicated diversity advantage is not realized with a predetermined, fixed, decision threshold.

The magnitude of shift employed in frequency shift communications varies widely among systems. In general, it might be expected that, the greater the shift employed, the less would be the correlation of fading on the separate frequencies. Recent observations on a predominantly single-hop HF circuit, indicate that a high degree of selective fading exists on systems using shifts as narrow as 350 cycles. Fig. 2 presents data taken on a relatively short HF path over a four-day period.

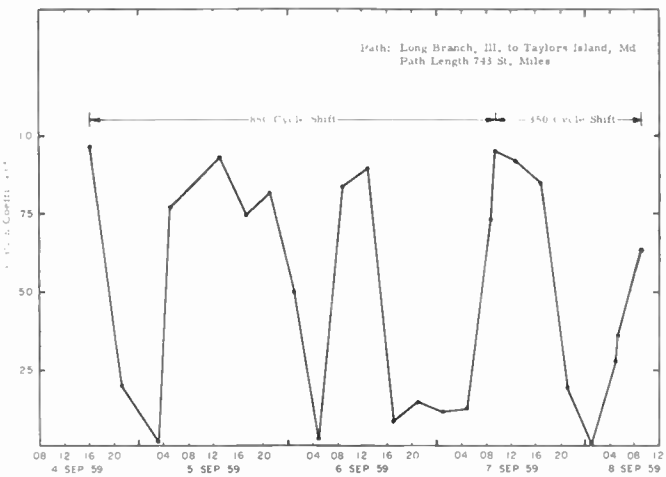

Fig. 2—Frequency correlation at 5 Mc.

The high correlation occurring during the midday period is probably brought about by dense D-layer ionization resulting in absorption of the higher-order modes. Low correlation is observed during the hours of darkness and is believed to result from multiple path interference, observed with reduced D-layer ionization.

Under conditions of selective fading, a fixed "zero" decision threshold can no longer be optimum. That this is true may best be shown by considering the extreme case illustrated in Fig. 3, which represents a detected FSK signal. The signal on the space frequency is shown as being reduced to zero amplitude, as a result of frequency selective fading, while the mark frequency remains at a high level. Decision failure occurs at the time indicated. If now the decision threshold is shifted to center, approximately half way between the two peaks of the received signal, the decision ambiguity is removed. In order for failure of the variable decision threshold to occur, the signal must fade simultaneously on both frequencies.

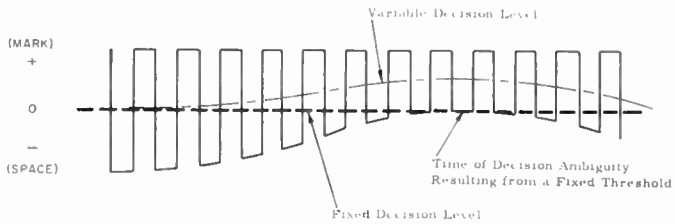

Fig. 3—Decision threshold effects for selectively fading FSK signals.

Theoretical Improvement

Where the fading of the separate mark and space frequencies is uncorrelated, simultaneous fading will rarely occur and the variable decision threshold technique would exhibit a diversity advantage. The mathematics required to derive a rigorous expression for the theoretical improvement of a variable threshold over a fixed threshold are involved and difficult to evaluate. An approximation to the theoretical improvement, however, may be more easily derived by considering the FSK signal as consisting of two separate AM signals. If the correlation of fading between the two frequencies is relatively independent, the probability of error should approximate that of two receivers working from diversity antennas on an on-off keyed (AM) signal.

Montgomery[2] has derived the following expressions for error probability in a nondiversity (AM) carrier binary system employing envelope detection:

$$P_{T,N+S} = 1 - \exp\left(-\frac{T^2}{N_0^2 + S_0^2}\right) \tag{1}$$

and

$$P_{N,T} = \exp\left(-\frac{T^2}{N_0^2}\right) \tag{2}$$

where

N_0^2 = long-term, mean-square value of noise envelope,
S_0^2 = long-term, mean-square value of carrier envelope,
T = threshold amplitude,
$P_{T,N+S}$ = probability that the signal plus noise is less than the threshold during a carrier-on or mark transmission,
$P_{N,T}$ = probability that the receiver output exceeds the threshold during a carrier-off or space transmission.

[2] G. F. Montgomery, "A comparison of amplitude and angle modulation for narrow band communications of binary-coded messages in fluctuation noise," Proc. IRE, vol. 42, pp. 447–454; February, 1954.

Extending Montgomery's expressions to an nth order diversity system which selects the receiver having the largest instantaneous output

$$P_{(n)T,N+S} = \left\{1 - \exp\left[-\frac{T^2}{N_0^2(1+R)}\right]\right\}^n \quad (3)$$

$$P_{(n)N,T} = 1 - \left\{1 - \exp\frac{-T^2}{N_0^2}\right\}^n \quad (4)$$

where

$$R = \frac{S_0^2}{N_0^2}.$$

$P_{(n)T,N+T}$ = the probability that the outputs of (n) receivers are simultaneously less than or equal to the threshold during a carrier-on transmission,

$P_{(n)N,T}$ = the probability that the output of at least one receiver is greater than or equal to T during a carrier-off transmission,

n = the order of diversity.

Assuming equal *a priori* probability for mark and space, the probability of error becomes

$$P_{(n)e} = \frac{1}{2}\left\{1 - \exp\left[-\frac{T^2}{N_0^2(1+R)}\right]\right\}^n + \frac{1}{2}\left\{1 - \left[1 - \exp\frac{-T^2}{N_0^2}\right]^n\right\}. \quad (5)$$

For a given average signal-to-noise ratio, the probability of error will be a minimum only at a specific threshold. The optimum value of threshold is determined by taking the derivative of the probability of error $P_{(n)e}$, with respect to T^2/N_0^2 and equating to zero.

$$\frac{d\left[P_{(n)e}\right]}{d\left[\frac{T^2}{N_0^2}\right]} = (N-1)\ln\left\{\frac{\left[1 - \exp\frac{-T^2}{N_0^2(R+1)}\right]}{\left[1 - \exp\frac{-T^2}{N_0^2}\right]}\right\} + \left(\frac{T^2}{N_0^2}\right)\left(\frac{R}{R+1}\right) - \ln(R+1) = 0. \quad (6)$$

The above is a transcendental equation which cannot be solved explicitly for the optimum threshold. A digital computer was used to search for that value of T^2/N_0^2 which satisfies (6) for specific values of R ranging from 5 to 40 db. These optimum values of T^2/N_0^2 were then used to evaluate (5) for dual AM diversity ($n=2$) and quadruple AM diversity ($n=4$). The resulting curves are shown in Fig. 4 and are labeled "Dual Diversity AM" and "Quadruple Diversity AM." Theoretical performance curves for nondiversity FSK and dual diversity FSK are also plotted in Fig. 4 for comparison with the theoretical AM performance. Theory indicates that, at binary error rates of one in ten thousand, processing the signal frequencies separately as dual diversity AM signals will, in the absence of multipath, result in a reduction of approximately 11 db in the required signal-to-noise ratio as compared to that necessary for the FSK decision. Similarly for the dual space diversity case, quadruple AM is approximately 3-db superior to the FSK case at the one in ten thousand binary error rate.

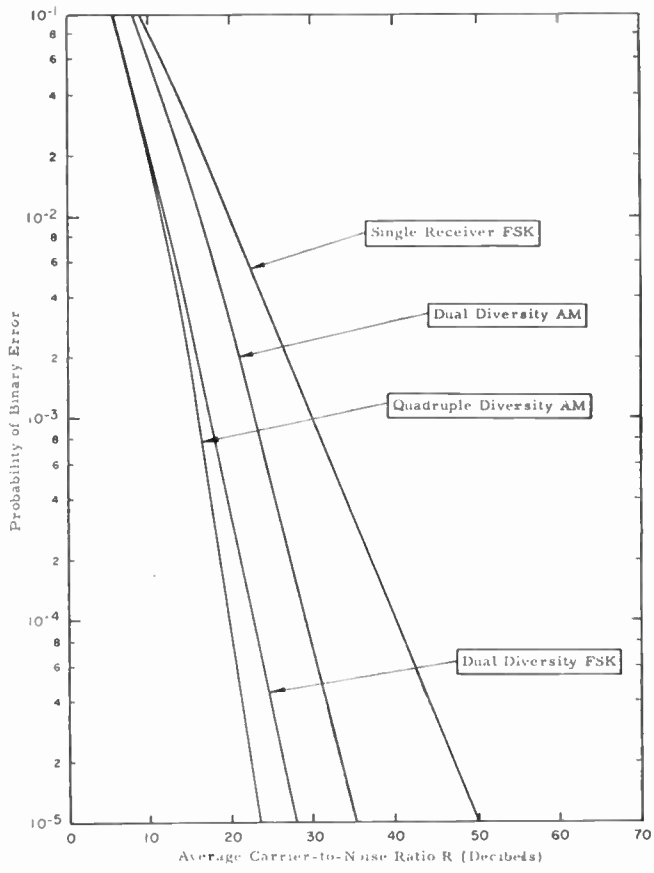

Fig. 4—Theoretical performance of FSK and AM diversity systems.

Operationally, it has been found that the automatic decision level adjustment would yield a greater improvement than that indicated by theory, by compensating for unbalance of the demodulator channels.

Theory of Operation

A large part of the potential diversity advantage can be achieved with simple and inexpensive circuitry, which would cause the received signal to center about a fixed threshold. If the transmission were limited to reversal keying, the desired effect could be accomplished with an RC high-pass filter which would average mark and space amplitudes.

Unfortunately, transmission systems are not limited to reversal keying. If RC coupling were to be used in practice, a varying mark-space duty factor would cause the decision threshold to vary from the desired level. A circuit which more closely approximates the desired operation is the dual clamp circuit, shown in Fig. 5. This approach was used by Allnatt, Jones and Law[3] in a

[3] J. W. Allnatt, E. D. Jones, and H. B. Law, "Frequency diversity in the reception of selectively fading binary frequency modulated signals," *Proc. IEE*, vol. 104B, pp. 98–110; March, 1957.

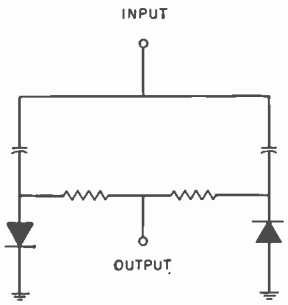

Fig. 5—Dual clamp circuit.

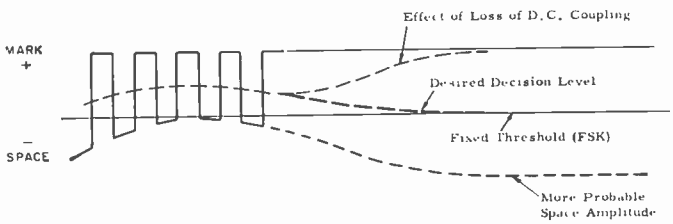

Fig. 6—Decision threshold effects illustrating the necessity of dc coupling.

device they termed an assessor. Although this circuit causes the signal to center about the desired threshold and is not affected by varying duty factor, the signal is still effectively capacity-coupled, and its response does not extend to dc.

In order to achieve the indicated diversity improvements, the data transmission rate must be greater than the fading rates and circuit time constants must be selected to allow the computer to follow signal fading rates without appreciable time delays. If transmitter keying inputs result in the signal remaining on one frequency for a period of time which is long when compared to the circuit time constants, it becomes essential that the frequency response of the threshold-varying device extend to dc. This characteristic is incorporated in the decision threshold computer and its effect is illustrated in Fig. 6. If the frequency response of the device does not extend to dc, the threshold is effectively shifted toward the received input signal level, eventually resulting in random decisions. During such periods, no information is available to indicate what the received amplitude of the opposite frequency would be if it were to be transmitted. Statistically, it appears that the amplitude of the other frequency is probably of an amplitude comparable to that of the frequency being received. This indicates that the decision level should be moved toward zero, the FSK decision level, during a single-frequency transmission period. If transmission coding can be provided, which would prevent the signal from remaining on one frequency for any period which would be long when compared to signal-fade rates, the problem would be less stringent. Such coding is not always convenient, and the decision level still would have a tendency to shift in a direction opposite to that desired. The decision threshold computer achieves the desired effect by gradually erasing the information stored in the coupling capacitors and, in effect, results in direct coupling when signal-keying conditions are such that amplitude levels of both frequencies cannot be accurately determined. The resulting transition between the two decision criteria is gradual and at a rate determined by circuit time constants derived from *a priori* fading information. The effective decision level is the "Desired Decision Level" of Fig. 6.

Test Program

The decision threshold computer has been adapted to ionospheric scatter and HF FSK communication systems. These systems were optimized and evaluated, using magnetic-tape recordings of received signals from typical propagation paths. The recordings consist of continuously repeated predetermined keying patterns and are made simultaneously with measurements of signal-to-noise ratio, fading characteristics and multipath conditions. The recordings are made from comparatively wide-band outputs prior to filtering and demodulation and are subsequently played back to the equipment to be evaluated. Outputs of the equipment under test are fed to an error-counting system, capable of recognizing and providing a cumulative count of equipment errors. Resulting error rate performances may then be compared to that theoretically obtainable with Gaussian noise and Rayleigh fading, or to those resulting from other design approaches. The recorded test signals have proven superior to the use of most propagation simulators in that, for practical applications, they are identical to the original signals and accurately simulate conditions for which equipment is intended to operate. Further, the same effect may be repeated as often as necessary to permit isolation of a subtle performance deficiency.

Signals recorded on several propagation paths were used to determine optimum time constants for the various applications of the DTC and to provide a performance evaluation. Typical results of the evaluation programs of equipments utilizing the variable decision level approach are shown in Figs. 7 and 8. Fig. 7 shows data obtained on ionospheric scatter equipment. An improvement of approximately 10 db at a probability of binary error of 1 in 10^4 bits is indicated for the single receiver case. Where dual space diversity is utilized in conjunction with the variable decision threshold technique, less improvement is noted, due to the diminishing returns of adding successively more diversity branches; however, a 3–5 db improvement is still noted at useful error rates.

Fig. 8 shows the results of the application of the DTC to a commercially available HF demodulator. Tests on the DTC-modified HF system show a gain of as much as 20 db in signal detectability. It may be noted that the performance still shows considerable degradation from that which may be theoretically obtainable. It is believed that a substantial part of this difference may be the result of propagation perturbations which in practice vary from the Gaussian noise and Rayleigh fading distributions that were assumed for the theoreti-

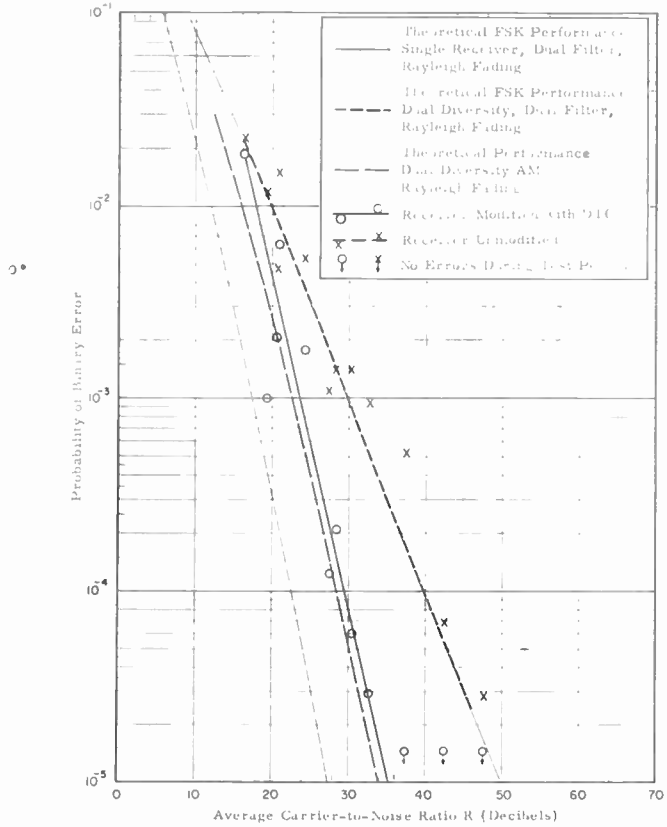

Fig. 7—Performance of single ionospheric scatter receiver with conventional FSK decision vs single ionospheric scatter receiver with decision threshold computer on 600-bit reversals.

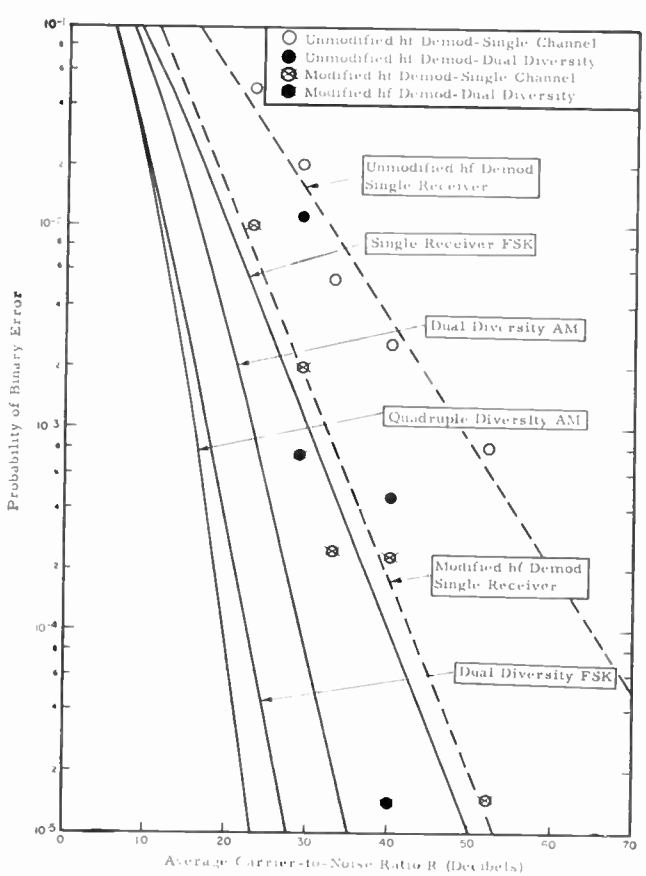

Fig. 8—Performance of unmodified HF demodulator as compared with modified HF demodulator with decision threshold computer on 45-bit reversals.

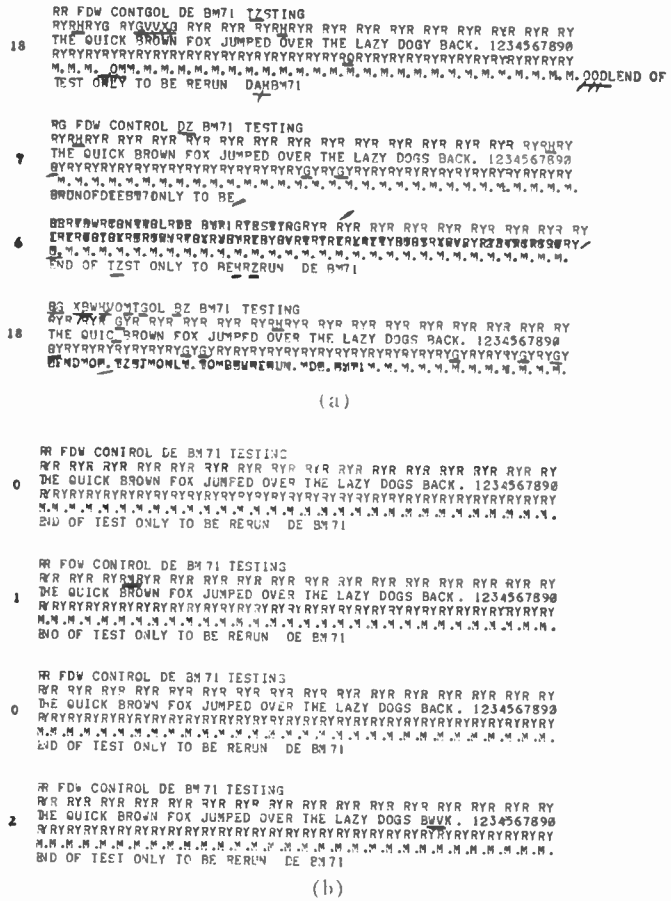

Fig. 9—Examples of simultaneously received teleprinter copy. (a) Unmodified HF demodulator; (b) modified HF demodulator with decision threshold computer.

cal calculations. More recent laboratory tests have indicated, however, that further improvement in demodulator performance may be achieved through more sophisticated filter design than was used in the modified equipment tested. The effect of the DTC modification on typical page copy is illustrated in Fig. 9.

Conclusions

The advantage of automatic decision level variation in binary transmission systems has been established. The DTC approach has been successfully adapted to existing ionospheric scatter and HF systems. Operational results of the DTC application to several scatter systems support those results achieved from the test tapes.

To achieve these results, careful consideration must be given to system parameters. The relation of time constants to fading rates is critical. The HF problem appears to be more severe as a result of greater variations in fading rates and impulse noise perturbations.

The DTC provides particular advantages where the use of dual spaced diversity systems is prevented by a lack of adequate real estate. Its potential for shipboard and aircraft installations is immediately obvious.

The bandwidth of a propagation medium is often referred to as that bandwidth over which a high correlation is maintained between frequencies. Additional orders of diversity have been a means by which the correlation bandwidth may be effectively increased. Use of

the decision threshold computer provides an economical method of increasing the order of diversity with FSK systems. In addition, use of this device may provide a means of high-speed data transmission at UHF. It is believed possible to extend the DTC technique to digital systems other than FSK.

ACKNOWLEDGMENT

The author would like to acknowledge the assistance of Robert L. Carrick, who performed the mathematical analysis contained in this paper and assisted in the experimental measurements.

Generalized Padé Approximation*

J. L. STEWART†, SENIOR MEMBER, IRE

Summary—**Approximation by minimizing the magnitude of the complex error phasor in the steady state is considered and relationships to conventional magnitude-only and phase-only methods are discussed. The particular case of the Taylor approximation about zero frequency is shown to be equivalent to the Taylor approximation in terms of the complex variable. Generalized examples are given which relate to rational approximations for transistor alpha, resistance-capacitance transmission lines, and the *Z* transform.**

I. INTRODUCTION

APPROXIMATION is herein understood to mean the determination of parameters of a function of given complexity in such a way that a different but known function is characterized in a reasonably accurate manner over a specified range of the variable. One purpose of approximation is to reduce difficulties in theoretical or numerical analysis by replacing a complicated function with a less complicated one. Another purpose is to find a relatively uncomplicated approximating function which, in turn, is a valid model for a physical system or device; approximation of this sort has as its ultimate objective the synthesis of a practical system with characteristics which are prescribed.

The adequacy of an approximation can be ascertained only in terms of an appropriate criterion of error. The present discussion is concerned with approximation of complex functions on the basis of an error criterion which specifies the magnitude of the vector (*i.e.*, phasor) difference between approximated and approximating functions. Relationships between this "error-magnitude" criterion and widely used magnitude-only or phase-only approximations are discussed here; it is demonstrated that the error-magnitude criterion includes other criteria as special cases through formulation of an "error-area" criterion.

The specific approximation of most concern here is the Taylor approximation for error-magnitude; although Taylor approximations for magnitude alone and for phase alone are well known, application for a combination of phase and magnitude is only partly recorded. A principal result is demonstration of equivalence of error-magnitude Taylor approximation about $\omega=0$ to Taylor approximation about any point on the real axis of the complex variable or p plane. The term Padé is adopted in order to specify Taylor approximation of a complex function of $j\omega$ rather than of a real function of frequency ω.

It is not to be implied that all of the concepts introduced here are new, although organization, interpretation, and application may show novelty. Tuttle discusses certain aspects of the problem in more detail than is typical for application in the steady state [1]. There are intimate relationships between the Padé method and approximation in the time domain; to a certain extent, these are described by Teasdale [2] and Ba Hli [3], among others. In addition, and apparently unrecognized before, certain Z transforms and Z forms turn out to be Padé approximations which further indicate frequency-time correspondences worthy of study [4]–[7].

The second part of this paper is devoted to examples where, for the most part, each is given without appreciable comment. Examples chosen indicate the following:

1) The class of low-pass Padé approximations can be extended to include j-axis transmission zeros and/or other types of constraints [1].
2) Most of the rational approximations for current gain alpha of a transistor are elementary Padé approximations [8], [9].
3) Transient solutions for the terminated general transmission line with transfer characteristics $\exp(-\gamma x)$ where γ is an irrational function of the Laplace variable may be solved by means of an obtainable rational approximation [10].
4) A general method for determining rational approximate Z transforms is indicated; approximations for the simple Laplace variable $1/p$ yield the Z transform (first-order approximation) and the Z form (second-order approximation) which have been used for time-domain analysis with considerable success and are closely related to general theories of integration [4]–[7].

* Received by the IRE, March 29, 1960; revised manuscript received, August 29, 1960.
† University of Arizona, Tucson, Ariz.

II. A Generalized Error Criterion

Let $G(j\omega)$ and $F(j\omega)$ be complex functions of variable ω which are single-valued and have no more than a finite number of discontinuities in a finite frequency interval. Plot loci of $F(j\omega)$ and $G(j\omega)$ on the complex plane. If these functions are to approximate one another in some sense, it is apropos to define a vector (phasor) error as

$$\epsilon(j\omega) = G(j\omega) - F(j\omega), \tag{1}$$

which is indicated in Fig. 1(a). On the basis of a suitable criterion, error is supposed to be small in a prescribed frequency interval $\omega_1 < \omega < \omega_2$.

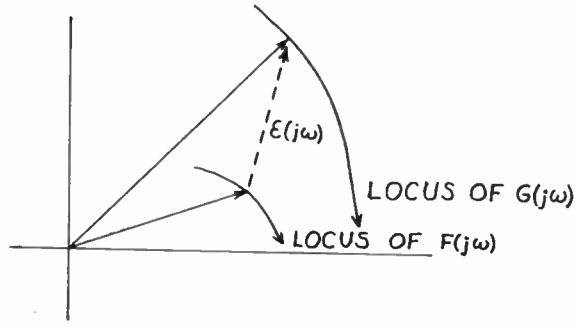

(a)

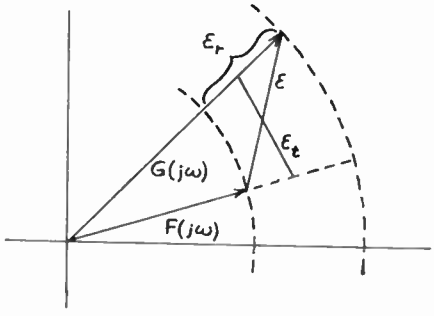

(b)

Fig. 1—Error components.

Although insight can be gained through consideration of the magnitude of the error phasor, its phase angle is not equally interpretable. Thus we are led to judge adequacy of an approximation in terms of the magnitude of the error phasor (actually its square-magnitude) according to

$$\begin{aligned} |\epsilon|^2 &= |G(j\omega) - F(j\omega)|^2 \\ &= |G(j\omega)|^2 + |F(j\omega)|^2 - G(j\omega)F(-j\omega) \\ &\quad - G(-j\omega)F(j\omega). \end{aligned} \tag{2}$$

Subsequent to manipulation by adding and subtracting $2|F(j\omega)G(j\omega)|$, (2) becomes

$$|\epsilon|^2 = \{|G(j\omega)| - |F(j\omega)|\}^2 + 2|F(j\omega)||G(j\omega)| \cdot \{1 - \cos[\operatorname{Arg} G(j\omega) - \operatorname{Arg} F(j\omega)]\} \tag{3}$$

in which individual terms can be interpreted as a radial component of error ϵ_r and a tangential component of error ϵ_t according to Fig. 1(b) as

$$\begin{aligned} |\epsilon_r| &= |G(j\omega)| - |F(j\omega)| \\ |\epsilon_t| &= \sqrt{2|F(j\omega)||G(j\omega)|\{1 - \cos[\operatorname{Arg} G(j\omega) - \operatorname{Arg} F(j\omega)]\}}, \end{aligned} \tag{4}$$

where it is observed that tangential error is defined at a radial distance equal to the geometric mean of $|F(j\omega)|$ and $|G(j\omega)|$. Total error square-magnitude may be determined for an equivalent right triangle as

$$|\epsilon|^2 = |\epsilon_r|^2 + |\epsilon_t|^2. \tag{5}$$

It may sometimes occur that the radial component of error is considered to be more important than is the tangential component, or conversely. In such cases, we are led to apply weighting functions so that the error criterion becomes

$$|\epsilon_e|^2 = R|\epsilon_r|^2 + T|\epsilon_t|^2, \tag{6}$$

where R and T are suitable weighting functions (which are functions of frequency in general) and where $|\epsilon_e|$ is the measure of error which is not necessarily proportional to error-magnitude $|\epsilon|$.

By inspection of Fig. 1(b), another error criterion may be proposed, and that is an error-area criterion as

$$A_\epsilon = |\epsilon_r||\epsilon_t|. \tag{7}$$

From the various error expressions given here, several conclusions may be reached. For the present, the manner in which error is made small is relatively unimportant (as, for example, Taylor or Tchebycheff approximation to zero, or points matching to zero, or approximation to zero in the least-squares sense, and so forth). What is important here is the basic definition for error itself.

Minimization of error-magnitude $|\epsilon|$ is an obvious optimal procedure. If radial and tangential components are weighted other than equally, it becomes optimal to minimize something other than error-magnitude. If radial errors are weighted very heavily, the approximation becomes one which essentially ignores tangential error altogether (and conversely).

The error-area criterion yields comparable results to the weighted-component concept for the special case when one component is very heavily weighted compared with the other. Note in this regard that error-area can be small with $|\epsilon_r|$ small even though $|\epsilon_t|$ is very

large, and conversely; clearly, the error-area concept may be a very misleading one.

Note that, if radial error alone is deemed to be important, the criterion of (6) (for weighting R constant) reduces to approximation as

$$|F(j\omega)|^2 \approx |G(j\omega)|^2, \tag{8}$$

which also obtains by considering only the effect of the radial component of error on error-area. The criterion of (8), which ignores phase altogether, is that employed in demonstrating well-known maximally flat and Tchebycheff approximations, among others.

In contrast, if tangential error alone is deemed to be important, and assuming in (6) that the product $T|FG|$ is constant over the approximated range, error minimization reduces to angle approximation as

$$\text{Arg } F(j\omega) \approx \text{Arg } G(j\omega) \tag{9}$$

or to the equivalent

$$\frac{d \text{ Arg } F(j\omega)}{d\omega} \approx \frac{d \text{ Arg } G(j\omega)}{d\omega}. \tag{10}$$

where phase slope is envelope delay. The phase criterion ignores magnitude altogether; most approximations as employed in design of delay lines are of this type.

If an approximating function has N parameters which can be adjusted, it can be made to approximate in some sense up to an order N. Three extreme cases are suggested, an Nth-order approximation to zero radial error, an Nth-order approximation to zero tangential error, and an Nth-order approximation to zero error-magnitude. In the error-magnitude case, roughly half of the parameters are assigned to reduction of radial error and the other half to reduction of the tangential error. Thus, the error-magnitude criterion is not in principle an optimum one unless both components of error are approximately equal in importance. It is not to be inferred that the error-magnitude criterion merely divides available parameter adjustments in a manner which separately considers each of the two components of error. To the contrary, the entire error function is minimized in the appropriate sense; in general, neither the radial nor the tangential component of error will by itself then be minimum in any sense.

III. Taylor Approximation

If error is expanded in a Taylor series about a center frequency ω_0 as

$$|\epsilon|^2 = \epsilon_0 + \epsilon_2(\omega - \omega_0)^2 + \epsilon_4(\omega - \omega_0)^4 + \cdots \tag{11}$$

and if coefficients $\epsilon_0, \epsilon_2, \epsilon_4, \cdots$ are set to zero in orderly sequence, the approximation is to error-magnitude in the Taylor sense with respect to frequency ω_0. If $\epsilon_{2k} = 0$ but $\epsilon_{2k+2} \neq 0$ for $k = 0, 1, 2, \cdots, n$, the order of the approximation is the nth.

A general restriction is next imposed as

$$G(p) \text{ and } F(p) \text{ are real for } p \text{ real}, \tag{12}$$

which states that poles and zeros occur in complex-conjugate pairs if complex. One consequence of this restriction is that real and imaginary parts of $F(j\omega)$ and $G(j\omega)$ are even and odd functions of ω, respectively, and hence square-magnitude error is an even function of ω. Certain very basic arguments pertaining to normal modes show that a model for a physical system, whether rational or not, must have the property of (12) [11].

Let us next consider the Taylor approximation for $\omega_0 = 0$ with the restriction of (12). First define real and imaginary parts as

$$\begin{aligned} G(j\omega) &= \text{Re } G(j\omega) + j \text{ Im } G(j\omega) \\ F(j\omega) &= \text{Re } F(j\omega) + j \text{ Im } F(j\omega), \end{aligned} \tag{13}$$

and define suitable Taylor series as

$$\begin{aligned} \text{Re } G(j\omega) &= A_0 + A_2\omega^2 + A_4\omega^4 + \cdots \\ \text{Im } G(j\omega) &= B_1\omega + B_3\omega^3 + \cdots \\ \text{Re } F(j\omega) &= C_0 + C_2\omega^2 + C_4\omega^4 + \cdots \\ \text{Im } F(j\omega) &= D_1\omega + D_3\omega^3 + \cdots. \end{aligned} \tag{14}$$

Square-magnitude error may now be written as

$$|\epsilon|^2 = (\text{Re } G - \text{Re } F)^2 + (\text{Im } G - \text{Im } F)^2, \tag{15}$$

from which the desired Taylor approximation may be obtained by equating coefficients of the powers of ω to zero in ascending order as:

$$\begin{aligned} &\omega^0\text{: } A_0 = C_0 \text{ gives 0th-order approximation} \\ &\omega^1\text{: } B_1 = D_1 \text{ gives 0th-order approximation} \\ &\omega^2\text{: } A_2 = C_2 \text{ gives 1st-order approximation} \\ &\omega^3\text{: } B_3 = D_3 \text{ gives 2nd-order approximation} \\ &\quad\vdots \qquad\qquad\qquad\quad \vdots \\ &\omega^q\text{: } B_q = D_q \\ &\text{or } A_q = C_q \text{ gives } (q-1)\text{th-order approximation} \end{aligned} \tag{16}$$

in which it is to be noted that adjustments of coefficients for the zeroth and first powers of ω give magnitude and frequency normalization, respectively; the order of the approximation has been defined so as not to yield a finite-order Taylor approximation by virtue of normalization alone.

Return now to a detailed examination of the way in which coefficients are adjusted. Subsequent to normalization, achievement of a first-order approximation requires consideration of only the real parts of $F(j\omega)$ and $G(j\omega)$; the second-order approximation subsequently involves only the imaginary parts; and so on. We are thus led to find Taylor series for the variable $p = j\omega$ as

$$\begin{aligned} G(p) &= G_0 + G_1p + G_2p^2 + G_3p^3 + \cdots \\ F(p) &= F_0 + F_1p + F_2p^2 + F_3p^3 + \cdots, \end{aligned} \tag{17}$$

and find real and imaginary parts of $G(j\omega)$ and $F(j\omega)$ in terms of the even and odd parts, respectively, of $G(p)$

and $F(p)$. We conclude that, if $F(p)$ and $G(p)$ are single-valued functions of variable p which have Taylor series about $p=0$ and if $F(p)$ and $G(p)$ are real for p real:

$F(j\omega)$ and $G(j\omega)$ approximate one another about $\omega=0$ in the Taylor sense for error-magnitude if $F(p)$ and $G(p)$ approximate one another in the Taylor sense about $p=0$. We will henceforth refer to this as *approximation in the Padé sense.*

Imagine the pole-zero plot of $F(p)$. Since poles and zeros are in complex-conjugate pairs if complex, it is evident that $F(p)$ may be transformed to $F(p+\alpha)=F(p')$ where α is real, with the result that $F(p')$ is real for p' real. From this we conclude that the Padé approximation for a function which is real on the real axis may be made in terms of the Taylor approximation of the complex variable about any regular point on the real axis; the origin may be only one such point. It does not follow that we may approximate about a complex point which has $\omega_0 \neq 0$ as $F(p-p_0)$; for such points, it does not necessarily follow that the real and imaginary parts of $F(u)=F(p-p_0)$ are even and odd functions of u, respectively. Approximation for $\omega_0=0$ thus permits interpretation of real frequencies (variable $j\omega$) as the complex variable p, or in effect, as a simple real variable. The simplicity provided by expansion about $\omega_0=0$ can thus not, in general, be realized for $\omega_0 \neq 0$ unless a suitable transformation $U(p)$ which converts $F(p)$ to $F[U(p)]$ can be determined (such as the familiar low-pass to band pass transformation $p+1/p$) [11].

Sometimes a function $F(p)$ does not have a Taylor series about some point on the real axis because of a removable singularity (that is, a pole of finite order). In such cases the proper expansion is made after removing the pole; subsequent introduction of the pole gives the Laurent series. If $F(p)$ does not have a Taylor series about a point on the real axis because of a branch point as, for example, the function $\exp \sqrt{pT}$ has at the origin, expansion may be made about a point on the real axis other than the branch point; analysis may often still be possible, provided suitable modifications in excitation and response waveforms are accepted.

IV. Examples

A. General Rational Fractions

Let $G(p)$ be approximated with a rational fraction which has undetermined or partly determined coefficients as

$$G(p) \approx F(p) = \frac{a_0 + a_1 p + a_2 p^2 + \cdots + a_m p^m}{b_0 + b_1 p + b_2 p^2 + \cdots + b_n p^n}, \quad (18)$$

which may be expanded subsequent to cross-multiplication as

$$(b_0 + b_1 p + \cdots)(G_0 + G_1 p + \cdots) \approx a_0 + a_1 p + \cdots, \quad (19)$$

where $G_0+G_1p+\cdots$ is the Taylor series about $p=0$ of function $G(p)$ which is to be approximated. Upon equating powers of p in (19) in ascending order, we get

$$\begin{aligned} p^0&: b_0G_0 = a_0 \\ p^1&: b_1G_0 + b_0G_1 = a_1 \\ p^2&: b_2G_0 + b_1G_1 + b_0G_2 = a_2 \\ p^3&: b_3G_0 + b_2G_1 + b_1G_2 + b_0G_3 = a_3, \end{aligned} \quad (20)$$

where the rule for forming the coefficient for p^q should be evident. Note that, for G_0 finite, neither a_0 nor b_0 can be zero and either a_0 or b_0 may be assumed to be unity at no loss in generality; in any case, one of the a_k or b_k, if not a_0 or b_0, may always be taken as unity.

A somewhat special case of the foregoing is for $G(p)=\exp(pT)$. In this event, the rational approximation $1/F(p)$ approximates $\exp(-pT)$ and is tabulated in several places for various degrees in p of numerator and denominator polynomials [1]. We give here only generalized formulas for coefficients obtained from (20) as

$$\begin{aligned} p^0&: b_0 = a_0 = 1 \\ p^1&: T + b_1 = a_1 \\ p^2&: T^2/2! + Tb_1/1! + b_2 = a_2 \\ &\vdots \\ p^q&: T^q/q! + T^{q-1}b_1/(q-1)! + T^{q-2}b_2/(q-2)! + \cdots \\ &\qquad + Tb_{q-1}/1! + b_q = a_q. \end{aligned} \quad (21)$$

Observe that the various Padé approximants may be obtained by substituting pT for x in the Taylor approximation of the real function of a real variable $\exp(x)$; this procedure was earlier shown to be valid in general. Padé approximants are often derived this way, which unfortunately hides the nature of the error criterion (which is, of course, minimization of error-magnitude in the Taylor sense).

The general formulas given here may be applied when some of the coefficients are specified. Suppose, for example, we wish to have a rational approximation to $\exp(-p)$ when there exist specified transmission zeros at $\pm j2$. The appropriate rational approximating function is assumed to be

$$F(p) = \frac{1 + a_1 p + a_2 p^2 + a_3 p^3}{1 + 0.25 p^2} \approx e^{+p}, \quad (22)$$

which is normalized as $a_0=b_0=1$. Equations from which coefficients may be found are (21) for $b_1=0$ and $b_k=0$ for $k>2$ and $a_k=0$ for $k>3$. There results

$$\frac{1}{F(p)} = \frac{1 + 0.25p^2}{1 + p + (3/4)p^2 + (5/12)p^3} \approx e^{-p}. \quad (23)$$

B. Transistor Alpha

A normalized expression for current gain of a transistor is

$$\alpha = \operatorname{sech}(a\sqrt{1+p}) = \frac{1}{\cosh(a\sqrt{1+p})}, \quad (24)$$

where

$$(\alpha)_{p=0} = \alpha_0 = \operatorname{sech} a \tag{25}$$

is the "nominal" current gain. In order to find rational approximations, we must first expand α into a Taylor series about $p=0$. It is slightly easier to expand $1/\alpha$ into such a series as

$$1/\alpha = G_0 + G_1 p + G_2 p^2 + \cdots, \tag{26}$$

where

$$G_0 = 1/\alpha_0$$
$$G_q = (1/q!)\left[d^q(1/\alpha)/dp^q\right]_{p=0} \tag{27}$$

are familiar coefficient values. Straightforward calculations yield

$$\frac{\alpha_0}{\alpha} = 1 + \left(\frac{aA}{2}\right)\frac{p}{1!} + \left(\frac{a^2 - aA}{4}\right)\frac{p^2}{2!} + \left(\frac{(a^3 + 3a)A - 3a^2}{8}\right)\frac{p^3}{3!} + \cdots, \tag{28}$$

where

$$A = \sqrt{1 - \alpha_0^2}. \tag{29}$$

With little difficulty, we now find the first few approximations for α as

$$\alpha = \alpha_0 \frac{1}{1 + \frac{aA}{2}p}$$

$$\alpha = \alpha_0 \frac{1}{1 + \frac{aA}{2}p + \frac{a^2 - aA}{8}p^2}$$

$$\alpha = \alpha_0 \frac{1 - \frac{a - A}{4A}p}{1 + \left(\frac{aA}{2} - \frac{a - A}{4A}\right)p}, \tag{30}$$

where p can be replaced by τp for the unnormalized case and where the approximations are discussed extensively in the literature (and note that a rational approximation need not be minimum phase) [8], [9].

C. Transmission Line

The terminated resistance-capacitance line has transfer function $\exp(-\sqrt{pT})$ [10]. We consider the normalized case $\exp(-\sqrt{p})$ for simplicity. Observe that the origin is not a regular point and hence special methods must be employed in order to obtain a Taylor series. Note that, in addition to the electrical transmission line, certain types of delay in servomechanisms and other mechanical and thermal phenomena have transfer functions of the type of interest here.

If $e(t)$ is applied to the line and if $E(p)$ is the Laplace transform of $e(t)$, response is

$$i(t) = \mathcal{L}^{-1}e^{-\sqrt{p}}E(p). \tag{31}$$

Now transform using $p+\alpha$ for p. There results

$$e^{-\alpha t}i(t) = \mathcal{L}^{-1}e^{-\sqrt{p+\alpha}}E(p+\alpha), \tag{32}$$

and we can thus determine response of the true line to excitation $e(t)$ by applying response $\exp(-\alpha t)e(t)$ to the modified line in order to obtain the desired result upon multiplying by $\exp(+\alpha t)$ as

$$i(t) = e^{+\alpha t}\mathcal{L}^{-1}e^{-\sqrt{p+\alpha}}E(p+\alpha). \tag{33}$$

Instead of a rational approximation to $\exp(-\sqrt{p})$ which does not have a Taylor series about $p=0$, we instead seek the Taylor series of $\exp(-\sqrt{p+\alpha})$ about $p=0$ which does exist for finite α; the expansion is in effect the Taylor series for $\exp(-\sqrt{p})$ about the point $p=+\alpha$. There results for the reciprocal for convenience

$$e^{\sqrt{p+\alpha}} = e^{\sqrt{\alpha}}\left(1 + \frac{1}{2\sqrt{\alpha}}p + \frac{\sqrt{\alpha} - 1}{8\alpha\sqrt{\alpha}}p^2 + \frac{\alpha\sqrt{\alpha} - 3\sqrt{\alpha} + 3}{48\alpha^2\sqrt{\alpha}}p^3 + \cdots\right) \tag{34}$$

which yields, for example, the unnormalized rational approximation

$$e^{-\sqrt{pT+\alpha}} \approx \frac{e^{-\sqrt{\alpha}}}{1 + \frac{1}{2\sqrt{\alpha}}pT + \frac{\sqrt{\alpha} - 1}{8\alpha\sqrt{\alpha}}p^2T^2}, \tag{35}$$

which indicates existence of a minimum value for the transformation parameter α in order that the rational approximations have no right-half-plane poles.

Of course, the general transmission line with transfer characteristic

$$e^{-\gamma x} = e^{-\sqrt{(R+pL)(G+pC)}\,x} \tag{36}$$

may be approximated in a similar fashion provided either $R=0$ or $G=0$; as in the case of the resistance-capacitance line, $\exp(-\gamma x)$ is irregular at $p=0$ if $G=0$, as is usually a valid assumption. Note that approximation to the general line can be made even if parameters R, L, C, and/or G are in themselves functions of p.

D. Z Transforms

The Z transform may be expressed in terms of sample points at intervals along a time-function curve [7]. If $g(t)$ is the time function which has Laplace transform $G(p)$, the Z transform is

$$Z[g(t)] = G^*(z) = A_0 + A_1z^{-1} + A_2z^{-2} + A_3z^{-3} + \cdots, \tag{37}$$

where incremental sample-point delay is obtained through

$$z = e^{pT}; \tag{38}$$

and hence the Z transform is an irrational function of p in general. The Z transform may be either a rational or an irrational function of z, depending upon whether (37) results from expansion of a rational fraction in z or not, respectively.

Let us assume that $G^*(z)$ can be found as a rational fraction in z, at least in approximation, as

$$G^*(z) = \frac{a_0 + a_1 z^{-1} + a_2 z^{-2} + \cdots + a_m z^{-m}}{b_0 + b_1 z^{-1} + b_2 z^{-2} + \cdots + b_n z^{-n}}, \quad (39)$$

where one of the coefficients may be prescribed (as unity, for example) at no loss in generality. Note that with $z = \exp(pT)$, $G^*(z)$ becomes the Laplace transform $G(p)$ and hence

$$G(p) = \frac{a_0 + a_1 e^{-pT} + \cdots + a_m e^{-mpT}}{b_0 + b_1 e^{-pT} + \cdots + b_n e^{-npT}}. \quad (40)$$

It often occurs that we wish to determine the Z transform for a waveform defined in terms of a rational Laplace transform. In this event, we seek to find coefficients a_k and b_k for an assumed degree of complexity (*i.e.*, values of m and n) so that (40) approximates a rational function of p. A specific case of interest is $G(p) = p^R$ where R is a positive integer. For this, expand exponentials in (40) in their power series and cross-multiply as in the usual Padé approximation. There results

$$b_0 p^R + \sum_{q=0}^{q=\infty} (-1)^q \frac{T^q p^{q+R}}{q!} (1^q b_1 + 2^q b_2 + \cdots + n^q b_n) \approx a_0 + \sum_{r=0}^{r=\infty} (-1)^r \frac{T^r p^r}{r!} (1^r a_1 + 2^r a_2 + \cdots + m^r a_m) \quad (41)$$

which, for any R, enables us to equate the coefficients of the lower powers of p. Of particular interest are first- and second-order approximations for $1/p$. We use $R = 1$ and invert the resulting solution to obtain

$$\frac{1}{p} \approx T \frac{z}{1 - z}$$
$$\frac{1}{p} \approx \frac{T}{2} \cdot \frac{z - 1}{z + 1}, \quad (42)$$

where the first-order approximation is the well known Z transform for a unit step function which has Laplace transform $1/p$ and where the second-order approximation is the Z form used in certain types of generalized analysis and in theories of integration [4]–[6].

V. Bibliography

[1] D. F. Tuttle, Jr., "Network Synthesis," John Wiley and Sons, Inc., New York, N. Y., pp. 761–782, 816; 1958.
[2] R. D. Teasdale, "Time domain approximation by use of Padé approximants," 1953 IRE Convention Record, pt. 5, pp. 89–94.
[3] E. Ba Hli, "A general method for time domain network synthesis," IRE Trans. on Circuit Theory, vol. CT-1, pp. 21–28; September, 1954.
[4] R. Boxer and S. Thaler, "A simplified method for solving linear and nonlinear systems," Proc. IRE, vol. 44, pp. 89–101; January, 1956.
[5] S. Thaler and R. Boxer, "An operational calculus for numerical analysis," 1956 IRE Convention Record, pt. 2, pp. 100–105.
[6] R. Boxer, "A note on numerical transform calculus," Proc. IRE, vol. 45, pp. 1401–1406; October, 1957.
[7] J. T. Tou, "Digital and Sampled-Data Control Systems," McGraw-Hill Book Co., Inc., New York, N. Y.; 1959.
[8] R. D. Middlebrook and R. M. Scarlett, "An approximation to alpha of a junction transistor," IRE Trans. on Electron Devices, vol. ED-3, pp. 25–29; January, 1956.
[9] R. M. Scarlett, "High-Frequency Equivalent Circuits for Junction Triodes," presented at WESCON, Los Angeles, Calif.; August, 1956.
[10] E. Weber, "Linear Transient Analysis," John Wiley and Sons, Inc., New York, N. Y., vol. 2; 1955.
[11] J. L. Stewart, "Fundamentals of Signal Theory," McGraw-Hill Book Co., Inc., New York, N. Y.; 1960.

A Study of Surface Roughness and Its Effect on the Backscattering Cross Section of Spheres*

R. E. HIATT†, senior member, ire, T. B. A. SENIOR†, and V. H. WESTON†

Summary—**The effect on the scattering cross section of a perfectly conducting object produced by surface roughness whose scale is only a small fraction of a wavelength is discussed. The object itself is assumed large compared with the wavelength. The roughness is assumed to be statistically random in nature and it is shown that this can be treated by means of an impedance boundary condition. This permits the use of known results to determine the resulting modification to the cross section of the unperturbed object. Experimental data obtained by measuring the backscattering cross section of a large rough sphere at three frequencies, *S*, *X* and *K* band, are presented. It is found that even for a sphere whose depth of roughness is as large as $10^{-2}\lambda$, the measured change in cross section is no more than about 0.1 db. This is in good agreement with the theoretical prediction.**

* Received by the IRE, July 6, 1960; revised manuscript received, August 29, 1960. The work described herein was carried out for the U. S. Air Force under Contracts AF 30(602)-1808, AF 30(602)-2099, and AF 19(604)-5470.

† Radiation Lab., Univ. of Michigan, Ann Arbor, Mich.

I. Introduction

During the last two years it has become apparent that a difference of opinion exists as to the influence of surface imperfections in model scattering experiments. On the one hand there are

those who believe that an rms surface finish good to $10^{-5}\lambda$ (approximately) is required if the effects of surface roughness are to be discounted, and that an increase in the roughness to $10^{-4}\lambda$ could produce a detectable change (of order 1 db) in the scattering cross section. In comparison with this, a tolerance of about $10^{-3}\lambda$ on the absolute dimensions of the body is regarded as sufficient.

The above viewpoint is held by several experimentalists of considerable reputation, and if the restrictions are indeed necessary it is questionable whether the scattering cross section of any practical shape can be predicted satisfactorily by means of model experiments. For example, individual rivets would then become important.

On the other hand, there are many who do not accept the necessity for these restrictions, and who feel that surface imperfections of as much as $10^{-2}\lambda$ will seldom (if ever) affect the scattering cross section in any detectable manner. The only exceptions are those cases where the return from the smooth (unperturbed) body is either small in magnitude (as in backscattering from an infinite cone nose-on), or the result of a particular phase relationship which is seriously disturbed by the presence of the roughness. This opinion is shared by the authors, and as a contribution towards a better understanding of roughness effects in general, some results obtained from a study of a particular type of roughness are presented here.

The type of roughness considered here is one in which the surface irregularities are distributed at random, but in a statistically uniform and isotropic manner. The surface slopes are assumed small, and the minimum (effective) radius of curvature (or dimension) of the mean (unperturbed) surface is assumed large compared with the wavelength. The effects of the surface roughness can then be discussed in terms of an impedance boundary condition applied at the mean surface, and this approach is described briefly in Section II. As an illustration the method has been used to determine the back scattering cross section of a rough sphere, and the results obtained appear in Section III. The details of the analysis are given in the Appendix.

In order to test the theoretical predictions a series of experiments has been carried out in which the scattering cross section of a suitably chosen rough sphere has been measured relative to the cross section of a smooth sphere of about the same diameter. Three different frequencies were employed thereby simulating three different scales of roughness. The results are presented in Section V and confirm that even for a sphere whose roughness depth is as large as $10^{-2}\lambda$ the change in cross section is no more than about 0.1 db. This is in reasonable agreement with the theory.

II. Approximate Boundary Conditions

Let us consider first an infinite perfectly conducting plane which is perturbed in some manner so as to yield a type of rough surface. Let $z=\zeta(x, y)$ be the amplitude of the perturbation measured from a mean surface which, for convenience, is taken to be the plane $z=0$. Then if the perturbed surface is defined in a statistical manner so that ζ is effectively a random variable, and if the statistical properties are uniform and isotropic, the boundary conditions at the actual surface $z=\zeta$ can be written as relations connecting the tangential components of the electric and magnetic fields at the mean surface $z=0$. The only characteristics of the surface which enter into these equations are the correlation function F (and its derivatives) and the standard deviation ζ_0 of the amplitudes. It is assumed that F is a function of the distance ρ between neighboring points on the surface, and falls rapidly to zero for $\rho \gg l$, where l can be interpreted as the scale of the irregularities (or the size of a typical "hump"). The details of the analysis are given in Senior,[1] who shows that the above results are valid providing ζ and its first derivatives are continuous and the slope of the surface is everywhere small. In the practical case to be investigated here we shall only be concerned with values of l for which $kl<1$, where $k=2\pi/\lambda$, and a sufficient condition upon the slope is then $\zeta_0 \ll l$.

The boundary conditions on the mean surface are functions of the angle at which the field is incident, and in any general application of the conditions this variation is a severe handicap. For the present purposes, however, only the approximate magnitude of the perturbation effect is required, and it seems reasonable to expect that the accuracy of the boundary condition will not be seriously impaired if an average is taken over all directions of the incident field. The boundary conditions which result from the averaging process are

$$E_x = -\eta Z H_y \tag{1}$$

$$E_y = \eta Z H_x \tag{2}$$

where $Z=1/Y$ is the intrinsic impedance of free space and η is a parameter defined in terms of the surface characteristics by

$$\eta = -\frac{ik\zeta_0^2}{4}\left[ik + \int_0^\infty \left\{\left(\frac{1}{\rho}\frac{\partial}{\partial\rho} + k^2\right)\left(FJ_0\left(\frac{k\rho}{\sqrt{2}}\right)\right) - \frac{k}{\sqrt{2}}\frac{\partial F}{\partial\rho}J_1\left(\frac{k\rho}{\sqrt{2}}\right)\right\} e^{ik\rho}d\rho\right]. \tag{3}$$

Eqs. (1) and (2) can be written as

$$E - (\hat{n}\cdot E)\hat{n} = \eta Z \hat{n} \wedge H, \tag{4}$$

where $\hat{n}$ is a unit vector normal in the outwards direction, and this will be recognized as the usual impedance boundary condition for a material whose effective surface impedance is η.

[1] T. B. A. Senior, "Impedance boundary conditions for statistically rough surfaces," submitted for publication in *Appl. Sci. Res.*

A boundary condition of the form (4) is frequently applied at the surface of a medium whose refractive index N is large compared with unity; η is then interpreted as a function of the electrical properties of the material and is proportional to $1/N$. A rigorous derivation of the boundary condition as applied to such materials is given in a paper by Senior,[2] where it is shown that (4) is also valid for surfaces of varying curvature providing

$$|\operatorname{Im} N|\, kd \gg 1,$$

where d is the smallest radius of curvature (or dimension) of the surface. If the permeability μ is not large compared with μ_0, a sufficient restriction upon d is

$$kd \gg |\operatorname{Im} \eta|. \tag{5}$$

Returning now to the boundary condition at a rough surface, this can be generalized so as to apply to a mean surface which is curved by an analysis similar in all respects to that given in Senior,[2] providing the minimum radius of curvature (or dimension) of the mean surface satisfies the inequality (5). In addition, it is noted that the roughness parameter η enters into the problem only via the boundary condition (4), and accordingly a rough (but perfectly conducting) surface is equivalent to an imperfectly conducting (but smooth) surface so far as its scattering properties are concerned. This enables us to associate an effective conductivity s with the rough surface. In the particular case $kl \ll 1$, (3) gives

$$\eta \sim i \frac{\sqrt{\pi}}{2} \frac{k\zeta_0^2}{l} \tag{6}$$

and hence for small scale roughnesses,

$$s \sim i \frac{4}{\pi} V \frac{l^2}{k\zeta_0^4} \text{ mhos/m}. \tag{7}$$

As an example, if $kl = 1/5$ and $k\zeta_0 = 1/100$,

$$s \sim \frac{10^5}{\lambda} \text{ mhos/m}$$

and at X band this is comparable to the conductivity of ordinary metals. In this instance at least it would not appear that the roughness can have any appreciable effect.

III. Scattering by a Rough Sphere

The impedance condition (4) is an approximation to the exact boundary conditions, and apart from any errors introduced by the averaging over the incident field directions, (4) is correct to the first order in η. Accordingly, in any solution obtained using this condition there is no physical justification for retaining terms which are of a higher order in η; and in consequence, if the fields are capable of expansion in series of ascending (positive) powers of η, the perfectly smooth approximation (corresponding to $\eta = 0$) can be inserted into the right-hand side of (4). In general, such expansions will be valid and lead to solutions which are essentially "perturbations" about the solutions for the surface without roughness.

We shall now use this fact to determine the backscattered field when a plane wave is incident on a uniformly rough sphere for which $ka \gg 1$, where a is the mean radius. If the incident field is polarized with its electric vector in the x direction, the scattered electric field at a distance R from the center of the sphere is

$$E_x = -\frac{a}{2R - a} e^{ik(R-2a)} \left\{ A_0 + \frac{A_1}{ka} + O(\overline{ka}^{-2}) \right\} \tag{8}$$

where

$$A_0 = 1 - 2\eta \tag{9}$$

$$A_1 = -\frac{2i(R-a)^2}{(2R-a)^2}(1 - 2\eta) + \frac{2R}{2R-a}(1-i)\eta, \tag{10}$$

and this result is valid if $|\eta| \ll (ka)^{-1/3}$. The detailed analysis is given in the Appendix.

Eq. (8) is of particular interest in showing the variation of the roughness effect as a function of the distance R. The dominant contribution to the over-all effect is provided by the term A_0 and this is independent of R. The first contribution which is a function of R comes from the term A_1 and is reduced in magnitude by the (large) factor ka in the denominator. As $R \to \infty$, $A_1 \to -i/2(1+2i\eta)$, but as the receiver approaches the sphere $A_1 \to 2(1-i)\eta$. Since $|\eta|$ is small compared with unity, the ratio of these two terms is approximately $4(1+i)\eta$, which implies a decrease in the effect of surface roughness as the receiver moves into the near field. In practice, however, it is unlikely that such a change would be detected in view of the factor ka by which the term A_1 is divided, and to a first approximation A_1 and all subsequent terms can be neglected. The magnitude of the scattered field is then

$$|E_x| \sim \frac{a}{2R-a} |1 - 2\eta| \tag{11}$$

which only differs from the "smooth" result by at most a few per cent for the type of roughness being considered here. Moreover, for $kl \ll 1$, η is purely imaginary and (11) shows that the cross section is increased by the presence of the small roughness. As kl increases, however, the approximate formula (6) ultimately ceases to apply, and the impedance assumes a resistive part as indicated by (3); the cross section of the sphere may then be either increased or decreased depending on the relative magnitudes of the real and imaginary parts of η. This is discussed at more length in Senior.[2]

[2] T. B. A. Senior, "Impedance boundary conditions for imperfectly conducting surfaces," submitted for publication in *Appl. Sci. Res.*

IV. An Experiment

To test the above conclusions and, at the same time, to obtain some direct measurements of the effect of roughness, an experiment was carried out in which the back scattering cross section of a rough sphere was measured against the cross section of a smooth (standard) sphere at a variety of different distances ranging from 16 feet to (about) 6 inches. Each sphere was cast in aluminum, a hemisphere at a time, and it was found that the casting process could be modified so as to provide a suitable degree of roughness. The first sphere was left in its rough initial state, while the second was machined to give a smooth sphere of radius approximately equal to the mean radius of the other. The dimensions (in cm) were found to be as follows:

	Rough Sphere	*Smooth Sphere*
a	12.857 ± 0.013	12.697 ± 0.010
ζ_0	0.037	- - - - - -
l	0.101	- - - - - -

where a is the mean radius (the variation is a consequence of slight asymmetries), ζ_0 is the rms amplitude of the roughness, and l is the scale. The measurement of ζ_0 and l was made using a vernier caliper, and although there was some variation from point to point on the sphere, the above values are typical of those obtained.

The two spheres are shown in Fig. 1 and the close-up photograph of the rough sphere in Fig. 2 gives some idea of both the type of surface and the degree of roughness.

In order to simulate three different degrees of roughness, the cross sections of the two spheres were measured at the frequencies 2.87, 9.7, and 23 kMc, corresponding to the wavelengths 10.5, 3.1, and 1.3 cm, respectively. The measurements were made in an indoor anechoic room 30 feet wide by 60 feet long using conventional equipment and technique. Particular care was taken to achieve the greatest possible accuracy, and it is believed that the results for the relative cross sections are good to about 0.2 db.

A block diagram of the equipment is shown in Fig. 3. At X band a cavity stabilized oscillator was employed, and at the S and K band frequencies the stability was obtained from a crystal oscillator. The receiver was of the microwave superheterodyne type using a separate mixer for each frequency band. The models were supported on a styrofoam column resting on a pedestal which could be rotated about its axis, and this in turn was mounted on a trolley to facilitate measurements as a function of range. A photograph of the room and part of the equipment is given in Fig. 4.

The comparison between the cross sections of the spheres was carried out in two different ways. In the first, the cross sections of the spheres were individually recorded as each was rotated through 360°. This procedure proved adequate at the lowest frequency where the roughness produced a negligible effect. At the higher frequencies point by point data were taken in addition

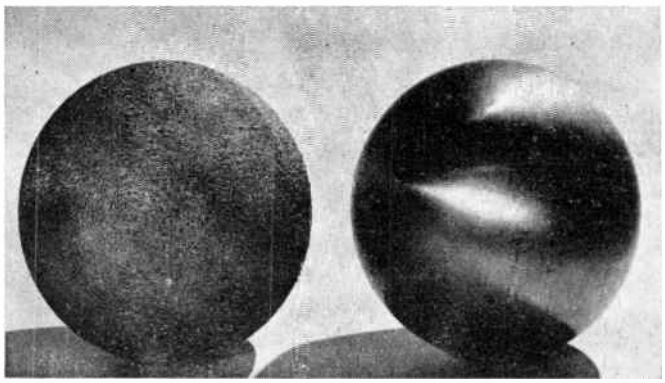

Fig. 1—Ten-inch metal spheres, rough and smooth surface.

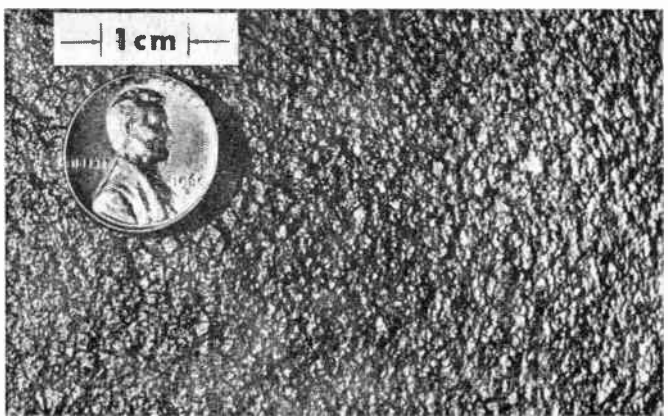

Fig. 2—Surface condition of rough ten-inch sphere.

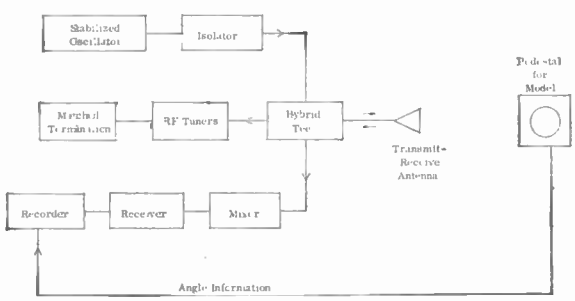

Fig. 3—Block diagram of equipment.

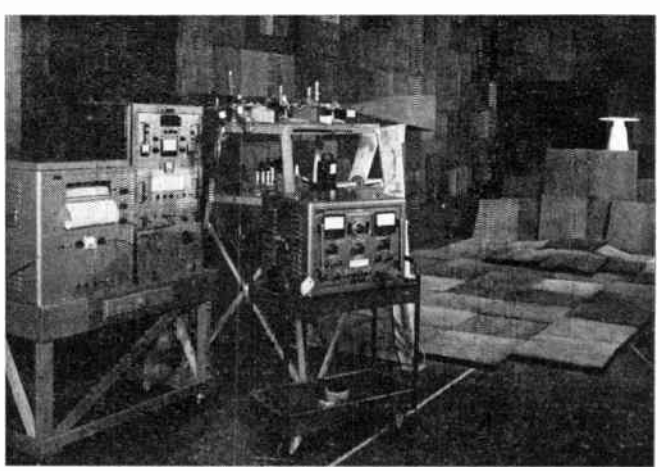

Fig. 4—Anechoic room and K-band equipment.

to the 360° plots. In obtaining these further data eight points on the rough sphere were selected, four on each hemisphere, in such a way that the plane of the junction between the two hemispheres was never parallel or perpendicular to either the direction of the illuminating beam or the electric vector. The antenna beam was then "directed" successively at each of these points, and the average signal recorded as the range was varied through $\pm\lambda/4$. The contribution due to the background was thereby minimized. The change in this contribution as a function of range could generally be kept to less than one or two decibels, and much of the time it was no more than one.

Interspersed between these eight readings, three readings were obtained with the smooth sphere, and the difference in averages was then recorded or plotted as one point (see, for example, Fig. 7). Point by point data of this type were obtained at both X and K bands, although at 23 kMc the number of readings was further increased to 24 by rotating the sphere through $\pm 5°$ at each of the above-mentioned eight points.

V. Results

At all the frequencies at which the experimental work was carried out, the values of kl are small compared with unity, and since $\zeta_0 \ll l$, (6) can be used to calculate the effective surface impedance consequent upon the presence of the roughness. Thus we have

$$\lambda = 10.5 \text{ cm}, \qquad \eta = 0.009i,$$
$$\lambda = 3.1 \text{ cm}, \qquad \eta = 0.03i,$$
$$\lambda = 1.3 \text{ cm}, \qquad \eta = 0.07i.$$

Using (8) now, the roughness is found to increase the backscattering cross section of the sphere by an amount which increases from 2×10^{-3} db at $\lambda = 10.5$ cm, through 2×10^{-2} db at $\lambda = 3.1$ cm to 10^{-1} db at $\lambda = 1.3$ cm. In addition, however, there is the change in the cross section of the rough sphere over the smooth (standard) sphere produced by its larger mean radius. At S band where the sphere is near the upper end of the resonant region the change is -0.1 db; for the X and K band frequencies the change is 0.1 db. These changes plus the theory outlined in Sections II and III then predict that the cross section of the rough sphere will exceed the cross section of the smooth (standard) sphere by the following amounts:

$$\lambda = 10.5 \text{ cm}, \qquad -0.10 \text{ db},$$
$$\lambda = 3.1 \text{ cm}, \qquad 0.12 \text{ db},$$
$$\lambda = 1.3 \text{ cm}, \qquad 0.20 \text{ db}.$$

Before going on to compare these with the values found experimentally, it may be of interest to list the degrees of roughness appropriate to the frequencies employed. If d denotes the total depth of the roughness (approximately $2\zeta_0$) and w denotes the total width of a typical bump (rather than the width between 3-db points used in the specification of the scale l), the various parameters are:

$\lambda(cm)$	ka	d/λ	w/λ
10.5	7.6	7×10^{-3}	3×10^{-2}
3.1	25.4	2×10^{-2}	10^{-1}
1.3	77.5	5×10^{-2}	2×10^{-1}

In view of the large values of ka it is not to be expected that any change in the relative cross sections as a function of distance will be detectable.

In Fig. 5 the experimental results at 2.87 kMc are shown in the form of 360° plots for three different ranges. Each plot contains four traces—one for the smooth sphere and one for each of the three orientations of the rough sphere—and in general the traces are more or less coincident with one another. By inspection of these traces (and other similar traces not presented here), it is concluded that there is no measurable effect due to the roughness at this frequency. In passing it should be noted that the thickness of the traces in Fig. 5 is of order 0.1 db, and accordingly a more detailed analysis would be necessary if the predicted change due to the different sphere radii is to be detected. Since this change is not truly a roughness effect, no such analysis was performed.

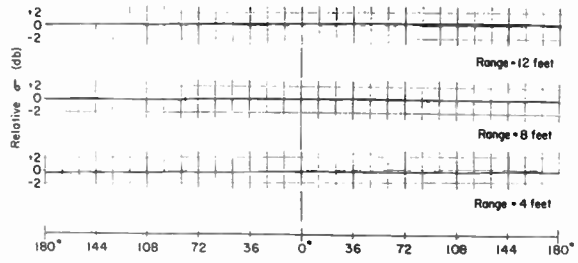

Fig. 5—Relative radar cross section, σ, of smooth and rough sphere at $\lambda = 10$ cm. Each of the three multiple traces show σ for the smooth sphere and for three different orientations of the rough sphere.

The 360° plots at 9.7 kMc are shown in Fig. 6. The effect of the surface roughness is quite apparent here, but the peak deviations from the smooth sphere return are limited to about 1 db, and the average difference in the returns is even less. This is brought out more clearly in Fig. 7 in which the point by point measurements are shown as a function of the range R. For comparison with the Rayleigh distance, the maximum range ($R = 16$ feet) is equivalent to $R = 9.4\ (a^2/\lambda)$, where a is the sphere radius, and at the minimum range ($R = 6$ inches) $R = 0.29(a^2/\lambda)$.

The results in Fig. 7 show no statistically significant range dependence, though there appears to be a tendency for the relative cross section to decrease with decreasing range. This is in accordance with the theory. When all the points in Fig. 7 are averaged regardless of range, the cross section of the rough sphere is found to be 0.12 db above that for the smooth sphere, and while

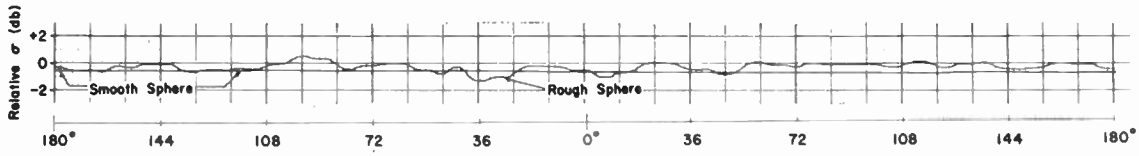

Fig. 6—Relative radar cross section, σ, of smooth and rough sphere at $\lambda = 3.1$ cm.

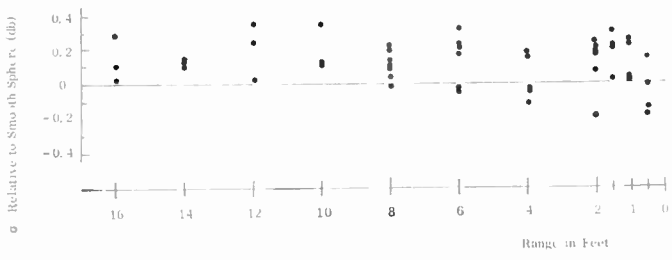

Fig. 7—Effect of range on the ratio of σ of rough to smooth sphere $\lambda = 3.1$ cm. Points plotted are the average of 16 or more readings.

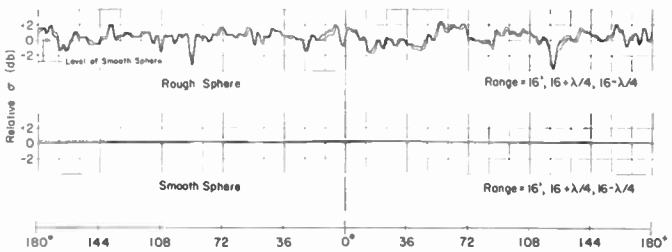

Fig. 8—Radar cross section, σ, of rough and and smooth sphere at $\lambda = 1.3$ cm.

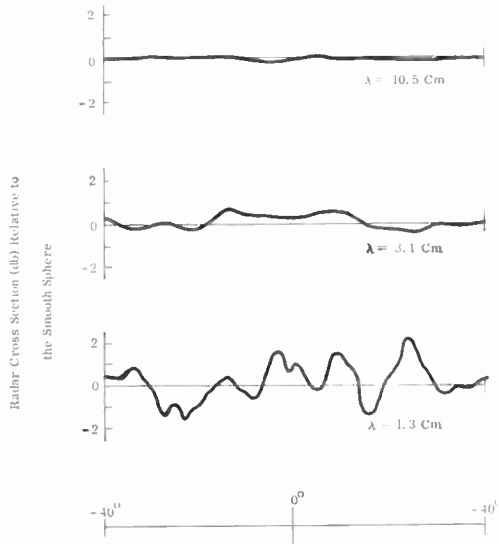

Fig. 9—Effect of surface roughness on backscatter pattern of 25 cm metal sphere. Average bump size about 0.7 mm deep by 3 mm wide.

the standard deviation of the experimental values is somewhat large (0.40 db), the average is in truly remarkable agreement with the theory. The extent of the agreement is, perhaps, a little fortuitous, but does provide confirmation of the theoretical approach.

The final set of 360° plots are given in Fig. 8 and are for 23 kMc. The surface roughness now has a marked effect, and the peak deviations from the cross section of the smooth sphere are as much as 4 db. The multiple traces shown result from changing the range by $\pm\lambda/4$ and serve to indicate the effect of the background signal. Such traces as these were entirely reproducible, and, if sufficient care was taken, the sphere could be removed from its pedestal and then replaced, with the same traces obtained once again.

At this frequency the bumps on the sphere are about $\lambda/5$ wide by $\lambda/20$ deep and it seems probable that the bumps are here acting singly or in combination of two or three at a time to produce the individual features in the traces. The fine structure in the traces is no more than 2° in width and corresponds to a displacement of the sphere's surface of approximately 0.4 cm. It can be seen from Fig. 2 that this is comparable to the width of the bumps, and under these circumstances a theory based on the random addition of the returns from many small irregularities is clearly inappropriate. It therefore comes as no surprise that the predicted change in cross section differs from that observed.

Information on the average change in measured cross section was obtained by the point by point method. Almost 800 readings were averaged regardless of range and showed that the cross section of the rough sphere exceeded that of the standard by 0.51 db. The standard deviation of the points was, however, 1.04 db.

In order to facilitate comparison of the returns at the three frequencies, sample recordings of the rough sphere data are given in Fig. 9. The way in which the roughness effect increases with increasing frequency is clearly visible.

VI. Theoretical Discussion

The theory outlined in Sections II and III is based on an impedance boundary condition derived in Senior.[1] This condition is accurate to the first order in the roughness effect providing the inclination of the actual surface to a mean surface is everywhere small, and providing the irregularities are distributed at random but in a statistically uniform and isotropic manner. If these restrictions are fulfilled, the main effect of the surface roughness is to modify slightly in phase and amplitude the field scattered by each surface element of the smooth body.

If any of the above restrictions are relaxed, the boundary condition may cease to hold. Thus, if the slopes of the irregularities are large, there is the possibility of scattering taking place from the sides of the individual humps, thus producing a field in a direction other than that for the smooth body and of a magnitude which is no longer negligible. If the surface of an infinite cone were roughened in this manner, a contribution could be expected which was not from the tip. Similarly, if the irregularities are not distributed at random, then in certain directions the fields produced by the individual element may add up in phase, and here again the boundary condition is not applicable. As an example of this, if small concentric grooves are cut in the sides of an infinite cone, a first-order modification to the field may result, particularly for backscattering in a direction normal to the rings.

If the surface irregularities do not satisfy the above restrictions, alternative methods must be employed for assessing the effect of the surface roughness, and only for certain special types of irregularity are appropriate methods available. Thus, for one or more isolated bumps whose dimensions are small compared with the wavelength, the total scattered field can be obtained by using the Rayleigh scattering formula for each individual bump and neglecting the interaction with the field of the smooth body. Since the cross section in Rayleigh scattering is proportional to the sixth power of a linear dimension, the percentage change in the total scattering cross section will be small unless the field of the unperturbed body is itself small, or the number of bumps is large. If, on the other hand, the surface perturbations are of a very regular kind and can be approximated by a series of corrugations, the effect may be estimated by using the known solutions for scattering by a corrugated sheet[3] or by a corrugated cylinder.[4] In this case, the perturbation field may be comparable to the field of the smooth body.

VII. Conclusions

In embarking on a study of surface roughness and its effect on radar scattering cross sections, one of the objectives was to consider the degree of surface finish which is necessary in model scattering experiments. As part of the experimental program the backscattering cross section of a suitably chosen rough sphere has been measured at *S*-, *X*-, and *K*-band frequencies and compared with the cross section of a smooth sphere of approximately the same diameter. It was found that even with a surface roughness which would normally be regarded as completely unacceptable for model work the change in cross section due to roughness was relatively small. Thus, at *X* band the sphere used had a roughness whose depth was 0.02 λ, but still the average change in cross section which could be attributed to the roughness was less than 0.1 db, and at *S* band no change could be detected. As is to be expected, the effect increases with increasing frequency, and at *K* band where the bumps were 0.05 λ in depth the scattering patterns were quite irregular.

On the theoretical side an analysis of the general problem of roughness has shown that geometrical irregularities characterized by small surface gradients and random but statistically uniform properties can be handled by the usual type of impedance boundary condition. This implies that the roughness produces a comparable effect to a change in the conductivity of the unperturbed surface. Results obtained with this approach are in good agreement with the experimental data.

Appendix

Backscattering from a Large Rough Sphere

Following the theory outlined in Section II it is assumed that the surface roughness produces an effective surface impedance η. The boundary condition which is applied at the surface $R=a$ is then

$$\boldsymbol{E} - (\hat{n}\cdot\boldsymbol{E})\hat{n} = \eta Z \hat{n} \wedge \boldsymbol{H}. \tag{12}$$

If the incident field is a plane wave traveling in the positive z direction with an electric vector

$$\boldsymbol{E}^i = \hat{\imath}_x e^{ikz-i\omega t} = e^{-i\omega t}\sum_{n=1} i^n \frac{2n+1}{n(n+1)}\left\{\boldsymbol{m}_{o1n}^{(1)} - i\boldsymbol{n}_{e1n}^{(1)}\right\},$$

where $\boldsymbol{m}_{o1n}$ and $\boldsymbol{n}_{e1n}$ are the spherical vector wave functions defined by Stratton,[5] the scattered field can be written as

$$\boldsymbol{E}^s = e^{-i\omega t}\sum_{n=1} i^n \frac{2n+1}{n(n+1)}\left\{a_n\boldsymbol{m}_{o1n}^{(3)} - ib_n\boldsymbol{n}_{e1n}^{(3)}\right\}$$

and by application of the boundary condition (12) the coefficients a_n and b_n are found to be

$$a_n = -\frac{\rho j_n(\rho) - i\eta[\rho j_n(\rho)]'}{\rho h_n(\rho) - i\eta[\rho h_n(\rho)]'} \tag{13}$$

$$b_n = -\frac{[\rho j_n(\rho)]' + i\eta\rho j_n(\rho)}{[\rho h_n(\rho)]' + i\eta\rho h_n(\rho)} \tag{14}$$

where $\rho = ka$ and the primes denote differentiation with respect to the entire argument. The backscattered field is then

$$\boldsymbol{E}^s = \hat{\imath}_x \sum_{n=1}^{\infty}(-i)^n(n+\tfrac{1}{2})\left\{a_n h_n(kR) + ib_n\frac{1}{kR}[kRh_n(kR)]'\right\}. \tag{15}$$

[3] P. C. Clemmow and V. H. Weston, "Diffraction by an Almost Circular Cylinder," University of Michigan, Ann Arbor, Rept. No. 2871-3-T; September, 1959.

[4] T. B. A. Senior, "The scattering of electromagnetic waves by a corrugated sheet," *Canad. J. Phys.*, vol. 37, pp. 787, 1572; July, December, 1959.

[5] J. A. Stratton, "Electromagnetic Theory," McGraw-Hill Book Co., Inc., New York, N. Y.; 1941.

To evaluate this expression for large ka it is convenient to separate out the portion appropriate to a smooth sphere ($\eta=0$). If $E(0)$ is the x component of the electric vector in the backscattered field for this case, and if $\boldsymbol{E}^s=\hat{\imath}_x E(\eta)$, (15) can be written in the form

$$E(\eta) = E(0) + \sum_{n=1}^{\infty} (-i)^n(n+\tfrac{1}{2})\left\{h_n(kR)[a_n(\eta)-a_n(0)] + i\frac{1}{kR}[kRh_n(kR)]'[b_n(\eta)-b_n(0)]\right\}, \quad (16)$$

where the new coefficients are defined by

$$a_n(\eta) - a_n(0) = \frac{\eta}{\rho h_n(\rho)}\{\rho h_n(\rho) - i\eta[\rho h_n(\rho)]'\}^{-1}$$

$$b_n(\eta) - b_n(0) = \frac{\eta}{[\rho h_n(\rho)]'}\{[\rho h_n(\rho)]' + i\eta\rho h_n(\rho)\}^{-1}.$$

If $|\eta|$ is sufficiently small,

$$a_n(\eta) - a_n(0) \sim \eta\{\rho h_n(\rho)\}^{-2}, \qquad |\eta| \ll 1 \quad (17)$$

$$b_n(\eta) - b_n(0) \sim \eta\{[\rho h_n(\rho)]'\}^{-2}, \qquad |\eta| \ll \rho^{-1/3} \quad (18)$$

and the coefficients will be replaced by these asymptotic values. This has the effect of neglecting the residues produced by the first-order poles of $a_n(\eta)-a_n(0)$ and $b_n(\eta)-b_n(0)$ when the series in (16) is transformed by means of a Watson transformation into a contour integral plus a residue series. Since these residues correspond to the diffracted field, the approximation represented by (17) and (18) is sufficient whenever the reflected field is dominant.

By using the relations

$$j_n(\rho)h_n'(\rho) - j_n'(\rho)h_n(\rho) = \frac{i}{\rho^2}$$

$$[\rho j_n(\rho)]'' + \left\{1 - \frac{n(n+1)}{\rho^2}\right\}\rho j_n(\rho) = 0$$

(16) can now be simplified to give

$$E(\eta) = \left[1 - i\eta\frac{\partial}{\partial\rho}\right]E(0) + \eta S \quad (19)$$

where

$$S = \sum_{n=1}^{\infty}(-i)^n(n+\tfrac{1}{2})\frac{n(n+1)[kRh_n(kR)]'}{kR\{\rho[\rho h_n(\rho)]'\}^2}. \quad (20)$$

Taking first the portion corresponding to a smooth sphere, the analysis in Weston[6] shows that

$$E(0) = -\frac{a}{2R-a}e^{ik(R-2a)}\cdot\left[1 + \frac{A_1(0)}{ka} + \frac{A_2(0)}{(ka)^2} + \cdots\right] \quad (21)$$

for large ka, where

$$A_1(0) = -\frac{2i(R-a)^2}{(2R-a)^2}, \quad (22)$$

$$A_2(0) = \frac{a(R-a)(2R^2-4Ra+3a^2)}{(2R-a)^4}. \quad (23)$$

The remaining task is to sum the series S, and for this purpose the Watson transform technique is used. If a contour C is drawn surrounding the poles of $\cos\nu\pi$ on the positive real axis of the ν plane, S can be written as

$$S = \sqrt{\frac{2}{\pi}}\frac{e^{i\pi/4}}{2kR\rho^2}\int_C \frac{e^{i\nu\pi/2}\nu(\nu^2-1/4)[\sqrt{kR}\,H_\nu(kR)]'}{\cos\nu\pi\{[\sqrt{\rho}\,H_\nu(\rho)]'\}^2}d\nu.$$

The contour C may now be deformed into a straight-line path from $-\infty$ to $+\infty$ and passing through the origin at an angle β to the positive real ν axis, where $-\pi/2<\beta<0$. The odd portion of the integrand then integrates to zero, so that

$$S = \sqrt{\frac{2}{\pi}}\frac{e^{3i\pi/4}}{kR\rho^2}\cdot\int_0^{\infty\exp(-i\beta)}\frac{\nu\tan\nu\pi(\nu^2-1/4)[\sqrt{kR}\,H_\nu(kR)]'}{e^{i\nu\pi/2}\{[\sqrt{\rho}\,H_\nu(\rho)]'\}^2}d\nu.$$

To evaluate this new integral it is convenient to break it into two parts by setting

$$\tan\nu\pi = \frac{ie^{-i\nu\pi}}{\cos\nu\pi} - i.$$

Taking first the integral S_1 corresponding to the first of these two terms, it is permissible to put $\beta=\pi/2$. Writing $\nu=-ip$ we then have

$$S_1 = -\sqrt{\frac{2}{\pi}}\frac{e^{i\pi/4}}{kR\rho^2}\int_0^{\infty} p(p^2+1/4)\frac{e^{-\pi p}}{\cosh\pi p}\cdot\frac{[\sqrt{kR}\,H_{ip}(kR)]'dp}{e^{-\pi p/2}\{[\sqrt{\rho}\,H_{ip}(\rho)]'\}^2}.$$

Since the dominant behavior of the integrand is provided by the factor $e^{-\pi p}/\cosh\pi p$, S_1 may be approximated as

$$S_1 \sim -\frac{1}{kR\rho^2}e^{ik(R-2a)}\int_0^{\infty} p(p^2+1/4)\frac{e^{-\pi p}}{\cosh\pi p}dp$$

and although this integral can be easily evaluated, for present purposes it is only necessary to note that

$$S_1 \sim \frac{1}{kR(ka)^2}e^{ik(R-2a)}\times\text{constant}.$$

[6] V. H. Weston, "Exact Near-Field and Far-Field Solution for the Back Scattering of a Pulse from a Perfectly Conducting Sphere," Univ. of Michigan, Ann Arbor, Rept. No. 2778-4-T; February, 1959.

The other integral S_2 is given by

$$S_2 = \sqrt{\frac{2}{\pi}}\,\frac{e^{i\pi/4}}{kR\rho^2} \cdot \int_0^{\infty \exp(-i\beta)} \nu(\nu^2 - 1/4)\,\frac{[\sqrt{kR}\,H_\nu(kr)]'\,d\nu}{e^{i\nu\pi/2}\{[\sqrt{\rho}\,H_\nu(\rho)]'\}^2}$$

and is evaluated by replacing the Hankel functions by their asymptotic expansions for $|\nu| < \sqrt{\rho}$.[7] We then have

$$[\sqrt{\rho}\,H_\nu(\rho)]' \sim \sqrt{\frac{2}{\pi}}\exp\left\{i\rho - (\nu - 1/2)i\frac{\pi}{2} + \frac{i\nu^2}{2\rho} - \frac{i}{8\rho}\right\}\left\{1 - (\nu^2 - 1/4)\frac{1}{4\rho^2} - \frac{i\nu^4}{24\rho^3} + \cdots\right\}$$

and the integral can now be approximated as

$$S_2 \sim \frac{e^{ik(R-2a)}}{kR\rho^2}\int_0^{\infty \exp(-i\beta)} \nu^3 \exp\left\{\frac{i\nu^2}{2}\left(\frac{1}{kR} - \frac{2}{ka}\right)\right\} d\nu = -\frac{2}{kR\left(2 - \frac{a}{R}\right)^2}\,e^{ik(R-2a)}\left\{1 + 0\left(\frac{1}{ka}\right)\right\}.$$

[7] J. M. C. Scott, "An Asymptotic Series for the Radar Scattering Cross Section of a Spherical Target," (British) Atomic Energy Res. Establ. Rept. T/M 30; 1949.

Hence,

$$S = -\frac{a}{2R - a}\,e^{ik(R-2a)}\left\{\frac{2R}{ka(2R - a)} + 0\left(\frac{1}{ka^2}\right)\right\} \quad (24)$$

and the backscattered field for the rough sphere is therefore

$$E(\eta) = -\frac{a}{2R - a}\,e^{ik(R-2a)} \cdot \left\{A_0(\eta) + \frac{A_1(\eta)}{ka} + \frac{A_2(\eta)}{(ka)^2} + \cdots\right\} \quad (25)$$

where

$$A_0(\eta) = 1 - 2\eta$$

$$A_1(\eta) = -\frac{2i(R - a)^2}{(2R - a)^2}(1 - 2\eta) + \frac{2R}{2R - a}\eta(1 - i).$$

This result holds for sufficiently large ka (such that the diffracted field is negligible) and for sufficiently small $|\eta|$ (*i.e.*, $|\eta| \ll (ka)^{-1/3}$).

Acknowledgment

The authors wish to express their thanks to Theodore Hon for his assistance with both the measurements and the illustrations.

Correspondence

Doppler Navigation and Tracking*

The series of papers by the personnel of Johns Hopkins in the April Space Electronics issue, on the use of Doppler techniques for satellite tracking and navigation were most interesting, and I would like to take this opportunity to expand on the fundamental principles and background underlying these projects.

The fundamental principle embodied in these navigation and tracking systems concerns the fact that at any instant a receiver will detect a Doppler and rate of change of Doppler frequency which is unique for that "target" position and velocity. As so aptly put by Drs. Weiffenbach and Guier, ". . . when properly utilized, each segment of the received Doppler curve provides useful information about the track of the satellite. . . ." Proper utilization will consist of some form of computational or apparatus curve fitting procedure. The realization that it is possible to resolve a moving "target" in azimuth and range, using CW transmission, is most interesting and powerful.

Space does not permit a theoretical analysis here; however, some of our experimental data will be of interest. The following discussion and data makes use of a moving aircraft to ground "target" configuration, as this was the first embodiment making use of these fundamental principles. A single target will return a Doppler frequency; *i.e.*, a Doppler curve which is a direct and analytic function of the aircraft path and velocity. Two targets are sufficient to establish aircraft position (given altitude and direction one target is sufficient, as is the case for a satellite of approximate known orbit). A more powerful aid to visualization of these principles of resolving a moving target in "azimuth" and "range" is provided by a Doppler mosaic. Fig. 1 shows such a mosaic oriented for a satellite with one-way propagation. This mosaic was originally developed for an aircraft with two-way propagation under conditions similar to those used for the experimental data (f_t—13.5 kmc, velocity—120 mph, Δf—as shown, $d\Delta f/dt$—×10) and simply relabeled to produce Fig. 1. Two sets of curves are shown, lines of constant Doppler frequency (radial lines converging at zero) and lines of constant rate of change of Doppler frequency (semi-elliptical curves, all tangent at the center). In three dimensions, the pattern is a figure of revolution around the velocity vector. Since we are concerned only with relative motion, consider the diagram attached to the satellite (or aircraft) with receiving sites (targets) moving through the pattern from right to left. The satellite path is assumed circular (altitude 400 miles), and thus a receiving station will follow the curved path (overhead pass) represented by the earth's surface. Off-course passes can be visualized in three dimensions as concentric circles around the earth's center and intersecting the mosaic above or below the plane of the paper.

The resolving power in determining satellite position is governed by equipment ability to measure Doppler frequency components in the presence of noise. The important point is that each element or segment of the Doppler curve can be properly weighted to provide a best "average" match or fit between the received signal (Doppler

* Received by the IRE, June 6, 1960.

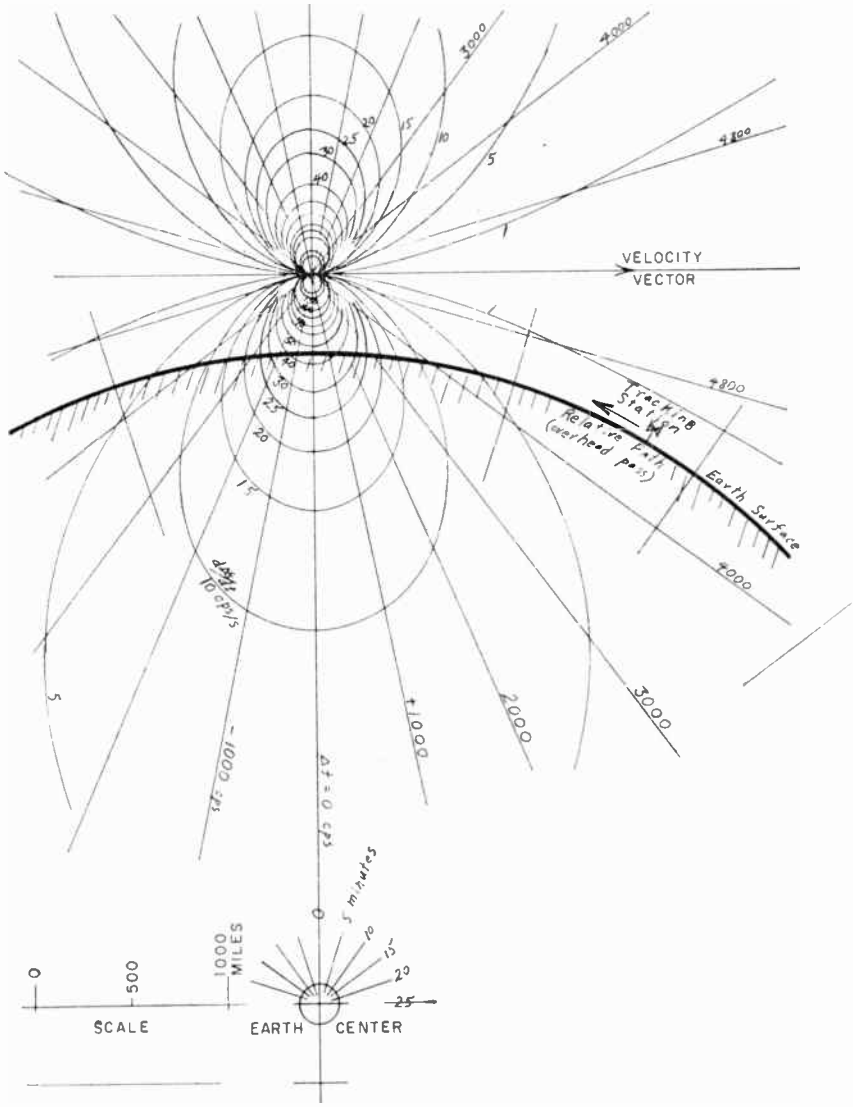

Fig. 1—Satellite Doppler mosaic.

Velocity—14,600 n mph
Period—100 minutes
Altitude—400 n miles
f_t—200 mc
f_d—5 kc
Δf—Doppler frequency.
$d\Delta f/dt$—Doppler rate.

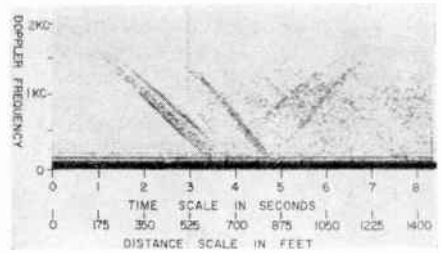

Fig. 2—Doppler curves of discrete ground targets.

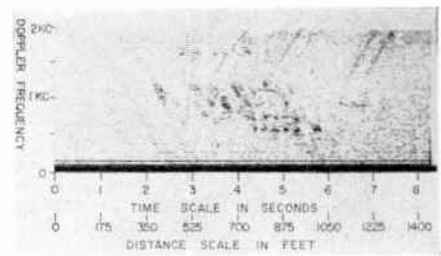

Fig. 3—Doppler curves of concentrated group buildings.

Fig. 4—Aerial photograph of buildings taken during run of Fig. 3. Position approximately indicated by zero on time-position scale.

curve) and a theoretical curve, *i.e.*, stored data in a computer or table.

The following experimental data was obtained by flying an *X*-band (9.25 kmc) CW device, along with the necessary instrumentation, in a Cessna 170B aircraft. The Doppler data was stored on a tape recorder for later ground analysis. The Doppler patterns were produced by analysis on a Kay Electric Company Sonalator, which provides a time vs frequency analysis. Suitable translation of this data will provide a "radar" map in the true sense.

Fig. 2 is a sonagraph of a set of rather discrete targets at the edge of a water-land boundary. The aircraft was proceeding over water to a large concrete dam, first target, with the second target situated in a heavily wooded background. The general nature of the Doppler curve and the relative positions of the various scatters (note slope variation) are apparent. A frequency calibration as well as a down range distance scale have been added.

Fig. 3 is a sonagraph of a multiplicity of target returns (a concentrated group of buildings) which contain a great deal of important and analyzable mapping information. Fig. 4 was taken with the aircraft moving from left to right in a northerly direction during the actual data run as analyzed in Fig. 3 (approximate photograph position indicated by zero on distance-time scale). By an odd set of circumstances, and I might add, by design, these flights were made in May, 1959, in the vicinity of the Johns Hopkins Applied Physics Laboratory, the buildings in the photographs.

Careful analysis will show the individual buildings as well as each of the trusses of the industrial type buildings to the north of the main laboratories. Visualization of target positions is somewhat analogous, in the frequency domain, to determining radar target locations by viewing an *A* scope in the time domain. The information content is quite astonishing when one considers that the bandwidth displayed is less than 2 kc with an apparent resolution of ten to twenty feet. Such data provide an indication of the accuracy that one should be able to realize in a blind landing or mapping application.

The above discussion evolves from a very long and arduous background. The principles were expounded in a document in 1956 entitled, "GODIVA—A Vehicle Guidance System." Copies of this document were circulated, and presentations were made to nearly all government agencies, industrial organizations and university groups actively engaged in guidance systems and/or Doppler radar technique developments at that time.

Through initiation of patent applications, this data was placed under secrecy order by the U. S. Government, and public disclosure could not be made. Numerous and varied program proposals have been made over these many years, including aircraft navigation, tracking, blind landing systems, "radar" mapping, etc. The Secrecy Order was removed effective March 29, 1960, obviously too late to permit our participation in the Space Electronics issue.

Ben R. Gardner
Consulting Engineer
P.O. Box 1267
Rancho Santa Fe, Calif.

WWV and WWVH Standard Frequency and Time Transmissions*

The frequencies of the National Bureau of Standards radio stations WWV and WWVH are kept in agreement with respect to each other and have been maintained as constant as possible with respect to an improved United States Frequency Standard (USFS) since December 1, 1957.

The nominal broadcast frequencies should, for the purpose of highly accurate scientific measurements, or of establishing high uniformity among frequencies, or for removing unavoidable variations in the broadcast frequencies, be corrected to the value of the USFS, as indicated in the table below.

The characteristics of the USFS, and its relation to time scales such as ET and UT2, have been described in a previous issue,[1] to which the reader is referred for a complete discussion.

The WWV and WWVH time signals are also kept in agreement with each other. Also they are locked to the nominal frequency of the transmissions and consequently may depart continuously from UT2. Corrections are determined and published by the U. S. Naval Observatory. The broadcast signals are maintained in close agreement with UT2 by properly offsetting the broadcast frequency from the USFS at the beginning of each year when necessary. This new system was commenced on January 1, 1960. The last time adjustment was a retardation adjustment of 0.02 s on December 16, 1959.

WWV Frequency
With Respect to U. S. Frequency Standard

1960 September 1600 UT	Parts in 10^{10}†
1	−148
2	−148
3	−148
4	−148
5	−148
6	−148
7	−148
8	−148
9‡	−148
10	−151
11	−150
12	−150
13	−150
14	−150
15	−149
16	−149
17	−149
18	−149
19	−149
20	−148
21	−148
22	−148
23	−148
24	−148
25	−148
26	−148
27	−148
28	−148
29	−147
30	−147

† A minus sign indicates that the broadcast frequency was low.

‡ The method of averaging is such that an adjustment of frequency appears on the day it is made. The frequency was decreased 3×10^{-10} on September 9.

National Bureau of Standards
Boulder, Colo.

* Received by the IRE, October 24, 1960.

[1] "National Standards of Time and Frequency in the United States," Proc. IRE, vol. 48, pp. 105–106; January, 1960.

Gain of a Traveling-Wave Parametric Amplifier Using Nonlinear Lossy Capacitors*

This letter presents an analysis of a traveling-wave parametric amplifier using nonlinear lossy capacitors. Tien and Suhl[1] have calculated the gain of a lossless transmission line parametric amplifier neglecting diode losses. The pump, signal, and idling frequencies were chosen to correspond to the case of the "inverting modulator" described by Manley and Rowe;[2] the frequencies are assumed to propagate with equal velocity along the circuit. Reverse biased diodes were considered to be the lossy capacitors, the resistive element being provided by the diode spreading resistance R_s only. The following transformation will be used:

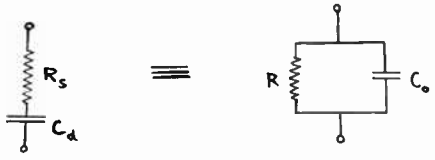

where

$$R = R_s(1 + Q^2) \approx R_sQ^2, \tag{1}$$

$$C_0 = \frac{C_d}{1 + \frac{1}{Q^2}} \approx C_d, \tag{2}$$

$$Q = \frac{1}{\omega C_d R_s}. \tag{3}$$

The approximate mean values for R and C_0 will be used in the analysis since the Q's are expected to be considerably greater than unity. It is evident that both components of the parallel representation of a diode are functions of frequency, although in the approximate expression the mean value of the diode capacitance C_0 is independent of frequency.

The model of the traveling-wave circuit is

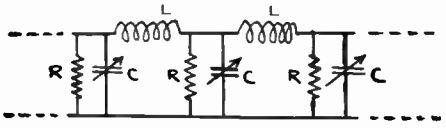

The mean value of the variable capacitor, C_0, comprises the distributed capacitance of the traveling-wave circuit per section.

It is assumed that the capacitance varies in the following manner:

$$C(zt) = C_0\left[1 + \tfrac{1}{2}\xi e^{j(\omega t - \beta z)} + \tfrac{1}{2}\xi e^{-j(\omega t - \beta z)}\right], \tag{4}$$

where

ω = pumping frequency,
ξ = fractional modulation of the diode capacitance.

It is assumed also that the line is energized by two waves $V_1(zt)$ and $V_2(zt)$ of frequencies ω_1 and ω_2 which are identified with the signal and the idling wave.

The differential equations for the line are as follows:

$$\frac{\partial V_1(zt)}{\partial z} = -L\frac{\partial I_1(zt)}{\partial t}, \tag{5}$$

$$\frac{\partial I_1(zt)}{\partial z} = -\frac{V_1(zt)}{R_1} - \frac{\partial}{\partial t}\left[C(zt)V_1(zt)\right] - \frac{\partial}{\partial t}\left[C(zt)V_2(zt)\right], \tag{6}$$

$$\frac{\partial V_2(zt)}{\partial z} = -L\frac{\partial I_2(zt)}{\partial t}, \tag{7}$$

$$\frac{\partial I_2(zt)}{\partial z} = -\frac{V_2(zt)}{R_2} - \frac{\partial}{\partial t}\left[C(zt)V_2(zt)\right] - \frac{\partial}{\partial t}\left[C(zt)V_1(zt)\right], \tag{8}$$

where R_1 and R_2 are the values of the equivalent parallel resistance of the diode at the frequencies ω_1 and ω_2, respectively. The terms in the square brackets are the coupling terms.

Assuming now

$$V_1(zt) = A_1(z)e^{j(\omega_1 t - \beta_1 z)} + A_1^*(z)e^{-j(\omega_1 t - \beta_1 z)}, \tag{9}$$

$$V_2(zt) = A_2(z)e^{j(\omega_2 t - \beta_2 z)} + A_2^*(z)e^{-j(\omega_2 t - \beta_2 z)}, \tag{10}$$

where $A(z)$'s are the amplitudes of the waves as functions of the distance z along the traveling-wave circuit; also assuming

$$\omega = \omega_1 + \omega_2 \tag{11}$$

$$\beta = \beta_1 + \beta_2 \tag{12}$$

where

$$\beta = \omega\sqrt{LC_0} \qquad \beta_1 = \omega_1\sqrt{LC_0}$$

$$\beta_2 = \omega_2\sqrt{LC_0}; \tag{13}$$

we obtain

$$\frac{\partial^2 A_1(z)}{\partial z^2} - j2\beta_1\frac{\partial A_1(z)}{\partial z} - j\frac{\omega_1 L}{R_1}A_1(z) + \frac{1}{2}\omega_1^2 LCA_2^*(z) = 0, \tag{14}$$

$$\frac{\partial^2 A_1^*(z)}{\partial z^2} + j2\beta_1\frac{\partial A_1^*(z)}{\partial z} + j\frac{\omega_1 L}{R_1}A_1^*(z) + \frac{1}{2}\omega_1^2 LCA_2(z) = 0. \tag{15}$$

Similar equations will be obtained for $A_2(z)$ and $A_2^*(z)$ by changing the subscripts from from 1 and 2 to 2 and 1, respectively. Since the amplitudes $A(z)$'s are slowly varying functions of z, the terms $\partial^2(A(z))/\partial z^2$ will be neglected.

Finally we obtain

$$\frac{\partial^2 A_1(z)}{\partial z^2} + \frac{C_0R_1}{2}(\beta_1\omega_1 + \beta_2\omega_2)\frac{\partial A_1(z)}{\partial z} + \frac{\beta_1\beta_2}{16}(4\omega_1\omega_2C_0^2R_s^2 - \xi^2)A_1(z) = 0. \tag{16}$$

Identical expressions will be obtained for $A_1^*(z)$, $A_2(z)$ and $A_2^*(z)$.

The solution of the above equation is

$$A_1(z) = a_1e^{\alpha_1 z} + b_1e^{\alpha_2 z},$$

* Received by the IRE, March 16, 1960; revised manuscript received, May 5, 1960.

[1] P. K. Tien and H. Suhl, "A traveling-wave ferromagnetic amplifier," Proc. IRE, vol. 46, pp. 700–706; April, 1958.

[2] J. M. Manley and H. E. Rowe, "Some general properties of nonlinear elements—part I. General energy relations," Proc. IRE, vol. 44, pp. 904–913; July, 1956.

where a_1 and b_1 are arbitrary complex constants to be determined from the boundary conditions, and the voltage gain per section in nepers is given by

$$\alpha_{1,(2)} = -\frac{1}{4} C_0 R_s(\beta_1\omega_1 + \beta_2\omega_2) \pm \frac{1}{4}\left[C_0^2 R_s^2(\beta_1\omega_1 - \beta_2\omega_2)^2 + \beta_1\beta_2\xi^2\right]^{1/2}, \quad (17)$$

with identical solutions for the other $A(z)$ functions.

In terms of the diode angular cutoff frequency at the average value of bias

$$\omega_c = \frac{1}{R_s C_0},$$

the gain per section is given by

$$\alpha_{1,(2)} = -\frac{1}{4}\frac{1}{\omega_c}(\beta_1\omega_1 + \beta_2\omega_2) \pm \left[\frac{1}{\omega_c^2}(\beta_1\omega_1 - \beta_2\omega_2)^2 + \beta_1\beta_2\xi^2\right]^{1/2}. \quad (18)$$

The amplitudes of the two progressive waves depend on the exponents α_1 and α_2, of which α_2 is always negative and gives rise to a strongly decaying wave. Amplification will be achieved only when the exponent α_1 is positive. Thus for amplification,

$$\alpha_1 > 0;$$

and this is satisfied by

$$\xi > 2\bar{\omega}C_0R_s = \frac{2}{Q} = \frac{2(\omega_1\omega_2)^{1/2}}{\omega_c} \quad (19)$$

where $\bar{\omega} = \sqrt{\omega_1\omega_2}$.

This condition gives the lower limit for the Q factor of diodes necessary to achieve amplification at a given fractional modulation of the capacitance.

Assuming 100 per cent modulation ($\xi = 1$), it is evident that for amplification the Q of the diode must be greater than 2. For a given diode, this condition gives also the maximum frequency at which parametric amplification may still be obtained and at lower frequencies the necessary minimum pump power to give the necessary modulation depth. Fig. 1 shows a family of curves of ξ corresponding to the threshold of amplification vs ω_1/ω_c, ω_p/ω_c being a parameter. These curves would lead one to believe that for a given value of capacitance modulation, gain is minimum at $\omega_1 = \omega_p/2$; however, the following calculations show this not to be true.

Substituting $\beta_1 = \omega_1/v$ and $\beta_2 = \omega_2/v$ in (18) and rewriting we obtain

$$\alpha\frac{v}{\omega_c} = \frac{1}{4}\left\{\left[\left(\frac{\omega_1^2}{\omega_c^2} - \frac{\omega_2^2}{\omega_c^2}\right)^2 + \frac{\omega_1\omega_2}{\omega_c^2}\xi^2\right]^{1/2} - \left(\frac{\omega_1^2}{\omega_c^2} + \frac{\omega_2^2}{\omega_c^2}\right)\right\}. \quad (20)$$

Fig. 2 shows graphical representation of (20); the pump frequency is fixed at 0.1 of the diode cutoff frequency. For values of ξ greater than 0.15 the gain is maximum when the signal frequency ω_1 is half the pump frequency ω_p.

Fig. 3 shows a family of curves relating gain with signal frequency, ω_p/ω_c being a parameter. The depth of modulation ξ is assumed constant at 0.5. For pump frequency equal or smaller than 0.4 of the diode cutoff frequency, the gain is maximum when the signal frequency is equal to half the pump frequency. The curves give an indication of the bandwidth of the amplifier. The maximum bandwidth is obtained when the pump frequency is equal to 0.4 of the diode cutoff frequency.

I would like to thank N. N. Hoffman for helpful discussions during my work on this problem.

W. Jasinski
Special Products Operation
Lansdale Div., Philco Corp.
Lansdale, Pa.

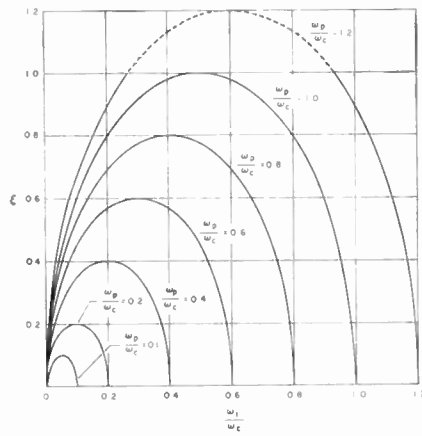

Fig. 1—Threshold of amplification.

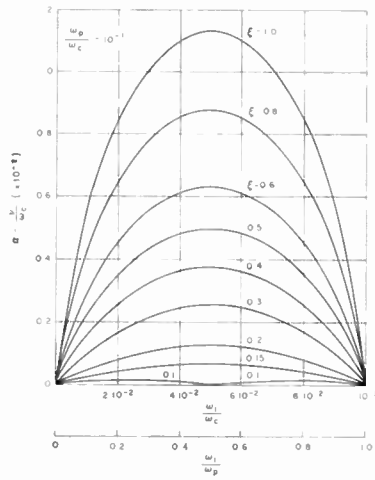

Fig. 2—$\alpha(v/\omega_c)$ vs (ω_1/ω_c); and $\alpha(v/\omega_c)$ vs (ω_1/ω_p).

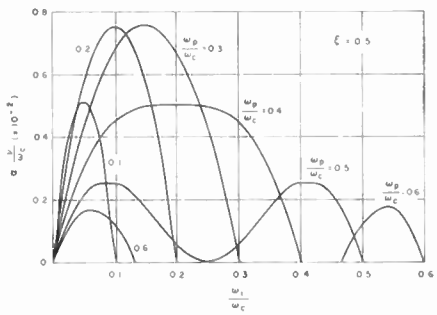

Fig. 3—$\alpha(v/\omega_c)$ vs (ω_1/ω_c).

Noise Figure Measurements Relating the Static and Dynamic Cutoff Frequencies of Parametric Diodes*

Variable-reactance semiconductor diodes suitable for parametric amplifier use are commonly characterized with respect to quality by the specification of a cutoff frequency based on the Q of the diode as a linear circuit element, *i.e.*,

$$f_c = \frac{1}{2\pi R_s C}. \quad (1)$$

The minimum capacity, near reverse breakdown, is ordinarily used in computing f_c. A number of convenient and comparable methods for measuring f_c have been described recently.[1,2]

From an analytical point of view, the degenerate-mode gain cutoff frequency is of considerable significance for simple three-frequency amplifiers, under small-signal conditions. This dynamic cutoff frequency is given by[3]

$$f_D = \frac{C_1}{2\pi R_s(C_0^2 - C_1^2)^{1/2}}, \quad (2)$$

where C_0 and C_1 are coefficients of the usual complex Fourier expansion of $C(t)$ for a hysteresis-free capacitor. If an expansion of elastance, $\sigma(t) = 1/C(t)$, is substituted for the capacitance version, an alternate, but equivalent expression for f_D is obtained,

$$f_D = \frac{\sigma_1}{2\pi R_s}. \quad (3)$$

A noise analysis for an appropriate open-circuit-stable model[4] can be made, and a minimum noise figure relationship obtained in terms of the operating frequencies normalized by f_D. For degenerate-mode conditions, the double-sideband standard noise figure F_0, at any signal frequency $f \leq f_D$, is given simply by

$$F_0 = \frac{1}{1 - \left(\frac{f}{f_D}\right)^2}. \quad (4)$$

for high-gain, band-center operation. A plot of F_0, in decibels according to (4), is shown in Fig. 1.

Parametric amplifier noise figure measurements have been carried out at the lower edge of the X-band, in an attempt to confirm the predicted noise behavior and to establish an experimental correlation between the static cutoff frequency f_c and the dynamic cutoff frequency f_D. The basic amplifier arrangement is shown in Fig. 2.

* Received by the IRE, August 12, 1960.

[1] N. Houlding, "Measurement of varactor quality," *Microwave J.*, vol. 3, pp. 40–45; January, 1960.

[2] S. T. Eng, "Characterization of Microwave Variable Capacitance Diodes," presented at the PGMTT Natl. Symp., San Diego, Calif.; May 9–11, 1960.

[3] C. S. Kim, "Parametric Converters and Amplifiers," General Electric Co., Syracuse, N. Y., Unpublished Rept.; May, 1958.

[4] C. R. Boyd, "A Generalized Approach to the Evaluation of n-Frequency Parametric Mixers," to be presented at the National Electronics Conf., Chicago, Ill.; October 10–12, 1960.

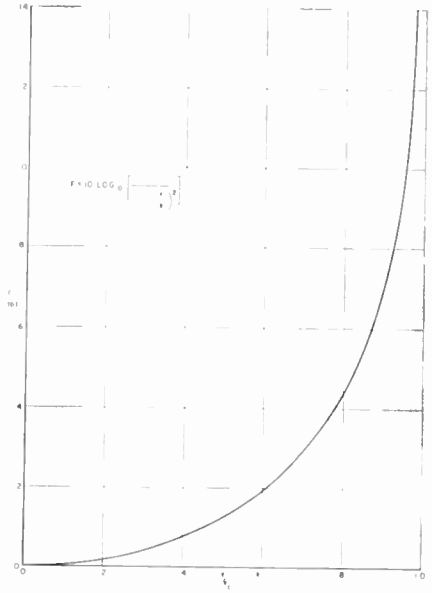

Fig. 1—Minimum noise figure, degenerate mode amplifier.

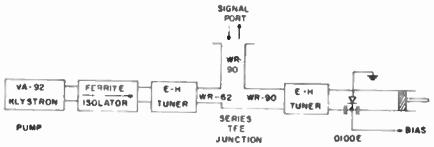

Fig. 2—Parametric amplifier circuit.

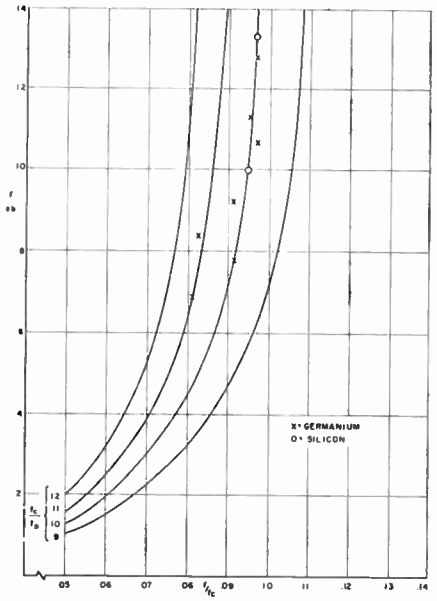

Fig. 3—Comparison of experimental data with computed performance.

Degenerate-mode amplification was obtained at about 8200 Mc with a number of diffused-junction mesa-type diodes, fabricated from silicon and germanium and having f_c values determined by the method of Houlding.[1] Noise figure was measured using an AIL-type 74 Noise Figure Indicator, with the gas-discharge noise source decoupled approximately 50 db from the amplifier through the use of several cascaded ferrite isolators. A conventional balanced mixer was used as the second stage, and the amplifier gain was adjusted to 15 db, on a single-sideband basis, for all measurements.

Fig. 3 shows the adjusted noise figure data obtained from these measurements, after accounting for insertion loss in the measuring circuit and second-stage noise contributions. The minimum noise figure achieved with each diode is plotted against the operating frequency normalized by the f_c of that diode. In addition, a family of computed noise figure curves for constant f_c/f_D ratios has been plotted over the experimental data. A qualitative correspondence between experimental and analytical behavior is evident, and an f_c/f_D ratio of 10 is indicated.

C. R. Boyd
Electronics Lab.,
General Electric Co.
Electronics Park, Syracuse, N. Y.

Gain Optimization in Low-Frequency Parametric Up-Converters by Multidiode Operation*

In the practical design of a low-frequency upconverter parametric amplifier, the theoretical gain given by earlier authors[1] is not always realizable, as shown by Kamal and Holub.[2]

It is the purpose of this note to suggest a completely new technique to optimize the gain in the low-frequency parametric upconverters. The method consists of using more than one variable capacitance diode at the same point. A first-order analysis is made only with two diodes, which demonstrates some very interesting facts. The method can also be extended to more than two diodes. The theoretical predictions are verified by an experimental amplifier.

Neglecting the series resistance R_s of the diode, a single-diode parametric upconverter can be represented in the $ABCD$ matrix form as[3]

$$\begin{bmatrix} -\frac{C_0}{C_1} & \frac{j}{\omega_u C_1} \\ j\omega_s C_1^* - j\frac{\omega_s C_0^2}{C_1} & -\frac{\omega_s}{\omega_u}\cdot\frac{C_0}{C_1} \end{bmatrix}, \quad (1)$$

where ω_s and ω_u represent the signal and upper sideband frequencies, respectively, the C_1^* is the conjugate of C_1.

The equivalent circuit of the amplifier including R_s can now be represented as in Fig. 1, and thus (1) can be written as

$$\begin{bmatrix} \left(-\frac{C_0}{C_1} - \frac{j\omega_s R_s C_0^2}{C_1} + j\omega_s C_1^* R_s\right) & \left(-\frac{C_0 R_s}{C_1} - \frac{j\omega_s R_s^2 C_0^2}{C_1} + j\omega_s C_1^* R_s^2 + \frac{j}{\omega_u C_1} - \frac{\omega_s C_0 R_s}{\omega_u C_1}\right) \\ \left(-\frac{j\omega_s C_0^2}{C} + j\omega_s C_1^*\right) & \left(-\frac{j\omega_s R_s C_0^2}{C_1} + j\omega_s C_1^* R_s - \frac{\omega_s C_0}{\omega_u C_1}\right) \end{bmatrix}. \quad (2)$$

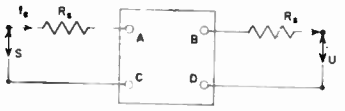

Fig. 1.

Transferring (2) into Y-matrix, one can write it in the form

$$\begin{bmatrix} Y_{11} & Y_{12} \\ Y_{21} & Y_{22} \end{bmatrix}. \quad (3)$$

For two symmetrical diodes in parallel, the admittance matrices add, giving

$$\begin{bmatrix} 2Y_{11} & 2Y_{12} \\ 2Y_{21} & 2Y_{22} \end{bmatrix}. \quad (4)$$

From the relationship between Y-matrices, the relation between double-diode and single-diode transmission matrices is given as

$$[\beta'] = \begin{bmatrix} A & \frac{B}{2} \\ 2C & D \end{bmatrix}, \quad (5)$$

where $[\beta']$ is the transmission matrix in the double-diode case, and A, B, C and D are the elements in the single-diode matrix.

Hence,

$$[B'] = \begin{bmatrix} \left(-\frac{C_0}{C_1} - \frac{j\omega_s R_s C_0^2}{C_1} + j\omega_s C_1^* R_s\right) & \left(-\frac{C_0 R_s}{2C_1} - \frac{j\omega_s R_s^2 C_0^2}{2C_1} + \frac{j\omega_s C_1^* R_s^2}{2} + \frac{j}{2\omega_u C_1} - \frac{\omega_s C_0 R_s}{2\omega_u C_1}\right) \\ \left(-\frac{2j\omega_s C_0^2}{C_1} + 2j\omega_s C_1^*\right) & \left(-\frac{j\omega_s R_s C_0^2}{C_1} + j\omega_s R_s C_1^* - \frac{\omega_s C_0}{\omega_u C_1}\right) \end{bmatrix}. \quad (6)$$

It is possible to split the matrix of (6) as

* Received by the IRE, June 17, 1960. This work was supported by the Magnavox Co., Fort Wayne, Ind.

[1] H. Rowe, "Some general properties of nonlinear elements II—small signal theory," Proc. IRE, vol. 46, p. 850; May, 1958.

[2] A. K. Kamal and A. J. Holub, "Gain inconsistencies in low frequency parametric upconverters," Proc. IRE (Correspondence), vol. 48, pp. 1784–1785; October, 1960.

[3] A. K. Kamal, "A parametric device as a nonreciprocal element," Proc. IRE, vol. 48, pp. 1424–1430; August, 1960.

$$\begin{bmatrix} \frac{1}{2} & 0 \\ 0 & 2 \end{bmatrix} \begin{bmatrix} 1 & 2R_s \\ 0 & 1 \end{bmatrix} \begin{bmatrix} 1 & 0 \\ \frac{j\omega_s C_0}{2} & 1 \end{bmatrix} \begin{bmatrix} 0 & \frac{2j}{|C_1|\sqrt{\omega_s\omega_u}} \\ \frac{j|C_1|\sqrt{\omega_u\omega_s}}{2} & 0 \end{bmatrix}$$

$$\begin{bmatrix} 1 & 0 \\ \frac{j\omega_u C_0}{2} & 1 \end{bmatrix} \begin{bmatrix} 1 & 2R_s \\ 0 & 1 \end{bmatrix} \begin{bmatrix} 2 & 0 \\ 0 & \frac{1}{2} \end{bmatrix}. \tag{7}$$

An interesting equivalent circuit that can be derived from the matrix of (7) is represented in Fig. 2, where

$$\begin{bmatrix} a & b \\ c & d \end{bmatrix} = \begin{bmatrix} 0 & \frac{2j}{|C_1|\sqrt{\omega_s\omega_u}} \\ \frac{j|C_1|\sqrt{\omega_s\omega_u}}{2} & 0 \end{bmatrix}. \tag{8}$$

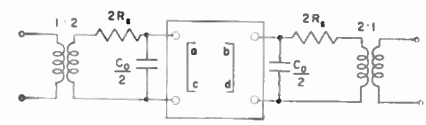

Fig. 2.

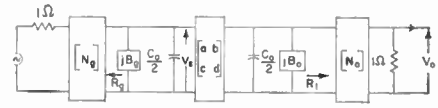

Fig. 3.

Following the procedure of Kamal and Hohnb,[2] the amplifier can be represented as shown in Fig. 3 where $[N_g]$ and $[N_0]$ are coupling networks matching the amplifier to the source and load, respectively.

$[N_g]$ and $[N_0]$ can be represented as

$$[N_g] = \begin{bmatrix} \frac{1}{\sqrt{R_g}} & 0 \\ 0 & \sqrt{R_g} \end{bmatrix}$$

$$[N_0] = \begin{bmatrix} \sqrt{R_L} & 0 \\ 0 & \frac{1}{\sqrt{R_L}} \end{bmatrix}$$

where R_g and R_L are transformed source and load impedances, respectively. In the above circuit representation, the series resistance of the diodes has been neglected since the net series resistance $2R_s$, when transferred to the source and load sides of the transformers in Fig. 2, becomes $R_s/2$ and, hence, can be neglected in comparison with the source and load impedances. Single-frequency operation is assumed so that the capacitances $C_0/2$ at the input and output are tuned out by the susceptances jB_u and jB_0.

The transfer matrix for the amplifier can now be written as

$$[T] = [TaQTb]$$

$$= \sqrt{\frac{\omega_s}{\omega_u}\cdot\frac{C_1^*}{C_1}} \begin{bmatrix} \frac{1}{\sqrt{R}} & 0 \\ 0 & \sqrt{R} \end{bmatrix} \begin{bmatrix} \frac{1}{2} & 0 \\ 0 & 2 \end{bmatrix} \begin{bmatrix} 0 & \frac{2j}{|C_1|\sqrt{\omega_s\omega_u}} \\ \frac{j|C_1|\sqrt{\omega_s\omega_u}}{2} & 0 \end{bmatrix}$$

$$\begin{bmatrix} 2 & 0 \\ 0 & \frac{1}{2} \end{bmatrix} \begin{bmatrix} \sqrt{R} & 0 \\ 0 & \frac{1}{\sqrt{R}} \end{bmatrix} \tag{9}$$

$$= \sqrt{\frac{\omega_s}{\omega_u}\cdot\frac{C_1^*}{C_1}} \begin{bmatrix} 0 & \frac{j}{2|C_1|R\sqrt{\omega_s\omega_u}} \\ 2j|C_1|R\sqrt{\omega_s\omega_u} & 0 \end{bmatrix}. \tag{10}$$

where $R = R_g = R_L$.

The power gain can be calculated from the relation[4]

$$G_p = \frac{P_u}{P_g} = \frac{4\left(\frac{\omega_u}{\omega_s}\right)}{\left|\sum_{ij} T_{ij}\right|^2} = \frac{4\frac{\omega_u}{\omega_s}}{2 + 4|C_1|^2R^2\omega_s\omega_u + \frac{1}{4|C_1|^2R^2\omega_s\omega_u}} = \frac{4\left(\frac{\omega_u}{\omega_s}\right)}{2 + \alpha' + \frac{1}{\alpha'}}. \tag{11}$$

where

$$\alpha' = 4|C_1|^2R^2\omega_s\omega_u.$$

From (11), we find the G_p is maximum only when

$$4|C_1|^2R^2\omega_u\omega_s = 1. \tag{12}$$

It is interesting to note that the parameter α', in the case of double-diode operation, is four times the parameter α of a single-diode case. This shows that with double-diode operation one can approach the unity value for α' far easier than in the case of a single-diode operation.

Following the procedure of Kamal and Hohnb,[2] the input impedance is found to be

$$Y_{in} = \frac{\alpha'}{R},$$

which is four times that of a single diode.

The experimental verification of the analysis was achieved with the following setup:

$f_s = 220$ mc
$f_p = 1120$ mc
$f_u = 1340$ mc
$C_0 = 10$ $\mu\mu$f for both capacitors
$R_g = R_L = R = 50$ ohms.

For this setup, maximum gain is given by

$$G_{p\max} = \frac{\omega_u}{\omega_s} = 6.1.$$

The input impedance measurement gave, for a single diode, $C_1 = 2.54$ pf. The gain for a single diode obtained under this setup is 3.8.

Assuming the above parameters for each single diode, the expected value of α' is 0.76 and $G_p = 5.97$, which was found to be in close agreement with the experimental results obtained. It is thus clear that with the existing diodes, the maximum possible gain can easily be obtained by means of multi-diode operation.

A. K. Kamal
M. Subramanian
Millimeter Wave Res. Lab.
School of Elec. Engrg.
Purdue Univ.
Lafayette, Ind.

[4] H. Seidal and G. Hermann, "Circuit aspects of parametric amplifiers," 1959 IRE Wescon Convention Record, pt. 2, pp. 83–90.

Idler Noise in Parametric Amplifiers*

Parametric amplifiers of the negative resistance type manifest a phenomenon known as idler noise, which presents a basic limitation to their usefulness as low-noise amplifiers. It will be shown here that idler noise is of a fundamental nature and is, therefore, impossible to eliminate. It arises

* Received by the IRE, June 6, 1960.

in fact from a much more general relation which appears as a constraint equation on gain processes in any lossless parametric system.

The most familiar type of parametric amplifier is one in which there is a pump at frequency ω_p, a signal at frequency ω_s, and an idler at frequency $\omega_i=\omega_p-\omega_s$. Noise figures calculated for either single diode amplifiers or traveling-wave structures are given for very high gain by

$$F = 1 + \omega_s/\omega_i \tag{1}$$

for loads at room temperature and lossless elements. The term ω_s/ω_i is caused by noise generated by amplifier loads at the idler frequency. Attempts to eliminate this noise by clever balancing schemes have invariably proved futile, and it has become accepted as an unavoidable side effect of the amplification process.

Consider more generally a parametric system that operates at a manifold of frequencies $\omega_s+n\omega_p$, where n can assume various positive or negative integral values. Depending upon the sign of $\omega_s+n\omega_p$, let these frequencies be referred to as positive or negative. While in practice it is possible for several of these frequencies to pass through a single-circuit port, we assign, on a purely formal basis, separate ports to different frequencies. Port j is thus associated with a particular frequency ω_j of the manifold. Several of the ω_j may, however, be identical, since a given frequency may be associated with several ports (such as input and output). Let a_j and b_j represent amplitudes of incident and reflected waves at port j, normalized such that $|a_j|^2$ and $|b_j|^2$ equal respective powers. Using matrix notation, let the vectors $\boldsymbol{a}$ and $\boldsymbol{b}$ represent, respectively, the manifolds a_j and b_j. In the linearized theory of parametric amplifiers, $\boldsymbol{a}$ and $\boldsymbol{b}$ are related by the equation

$$\boldsymbol{b} = \boldsymbol{S}\boldsymbol{a}, \tag{2}$$

where $\boldsymbol{S}$ is a scattering matrix characterizing the system. Note that the normalization constants involved in the definition of $\boldsymbol{S}$ are chosen equal to the network terminations.

Gain is defined as follows. Let power be incident only at a single port, *e.g.*, port j. The gain factor g_{kj} is then defined as the ratio of output power at port k to the incident power. Putting $a_m=0$ for all m except for $m=j$, one finds

$$g_{kj} = |b_k|^2/|a_j|^2 = |S_{kj}|^2. \tag{3}$$

The starting point in establishing constraints on the g_{kj}'s is the Manley and Rowe relation,[1] which in terms of the above formalism is given by

$$\sum_j \frac{|a_j|^2}{\pm\omega_j} = \sum_j \frac{|b_j|^2}{\pm\omega_j}, \tag{4}$$

where a plus or minus sign is used, depending upon the sign of ω_j as defined above. Let $\boldsymbol{\Omega}$ be a diagonal matrix whose jth diagonal element equals $\pm\omega_j$. Then (4) can be rewritten in the matrix form

$$\tilde{\boldsymbol{a}}\boldsymbol{\Omega}^{-1}\boldsymbol{a} = \tilde{\boldsymbol{b}}\boldsymbol{\Omega}^{-1}\boldsymbol{b} = \tilde{\boldsymbol{a}}\tilde{\boldsymbol{S}}\boldsymbol{\Omega}^{-1}\boldsymbol{S}\boldsymbol{a}, \tag{5}$$

where the tilde($\sim$) denotes the complex conjugate of the transpose of a given matrix. Since this holds for all $\boldsymbol{a}$, we have

$$\tilde{\boldsymbol{S}}\boldsymbol{\Omega}^{-1}\boldsymbol{S} = \boldsymbol{\Omega}^{-1}. \tag{6}$$

The jth diagonal element of this matrix equation is

$$\sum_k \pm \tilde{S}_{jk}\omega_k^{-1}S_{kj} = \omega_j^{-1}.$$

Since, by definition, $\tilde{S}_{jk}=S_{kj}^*$,

$$\sum_k \pm\frac{\omega_j}{\omega_k}|S_{kj}|^2 = \sum_k \pm\frac{\omega_j}{\omega_k}g_{kj} = 1 \tag{7}$$

where plus or minus signs are used, depending upon whether ω_j and ω_k are of the same or of different signs. Eq. (7) is the first constraint relation on gain factors. It is simply a restatement of the Manley and Rowe relation for the case in which power is introduced only at port j, and the summation is performed over output power through all ports.

Of more interest is a less obvious relation which may be obtained by reversing the role of input and output ports in (7); *i.e.*, performing a time reversal operation on the system. To derive this relation, we consider $\boldsymbol{S}^{-1}$, which describes the time-reversed scattering process. It can be readily checked that $\boldsymbol{S}^{-1}$ also obeys (6); *i.e.*,

$$\tilde{\boldsymbol{S}}^{-1}\boldsymbol{\Omega}^{-1}\boldsymbol{S}^{-1} = \boldsymbol{\Omega}^{-1}, \tag{8}$$

as one would expect from the reversible nature of the Manley and Rowe relation. Taking the inverse of (8), one obtains the equation

$$\boldsymbol{S}\boldsymbol{\Omega}\tilde{\boldsymbol{S}} = \boldsymbol{\Omega}, \tag{9}$$

the jth diagonal element of which is given by

$$\sum \pm S_{jk}\omega_k\tilde{S}_{kj} = \pm\omega_j.$$

Again, since $S_{kj}=S_{jk}^*$, we get

$$\sum_k \pm|\frac{\omega_k}{\omega_j}S_{jk}|^2 = \sum_k \pm\frac{\omega_k}{\omega_j}g_{jk} = 1. \tag{10}$$

This is the second gain constraint relation. Note that the summation is over all input ports k for a single fixed output port j. It is a constraint on "where gain must come from." According to it, it is impossible to eliminate undesirable forms of gain which result in excess noise without affecting desirable gain as well.

From (7) and (10), it possible to draw quite general conclusions on the limitations of parametric systems. Greatest physical insight into noise processes would perhaps be gained by formulating a theory of parametric systems within a thermodynamic framework. Since such a discussion would be outside the scope of this letter, we limit ourselves here to the simplest application, namely, a derivation of idler noise for the example of a negative resistance amplifier, in which a signal at ω_s and a single idler at $\omega_i=\omega_p-\omega_s$ are the only small signal frequencies present. Input and output are both taken at ω_s, and the input and output ports are designated by 1 and 2, respectively. In (10) we can separate the sum into two parts, the first consisting of summation over all signal ports, and the second of summation over all idler ports, to give

$$\sum_{k(\text{sig})} g_{2k} - \frac{\omega_i}{\omega_s}\sum_{k(\text{idl})} g_{2k} = 1. \tag{11}$$

Assuming all loads to be at room temperature, the incident noise power at any port is given by kTB, where B is the bandwidth, and the total noise output at port 2 is

$$N_{\text{out}} = kTB\left[\sum_{k(\text{sig})} g_{2k} + \sum_{k(\text{idl})} g_{2k}\right]. \tag{12}$$

Making use of (11), this gives

$$N_{\text{out}} = kTB\left[(1+\omega_s/\omega_i)\sum_{k(\text{sig})} g_{2k} - \omega_s/\omega_i\right].$$

For large gain, approximately,

$$N_{\text{out}} \simeq kTB\left[(1+\omega_s/\omega_i)\sum_{k(\text{sig})} g_{2k}\right]. \tag{13}$$

The noise figure definition is given by

$$F = \frac{N_{\text{out}}}{g_{21}kTB}. \tag{14}$$

Hence, according to (13),

$$F = (1+\omega_s/\omega_i)\sum_{k(\text{sig})} g_{2k}/g_{21}.$$

The minimum noise figure is obtained when g_{21} is the only nonvanishing among the g_{2k} (where k goes over all signal ports). It is given by

$$F = 1 + \omega_s/\omega_i. \tag{15}$$

A similar equation is obtained when the output is taken at the idler frequency ω_i. In deriving this equation, no assumptions whatsoever have been made as to the particular circuit or the number of elements in it. Similar idler noise contributions are also obtained in amplifiers employing a larger number of frequencies.

The off-diagonal terms of the matrix (9) give a somewhat different constraint, one which relates to scattering into two different ports. It is of interest only in a system in which output is extracted from two ports, such as a double sideband amplifier followed by a detector stage in which the pump serves as local oscillator.

The above relations were evolved in the course of discussions with Harold Seidel, to whom the author is greatly indebted.

GABRIEL HERRMANN
Sylvania Electric Products, Inc.
Microwave Physics Lab.
Mountain View, Calif.
Formerly at
Bell Telephone Labs., Inc.
Murray Hill, N. J.

[1] J. M. Manley and H. E. Rowe, "Some general properties of nonlinear elements," PROC. IRE, vol. 44, pp. 904–913; July, 1956.

Esaki Diode Amplifiers at 7, 11, and 26 KMC*

Gallium arsenide Esaki diode amplifiers have been operated with stable gains up to 38 db at 6.8 kmc and 10.8 kmc, and 36 db at 25.8 kmc. The basic amplifier consists of a reflection cavity containing the diode with

* Received by the IRE, August 15, 1960.

the input and output separated by means of a circulator or directional coupler.

Small junction diodes were prepared by alloying a point of pure tin or tin containing 5 per cent tellurium to zinc-doped gallium arsenide ($\rho = 0.0015$ ohm-cm).[1] Peak currents ranged from 0.5 to 1 ma with peak-to-valley ratios of 3 to 1 or better.

The reflection cavity which has been described previously[1] was cylindrical in shape with the diode shunting the apex of a reentrant cone to the opposite face. The cavity operated in the dominant mode for which the diameter is essentially half of a wavelength. Microwave power was coupled into and out of the cavity by means of a large coupling loop on the end of a coaxial line fed from waveguide. Except at the highest frequency, a small range of loop positions within the cavity could be found over which oscillation could be quenched in the entire negative resistance region of the diode characteristic. With the loop set in the center of this range, a slide-screw tuner in the waveguide served as a fine control on the gain which could be varied from 5 to 38 db by insertion of the screw. At 25.8 kmc the loop was soldered to the interior of the cavity, and all tuning adjustments had to be made in the waveguide.

A portion of the current-voltage characteristic, and the gain as a function of bias at 10.8 kmc for a particular adjustment is shown in Fig. 1. The peak gain is 19.4 db

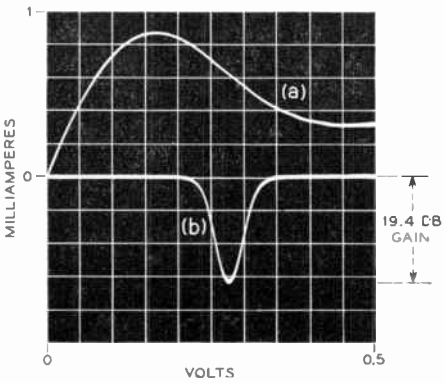

Fig. 1—(a) Current-voltage characteristic of a GaAs Esaki diode operating in an amplifier at 10.8 kmc. (b) Detected power output at 10.8 kmc as a function of bias voltage for a constant input voltage. Peak gain is 19.4 db.

and drops very rapidly for small bias deviations on either side of the point of maximum negative slope of the I-V characteristic. Fig. 2 shows the saturation characteristic of this amplifier. When the gain is high, it is particularly sensitive to small changes in the negative resistance (or average negative resistance for finite amplitude signals). At the bias for maximum gain the diode resistance is a minimum, and therefore the gain drops for small bias changes or for finite amplitude signal swings.

Fig. 3 shows the bandwidth vs gain for an amplifier operating at 10.8 kmc. As is

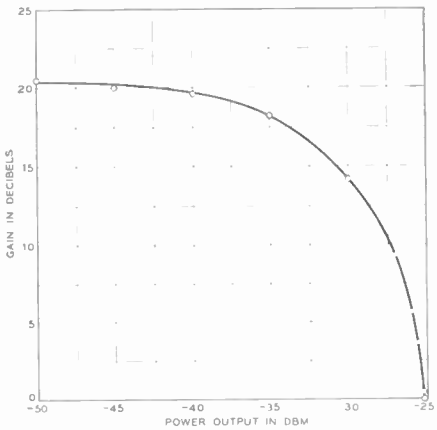

Fig. 2—Saturation characteristic of the 10.8 kmc amplifier.

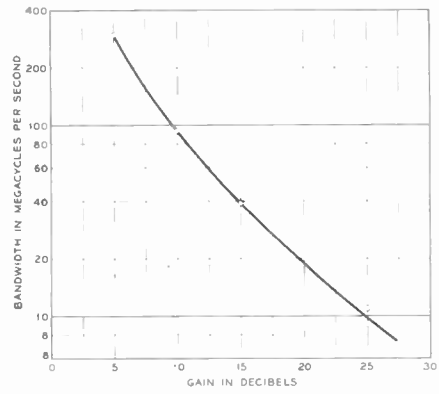

Fig. 3—Bandwidth-gain relationship for the 10.8 kmc amplifier.

typical of a reflection amplifier, the gain and frequency response were found to be dependent upon reflections from the circulator. With a poorly matched circulator, peaks in gain could be found at several frequencies; and a strong tendency to break into oscillation at an unwanted frequency often interfered with gain adjustments.

Measured noise figures were 7.5 db at 6.8 kmc (25-db gain), 10.7 db at 9.7 kmc (22-db gain), and 11.5 db at 10.8 kmc (26-db gain). Noise measurements were not made at 25.8 kmc. These figures are higher than the 7-db figure obtained at 4.5 kmc with a germanium diode by Yariv, Cook and Butzien[2] and considerably higher than one would expect from the expressions given by Chang[3] and others.[4] The large noise figures result from circuit losses as well as from excessive diode shot noise.

The authors would like to thank F. A. Braun for constructing the cavities, C. A. Burrus for providing the gallium arsenide, and N. E. Chasek for the noise figure measurement at 6.8 kmc.

R. F. Trambarulo
Bell Telephone Labs., Inc.
Holmdel, N. J.

[1] R. Trambarulo and C. A. Burrus, "Esaki diode microwave oscillators," Proc. IRE, vol. 48, p. 1776; October, 1960. Also, C. A. Burrus, private communication.

[2] A. Yariv, J. S. Cook, and P. E. Butzien, "Operation of an Esaki diode microwave amplifier," Proc. IRE, vol. 48, p. 1155; June, 1960.

[3] K. K. N. Chang, "Low noise tunnel-diode amplifier," Proc. IRE, vol. 47, pp. 1268–1269; July, 1959.

[4] M. E. Hines and W. W. Anderson, "Noise performance theory of Esaki (tunnel) diode amplifier," Proc. IRE, vol. 48, p. 789; April, 1960.

A Broad-Band Hybrid Coupled Tunnel Diode Down Converter*

Recent work on tunnel diode traveling-wave amplifiers demonstrated the need for a low-noise broad-band radio frequency mixer that provides isolation between the tunnel diode amplifier and the local oscillator. It was found that the presence of even small amounts of local oscillator signal greatly reduced amplifier gain. A hybrid coupled tunnel diode down converter which has the required isolation, moderate power gain, a very large bandwidth, a reasonable noise figure, and absolute stability has been constructed and tested.

A pair of matched tunnel diodes (G.E. 1N2939) and a balanced IF circuit are connected to two arms of a Sage 751 hybrid as shown in Fig. 1. The 30-Mc transformer consists of a balanced tank circuit with the center tap of the inductor opened so that the tunnel diodes may be individually biased. When biased near the peak current point in the positive conductance region of the I-V characteristic as indicated in Fig. 2, the tunnel diodes appear as positive balanced loads to the local oscillator and hybrid action causes cancellation of the local oscillator signal at the signal input terminals.

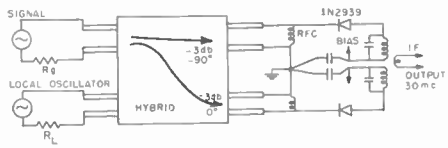

Fig. 1—Block diagram of hybrid coupled tunnel diode down converter.

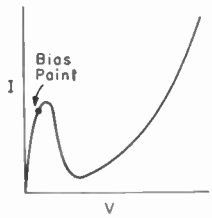

Fig. 2—Tunnel diode I-V characteristic.

When driven by the local oscillator the tunnel diodes and IF circuit appear as balanced negative conductances to the incoming signal. Hybrid action isolates the input terminal from the signal source when the local oscillator terminal is terminated in a matched load.

Measurements indicate that power gain and noise figure are critically dependent upon the power input from the local oscillator. A power input of 10 μ watts was required to yield maximum power gain and minimum noise figure. Hybrid action attenuates the local oscillator signal at the input terminal at least 20 db when the tunnel diodes are carefully matched.

Stable small signal conversion gains up to 10 db were measured at 400 Mc. A two-

* Received by the IRE, August 22, 1960.

channel noise figure of 7 db was measured with a Hewlett-Packard 342A noise figure meter at 400 Mc. At higher frequencies power gain and noise figure deteriorate due to the cutoff frequency of the tunnel diodes that were used. With matched tunnel diodes the down converter is both open and short circuit stable at the input terminals without the use of a nonreciprocal device. Additional selectivity may be obtained by employing tuned circuits or filters at the input terminals without affecting stability. Dynamic response of the down converter is shown in Fig. 3.

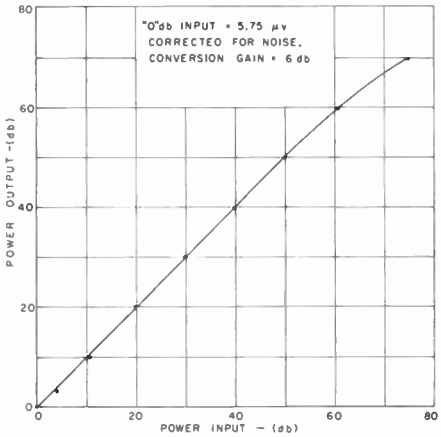

Fig. 3—Dynamic response of tunnel diode down converter.

It is felt that further refinements will improve the performance of the device. In particular, the use of gallium arsenide tunnel diodes may lower the noise figure to a more acceptable value. The use of two octave hybrids which are available, and improved tunnel diodes, should make it possible to construct a down converter with a 6:1 frequency range. Even in its present stage of development the hybrid coupled tunnel diode down converter offers considerable advantage over the conventional crystal mixer in the UHF band.

W. J. Robertson
Antenna Lab.
The Ohio State University
Columbus, Ohio

Millimeter Wave Esaki Diode Oscillators*

Esaki diode oscillators operating at frequencies to about 40 kMc (7.5 mm wavelength) have been reported recently from the Bell Telephone Laboratories.[1] The diodes employed were small area alloyed junctions made by electrically "forming" a point contact between tin and p-type gallium arsenide.[2,3]

More recently the high frequency limit at which fundamental oscillations have been observed has been extended to 103 kMc (2.9 mm wavelength). The Esaki diodes used in these latter experiments were made by electrically "forming" a point contact between zinc and heavily doped ($\rho = 0.0007$–0.0009 ohm-cm) n-type gallium arsenide.[2] Peak currents of these diodes ranged from a few hundred microamperes to several milliamperes, with peak-to-valley ratios of 3 to 1 or better.

The circuits employed were similar to those of Trambarulo and Burrus.[1] They consisted of reduced height rectangular waveguides into which the Esaki diodes were built, with a movable shorting piston inserted behind the diode. The Esaki diode was followed by an attenuator, cavity wavemeter and video detector diode. The rectified output of the detector was fed directly to an oscilloscope preamplifier. Bias for the oscillator was supplied from low impedance dc or 60-cps ac sources.

The frequency of oscillation depended upon both the waveguide size and the diode. Fundamental oscillations from frequencies near the waveguide cutoff to more than three times this frequency were observed in the same circuit, depending upon the particular diode employed, with each diode oscillating over a different range of frequencies. Both "strong" and "weak" oscillations, as defined in the literature,[1] were observed.

The highest frequency fundamental oscillation observed to date was at 103 kMc. The diode had a peak current of 600 μa and was mounted in 0.122×0.010 inch waveguide (48.4 kMc low frequency cutoff). Oscillation occurred from 93 to 103 kMc, tunable over this range by movement of the waveguide piston. At regular intervals of the piston position the oscillation was completely suppressed. This suppression was evidenced by a gradual shrinkage in the length and amplitude of the s-shaped indication of oscillation in the negative resistance portion of the diode characteristic, and by simultaneous diminution and disappearance of detected microwave output.

Fig. 1 shows an example of the voltage-current character stic of an oscillating Esaki diode and the corresponding detected microwave output.

In a few instances the frequency of oscillation could be varied 33 to 38 per cent by movement of the waveguide piston. The frequency variation more commonly obtained by such tuning, however, was 10 to 25 per cent. The frequency sweep provided by the diode bias variation was usually 0.5 to 2 per cent.

Diodes employed in the 50 to 100-kMc oscillators had peak currents in the 0.5 to 2 ma range. Diodes having lower peak currents did not oscillate in the circuits employed, and those with higher peak currents usually oscillated at frequencies below the waveguide cutoff so that only harmonic output could be observed.

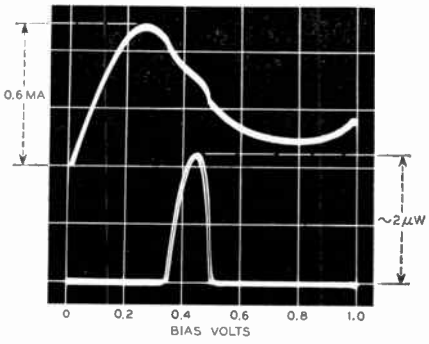

Fig. 1—Oscilloscope tracing of the 60-cps voltage-current characteristic of an oscillating Esaki diode (upper trace), and the corresponding detected microwave output at 80 kMc.

Some indication of the power output of the oscillators was obtained by use of a video detector diode calibrated at 58 kMc against a calorimeter.[4] On the basis of measurements with this diode, the maximum power so far obtained was 25 μw, or approximately −16 dbm, at 50 kMc, falling off to about 2 μw at 90 kMc and a few tenths of a microwatt at 100 kMc.

We should expect that the high frequency limit of oscillation, the operating efficiency and the tuning range of the oscillators might be increased with more nearly optimum circuitry.

C. A. Burrus
Bell Telephone Labs., Inc.
Holmdel, N. J.

[4] W. M. Sharpless, "A calorimeter for power measurements at millimeter wavelengths," IRE Trans. on Microwave Theory and Techniques, vol. MTT-2, pp. 45–47; September, 1954.

The Effect of Rain on the Noise Level of a Microwave Receiving System*

A low-noise receiving system,[1] using a high-gain horn-reflector antenna and a traveling-wave solid-state maser, is currently being used to measure zenith sky-noise temperatures for various sky conditions, at a frequency of 6 kMc. This study is directed towards evaluating the variability in noise level for receivers to be used in space communications.[2] The measured input noise temperature consists of a constant term, which includes noise contributed by the maser, waveguide, and residual in the antenna; these amount to 17° K. An additional term is the sky temperature, which varies as a function of atmospheric absorption in the volume of the sky subtended by the an-

* Received by the IRE, September 20, 1960.
[1] R. F. Trambarulo and C. A. Burrus, "Esaki diode oscillators from 3 to 40 kMc," Proc. IRE, vol. 48, pp. 1776–1777; October, 1960.

[2] C. A. Burrus, unpublished work.
[3] These diodes have been used as amplifiers at frequencies to 26 kMc. (R. F. Trambarulo, "Esaki diode amplifiers at 7, 11, and 26 kMc," in this issue, p. 2022.)

* Received by the IRE, August 11, 1960.
[1] R. W. DeGrasse, D. C. Hogg, E. A. Ohm and H. E. D. Scovil, "Ultra-low noise measurements using a horn reflector antenna and a traveling wave maser," *J. Appl. Phys.*, vol. 30, p. 2013; 1959.
[2] J. R. Pierce and R. Kompfner, "Transoceanic communication by means of satellites," Proc. IRE, vol. 47, pp. 372–380; March, 1959.

tenna beam; on a clear day, the sky noise[3] is about 3° K, which increases the input noise to 20° K.

Much higher noise levels are observed when rain occurs or is imminent at the receiver location. It is natural to expect wide variations in zenith sky-noise temperature, when a rain storm is in the vicinity of the receiver, for it is during this period that the precipitation in the antenna beam is undergoing relatively rapid changes due to movement of the clouds by the wind.

Observed sky temperatures for a rain that occurred during the evening of June 24, 1960, are shown in the figures, along with ground rain rate obtained from a tipping-bucket rain gauge located 50 feet from the antenna. These data were selected as representative of the changes which usually occur in zenith sky temperatures just prior to and on arrival of the rain at the ground. The sky temperature, before the actual arrival of the rain and after its departure from the location, may undergo variations on the order of several degrees. It should be noted in Fig. 1 that an abrupt increase in sky

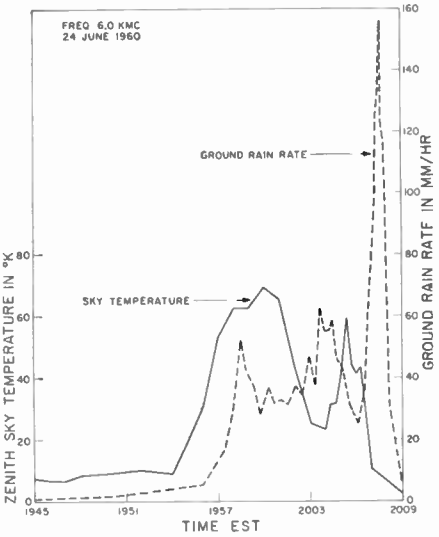

Fig. 1

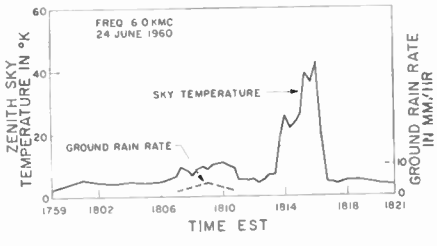

Fig. 2

noise is observed well before any significant rain is measured at the ground, thus the sky noise is a precursor of the rain.

Of special interest are the data shown in the last portion of Fig. 2; note that although the sky temperature increases more than 40°, no rain is recorded at the ground. As stated previously, the observed noise levels vary widely with atmospheric conditions, sky temperatures in excess of 120° K having been observed during storms.

D. C. Hogg
R. A. Semplak
Bell Telephone Labs., Inc.
Holmdel, N. J.

[3] D. C. Hogg, "Effective antenna temperatures due to oxygen and water vapor in the atmosphere," *J. Appl. Phys.*, vol. 30, pp. 1417–1419; September, 1959.

Electronically-Tunable Traveling-Wave Masers at L and S Bands*

Operating solid-state masers for the lower microwave frequencies using ruby-loaded cavity structures have previously been reported.[1–7] Furthermore, masers utilizing distributed structures giving nonreciprocal gain have resulted in a significant advance in the state-of-the-art.[8,9,5] It is the purpose of this note to report on electronically-tunable traveling-wave maser operation in the L- and S-band regions utilizing ruby as the active material.

Emphasis in this work was placed upon tunability. In general, the tuning range is inversely proportional, and the TWM gain in db is directly proportional to the slowing factor S of the slow-wave structure (where S = velocity of light/group velocity). It follows that a required tuning range tends to limit the gain per unit length that is obtainable.

The test data for tunable traveling-wave maser sections operated in three frequency regions is given in Table I. As can be seen, tuning ranges of 250 Mc or more have been obtained with sufficiently high gains to yield reasonable structure lengths. The active length of all structures was $1\frac{7}{8}$ inches and the ruby chromium content was nominally 0.05 per cent. The lower gain of structure I is due in part to the smaller electrical length at the lower signal frequency. Electronic gains measured at 4.2° K were approximately 40 per cent of those reported in Table I which were taken at 1.6 to 1.8° K. The magnetic fields and pump frequencies used were close to the values predicted from the energy level diagrams for three-level maser operation, ranging from 1.75 to 2.45 kilo-oersteds and 10,900 to 12,800 Mc, respectively. The nonmagnetic losses in the experimental structures were 2 db for structure I, and 1 db for structures II and III at liquid helium temperatures. The bandwidth measured in the test structures extrapolates to a 25-Mc bandwidth in a full-length structure, having an electronic gain of 30 db. The effective magnetic Q, calculated from the data in Table I, is approximately 70 for all three structures.

TABLE I
Tunable Traveling-Wave Maser Test Data

Structure Number	Tuning Range (Mc)	Electronic Tuning Range	Average Electronic Gain (db)	Liquid Helium Operating Temperature (°K)	Midband Structure Slowing Factor	Saturation Output Power (dbm)	Ferrite Isolator Reverse Loss at Helium Temperature (db)	Structure Length for 30-db Electronic Gain
I	1120 to 1370	20 per cent	6.5	1.6	98	−23	—	8.5 inches
II	1850 to 2150	15 per cent	9.4	1.7	75	−22	—	6.0 inches
III	2100 to 2400	13 per cent	9.1	1.8	72	—	19	6.2 inches

The slow-wave structure that we employed is similar to the comb-structure pioneered by the workers of Bell Telephone Laboratories.[8] We placed active ruby on both sides of the comb; this was done since, for the 90° orientation of the ruby C-axis relative to the applied magnetic field, the matrix elements for the signal transition become increasingly linearly-polarized as the signal frequency is decreased. This results in a significant increase in the gain in db per unit length. By judicious dielectric loading, the cutoff frequencies of the slow-wave structures are readily adjusted to yield the desired pass band. The ruby C-axis was oriented parallel to the direction of propagation. This orientation yielded higher gains than the more standard 60° orientation, as expected from the calculated matrix elements,[10]

All of the measurements were obtained by varying only the applied magnetic field and the pump frequency. No mechanical tuning was necessary because a multiple resonance effect at the pump frequency results in a high degree of absorption of pump

* Received by the IRE, August 12, 1960. This work was supported in part by the U. S. AF Wright Air Dev. Div., under Contract AF33(600)38862, and in part by the Dept. of Defense.

[1] F. Arams and S. Okwit, "Packaged Tunable L-Band Maser System," presented at PGMTT Symp., Harvard University, Cambridge, Mass., June, 1959; Proc. IRE, vol. 48, pp. 866–874; May, 1960.

[2] A. Penzias, "Maser Amplifier for 21 CM Radiation," Columbia University Rad. Lab., New York, N. Y., Quarterly Progress Repts.; 1958–1960.

[3] B. F. C. Cooper and J. V. Jelley, "Maser for Radio Astronomy Observations at 21 CM," presented at Northeast Electronics Res. and Engrg. Meeting, Boston, Mass.; November, 1959.

[4] B. Bolger, B. J. Robinson, and J. Ubbink, "Some characteristics of a maser at 1420 MHz," *Physica*, vol. 26, pp. 1–18; January, 1960.

[5] W. S. C. Chang, J. Cronack, and A. E. Siegman, "Cavity and Traveling-Wave Masers Using Ruby at S-Band," Stanford University Electronics Labs., Stanford, Calif., Tech. Rept. 155-2; July 28, 1959.

[6] W. H. Higa, "Excitation of an L-Band Ruby Maser," in "Quantum Electronics," Columbia University Press, New York, N. Y., pp. 298–301; 1960.

[7] J. E. Geusic, E. O. Schulz-DuBois, R. W. DeGrasse, and H. E. D. Scovil, "Three-level spin refrigeration and maser action at 1500 Mc/sec," *J. Appl. Phys.*, vol. 30, pp. 1113–1114; July, 1959.

[8] R. W. DeGrasse, E. O. Schulz-DuBois, and H. E. D. Scovil, "Three-level solid-state traveling-wave maser," *Bell Sys. Tech. J.*, vol. 38, pp. 305–334; March, 1959.

[9] E. O. Schulz-DuBois, H. E. D. Scovil, and R. W. DeGrasse, "Use of active material in three-level solid-state masers," *Bell Sys. Tech. J.*, vol. 38, pp. 335–352; March, 1959.

[10] W. S. Chang and A. E. Siegman, "Characteristics of Ruby for Maser Applications," Stanford University Electronics Labs., Stanford, Calif., Tech. Rept. 156-2; September 30, 1958.

power by the ruby throughout the tuning range. Pump power is obtainable from a backward-wave oscillator, so that the TWM can be antenna-feed mounted for minimum receiver noise figure, with electronic tuning from a remote location. Further work is in progress.

S. Okwit
F. R. Arams
J. G. Smith
Airborne Instruments Lab.
Div. of Cutler-Hammer, Inc.
Melville, Long Island, N. Y.

Laurent-Cauchy Transforms for Analysis of Linear Systems Described by Differential-Difference and Sum Equations*

The paper by Y. H. Ku and A. A. Wolf[1] constitutes one of the several useful contributions that these authors have made in the field of systems analysis and other allied subjects, and they are to be commended for this new addition to their work.

As the authors have pointed out in their conclusion, Laurent-Cauchy's transforms reduce to the Z transform method by simple modification in the notation of the parameters. Because of this close identity, I am taking the liberty in this discussion of pointing out some of the latest work done in the latter transform[2] which may clarify or add to the contributions of this paper. To clarify the contents of this discussion, this author finds it expedient to itemize the text into the following three points:

1) One of the major points in this paper[1] is the derivation of the complex convolution of $\mathcal{L}_c[\beta_k h_k(s)]$ as given in (54) and (55), which is written with the assumption (in the following discussion) that h_k is not a function of (t), thus s does not appear in (54). Therefore (54) with (55) can be written

$$\mathcal{L}_c[\beta_k h_k] = \frac{1}{2\pi j}\int_c B(\gamma)\gamma^{-1} H\left(\frac{\rho}{\gamma}\right) d\gamma = \sum_{k=0}^{\infty} \beta_k h_k \rho^{-k}. \quad (1)$$

Eq. (1) is identical to the Z transform of the multiplication of two time sequences.[2,3] It should be pointed out that to evaluate (1), one can evaluate the residues inside the circle which enclose only the poles of $\gamma^{-1}B(\gamma)$ in a positive sense, or, alternately, by obtaining the residue of $H(\rho/\gamma)$ outside this circle with the path of integration taken in the negative sense. It is important to clarify the contour c in this relation, for it might lead to some simplification in the results as will be observed from the following.

One application of (1) is to obtain some of the summation theorems, as a special case, without having to discuss some of the mathematical steps involved on p. 928.[1]

a) To obtain

$$\sum_{n=0}^{\infty} f_n,$$

one can replace β_k by f_n and h_k by a unit step whose $\mathcal{L}_c$ transform is $\gamma/\gamma-1$ and let γ equal ρ and $\rho\to 1$ in (1), thus,

$$\sum_{n=0}^{\infty} f_n = \frac{1}{2\pi j}\int_c \frac{F(\rho)}{\rho(1-\rho)}\, d\rho. \quad (2)$$

The above equation is identical to (63).[1] However, the path c can be taken in a negative sense to include the pole $\rho=1$ only, thus,

$$\sum_{n=0}^{\infty} f_n = -\left[-\lim_{\rho\to 1}\rho^{-1}F(\rho)\right] = \lim_{\rho\to 1} F(\rho). \quad (3)$$

Similarly, one can write β_k = unit step, h_k for f_n and let $\rho=1$. Thus from (1),

$$\sum_{n=0}^{\infty} f_n = \frac{1}{2\pi j}\int_c \frac{F(1/\rho)}{\rho-1}\, d\rho, \quad (4)$$

where the contour c in this case would enclose the pole $\rho=1$ in a positive sense, which would yield for (4),

$$\sum_{n=0}^{\infty} f_n = \lim_{\rho\to 1} F(1/\rho) = \lim_{\rho\to 1} F(\rho). \quad (5)$$

It is seen that (4) is not exactly identical to the equation of Case II, as given on p. 931,[1] when $f_n = h_n$. Furthermore, one need not integrate to obtain this identity[1-3]

$$\sum_{n=0}^{\infty} f_n = \lim_{\rho\to 1} F(\rho),$$

but simply replace ρ by unity and $\beta_k h_k$ by f_n in the right hand side of the expression of (1). The fact that the authors' summation is given in three forms [as Cases I and II (p. 931) and (63)] seems rather puzzling to this author.

As a remark on this point one can also obtain (68)[1] from (1) by replacing γ by ρ, ρ by unity, y_n and f_n by β_k and h_k, respectively. However, the contour c should be defined accordingly for the sake of simplification in evaluating the residues. Similar to a), but replacing h_k by $[u_n - u_{n-(k+1)}]$, one can readily obtain (67).[1]

2) The second point (which the authors are probably aware of) comes up only in special cases, and is included in this discussion only as a point of caution to the reader, that is, the special case when $\beta_k = 1/k$ and $\lim_{k\to 0} h_k = 0$. Using the convolution integral in this case, special care should be exercised for the $\lim_{k\to 0} h_k/k$ if it exists. In this case, it might be difficult to use (1) in view of the fact that the $\mathcal{L}_c(1/k)$ ought to be known; therefore, an alternate equivalent formula is indicated (without going into the details) and is[2]

$$\mathcal{L}_c\left[\frac{h_k}{k}\right] = \int_{\rho}^{\infty} \rho^{-1}F(\rho)d\rho + \lim_{k\to 0}\frac{h_k}{k}. \quad (6)$$

Although the above comment might seem irrelevant to the general contents of this paper, in view of this situation, I do not agree with the authors' functional entry of $[-(1/n)]$ in Table I[1] (p. 930) which I believe should read[2-4]

$$\mathcal{L}_c\left[-\frac{1}{n}\right] = \mathcal{L}_c\left[-\frac{u_{n-1}}{n}\right] = -\ln\frac{\rho}{\rho-1}, \quad \text{for } n>0.$$

In my opinion, the source of this difficulty lies in the application of the functional entry of

$$\frac{h_{n+2}}{n+1}, \quad \begin{cases} h_0 = 0 \\ h_1 = 0 \end{cases} \quad \text{(on p. 931)}[1]$$

to the case $[-(1/n)]$. In concluding this point, I would like to mention some of the functions which need the special care for their Laurent-Cauchy transform, *i.e.*,

$$\frac{1-e^{-\alpha n}}{n}, \quad \frac{\sin \alpha n}{n}.$$

3) Although this transform has been applied mainly to the solution of linear difference equations, extension of the convolution integral to solution of certain types of nonlinear difference equations is amenable, and work along this line (by this author) has shown some promise of this extension. Further application of this convolution to linear difference equations with periodic functions, or equivalently, to the modified Z transform case, is discussed elsewhere.[2]

Before concluding this note, one or two minor technical points are indicated:

a) A misprint appears in Table I[1] (p. 930). Entry 18 should read

$$\sum_{k=0}^{n} k h_k g_{n-k};$$

$n^{[k]}$ (in the fourth line from the bottom of p. 930) should read

$$n^{[k]} = n(n-1)\cdots(n-k+1),$$

and the functional entry of $(-n^3 h_n)$ (on p. 930) should read

$$\rho^3 H'''(\rho) + 3\rho^2 H''(\rho) + \rho H'(\rho).$$

b) For obtaining

$$\sum_{n=0}^{\infty} y_n^2$$

(on p. 931), which is the equivalent discrete form of Perseval's theorem, one may not need to evaluate the residues of the integrand, but this sum is given as a ratio of two determinants whose elements are the coefficients of powers of "ρ" in $Y(\rho)$ and this sum has been tabulated up to fourth-order systems.[5]

(c) In addition to the summation list indicated by the authors, the following could be added:[2]

$$\sum_{n=0}^{\infty}\frac{f_n}{n} = \int_1^{\infty}\rho^{-1}F(\rho)d\rho + \lim_{n\to 0}\frac{f_n}{n}.$$

* Received by the IRE, May 23, 1960.

[1] Y. H. Ku and A. A. Wolf, "Laurent-Cauchy transforms for analysis of linear systems described by differential-difference and sum equations," Proc. IRE, vol. 48, pp. 923–931; May, 1960.

[2] E. I. Jury, "Contribution to the modified z-transform," *J. Franklin Inst.*, vol. 270, pp. 114–129; August, 1960.

[3] J. Cypkin, "Theory of Pulse Systems," State Press for Physics and Mathematical Literature, Moscow, Russia; 1958. (In Russian.)

[4] W. M. Stone, "A list of generalized Laplace transforms," *Iowa State College J. Sci.*, vol. 22, pp. 215–225; April, 1948.

[5] H. B. Bharucha, "Analysis of Integral-Square Error in Sampled-Data Control Systems," Electronics Res. Lab., University of California, Berkeley, I.E.R. Rept., Ser. No. 60, Issue No. 206; June 30, 1958.

In conclusion, this author is of the opinion that this paper is of important value, in particular the entries in Table I,[1] and the points raised in this note are hoped to be useful to its contents.

E. I. Jury
University of California
Dept of Electrical Engrg.
Berkeley, Calif.

Author's Comments[6]

The authors would like to extend their thanks to Dr. Jury for his very kind and encouraging remarks in his discussion of our paper on the Laurent-Cauchy transform. We would also like to thank those correspondents who wrote encouraging comments on this work.

Dr. Jury has discussed several points concerned mainly with subtleties of a theoretical nature involving evaluation of certain transform forms which, in general, are in fundamental agreement with the main theme of the paper. Because of space limitations we were unable to give a more detailed account of all of these subtleties.

Let us briefly discuss one such subtlety. The Laurent-Cauchy transform belongs to a general class of transforms, as was pointed out in the paper. If one takes the Taylor-Cauchy transform as a starting point, he is able to obtain all of the integral and integral-sum transforms containing kernels of elementary functions by using mappings of elementary functions. A simple algebraic mapping produced the Laurent-Cauchy transform. In addition, one can obtain integral and integral-sum transforms containing kernels of higher transcendental functions, like the Fourier-Bessel transform which is particularly useful in the analysis of a class of radiation problems. It is, therefore, not surprising that a marked similarity exists between the Laurent-Cauchy and Z transforms. It is very easy to show, in a similar manner, that the Taylor-Cauchy transform maps into the Fourier series by a simple mapping involving the exponential function $e^{j\theta}$, and a simple interpretation of notation.

The important thing to consider in dealing with this class of transforms is the limitations on the functions admissible as transform candidates and the scope of problems that can be solved. For example, as Dr. Jury has pointed out, the Laurent-Cauchy transform, while generally applicable to the solution of linear differential-difference and sum equations, may be applied to certain nonlinear difference equations. Unfortunately, the latter case is not, in general, possible as a means of solution. For example, suppose a nonlinear difference equation of the nonrecursive type is Laurent-Cauchy transformable into a nonlinear differential equation belonging to the class described, then a second transformation of the Taylor-Cauchy type is required to give rise to a new nonlinear difference equation of the recurrence-convolution type which is always solvable as discussed elsewhere.

Another problem mentioned, but not considered in any detail, is the question dealing with random inputs. This question is taken up somewhat in [6] and in greater detail in [7].

A vast number of problems are yet to be solved in this area of generalized transforms belonging to a general class of auxiliary forcing functions.

Y. H. Ku
The Moore School of Elec. Engrg.
University of Pennsylvania
Philadelphia, Pa.
A. A. Wolf
Stromberg-Carlson Div.
General Dynamics Corp.
Rochester, N. Y.

Bibliography

[1] Y. H. Ku and A. A. Wolf, "Laurent-Cauchy transforms for analysis of linear systems described by differential-difference and sum equations," Proc. IRE, vol. 48, pp. 923–931; May, 1960.
[2] Y. H. Ku, A. A. Wolf and J. H. Dietz, "Taylor-Cauchy transforms for analysis of a class of nonlinear systems," Proc. IRE, vol. 48, pp. 912–922; May, 1960.
[3] A. A. Wolf, "A Mathematical Theory for the Analysis of a Class of Nonlinear Systems," Ph.D. dissertation, University of Pennsylvania, Philadelphia; June, 1958.
[4] A. A. Wolf, "Recurrence relations in the solution of a certain class of nonlinear systems," *Trans. AIEE*, vol. 78, pp. 830–834; January, 1960.
[5] A. A. Wolf, "Generalized recurrence relations in the analysis of nonlinear systems," *Trans. AIEE*, vol. 79, to be published in pt. 1, 1960.
[6] Y. H. Ku and A. A. Wolf, "Transform ensemble method for the analysis of linear and nonlinear systems with random inputs," *Proc. NEC*, vol. 15, pp. 441–455; 1959.
[7] A. A. Wolf, "Poles and Zeros of a Random Process in Linear and Nonlinear Systems," *Proc. NEC*, vol. 16; 1960.

[6] Received by the IRE, June 8, 1960.

The Relation of the Satellite Ionization Phenomenon to the Radiation Belts*

Observations at The Ohio State University Radio Observatory have been reported which indicate a close correlation between the occurrence of satellite induced ionization and passes of the satellite through the auroral or Van Allen belts.[1–3] However, little or no information has been available as to the exact position of these belts on any particular pass.

Recently, telemetering equipment was installed at The Ohio State University so that it has been possible to monitor the counting rates of the Anton 112 and 302 Geiger counters carried by Explorer VII (1959 Iota 1) whenever the satellite's transmitter was within range of Columbus, Ohio. Ten to twenty minutes of data per pass for 5 to 6 passes per day have been obtained. The experiment involving these counters was prepared by the Department of Physics and Astronomy of the State University of Iowa for monitoring, among other things, the spatial and temporal variations of the geomagnetically-trapped corpuscular radiation.[4] In addition to monitoring the Explorer VII transmitter (19.991 mc) and the counting rates of its Geiger counters, records have been made at The Ohio State University Radio Observatory of the signals of WWV (near Washington, D. C.) on 15 mc and also much of the time on 10 and 20 mc. The receivers for WWV were all tuned a kilocycle or so to the high-frequency side of the carrier to favor any Doppler shifts in frequency. This method of tuning has been found to improve the correlation between WWV enhancements and satellite passes and has already been reported.[2]

During the two months (March and April, 1960) that we have monitored the telemetering information from Explorer VII, we have noted that many of the strongest WWV enhancements have occurred at or very close to the time when the counting rates of the Geiger counters aboard the satellite were at peak values. That is, the WWV enhancements occurred at about the time that the satellite was passing through the most intense parts of the lower horn of the outer Van Allen belt. We noted further that many of these events were accompanied by another phenomenon, namely a partial or complete fadeout of the signal from Explorer VII. These fades or "drop outs" of the signals from the satellite, when in association with a WWV enhancement, are suggestive of ionization patches or clouds occurring between the satellite and Columbus which attenuate or scatter the signal from the satellite transmitter while at the same time acting as reflecting or backscattering regions for the WWV signals.

A typical example of the phenomenon is illustrated in Fig. 1. The upper record shows the 15.001-mc signal level from WWV for the morning of March 31, 1960, with a large enhancement at 5:50 A.M. EST. At almost the same time there is a drop in the level of the signal from Explorer VII, as shown by the lower trace of the two channel record. The counting rates of the Anton 112 (shielded) and 302 (unshielded) Geiger counters aboard Explorer VII are given for this pass in Fig. 2. It is apparent that the rates of both counters were at a peak at the time of the WWV enhancement and the drop in the Explorer VII signal. Note that time increases from left to right in Fig. 2 but from right to left in Fig. 1.

The track of Explorer VII across North America for this pass is presented in Fig. 3. A curve showing the trend in the rate of the 302 counter is superposed on the track. The locations of the WWV burst or enhancement and the "drop out" of the Explorer VII signal are also indicated. We believe that the nearly simultaneous occurrence of the WWV burst, the "drop out" and the peak counting rate is significant. The peak counting rate may be regarded as defining the position of

* Received by the IRE, May 16, 1960.

[1] J. D. Kraus, R. C. Higgy, D. J. Scheer, and W. R. Crone, "Observations of ionization induced by artificial earth satellites," *Nature*, vol. 185, pp. 520–521; February 20, 1960.
[2] J. D. Kraus, R. C. Higgy, and W. R. Crone, "The satellite ionization phenomenon," Proc. IRE, vol. 48, pp. 672–678; April, 1960.
[3] J. D. Kraus, "Evidence of satellite induced ionization effects between hemispheres," Proc. IRE, (Correspondence), vol. 48, pp. 1913–1914; November, 1960.
[4] G. H. Ludwig and W. A. Whelpley, "Corpuscular Radiation Experiment of Satellite 1959 Iota (Explorer VII)," Dept. of Physics and Astronomy, State University of Iowa, Iowa City, Iowa, no. 59-30; December, 1959.

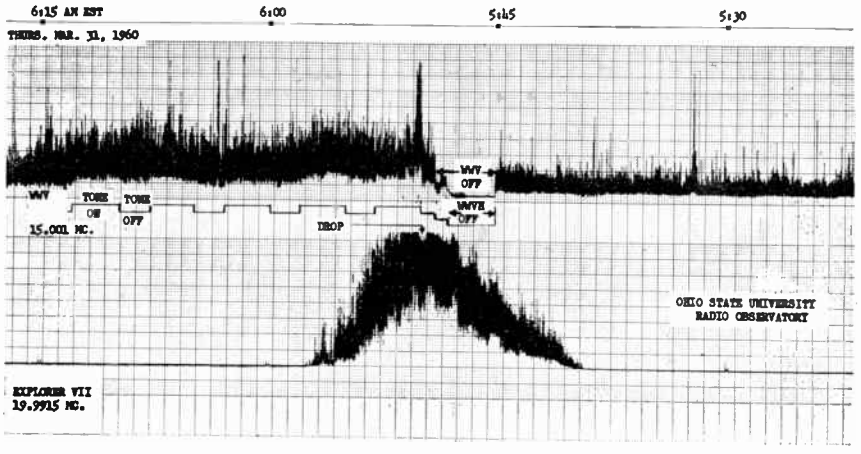

Fig. 1—WWV 15.001-mc signal (upper trace) and Explorer VII 19.9915-mc signal (lower trace) as recorded at The Ohio State University Radio Observatory on the morning of March 31, 1960. A burst or enhancement of WWV occurs at 5:50 A.M. At approximately the same time there is a drop in the signal from the satellite. The counting rates of the Geiger tubes aboard Explorer VII also reached a peak at 5:50 A.M. (see Fig. 2). The wavy lower edge of the WWV signal after 5:50 is due to the alternate tone-on (440 or 600 cps) and tone-off periods of WWV.

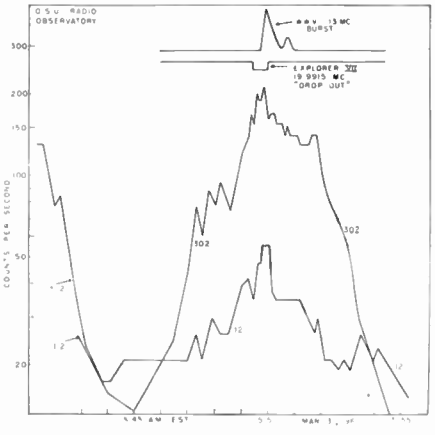

Fig. 2—Radiation counting rates of the Anton 302 (unshielded) and 112 (shielded) Geiger tubes aboard Explorer VII for the pass of Fig. 1.

the outer Van Allen belt on a particular pass for the particles producing the counts. On this pass Explorer VII passed through the belt northbound over southern Alberta and southbound over Maine.

Sometimes the drop outs of the Explorer VII signal are sufficiently deep to make the telemetered information unreadable. This was not the case for the example given above, but it is the case in some others. Dr. Brian J. O'Brien at the State University of Iowa has observed a loss of telemetering information when the satellite was in or near the most intense part of the Van Allen belt on a number of occasions.[5] In particular, he noted this effect on trips of Explorer VII through the outer Van Allen belt on at least one pass per day for 15 consecutive days during November, 1959. The fade was noted in the most intense part of the belt or just north of it on all northbound passes and in the neighborhood of the peak on some southbound passes. The most consistent pass, on which he noted the effect without exception, was one of a sequence which occurred some minutes earlier each day. Our observations indicate that the phenomenon is usually not so consistent from day to day as in the sequence observed by Dr. O'Brien, being more of a sporadic effect. Drop outs have also been noted in the signals of Sputnik III at the time of WWV enhancements and radar echoes as previously reported.[1,3]

[5] Private communication from G. H. Ludwig to J. D. Kraus, April 14, 1960.

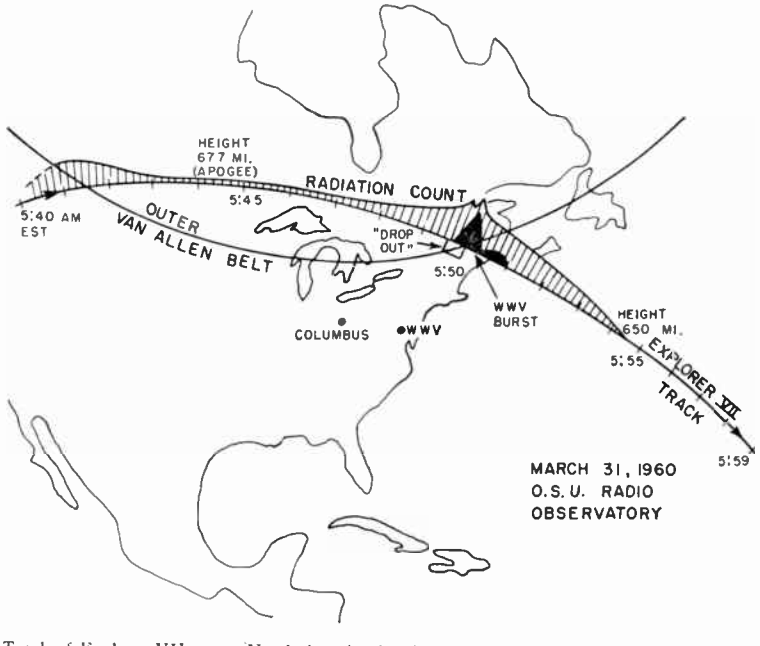

Fig. 3—Track of Explorer VII across North America for the pass of Fig. 1 with radiation counting rate data superposed on the track. A WWV burst and a drop in the Explorer VII signal occurred at the time the satellite was in the most intense part of the Van Allen belt.

The above observations suggest ionization may be induced by the satellite in the most intense part of the radiation belt due to encounters between the satellite and regions of high particle density and/or energy. The actual mechanism by which the ionization is induced is not clear. It may even be that the particles responsible do not register on the Geiger counters aboard Explorer VII, but are merely associated in some way with the particles which do.

The authors wish to acknowledge the assistance of R. E. Townsend, A. G. Herriman, and S. R. O'Donnell in making the observations. We also greatly appreciate the assistance of C. E. McLain of the Army Rocket and Guided Missile Agency in obtaining the telemetering equipment and the advice of Dr. G. H. Ludwig, who constructed the counting equipment aboard Explorer VII, Dr. B. J. O'Brien, and P. Rothwell, all of the Department of Physics and Astronomy of the State University of Iowa, in interpreting the telemetered data. The orbit data on Explorer VII was provided by courtesy of the Smithsonian Astrophysical Observatory. The work was supported in part by the Army Rocket and Guided Missile Agency through a contract with the Ohio State University Research Foundation, and in part by the University's Fund for Basic Research.

J. D. Kraus
R. C. Higgy
Radio Observatory
Dept. of Elec. Engrg.
Ohio State University
Columbus 10, Ohio

Some Characteristics of the Signal Received from 1958 δ^2*

Introduction

The study of the rapid fluctuation in the received signal strength from artificial earth satellites has led to a better understanding of the irregularities in electron density which exist in the ionosphere. In particular, the dimensions and locations of these inhomo-

* Received by the IRE, May 11, 1960. This work has been performed under Grant No. NsG 30-60 from the Natl. Aeronautics and Space Admin.

geneities have been investigated.[1-4] This note may serve as additional confirmation of some of the work mentioned above and, in addition, will report several new features of the received satellite radio signals.

Scintillation

Over 200 passages of 1958 δ^2 (Sputnik III) were observed in the period between June, 1958, and April, 1959. The amplitude of the 20-mc signal was recorded on an oscillograph whose frequency response was flat to about 50 cps. From these records a selection was made of 82 nighttime passages for which the zenith angle was less than 30° at the point of closest approach (proximal point). The daytime records were excluded because the occurrence of scintillation was far less frequent than for the nighttime period. Vertical-incidence ionograms were recorded at Stanford University near the time of each satellite passage and, from these, the presence of spread-F and sporadic-E was determined. Table 1 shows the number of occurrences for each of the eight possible combinations of scintillation, spread-F and sporadic-E. In this table scintillation was affirmed only when it was observed near the proximal point.

TABLE 1

Case	Observation of Scintillation	Spread-F	Sporadic-E	Number of Passages
1	Yes	Yes	Yes	9
2	Yes	Yes	No	18
3	Yes	No	Yes	0
4	Yes	No	No	2
5	No	Yes	Yes	3
6	No	Yes	No	2
7	No	No	Yes	23
8	No	No	No	25

An inspection of the various combinations reveals that not only does scintillation usually accompany spread-F (27 out of 32 cases), but also that scintillation is seldom observed without spread-F (2 out of 29 cases). Rows three and seven show no correlation between scintillation and sporadic-E.

Satellite passages as low as 230 km and as high as 1400 km are included in the data. Scintillation was observed on some nighttime passages as low as 250 km; on these passages a very slow Faraday rotation rate implied that the satellite was in the lower portion of the F layer.

Field Aligned Irregularities

On a number of occasions when spread-F was absent on the vertical-incidence sounder, scintillation was observed to the north but not overhead. Radar backscatter records obtained in the Stanford IGY program[5] were investigated on these occasions. Some of these backscatter records showed echoes from field-aligned ionization at a range of about 1000 km to the north. When the ray path between the satellite and the receiver appeared to intersect the region from which the radar echoes were obtained, scintillation of the satellite signals was found. Fig. 1 is an example of this. The cross-hatched area shows the range and azimuth at which field-aligned F-region echoes were obtained using a frequency of 18 mc. The solid line shows the subsatellite position during the time strong scintillation was observed.

Skip Distance Phenomena

As Yeh and Swenson[3] and Dewan[6] have noted, the sudden disappearance of a strong, fluctuating signal frequently occurred as the satellite passed into the "skip" region at a height below the F-region maximum density. The rapid fluctuation resulted from slightly different Doppler shifts imparted to the upper and lower rays. A similar increase of signal amplitude usually appeared as the satellite passed out of the skip region. We have observed on many occasions that the signal strength variations were more complex, with build-ups occurring in pairs with a time separation of 2 to 20 seconds as shown in Fig. 2. The formation of these pairs can be explained on the basis of magneto-ionic theory, from which it may be determined that the ordinary and extraordinary waves have slightly different skip distances. The separation of the skip distance is found to depend upon the magnitude of the component of the earth's magnetic field resolved along the direction of the ray at the reflection height in the ionosphere. Thus, N-S propagation results in a greater skip distance difference between ordinary and extraordinary waves than does E-W propagation. Using a graphical method for determining the difference in skip distance given by Smith,[7] one can estimate the magnitude of this variation using the appropriate transmission curves. In Fig. 2 we have the record of a southeast bound passage of 1958 δ^2, which crossed Stanford's latitude to the east. One can observe that the spacing of the pair before the proximal point (6.5 seconds) is greater than the spacing after the proximal point (2.5 seconds), which is in agreement with the qualitative explanation given above. The time separations of each pair are also consistent with the satellite velocity and skip distance separation estimated with the use of the transmission charts.

The propagation mode appears to be that sketched pictorially in Fig. 3, where the solid curves (O and X denote ordinary and extraordinary waves) represent the two skip distances and move along the ground with the satellite motion. The dotted curves represent the ordinary wave upper and lower rays, while dashed curves represent the upper and lower extraordinary rays. As the O skip distance approaches the receiver, the dotted curves will coalesce into the O skip ray. A few seconds later, the dashed curves combine to form the X skip ray. After that, only the direct ray is possible until the satellite once again exceeds the X skip distance.

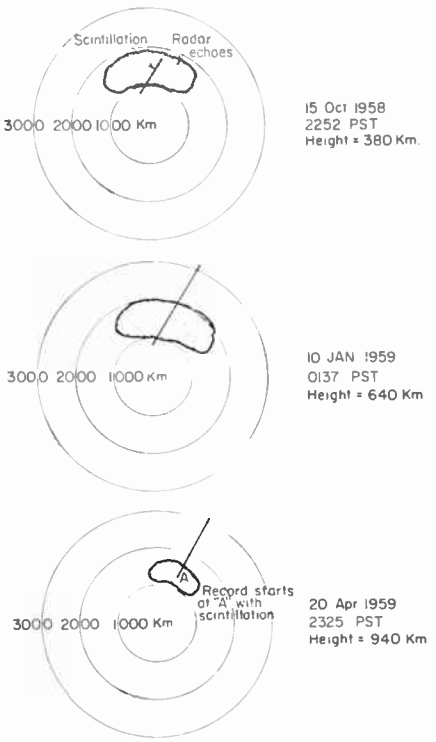

Fig. 1—Field aligned echoes and scintillation.

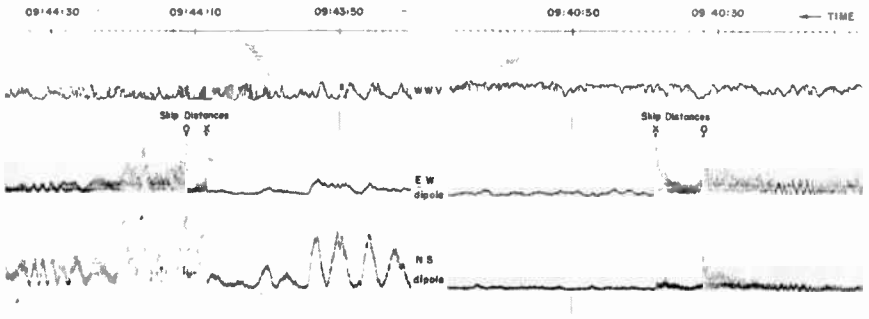

Fig. 2—Southeast bound passage of 1958 $\delta 2$ on March 30, 1960 with proximal point at 09:42:27 PST.

[1] O. B. Slee, "Radio scintillation of Satellite 1958α," *Nature*, vol. 181, pp. 1610–1612; 1958.
[2] G. S. Kent, "High-frequency fading observed on the 40-mc wave radiated from artificial satellite 1957α," *J. Atmos. Terrest. Phys.*, vol. 16, pp. 10–20; 1959.
[3] K. C. Yeh and G. W. Swenson, Jr., "The scintillation of radio signals from satellites," *J. Geophys. Res.*, vol. 64., pp. 2281–2286; December, 1959.
[4] R. Parthasarathy, R. P. Basler, and R. N. Dewitt, "A new method for studying the auroral ionosphere using earth satellites," PROC. IRE, vol. 47 p. 1660; September, 1959.
[5] A. M. Peterson, R. D. Egan and D. S. Pratt, "The IGY three-frequency backscatter sounder," PROC. IRE, vol. 47, pp. 300–314; February, 1959.
[6] E. Dewan, "An interesting propagation effect of Sputnik I," U. S. Dept. of Commerce, Office of Tech. Services, Washington, D. C., ASTIA Doc. No. AD 160760, pp. 1–22; December, 1958.
[7] N. Smith, "The relation of radio sky-wave transmission to ionospheric measurements," PROC. IRE vol. 27, pp. 332–347; May, 1939.

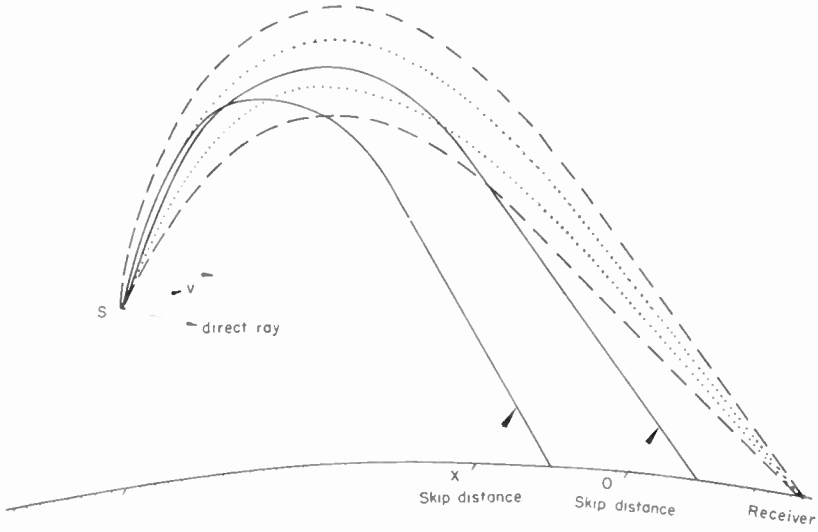

Fig. 3—Sketch of propagation modes. The dotted curves represent the ordinary waves and the dashed curves the extraordinary waves.

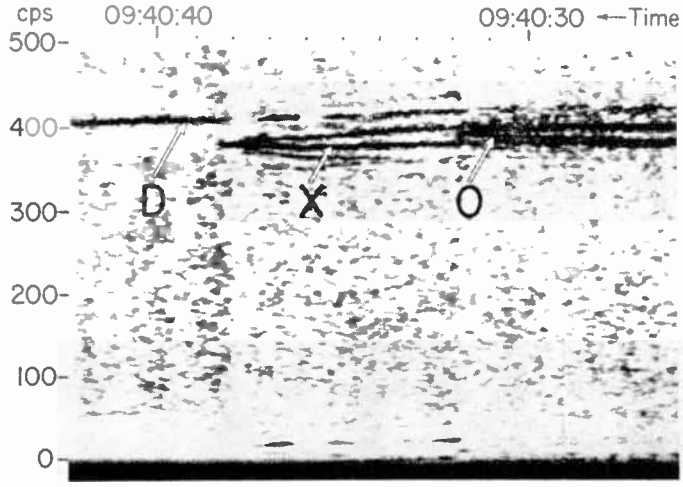

Fig. 4—Spectrum analysis of the received signals as the satellite passed into the O and X skip regions. The component D is the direct ray from the satellite.

In general, the Doppler shifts imparted to each of the rays will be different, due to the different angle of departure for each ray from the satellite.

A spectrum analysis (Fig. 4) of the signal during the first pair (Fig. 2) confirms the phenomenon described above, that is, the frequencies of the upper and lower rays of the ordinary mode coalesce at the ordinary wave skip distance, and similarly the upper and lower rays of the extraordinary wave coalesce at the extraordinary wave skip distance. The spectrogram also shows the Doppler shift of the direct ray.

The assistance of S. C. Hall in the collection of data is gratefully acknowledged.

F. DE MENDONCA
O. G. VILLARD, JR.
O. K. GARRIOT
Radioscience Lab.
Stanford University
Stanford, Calif.

Digitized Maximum Principle*

The maximum principle of Boltyanskii, Gamkrelidze, and Pontryagin[1,2] for minimal time or maximal range control of nonlinear continuous systems can be readily extended to sampled-data systems. This note states and derives such a digitized version of the maximum principle.

The main application of the digitized maximum principle is perhaps not so much in optimal control of nonlinear sampled-data systems *per se*, but in digital computation of optimal control of nonlinear continuous systems. No matter what method one chooses, a necessary step is converting the differential equations into discrete-time form. How to do this efficiently and accurately is not a concern of the present note. However, once this is done, the digitized maximum principle offers a computation process which is simple, straightforward and exact. The only error is the computer round-off error. The dynamical system is described by

$$x_i(n+1) = f_i[\mathbf{x}(n), \mathbf{y}(n)] \qquad i = 1, 2, \cdots, m, \tag{1}$$

where the vectors $\mathbf{x}(n)$, $\mathbf{y}(n)$ represent x_1, x_2, $\cdots$, x_m, and y_1, y_2, $\cdots$, $y_{m'}$ respectively, at the nth sampling instant. There is a system of constraints on $\mathbf{y}$ of the type

$$|y_i| \leq 1 \quad i = 1, 2, \cdots, m'. \tag{2}$$

The problem is to select $\mathbf{y}(n)$ within (2) to accomplish either of the following:

1) bringing the representative point of the system in space X^m from an initial point $\mathbf{x}=\mathbf{a}$ to a terminal point $\mathbf{x}=\mathbf{b}$ in minimum number of steps (minimal time problem),

2) maximizing $\mathbf{h}\cdot[\mathbf{x}(N)-\mathbf{x}(0)]$ where $\mathbf{h}$ is a given constant vector (maximal range problem, of which Mayer's problem is a special case).

The following assumptions are made:

a) the functions $f_i(x, y)$ have continuous first partial derivatives, and

b) $Nm' > m$.

Let $\Omega_N(a)$ represent the set of all possible terminal points of the system at the end of N steps starting from $\mathbf{a}$. Since the allowable range of $\mathbf{y}$ is continuous, $\Omega_N(a)$ forms a continuous region in X^m. For the maximal range problem, the terminal point is the tangential point of a plane perpendicular to $\mathbf{h}$ on the far side (from $\mathbf{a}$) of $\Omega_N(a)$. For the minimal time problem, an N can be found such that $\mathbf{b}$ belongs to $\Omega_N(a)$ but does not belong to any $\Omega_{N'}(a)$, $N' < N$. If $\mathbf{b}$ is an interior point of $\Omega_N(a)$, there are, in general, infinitely many optimal trajectories. To limit the present derivation to cases where a unique solution is possible, a third assumption on the selected terminal point is added to the previous two:

c) the terminal point $\mathbf{b}$ is an exterior point (on the surface) of $\Omega_N(a)$.

Let $\boldsymbol{\lambda}$ be a normal at $\mathbf{b}$ of the boundary surface of $\Omega_N(a)$ pointing outward from $\Omega_N(a)$.[3] Let $\mathbf{b}'$ be the terminal point of an adjacent trajectory resulting from $\mathbf{y}'(n) = \mathbf{y}(n) + \delta\mathbf{y}(n)$, and $|y_i'(n)| \leq 1$, $n = 1, 2, \cdots, m'$. Then $\mathbf{b}'$ belongs to $\Omega_N(a)$ and

$$\boldsymbol{\lambda}\cdot\delta\mathbf{x}(N) = \boldsymbol{\lambda}\cdot(\mathbf{b}' - \mathbf{b}) \leq 0. \tag{3}$$

Inequality (3) holds for the first order variations. To the same approximation, (1) gives

$$\delta x_i(n+1) = \sum_j \left(\frac{\partial f_i}{\partial x_j}\right)_n \delta x_j(n) + \sum_k \left(\frac{\partial f_i}{\partial y_k}\right)_n \delta y_k(n), \tag{4}$$

* Received by the IRE, June 6, 1960.

[1] V. G. Boltyanskii, R. V. Gamkrelidze and L. S. Pontryagin, "On the theory of optimal process," *C.R. Acad. Nauk SSSR*, vol. 110, pp. 7–10; July, 1956.

[2] L. A. Zadeh, "Minimal Time Problems and Maximum Principle," presented at Winter General Meeting—AIEE, New York, N. Y.; February, 1960.

[3] In order to establish (3), it is only necessary to show that $\boldsymbol{\lambda}$ exists for a subregion $\Omega_N(a, b, \epsilon)$ consisting of end points of adjacent trajectories with $|\delta y_i(n)| \leq \epsilon$ for all i and n. This weaker condition follows from (6).

where the subscript n indicates that the partial derivatives are evaluated for points $x(n)$, $y(n)$ on the optimal trajectory from a to b. For any particular optimal trajectory these derivatives are functions of n only. Eq. (4) is linear in the first order variations $\delta x(n)$ and $\delta y(n)$, with the boundary condition $\delta x(0)=0$.

It is convenient to express (4) in matrix form: δx and δy can be written as column vectors. Let $F(n)$ and $B(n)$ represent $m\times m$ and $m\times m'$ matrices with $(\partial f_i/\partial x_j)_n$ and $(\partial f_i/\partial y_j)_n$ as their respective elements of the ith row and jth column. Eq. (4) can be written as

$$\delta x(n+1) = F(n)\delta x(n) + B(n)\delta y(n). \quad (5)$$

The solution is

$$\delta x(N) = \sum_{n=0}^{n=N-1} A(n)B(n)\delta y(n), \quad (6)$$

where $A(N-1)=1$, and for $n<N-2$,

$$A(n) = F(N-1)F(N-2),\cdots,F(n+1) = A(n+1)F(n+1). \quad (7)$$

Let λ' represent the row vector with λ_i as its elements. Inequality (3) can be written as

$$\lambda'\delta x(N) = \sum_{n=0}^{n=N-1} \lambda' A(n)B(n)\delta y(n) \leq 0. \quad (8)$$

Since the $\delta y(n)$'s are independent, (8) is equivalent to

$$\lambda' A(n)B(n)\delta y(n) \leq 0, \quad n = 0, 1, \cdots, N-1. \quad (9)$$

Let $\psi'(n)=\lambda' A(n)$. Then $\psi'(n)$ satisfies

$$\psi'(N-1) = \lambda', \quad \psi'(n-1) = \psi'(n)F(n), \quad n = 1, 2, \cdots, N-1. \quad (10)$$

Inequality (9) is equivalent to maximizing $\psi'(n)f[x(n), y(n)]$ by the choice of $y(n)$ with $\psi'(n)$ and $x(n)$ considered fixed. Since only the first order variations have been considered in the above derivation, the possibility that the optimum $y(n)$ is a stationary point is not ruled out. The digitized maximum principle can be stated as follows:

Along an optimal trajectory $\psi'(n)f[x(n), y(n)]$ is either maximum or stationary with respect to infinitesimal variations of $y(n)$.

Computationwise, it is convenient to start from the terminal point and compute backwards. For the minimal time problem λ depends on the initial point a but there is no known relationship between λ and a. However, as the problem usually is knowing the terminal point b, what are the best $y(t)$'s for different initial points a? The mapping between λ and a is automatically carried out in the computing process. For the maximal range problem $\lambda=h$, but b is unknown for any given a and the same situation holds.

S. S. L. Chang
Dept. of Elec. Engrg.
New York University
University Heights
New York, N. Y.

Volume Density of Radio Echoes from Meteor Trails*

A type of radio linkage between two stations is based on the scattering properties of meteor trails in the high earth atmosphere. It is well known that a meteor leaves an ionized trail, when traveling through the atmosphere, which can scatter e.m. radiation. Consequently, if a trail is illuminated by a transmitter T, an echo may reach a receiver R and the likage between T and R through the trail can take place.

Two conditions must be fulfilled by a trail for giving rise to the linkage. One is a geometrical condition; the other, energetical. A trail will be called *geometrically useful* for a linkage, if it is tangent to an ellipsoid with foci at T and R, at a point P of the illuminated zone. The point P will be called *reflection point* of the trail. A geometrical useful trail is also *energetically* useful, if the ionization at P is high enough to give rise to an echo which reaches the receiver with a power above the threshold power of the receiver.

Now the problem is to determine the number of echoes received per unit time by a receiver as a function of the region of the sky where the receiver beam crosses the transmitter beam. This problem has been approached by a number of authors.[1,2] Recently,[3] we developed a method which substantially differs from those found in the literature, and which will be briefly described in the sequel.

First at all, we introduce a volume density of radio echoes Δ, which is defined as follows.

Let us consider an elementary volume dV around a point P_0 of the sky (Fig. 1). Among the trails which cross dV, there are some which have the reflection point inside dV. Their number represents the number of geometrically useful trails to be associated with dV. In order to determine it, let us consider a point P on the surface $d\Sigma$ bounding dV, and the ellipsoid through P with foci at T and R. A trail has the reflection point at P if it passes through P and lies on the plane π tangent at P to the ellipsoid. Consider now a trail s' passing through P under an angle ϵ' with the plane π. Let β be the angle between the projection of s' on π and the projection τ of the normal t to $d\Sigma$ at P. This trail crosses $d\Sigma$ at another point P'. Consider the ellipsoid through P' with foci at T and R. If s' is tangent at P' to this ellipsoid, the trail directed as s' has the reflection point at P'. Every trail through P, corresponding to the same value of β and contained in the angle between s' and its projection on π, has the reflection point inside dV. By varying β, the directions s' describe a surface π'. The plane π and the surface π' determine a solid angle $d\Omega$, which has the property that all, and alone, the trails through P contained within $d\Omega$ have the reflection point inside dV. We can write

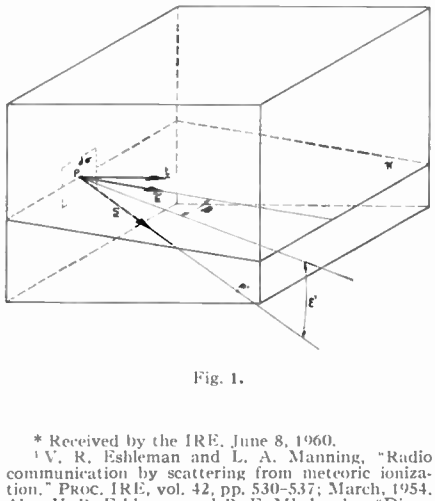

Fig. 1.

$$d\Omega = \int d\omega \quad (1)$$

with

$$d\omega = \epsilon' d\beta. \quad (2)$$

Obviously, ϵ' is a function of β, and depends upon the coordinates of P_0, on the shape of $d\Sigma$, on the position of P on $d\Sigma$. However, it may be considered constant for the points of an area $d\sigma$ of $d\Sigma$ around P, small compared with $d\Sigma$. As a consequence, we are in a position to write the number dN of geometrically useful trails to be associated with dV, entering dV through $d\sigma$, as follows:

$$dN = \int_{d\Omega} n(s)t\cdot s\,d\sigma\,d\omega = d\sigma\int_{-\pi/2}^{\pi/2} n(s)t\cdot s\,\epsilon'\,d\beta, \quad (3)$$

where s indicates a direction within $d\omega$, and $n(s)$ represents the number of meteors flowing per unit time, and per unit solid angle around s, through the unit surface normal to s. The limits $-\pi/2$, $+\pi/2$ of the integration with respect to β have been so chosen as to count the trails only one time, when *enter* dV. The total number $\Delta' dV$ of geometrically useful trails to be associated with dV is simply obtained by integrating dN over $d\Sigma$:

$$\Delta' dV = \int_{d\Sigma} d\sigma \int_{-\pi/2}^{\pi/2} n(s)t\cdot s\epsilon'\,d\beta. \quad (4)$$

Here Δ' represents the volume density of reflection points.

Generally speaking, it is not an easy matter to determine ϵ' as a function of β and of point P on $d\Sigma$, nor to carry out the integrations with respect to $d\beta$ and $d\sigma$. However, we note that the density is independent of the shape of the volume assumed for evaluating it. Accordingly, if we consider a dV of suitable shape, the difficulties may be reduced. In the case of backscatter, we found[3] that all mathematical difficulties disappear if one chooses dV shaped as in Fig. 2; that is, bounded by a conical surface $d\Sigma_c$ belonging to a cone with the vertex at the radar

* Received by the IRE, June 8, 1960.

[1] V. R. Eshleman and L. A. Manning, "Radio communication by scattering from meteoric ionization," Proc. IRE, vol. 42, pp. 530–537; March, 1954. Also, V. R. Eshleman and R. F. Mlodnosky, "Directional characteristics of meteor propagation derived from radar measurements," Proc. IRE, vol. 45, pp. 1715–1724; December, 1957.

[2] R. E. Pugh, "The number density meteor trails observable by the forward-scattering of radio waves," *Canad. J. Phys.*, vol. 34, pp. 997–1004; October, 1956. Also C. O. Hines and R. E. Pugh "The spatial distribution of signal sources in meteoric forward-scattering," *Canad. J. Phys.*, vol. 34—pp. 1005–1015; October, 1956.

[3] N. Carrara, P. F. Checcacci, A. Consortini, and L. Ronchi, "Volume Density of Radio Echoes from Meteor Trails," Tech. Note No. 3, of Contract AF 61 (052)-227 between the Air Res. and Dev. Command and the Centro Microonde; 1959.

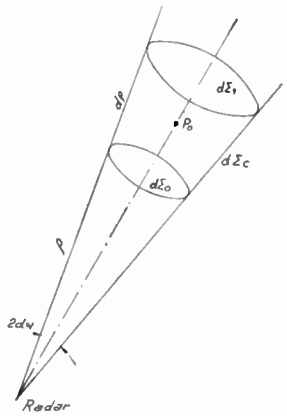

Fig. 2.

and semiaperture $d\alpha$, and by two spherical surfaces $d\Sigma_0$, $d\Sigma_1$, belonging to two spheres centered at the radar and with radii ρ, $\rho+d\rho$, respectively. In this case we found that the integration over $d\Sigma$ can be limited at $d\Sigma_c$, and that

$$\epsilon' = 2d\alpha \cos\beta$$

for all points of $d\Sigma_c$. On the other hand, t and τ coincide, so that $t \cdot s = \cos\beta$. Then, if η is an angle specifying P over $d\Sigma_c$, one can put

$$d\sigma = \rho d\alpha d\eta d\rho.$$

As a result, we found

$$\Delta' = \frac{2}{\rho}\int_0^{2\pi} d\eta \int_{-\pi/2}^{\pi/2} n(s)\cos^2\beta d\beta. \quad (5)$$

We wish to outline that this result is exact, as only higher order infinitesimal quantities have been neglected in deriving it, and that it rests upon no arbitrary assumptions.

The case of forward scatter is now being developed and turns out to be surprisingly easy to be treated, in spite of the more complex geometry to be taken into account.

In order to pass from Δ' to Δ, one has to substitute for $n(s)$ a function $N(s, P)$, which takes into account the fact that only a part of the meteors with direction s originates at P such an ionization that the echo is revealed by the radar. The treatment of this second part of the problem requires the laws of the meteor evaporation and of scattering of radiation by meteor trails to be known.

For the meteor evaporation we have assumed the simplified Herlofson theory[4] to hold, which gives the expression of the linear ionization density q along a trail in terms of the mass and velocity of the meteor as well as of the atmospheric pressure.

From the expression of the power scattered by a trail and arriving at a receiver,[5] one can evaluate the minimum value $\bar{q}$ of q for which the echo is revealed by the receiver, in terms of the distance from the reflection point to the radar and of the characteristics of the radar itself. Then, from the Herlofson theory, one can determine, for a given value of the velocity v of the meteor, the minimum value M_0 of the mass M which gives rise to the value $\bar{q}$ at the reflection point. M_0 turns out to be a function of the coordinates of the reflection point, of the direction s of the trail, and of v, as well as of the characteristics of the radar.

Now let $F(M)dM$ and $G(v)dv$ be the probabilities that a meteor has the mass between M and $M+dM$ and the velocity between v and $v+dv$, respectively. Recalling the meaning of $n(s)$, if s is a geometrically useful direction to be associated with a dV around a point P_0, one can write that

$$N(s, P_0) = n(s)\int_0^\infty G(v)dv \int_{M_0(s,P_0,v)}^\infty F(M)dM \quad (6)$$

represents the number of trails with direction s which give rise to detectable echoes. This quantity (6) is to be introduced into (5) in order to determine the volume density of radio echoes.

In Carrara, *et al.*,[3] we have developed the case of the back-scatter. Of course, the results obtained depend, even if not in an essential way, on the assumed law for the evaporation process, and can be modified and improved. Consequently, they are not given here, since the main purpose of the present note is to describe the method we have elaborated.

A general result we wish to emphasize is that the density of radio echoes depends also upon the characteristics of the radar used.

Once Δ is known, the number of echoes received by the radar per unit time may be obtained by integrating ΔdV on the volume illuminated by the radar. This integration is to be carried out without putting arbitrary limits to the sky region where the meteor evaporation takes place. Finally, we note that with our method, the meteor scattering is treated in the same way as the usual scattering from a volume containing scatterers with a given density.

Nello Carrara
Pier F. Checcacci
Laura Ronchi
Centro Microonde
Florence, Italy

Point-Pair Reading Logic*

While its primary concern is not with character recognition, the paper by Browning and Bledsoe[1] appears to contain principles which are applicable and potentially effective for character recognition. After a careful study of the principles, it became apparent that the advantages of the technique, which we shall refer to as point-paired reading, are limited in some respects. The exact nature of the limitations is not entirely clear because of the random aspect of the technique. It was found, however, that one might assume an extended version of the point-paired reading principle which is not random. In this extended version, to be described later, the effectiveness is clearly greater than the random machine that might be built in accordance with the technique of point-pairing. Even so, the more effective machine fails in a situation in which a simple point-by-point comparison device, using two references, successfully reads a reasonably distorted character.

We shall consider the latter two devices as operating on an N point, two-dimensional field. Each of the machines will have stored, as a reference, an alphabet of M characters in two possible type fonts, one a variation of the other. The number of similar points between the two fonts will be at least b_0. When an unknown character is presented to the machine, the machine will form a set of sums which, in a general sense, will measure the similarity of the unknown character with each reference character. In all, M sums are formed. The final output will be based upon a decision as to the largest sum.

If we consider the point-by-point comparison device, it will form its measure of similarity of the unknown character to each reference character by counting the point-for-point similarities. Since two fonts exist for the reference character, we shall choose the larger of the two sums as the one presented to the output.

The point-pair device considers the binary states of pairs of points. In the Browning-Bledsoe machine, these pairs were selected at random so that $N/2$ pairs, each pair exclusive of the others, were picked. For our extended version of the machine, we shall consider one in which there exists every possible pairing of a point with itself and all other points. This should prove to be a more powerful version than the one proposed by Browning and Bledsoe. Since it includes the pairs involved in all possible random-pair configurations, it should, therefore, perform as well as any of them. The reference for each character consists of storing any of the four possible states which can occur for a particular character and pair.

The output measure of each character is the number of coincidences of the unknown character pair-states, with the allowed pair-states for the particular character of the alphabet being considered.

We shall now present a character to the machine and calculate the outputs from two character channels for

1) the point machine and
2) the paired-point machine.

Any unknown character must agree with both reference characters in some fraction of points y. It will agree with only one reference by some fraction of points x, and the other reference by some fraction z. As an example, consider a letter C to be compared with two type fonts of the letter O shown in Fig. 1. The unknown character agrees with the second "O" or O_2 in the white area X and with the first "O" or O_1 in white area Z.

[4] N. Herlofson, "Theory of meteor ionization," *Repts. Progr. Phys.*, vol. 11, pp. 444–454; July, 1948.
[5] For the underdense trails, see footnote 1. For the overdense trails, see P. A. Forsythe and C. O. Hines, "The forward-scattering of radio waves from overdense meteor trails," *Canad. J. Phys.*, vol. 35, pp. 1033–1040; October, 1957. Also P. A. Forsythe, "The forward-scattered radio signals from an overdense meteor trail," *Canad. J. Phys.*, vol. 36, pp. 1112–1120; November, 1958. Also L. A. Manning, "Oblique echoes from overdense meteor trails," *J. Atmos. Terr. Phys.*, vol. 14, pp. 82–93; January, 1959.

* Received by the IRE, June 23, 1960.
[1] W. W. Bledsoe and I. Browning, "Pattern Recognition and Reading by Machine," presented at Eastern Joint Computer Conference, Boston, Mass.; December, 1959.

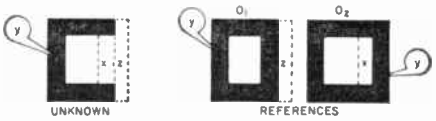

Fig. 1—Comparison of an unknown figure with the character *O*.

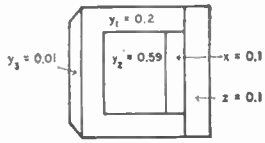

Fig. 2—Breakdown of character area.

Fig. 3—Comparison of an unknown figure with the character *C*.

The point-by-point comparison device has an output for any character-measuring unit of either $x+y$ (the number of points by which the unknown agrees with one reference) or $y+z$. If $x>z$, its output will be $x+y$.

For the same character, we can now compute the output of the paired-point reader. This output will be the fraction of all possible pairs which have allowable binary states. For example, the number of pairs which are formed from points in Y, paired with points in X, Y, or Z, are $y(x+y+z)$; similarly for X and Z, so that the output sum is $x(x+y)+y(x+y+z)+z(y+z) = (x+y)^2+2yz+z^2$.

If the result had been $(x+y)^2$, there would be an unambiguous relation between the output of the comparison device and the paired-point device. However, the terms $2yz+z^2(=h)$ destroy this one-to-one relation so that the largest value of the indications may no longer signify the proper character. The degree to which this is a significant factor depends upon whether h is large. To determine if this is true, we calculate the maximum value of h within the convex space

$$x + y + z \leq 1$$

$$x \geq z$$

$$y \geq b_0$$

$$x \geq 0,\ y \geq 0,\ z \geq 0$$

(the 3-dimensional space within which acceptable values of x, y, and z must fall),

in which

$$h = 2yz + z^2.$$

The solution to this system of equations, although not performed here, may be shown to be

$$\text{for } b_0 > \tfrac{1}{3}$$

$$(x,\ y,\ z)\ \max = \left[\tfrac{1}{2}(1 - b_0),\ b_0,\ \tfrac{1}{2}(1 - b_0)\right].$$

This gives

$$h \text{ maximum} = \tfrac{1}{4}(1 - b_0)(1 + 3b_0).$$

In order to appreciate the meaning of these results, we may assign reasonable values to the C and O example (Fig. 2). For the O measure, when looking at a C, let $b_0=0.8$, $x=0.1$, $y=0.8$, $z=0.1$. These values may exist while the C agrees with the reference C by 0.99. (See Fig. 3.) The outputs of the pairing device are 0.98 for the C, 0.98 for the O. For an almost perfect C which agrees with either O by only 0.90 point, the point-pairing machine has given equal outputs! The simple matching device described earlier will give an output of 0.99 for the C and 0.90 for the O.

While many examples may be submitted to demonstrate the effectiveness of a system, yet if one reasonable example can be shown for which a system fails, the validity of the technique becomes subject to question. The essence of these remarks is that for many paired-point configurations, negative examples may be found by applying criteria similar to the above. In these cases, the point-paired principles must be less effective than a simpler technique, such as point-by-point comparison.

J. M. Bailey, Jr.
Radio Corp. of America
Electronic Data Processing Div.
Camden, N. J.

Ferrimagnetic Linewidth of Single Crystals of Barium Ferrite ($BaFe_{12}O_{19}$)*

Oriented polycrystalline barium ferrite[1] has been used as the gyromagnetic element in resonance isolators operating in the millimeter region[2] because its high magnetic anisotropy field of 17,000 oersteds[3] greatly reduces the external magnetic field required for resonance. The narrowest linewidth of oriented polycrystalline barium ferrite obtained at Philips Laboratories, Irvington-on-Hudson, N. Y., was 1200 oersteds. Since for some applications, such as filters and parametric amplifiers, an extremely narrow linewidth is desirable, it was felt that a determination of the single crystal linewidth of barium ferrite would be of interest.

Measurements were made at both Philips Laboratories[3] and the U. S. Army Signal Research and Development Laboratory.[4] At Philips, measurements were made by placing a small polished wafer 1×20×40 mils, ground from a single crystal of barium ferrite, in a rectangular waveguide, and determining the variation in transmitted power as a function of the applied field. The test frequency was 55.5 kilomegacycles. The narrowest linewidth obtained was 50 oersteds. The field required for resonance was 7600 oersteds, which is in excellent agreement with the above value of the anisotropy field.

Measurements at USASRDL were made by placing a small spheroid one half wavelength from the shorted end of a section of waveguide, and determining the variation in VSWR as a function of the applied field. The spheroid was oblate with major and minor axes of 19 and 15.5 mils, respectively. The test frequency was 57.7 kilomegacycles. The narrowest linewidth obtained was 53 oersteds. The field required for resonance was 5000 oersteds, which again is in excellent agreement with the anisotropy field.

The single crystals were grown at the U. S. Army Signal Research and Development Laboratory.[5]

Isidore Bady
Thomas Collins
USASRDL
Ft. Monmouth, N. J.
Dominick J. DeBitetto
Frits K. du Pré
Philips Labs.
Irvington-on-Hudson, N. Y.

* Received by the IRE, April 21, 1960.

[1] J. J. Went, G. W. Rathenau, E. W. Gorter and G. W. van Oosterhout, *Philips Tech. Rev.*, vol. 13, pp. 194–208; January, 1952.

[2] L. C. Kravitz and G. S. Heller, "Resonance isolator at 70 kmc," Proc. IRE, vol. 57, p. 331; February, 1959.

[3] F. K. du Pré, D. J. De Bitetto, F. G. Brockman, and G. W. Steneck, Jr., "Hexagonal Magnetic Materials for Microwave Applications," Final Rept., Signal Corps Contract DA-36-039-SC-78071, Philips Labs., Irvington-on-Hudson, N. Y.; June, 1958–1959.

[4] I. Bady and T. Collins, USASRDL Tech. Rept. No. 2116, Ft. Monmouth, N. J.; May, 1960.

[5] F. Leonhardt and R. Gambino, "Growth of Barium Ferrite single crystals," presented at meeting of Electronic Div. Am. Ceramic Soc., Detroit, Mich.; September 23, 1959.

The Influence of Sunspot Number on Transmitter Power Requirements for HF Ionospheric Circuits*

It is well known that during periods of high sunspot activity, transmission at higher frequencies is possible with less power. This investigation is an attempt to determine the order of magnitude of decrease in power permissible with increasing sunspot number.

In free space, the attenuation of radio waves is due only to distance. At some distance d, let the unabsorbed field intensity be E_0. In the case of an absorbing medium, however, the wave suffers additional attenuation and the absorbed field intensity E at a distance d is then given as

$$E = E_0 e^{-\alpha d}\ \mu\text{v/m}, \qquad (1)$$

where

E_0 = unabsorbed field intensity in μv/m,
α = average attenuation constant in nepers/km,
d = ray path length in km.

* Received by the IRF, May 27, 1960.

The absorption index A is defined as

$$A = \log_{10} \frac{E_0}{E} \left(\frac{\text{db}}{20}\right). \quad (2)$$

Thus, the absorption index in db is

$$A' = 20A = 20\alpha d \log_{10} e = 8.686\alpha d \text{ db}. \quad (3)$$

Note that the absorption index is an absolute measure of the attenuation for a particular path length d, in contrast with the attenuation constant α, which is the attenuation per unit length.

From experimental data it has been found that the absorbed field intensity can be represented as

$$E = E_0 \times 10^{-Sd/20} \mu\text{v/m}. \quad (4)$$

The attenuation constant S is a product of four terms:

$$S = S_0 J Q \overline{K} \text{ db/km}, \quad (5)$$

where

S_0 = frequency variation factor in db/km,
J = seasonal variation factor,
Q = solar variation factor,
$\overline{K}$ = average diurnal variation factor.

The last three factors ($JQ\overline{K}$) are dimensionless. From (2), (4), and (5),

$$A' = 20 \log_{10} \frac{E_0}{E} = 20 \left(\frac{S_0 J Q \overline{K} d}{20}\right)$$

$$A' = S_0 J Q \overline{K} d \text{ db}. \quad (6)$$

From Signal Corps technical report no. 9,[1] the absorption index in db is stated as

$$A' = \frac{615.5 n \sec\phi (1 + .0037s)(\cos .881\psi)^{1.30}}{(f + f_H)^{1.98}} \text{ db}, \quad (7)$$

where

n = number of hops,
ϕ = angle between the ray path and the perpendicular to the earth at a height of 100 km,
s = twelve-month running average Zurich sunspot number,
ψ = sun's zenith angle at the ionosphere reflection point,
f = operating frequency in mc,
f_H = gyrofrequency in mc at 100 km height.

The term $n \sec\phi$ represents the distance and obliquity factor, $(1+.0037s)$ represents the solar variation factor, $(\cos .881\psi)^{1.30}$ represents the diurnal variation factor, with the constant term of the frequency variation factor and an average value for the seasonal variation factor contained in the constant 615.5.

Since the objective of this report is to determine the required change in radiated power as a function of sunspot number only, (7) becomes

$$A' = \frac{C(1 + .0037s)}{(f + f_H)^{1.98}} \text{ db}, \quad (8)$$

where

C = constant.

It is assumed that, for different sunspot numbers, transmission is made over the same circuit, via the same mode, and at the same time and month.

Thus, in such a case, the sunspot number corresponds to the yearly variation of the absorption index.

Eq. (8) cannot be simplified further without imposing special conditions since the change of the maximum usable frequency (muf) with sunspot number depends on the geographic location, month, and local time at the control point (s). Designate the sum of the operating frequency plus the gyrofrequency as f'. Then, the total operating frequency plus gyrofrequency at sunspot number zero is f_0'. At some other sunspot number s, $f' = f_s'$, and

$$f_s' = m f_0', \quad (9)$$

where

m = percentage increase in total muf plus gyrofrequency from sunspot number zero.

The absorption index at sunspot number zero is A_0'.

$$A_0' = \frac{C}{(f_0')^{1.98}} \text{ db}. \quad (10)$$

At sunspot number s, then,

$$A_s' = \frac{C(1 + .0037s)}{(f_s')^{1.98}} = \frac{C(1 + .0037s)}{(m f_0')^{1.98}}$$

$$= \frac{C}{(f_0')^{1.98}} \frac{(1 + .0037s)}{m^{1.98}}$$

$$= (1 + .0037s) \frac{A_0'}{m'} \text{ db}, \quad (11)$$

where

$$m' = m^{1.98}.$$

From (2),

$$A = \log_{10} \frac{E_0}{E} = \log_{10} \frac{B\sqrt{W}}{E}$$

$$= \log_{10} \frac{B}{E} + \log_{10} \sqrt{W} \text{ db},$$

where

B = constant for the same circuit $= 1.765/d \times 10^3 \times (0.63)^{n-1}$,
W = effective radiated power in kw $= \frac{1}{2} G_T W_0$,
G_T = directivity of antenna over isotropic radiator in direction of transmission,
W_0 = total radiated power in kw

$$\log_{10} \sqrt{W} = A - \log_{10} \frac{B}{E}. \quad (12)$$

For $s = 0$,

$$\log_{10} \sqrt{W_0} = A_0 - \log_{10} \frac{B}{E}.$$

For any sunspot number s,

$$\log_{10} \sqrt{W_s} = A_s - \log_{10} \frac{B}{E}.$$

Subtracting,

$$\log_{10} \sqrt{W_0} - \log_{10} \sqrt{W_s} = A_0 - A_s$$

$$10 \log_{10} \frac{\sqrt{W_0}}{\sqrt{W_s}} = A_0' - A_s'$$

$$10 \log_{10} \frac{W_s}{W_0} = 2(A_s' - A_0')$$

$$= 2\left[(1 + .0037s)\frac{A_0'}{m'} - A_0'\right]$$

$$P' = \left[\frac{2(1 + .0037s)}{m'} - 2\right] A_0' \text{ db}. \quad (13)$$

Eq. (13) is the normalized power as a function of sunspot number and operating frequency.

Case I

$m' = 1$ (constant operating frequency)

$$P_I' = [2(1 + .0037s) - 2] A_0' \text{ db}. \quad (14)$$

This curve is plotted in Fig. 1. For a constant frequency, then, greater transmitter power is required for large sunspot numbers.

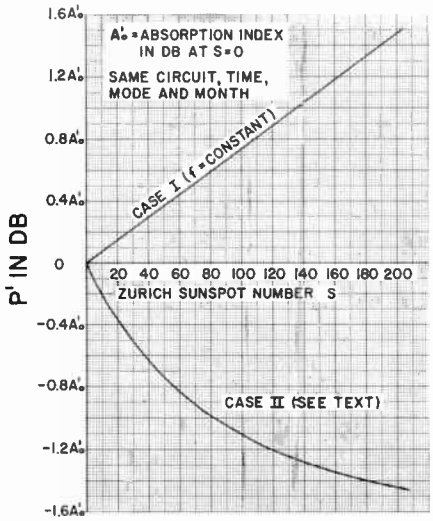

Fig. 1—Increase in transmitted power vs sunspot number referred to power at $s=0$ for constant receiver field intensity.

Case II

$m' = f(s)$. (Operating frequency a function of s.)

Due to the increase in ionization of the ionosphere during high sunspot activity, higher operating frequencies are permissible. For the $F2$ layer in certain mid-latitude and equatorial regions, the operating frequency plus the gyrofrequency may be approximately expressed as

$$f_s' = f_0' + \frac{s}{130} f_0' \text{ mc}, \quad (15)$$

where f_0 = operating frequency during sunspot minimum ($s = 0$) in mc.

[1] P. O. Laitinen and G. W. Haydon, "Analysis and Prediction of Sky-Wave Field Intensities in the High Frequency Band," Radio Propagation Unit Tech. Rept. No. 9; March, 1956.

$$m' = \left(1 + \frac{s}{130}\right)^{1.98}.$$

Assuming such a frequency variation, then, the normalized power becomes

$$P_{II}' = \left[\frac{2(1 + .0037s)}{\left(1 + \frac{s}{130}\right)^{1.98}} - 2\right] A_0' \text{ db.} \quad (16)$$

This curve is plotted in Fig. 1. Note that, for a frequency variation as expressed by (15), the power requirements are less during high sunspot activity. Thus, although the attenuation increases with large sunspot numbers for a fixed frequency, the permissible use of higher frequencies during high sunspot activity results in a decrease in attenuation and transmitter power requirements.

To determine the actual change in power requirements, it is necessary to calculate only the absorption index for zero sunspot number, A_0', from (7). Then substitute A_0' in the expression for P', obtained from Fig. 1. In the general case, when the operating frequency is f_s at some sunspot number s, P' is calculated from (13). The actual power can be calculated from (12).

Example

Assume that the absorption index for a particular circuit is 10 db during sunspot minimum, and that the frequency change for other sunspot numbers corresponds to Case II. For $s = 130$, then, the transmitted power may be decreased by 12.5 db, assuming that transmission is made over the same circuit, via the same mode, and during the same time and month.

$$A_0' = 10 \text{ db}$$
$$P_{125}' = -1.25A_0' = -12.5 \text{ db}.$$

Frank T. Koide
Collins Radio Co.
Cedar Rapids, Iowa

An Experimental Wide-Tuning Range Inverted Magnetron*

The general problem of tuning of interdigital magnetrons by coaxial lines has been investigated by one of the authors.[1] This investigation suggested the possibility of obtaining wide-tuning ranges in an inverted interdigital magnetron. The tuning is accomplished by a sliding plunger in a coaxial line coupled strongly to the region enclosed by the fingers.

An experimental inverted interdigital magnetron, tuned by a coaxial line, was fabricated with a view to try out the fabrication procedure, to study the operation, and to get an actual scale model for the cold tests needed for detailed design of output couplers. It may be mentioned that the previous cold test model, on which the general problem had been studied, worked in the UHF range. It was unwieldy to try different coupling methods on it because of the large size of the output coupling line required.

A diagrammatic representation of the tube and the salient dimensions are given in Fig. 1. The cathode surrounding the anode consisted of a plain nickel sleeve, with oxide coating on the inside surface. It had molybdenum end hats. A part of the tuner coaxial line was built into the tube proper, ending in a glass window. (Here a ceramic window would be an advantage.) The tuning plunger had contacting fingers sliding in an air-filled coaxial line, which was joined on to the vacuum tube, forming a continuation of the tuner line in it.

A trial method of output coupling was adopted, namely, by means of a loop in the region of the cavity which lies outside the cathode. This method of coupling was chosen for its ease of construction which was an advantage in the case of an exploratory tube. Later measurements showed that the tube was strongly under-coupled.

The tube was designed to operate in the frequency band of 1000 to 2000 mc. The anode consisted of 12 fingers of circular

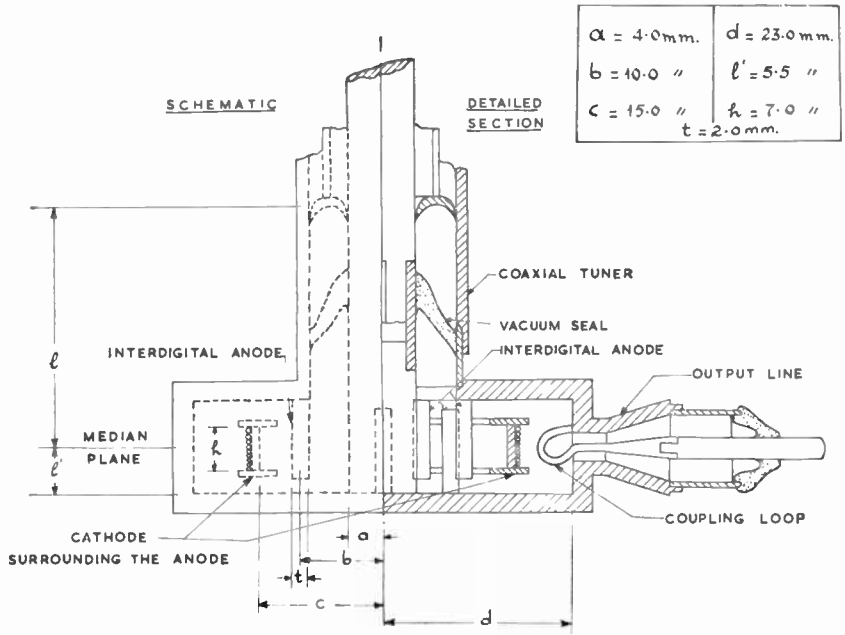

Fig. 1—Diagrammatic representation of tunable inverted magnetron.

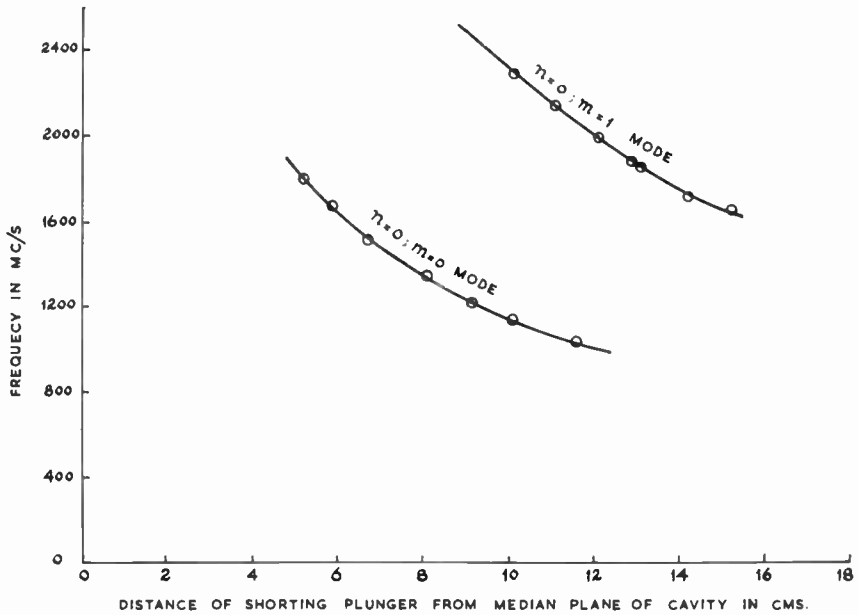

Fig. 2—Tuning curve obtained with experimental tube. (n represents azimuthal order and m represents the number of nodes of electric field in the tuner line, in addition to the one at the shorting plunger.)

* Received by the IRE, May 17, 1960.
[1] A. Singh, "Tuning of interdigital magnetrons by coaxial lines," *J. Electronics and Control*, vol. 3, pp. 183–193; August, 1957.

cross section. For $N=12$, for a normal magnetron, the optimum ratio[2] of cathode to anode radius is $(12-4)/(12+4)$, *i.e.*, $\frac{1}{2}$. The ratio of distance between adjacent segments to distance between cathode and anode is of greater importance in the interaction between electrons and electromagnetic field than the ratio of cathode to anode radius. In order to preserve the former unchanged, the latter was made 3:2 for the inverted magnetron tube.

The scaling parameters for the voltage and magnetic field were respectively 690 volts and 180 gauss. Operation was at ten times these values. In the absence of a suitable dc supply, the operating tests were carried out by means of a pulsed supply. However, since the cathode has a relatively large area, emission density or heating by back-bombardment are not likely to prove bottlenecks for CW operation at similar power levels.

The tuning curve obtained in operation is shown in Fig. 2. It is seen that its nature is the same as that anticipated from the general analysis earlier. A tuning range of 1.8:1 is obtained with the lower frequency branch alone. The two overlapping branches of the tuning curve together cover a frequency range of 2.3:1.

The power output lay between 40 and 300 mw, over the tuning range of 1.8:1. A major cause of holding down the power was the low circuit efficiency. The latter was measured by using the tube as a cold test model. Typical values of the Q_{unloaded}, Q_{loaded}, Q_{external} and circuit efficiency were 102, 98, 2500, and 4 per cent respectively. This leads to the conclusion that, given other methods of coupling with good circuit efficiency, appreciably larger powers may be expected. It may be mentioned that Hull[3] obtained pulse power output of the order of 50 kw from an untuned inverted interdigital magnetron.

Two additional methods of coupling have been studied. One method uses probes capacitively coupled to the fingers. The other one uses an iris between the tuner coaxial line and the output coaxial line. Both can give good circuit efficiency. A design approach has been developed for the case of iris coupling, by which a fairly uniform Q_{external} (within ± 12 per cent) can be obtained over a wide tuning range (1.8:1). A more detailed communication on this will follow.

It was also observed in the cold tests, that when the cathode leads were shorted to the cavity, the unloaded Q remained unchanged to within the limits of experimental error. Since no cathode decoupling chokes had been used, this lends support to the possibility of dispensing with such chokes.

AMARJIT SINGH
Central Electronics Engrg. Res. Inst., Pilani
Rajasthan, India
N. C. VAIDYA
National Physical Lab.
New Delhi, India

Calculating the Spectrum Power Density of a Signal*

The spectrum density of a signal may be measured in the laboratory by using a narrow-band filter, a wide-band amplifier (if gain is required), and a power monitoring detector as illustrated in Fig. 1. The Q of the filter is chosen to be compatible with the spectrum variations of the signal under test and, in general, the bandwidth of the filter is much less than that encompassed by the signal.

If the filter had an ideal rectangular bandpass, the power density would be computed directly by dividing the reading of the monitoring detector by the bandwidth of the filter. However, in the most practical instance, the filter may have the characteristic response of a single tuned circuit. Under these circumstances, more power is incident on the detector then would have been had the ideal rectangular filter with the same bandwidth been used. Therefore, the readings obtained must be reduced by some factor. By assuming that the Q of the filter is much greater than unity (*i.e.*, arithmetic symmetry), it is well known and can readily be verified that this factor is $2/\pi$.[1]

It is interesting to note that this same factor is valid for the low Q case where the assumption of even symmetry no longer applies. With the aid of Fig. 2, the proof follows:

The signal at the power monitor, $D(\omega)$, may be expressed as

$$D(\omega) = S(\omega) \cdot H(\omega) \cdot K.$$

By adjusting the gain of the wide-band amplifier appropriately (*i.e.*, $H(\omega_0) \cdot K = 1$), the transfer function of the single tuned circuit and amplifier may be expressed as

$$K \cdot H(\omega) = \frac{1}{1 + jQ\left(\frac{\omega}{\omega_0} - \frac{\omega_0}{\omega}\right)}$$

where $\omega_0^2 \equiv 1/LC$ and $Q \equiv R/\omega_0 L$.

Using Parseval's Theorem, the power at the monitor may be expressed in terms of the frequency spectrum.

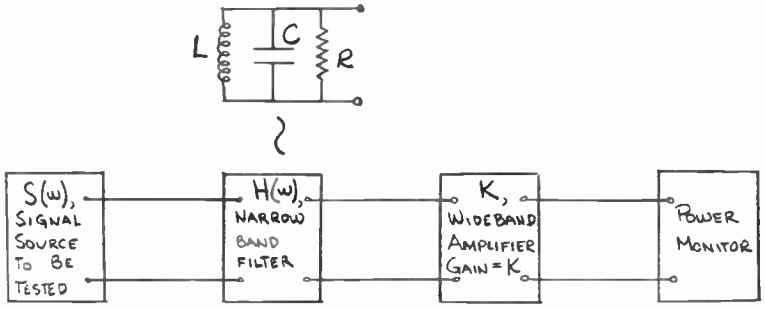

Fig. 1—Laboratory configuration.

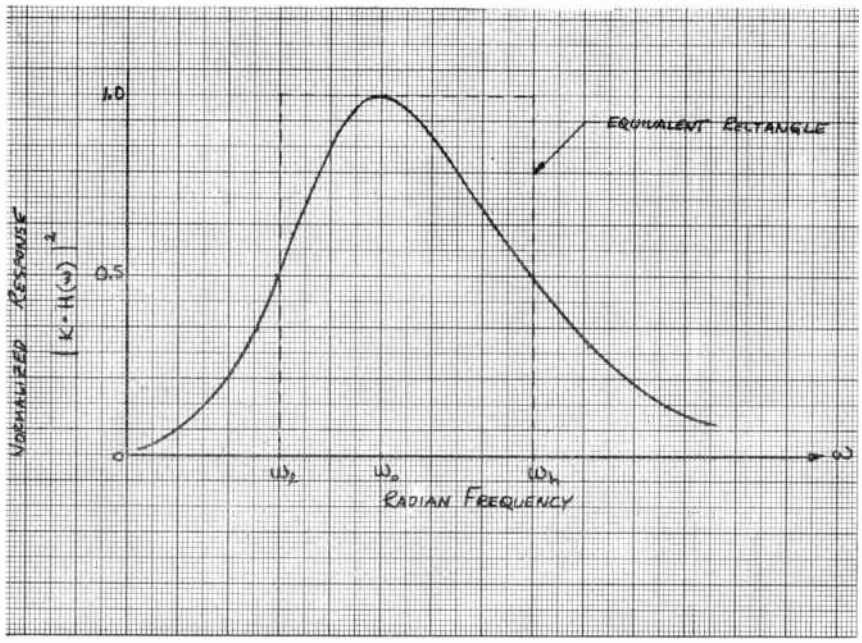

Fig. 2—Power spectrum vs radian frequency for single tuned circuit and amplifier.

[2] G. B. Collins, "Microwave Magnetrons," McGraw-Hill Book Co., New York, N. Y., p. 23; 1948.
[3] J. F. Hull, "Inverted magnetron," PROC. IRE, vol. 40, pp. 1038–1041; September, 1952.

* Received by the IRE, May 5, 1960.

[1] G. Valley and H. Wallman, "Vacuum Tube Amplifiers," M.I.T. Rad. Lab. Ser., McGraw-Hill Book Co., Inc., New York, N. Y., vol. 18, p. 169; 1948.

Power at monitor

$$= \int_{-\infty}^{\infty} D^2(t)dt = \int_{-\infty}^{\infty} |D(\omega)|^2 d\omega.$$

Positive frequencies alone need be considered since only the ratio of two areas are desired. Substituting for $D(\omega)$ and using the law of the mean [*i.e.*, $S(\omega)$ may be assumed constant within the bandwidth of the filter],

Power at monitor $|_{\text{filter}}$

$$= S^2(\omega) \int_0^{\infty} \frac{d\omega}{1 + Q^2\left(\frac{\omega}{\omega_0} - \frac{\omega_0}{\omega}\right)^2}. \quad (1)$$

The 3-db radian bandwidth $\omega_h - \omega_e$ can be found by setting $\omega/\omega_0 = x$ and letting

$$Q\left(x - \frac{1}{x}\right) = \pm 1.$$

Solving for x_h and x_e,

$$x_h = \frac{1/Q \pm \sqrt{1/Q^2 + 4}}{2}$$

and

$$x_e = \frac{-1/Q \pm \sqrt{1/Q^2 + 4}}{2};$$

$$x_h - x_e = \frac{\omega_h - \omega_e}{\omega_0} = \frac{1}{Q}.$$

This is shown in Fig. 2.

The power at the monitor assuming a rectangular pass band is:

Power at monitor $|_{\text{rect.}}$

F, the ratio of (1)/(2) is then the reciprocal of the desired correction factor

$$F = \frac{S^2(\omega) \int_0^{\infty} \frac{d\omega}{1 + Q^2\left(\frac{\omega}{\omega_0} - \frac{\omega_0}{\omega}\right)^2}}{S^2(\omega)(1)^2(\omega_h - \omega_e)}.$$

Letting $x = \omega/\omega_0$, this reduces to

$$F = Q \int_0^{\infty} \frac{dx}{1 + Q^2\left(x - \frac{1}{x}\right)^2}. \quad (3)$$

This integral may be solved as follows:

Let

$$y = \frac{1}{x}, \quad \text{then} \quad dy = -\frac{1}{x^2}dx.$$

Substituting and reversing the limits,

$$F = Q \int_0^{\infty} \frac{1/y^2 dy}{1 + Q^2\left(y - \frac{1}{y}\right)^2}.$$

Using the dummy variable theorem from calculus,

$$F = Q \int_0^{\infty} \frac{1/x^2 dx}{1 + Q^2\left(x - \frac{1}{x}\right)^2}. \quad (4)$$

Adding (3) to (4),

$$2F = Q \int_0^{\infty} \frac{\left(1 + \frac{1}{x^2}\right)}{1 + Q^2\left(x - \frac{1}{x}\right)^2} dx. \quad (5)$$

By making the final substitution

$$z = Q\left(x - \frac{1}{x}\right),$$

(5) may be solved for F.

$$F = \frac{1}{2} \int_{-\infty}^{\infty} \frac{dz}{1 + z^2} = \pi/2, \text{ Q.E.D.}$$

GERALD F. ROSS
Sperry Gyroscope Co.
Great Neck, N. Y.

Self-Setting Cross-Correlators*

Interest in conjugate filters has led to the consideration of horizontal modulation systems in which a single signal pulse is first transformed into a video signal consisting of a quasi-random series of positive or negative pulses, spaced at a given time interval, and representable by the series $a_1, a_2, \cdots, a_n$, where $a_i = \pm 1$. When that video pulse is fed to the input of a balanced, lumped constant delay line with tapped points connected to a bus and spaced at the same given time interval, and when the taps are positive or negative in accordance with the series or code, $a_n, a_{n-1}, \cdots, a_1$ (and are also of increasing magnitude to compensate for the attenuation of the delay line), then the output of the bus will be the autocorrelation of the a_i series:

$$C_j = \sum_{i=1}^{i=n-j} a_i a_{i+j}.$$

This output is characterized by a "correlation peak" flanked by a symmetric tailing of diminishing average amplitude, the over-all average amplitude of the tailing being of the order of $1/\sqrt{n}$ the amplitude of the correlation peak. There are several other possible applications of the tapped delay line, such as character recognition. In this particular application, alphabetic or other characters are scanned vertically in a continuous horizontally extended raster, the signals thus generated are fed to a tapped delay line, and several systems of taps serve to recognize several or all the characters scanned, regardless of slight vertical or horizontal errors of registration.

More generally, the tapped delay line may be considered as a means for obtaining the cross-correlation function between the function representable by any one system of taps, and the time series fed to the delay line input.

In general, the tapping should be capacitive, in order to avoid the additional attenuation which would be incurred with resistive tapping, and several methods for effecting this tapping are available. For instance, the line can be permanently tapped with soldered connections. Alternately, switches may be provided, to tap one side or the other, on the basis that the tapping function is reduced to a binary number, the first binit of which is utilized, *i.e.*, the sign of the number. Again, spring-back switches may be utilized, which are set by properly punched cards.

There is yet a basically different method, namely the one implied by the title of this note. With this method, the tapping function is first inserted as a signal in the delay line input, and when the first portion of the signal reaches the end of the delay line, a special signal causes each or every other delay line section to be tapped in accordance with the sign of the tapping function.

A possible circuit for accomplishing this is illustrated by Fig. 1. At each of the tapping points, which are at alternate sections, there is a by-stable transistor flip-flop, and in normal cross-correlating operation, this flip-flop controls the voltage of two diodes, D_1. These diodes are biased negatively, and do not conduct, but their capacitances are controlled by their bias voltage. The one diode out of each pair with the least bias has the higher capacitance, and thus taps that

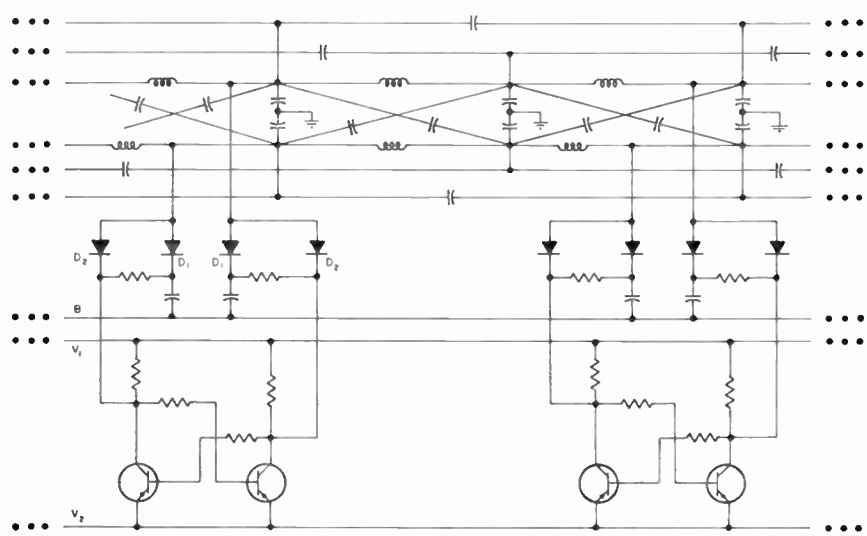

Fig. 1—Section of self-setting cross-correlator.

* Received by the IRE, April 21, 1960.

side of the delay line to which it is connected.

When it is desired to change the state of the flip-flop in accordance with a new tapping function which has been fed into the delay line, the $V_1 - V_2$ voltage difference is first collapsed, so as to erase the flip-flop memories. At the precise instant when the tapping function occupies exactly the full length of the delay line, the following two operations are performed in a time small compared to the time delay per section: first, the voltage of the flip-flop supply and return is lowered to ground voltage, so that one or the other of the D_2 diodes is brought into conductivity, depending upon the polarity of the tapping function at that instant and at that point. Second, the normal voltage difference $V_1 - V_2$ is reinstated, so that the flip-flop assumes a new state triggered by the conductivity of one of the D_2 diodes. After this has been accomplished, the voltages V_1 and V_2 can be lifted, at relative leisure, sufficiently above ground to assure the biasing to nonconduction of all diodes, and the proper capacity control of the D_1 diodes. The cross-correlator is now ready for the resumption of operation, and the cross-correlative function is delivered by bus B.

MARCEL J. E. GOLAY
Philco Corp.
Philadelphia, Pa.

A Necessary Condition on Coefficients of Hurwitz Polynomials*

In this note, we present a simple coefficient condition that every polynomial with negative real zeros must satisfy. This condition enables us to obtain a necessary condition on the coefficients of Hurwitz polynomials. Consider polynomial

$$p_n = a_n s^n + a_{n-1}s^{n-1} + \cdots + a_0, \quad (1)$$

which has only zeros on the negative real axis. We will show that

$$\text{Min } [a_0, a_1, \cdots, a_n] = \text{Min } [a_0, a_n], \quad (2)$$

and furthermore, there are no local minima. More precisely, this result may be stated as follows:

Theorem: If polynomial (1) has only negative real zeros, then

$$\begin{cases} a_i \le a_{i-1} \\ a_i \le a_{i+1} \end{cases} \quad 0 < i < n \quad (3)$$

cannot simultaneously be satisfied.

Proof: We will prove this theorem by induction. The lowest order polynomial considered is

$$p_2 = a_2 s^2 + a_1 s + a_0. \quad (4)$$

Polynomial (4) must have only negative real zeros; therefore, $a_i > 0$ (for $i = 0, 1, 2$) and

$$a_1^2 - 4a_2a_0 \ge 0. \quad (5)$$

Let us assume that $a_1 \le a_2$, which implies that $a_1 - 4a_0 \ge 0$ or $a_1 > a_0$. Hence, our assertion is valid for $n = 2$. To complete the induction, let us assume the theorem is valid for polynomials of order up to $n-1$. We must show that it is also valid for polynomial of order n. Since all zeros of polynomial p_n are assumed to be on the negative real axis, we have in general

$$p_n = (b_1 s + b_0)p_{n-1} \quad (6)$$

or

$$p_n = b_1a_{n-1}s^n + (b_0a_{n-1} + b_1a_{n-2})s^{n-1} + \cdots + (b_0a_j + b_1a_{j-1})s^j + \cdots + a_0b_0. \quad (7)$$

We must show that

$$\begin{cases} b_0a_j + b_1a_{j-1} \le b_0a_{j-1} + b_1a_{j-2} \\ b_0a_j + b_1a_{j-1} \le b_0a_{j+1} + b_1a_j \end{cases} \quad 0 < j \le n-1^1 \quad (8)$$

cannot be satisfied simultaneously. The inequalities of (8) may be written as

$$\begin{cases} b_0(a_j - a_{j-1}) \le b_1(a_{j-2} - a_{j-1}) \\ b_0(a_j - a_{j+1}) \le b_1(a_j - a_{j-1}). \end{cases} \quad 0 < j \le n-1 \quad (9)$$

We will consider two different cases:

1) $a_j \le a_{j-1}$, which implies that $a_j > a_{j+1}$, which in turn means that the second inequality in (9) cannot be satisfied.

2) $a_j \ge a_{j-1}$, which implies that $a_{j-1} > a_{j-2}$, which means that the first of the inequalities of (9) cannot be satisfied.

A useful corollary to this theorem is the following.

Corollary: If

$$f(s) = a_n s^n + a_{n-1}s^{n-1} + \cdots + a_0 \quad (10)$$

has no zeros in the right half plane, then

$$\begin{cases} a_i \le a_{i-2} \\ a_i \le a_{i+2} \end{cases} \quad 1 < i < n-1 \quad (11)$$

cannot be satisfied simultaneously.

Proof: If $f(s)$ is such a polynomial, then

$$f_e = a_0 + a_2 s^2 + a_4 s^4 + \cdots \quad (12)$$

and

$$f_0 = a_1 s + a_3 s^3 + a_5 s^5 + \cdots \quad (13)$$

are polynomials with zeros only on the imaginary axis.[2,3] Replacing s^2 by λ, we obtain

$$f_e(\lambda) = a_0 + a_2\lambda + a_4\lambda^2 + \cdots \quad (14)$$

and

$$f_0(\lambda) = \sqrt{\lambda}(a_1 + a_3\lambda + a_5\lambda^2 + \cdots). \quad (15)$$

The zeros of $f_e(\lambda)$ and $f_0(\lambda)$ will lie on the negative real axis, therefore the result of the theorem applies. This proves the corollary.

These results provide a preliminary testing procedure for identifying a class of non-Hurwitz polynomials, and also determining whether a polynomial may have only negative real zeros.

S. L. HAKIMI
Dept. of Elec. Engrg.
University of Illinois
Urbana, Ill.

* Received by the IRE, May 16, 1960; revised manuscript received, May 31, 1960. This work was supported by the Office of Ordnance Res., U. S. Army.

[1] $a_k = 0$ for $k < 0$ and $k > n-1$.

[2] E. A. Guillemin, "The Mathematics of Circuit Analysis," John Wiley and Sons, Inc., New York, N. Y., 1949.
[3] M. Marden, "The Geometry of the Zeros of a Polynomial in a Complex Variable," Am. Math. Society, New York, N. Y., 1949.

Relativity and the Scientific Method*

In a recent letter, C. A. Mead[1] calls for the application of the scientific method to the evaluation of the theory of relativity. By this he apparently means that, "the success of a theory may thus be judged by the manner in which it fulfills this objective"; namely, "to predict the outcome of new experiments." The theory must be discarded if, and apparently only if, "it can be shown that a prediction of the theory is in clear contradiction to the behavior of nature as observed by a well-performed experiment."

Judged by this standard, the caloric theory of heat should still be firmly established. Actually it is no violation of the scientific method to prefer the kinetic theory of heat. This is done for two reasons: 1) it coordinates a wider variety of phenomena and, 2) it reduces the number of independent assumptions.

The theory of relativity has recently been put in exactly the same category as the caloric theory by the development of a mechanistic theory of physical phenomena.[2] This provides an interpretation of all the phenomena covered by the relativity theory plus those of electrostatics and quantum electrodynamics and furnishes a particle model which conforms to relativistic mechanics. In so doing, it eliminates the necessity for all assumptions except those of Newtonian mechanics. It is a matter of choosing the right model.

R. V. L. HARTLEY
174 Summit Ave.
Summit, N. J.

* Received by the IRE, June 24, 1960.

[1] C. A. Mead, "Relativity and the scientific method," PROC. IRE, vol. 48, pp. 1160–1161; June, 1960.
[2] R. V. L. Hartley, "A Mechanistic Theory of Extra-Atomic Physics," *Phil. Sci.*, vol. 26, pp. 295–309; October, 1959.

Field Effect on Silicon Transistors*

The above paper[1] discusses observations made by applying voltages to a ring electrode on a special silicon transistor. Work that we have done on germanium transistors[2] has shown that it is possible to observe the changes in α' with surface barrier height by using a probe rather than a ring. This makes it a relatively simple matter to study many types of commercial transistors directly. The method we used, as shown in section 3.1 of the above reference[2] also has the advantage of indicating the curvature of the S vs ϕ_s curve at the operating point. This assists in differentiating between points on the curve at which the tangents are equal, even if only a small field can be applied.

It has been found by our research depart-

* Received by the IRE, May 24, 1960.

[1] B. Schwartz and M. Levy, PROC. IRE, vol. 48, pp. 317–320; March, 1960.
[2] J. R. A Beale, D. E. Thomas, and T. B. Watkins, *Proc. Phys. Soc.*, vol. 72, pp. 910–914; November, 1958.

ment at Southampton that using these techniques similar results can be obtained on production silicon transistors.[3]

J. R. A. Beale
D. E. Thomas
T. B. Watkins
Mullard Research Lab.
Salsford
Surrey, Eng.

[3] F. D. Morton, private communication.

Steady-State Transforms*

Professor Jury[1] has presented a method of obtaining the steady-state response, in closed form, of a linear system to nonsinusoidal periodic inputs. The method involves the use of the modified z-transform, along with a limiting process necessitated by the final value theorem.

An alternate method of solving this same type of problem is that of the use of steady-state transforms.[2-4] The method involves first, the finding of the direct transform of the driving function by integration[2] or by the use of steady-state transform tables.[5] The direct transform is then multiplied by the transfer function of the driven system, and the result is the direct transform of the output steady-state wave. The required time function in closed form may be obtained by integration,[2] or by use of the steady-state transform tables.[5] The purpose of this note is to illustrate the application of these transform tables to the two examples suggested by Professor Jury.

Example I: This example[1] is that of Fig. 1 of the first reference, and consists of a rectified sine wave applied to a parallel RC circuit in series with another resistance. The problem is to obtain the steady-state output voltage across the parallel RC circuit. From no. 4 of Table I of the steady-state transform tables,[5] the direct transform of the input voltage is

$$V_i(p) = S[v_i(t)] = \left(\frac{E\pi}{T}\right)\left[\frac{1+e^{-pT}}{p^2+(\pi/T)^2}\right], \quad (1)$$

where S indicates the operation of obtaining the direct steady-state transform. The transform of the output voltage, $V_o(t)$, across the parallel RC circuit is obtained by multiplying (1) by the transfer function.

$$V_0(p) = S[v_0(t)] = \left(\frac{E\pi}{T}\right)\left[\frac{1+e^{-pT}}{p^2+(\pi/T)^2}\right]\left[\frac{1}{R_1C(p+a)}\right] = K\frac{(1+e^{-pT})}{[p^2+(\pi/T)^2](p+a)} \quad (2)$$

where $K=(E\pi/R_1CT)$ and $a=(R_1+R_2)/R_1R_2C$. The output voltage may be obtained by taking the inverse steady-state transform of (2). By the use of no. 21 of Table II, of the steady-state transform tables,[5] the output steady-state voltage in closed form is

$$v_0(t) = S^{-1}[V_0(p)] = S^{-1}\left\{\frac{K(1+e^{-pT})}{[p^2+(\pi/T)^2](p+a)}\right\} = \frac{2Ke^{-at}}{[a^2+(\pi/T)^2](1-e^{-aT})} + \frac{KT\sin[(\pi t/T)-\alpha]}{\pi[a^2+(\pi/T)^2]^{1/2}}, \quad (3)$$

where $0<t<T$

$$\alpha = \arctan(\pi/aT)$$

and S^{-1} indicates the operation of obtaining the inverse steady-state transform. This agrees with the previous result.[1]

Example II: This example[1] is that of Fig. 2 of the first reference, and consists of a periodic double pulse applied to a series RL circuit. The problem is to obtain the steady-state voltage across the resistance. From no. 3, Table I,

$$V_i(p) = (1/p)[1-e^{-ph_1}+e^{-pT_1}-e^{-p(T_1+h_2)}]. \quad (4)$$

When (4) is multiplied by the transfer function, the transform of the output voltage is

$$V_0(p) = \left(\frac{R}{L}\right)\left[\frac{1-e^{-ph_1}+e^{-pT_1}-e^{-p(T_1+h_2)}}{p(p+R/L)}\right]. \quad (5)$$

To obtain the steady-state output voltage in closed form, no. 8 of Table II, of the transform tables,[5] is used. The result is

$$v_0(t) = \begin{cases} \left(\frac{L}{R}\right)\left\{1-\frac{e^{-Rt/L}}{(1-e^{-RT/L})}\left[1-e^{-(T-h_1)R/L}+e^{-(T-T_1)R/L}-e^{-(T-T_1-h_2)R/L}\right]\right\}, & 0<t<h_1 \\ \left(\frac{L}{R}\right)\frac{e^{-Rt/L}}{1-e^{-RT/L}}\left[-1+e^{Rh_1/L}-e^{-(T-T_1)R/L}+e^{-(T-T_1-h_2)R/L}\right], & h_1<t<T_1 \\ \left(\frac{L}{R}\right)\left\{1-\frac{e^{-Rt/L}}{(1-e^{-RT/L})}\left[1-e^{Rh_1/L}+e^{RT_1/L}-e^{-(T-T_1-h_2)R/L}\right]\right\}, & T_1<t<(T_1+h_2) \\ \left(\frac{L}{R}\right)\frac{e^{-Rt/L}}{(1-e^{-RT/L})}\left[-1+e^{Rh_1/L}-e^{RT_1/L}+e^{(T_1+h_2)R/L}\right], & (T_1+h_2)<t<T. \end{cases} \quad (6)$$

Again this agrees with the previous result.[1]

The steady-state transforms may also be evaluated as a Fourier series,[2,6] and thus may be used to obtain the closed form of an infinite convergent Fourier series. It is hoped that in the near future a paper on this particular use of steady-state transforms will be presented.

D. L. Waidelich
Dept. of Elec. Engrg.
University of Missouri
Columbia, Mo.

* Received by the IRE, June 17, 1960.

[1] E. I. Jury, "A note on the steady-state response of linear time-invariant systems to general periodic input," Proc. IRE, vol. 48, pp. 942–944; May, 1960.

[2] D. L. Waidelich, "The steady-state operational calculus," Proc. IRE, vol. 34, pp. 78–83; February, 1946.

[3] D. L. Waidelich, "Response of circuits to steady-state pulses," Proc. IRE, vol. 37, pp. 1396–1401; December, 1949.

[4] D. L. Waidelich, "Steady-state waves on transmission lines," *Trans. AIEE*, vol. 69, pp. 1521–1524; 1950.

[5] J. N. Warfield and D. L. Waidelich, "A Table of Steady-State Transforms," University of Missouri, Columbia Engrg. Exper. Station, Res. Rept. No. 1; 1953.

[6] D. L. Waidelich, "Steady state currents of electrical networks," *J. Appl. Phys.*, vol. 13, pp. 706–712; November, 1942.

Measurement of Phase Deviations in Ramsey-Type Cavities of Atomic Beam Frequency Standards*

Double oscillating field excitation (Ramsey-type cavity) is now used exclusively in high-precision atomic beam spectrometers and frequency standards. Its advantages over the single field excitation are well known.[1] Special care has to be taken, however, to reduce the phase difference between the two excitation fields to fractions of a degree if an accuracy of better than $1p:10^{10}$ should be achieved with a Cs beam standard, utilizing a line width of some 120 cps at 9.2 kmc.[2,3] The fractional frequency shift, $\Delta f/f$, resulting from a phase difference, $\Delta\phi°$, and an atomic resonance line characterized by Q is given by

$$\frac{\Delta f}{f} = \frac{\Delta\phi}{180}\,\frac{1}{Q}. \quad (1)$$

The shift associated with a given beam apparatus will be equal in size but opposite in sign if the cavity is traversed by the beam in reversed direction.

In the spring of 1958, we proposed to utilize this effect for either checking out cavity systems for production models of Cs beam standards or for increasing the accuracy of laboratory models of such standards, by building the vacuum envelope of the beam tube around the cavity system in the form of a drum, which would allow a 180° precision rotation of the cavity system under vacuum. The microwave signals could be fed into the rotable cavity through a waveguide with a vacuum-proof rotary waveguide joint. Because of the rotary joint, this method is obviously not suitable for sealed systems but only for continuously pumped systems, which would be most pertinent for the above-mentioned applications, anyway. The necessary mechanical tolerances involved are close but obtainable at the present time. The accuracy of such a device for determining the effective cavity phase error is about $1p:10^{11}$. Once the cavity is installed in its usual position number 1, the measurement procedure is relatively simple. The beam device is put in operation and the output signal (*e.g.*, 100 mc) is measured in terms of any other standard which has a stability comparable to that of Atomichron NC1001. The beat note is observed over a period of about 1 hour, after which the fre-

* Received by the IRE, June 14, 1960.

[1] N. F. Ramsey, "Molecular Beams," Oxford University Press, New York, N. Y.; 1956.

[2] W. Molimberger, "Militarized Atomic CS Beam Frequency Standard," National Co., Malden, Mass., Semifinal Rept., Signal Corps Contract DA-36-039 SC-74863; 1959.

[3] J. Holloway, *et al.*, "Comparison and evaluation of cesium atomic beam frequency standards," Proc. IRE, vol. 47, pp. 1730–1736; October, 1959.

quency of the reference standard is adjusted to zero beat, in order to maximize the measurement precision. Then the test cavity is rotated under vacuum through 180° to bring the cavity in position number 2. The new beat frequency is measured, and it is determined if the test standard with cavity position number 2 is higher or lower in frequency than the reference standard. If the rotation showed a frequency change, $-2\Delta f$, we have found that the frequency of the standard under test with the cavity operated in normal position number 1 has a fractional error $+\Delta f/f$, and that the excitation field closest to the detector leads the other field by an effective amount, $\Delta\phi_r°$, which can be calculated from (1). This phase shift may be called effective because the presence of a phase shift $\Delta\phi°$ in a servo controlled system using modulation of the excitation signal gives rise to an additional small frequency shift caused by a "mathematical" effect.[3] If it should be desired to measure the pure cavity phase shift $\Delta\phi°$, undisturbed by this "mathematical" effect, one has to open the servo loop and measure the dc resonance curve.[4]

The advantage of cavity rotation under vacuum over the method of removing the cavity from the system, turning it around and reinstalling it—as practiced occasionally—is obvious. It saves considerable time, and leaves all other conditions unchanged.

FRIEDRICH H. REDER
U. S. Army Signal and Dev. Lab.
Fort Monmouth, N. J.

[4] F. Reder, "Proposed feasibility study of frequency shift in sealed atomic beam frequency standards," PROC. IRE, vol. 47, pp. 1656–1657; September, 1959.

Broad-Band Amplifier of Nearly Forty Years Ago*

Soon after the advent of broadcasting, attempts were made to improve the performance of receivers with nonoscillating detectors, since the simple grid bend detector is a relatively insensitive device. As a result, many types of transformers were marketed which were intended to provide untuned radio-frequency amplification over the frequency range 500 to 1400 kc. These were probably the earliest broad-band amplifiers used in the communications industry. Only triode tubes were available, and neutralization had not yet been invented.

A variety of these transformers have been collected, and their performance measured. Most designs are quite crude, providing negligible gain and bandwidth. However, one manufacturer seems to have had inspired engineers who brought out transformers designed as stagger tuned triplets. The realization of the desirability of low capacity is evidenced by progressive bank windings. Thin strips of silicon iron form the open type core. Its main function is providing loss to broaden the circuits. Transformer characteristics are given in Table I. A test setup was made using type UV201A tubes operating at normal rating because type UV201 tubes are not presently available. The results are shown in Fig. 1. This performance can only be achieved when the transformers are connected in order R-2, R-3, R-4. Any other sequence gives a more distorted over-all response because of inauspicious feedback within the unneutralized triode tubes. When two triplets are connected in series, this order is upset with the associated large feedback and response curve of Fig. 2. The transconductance of these tubes varies rapidly with plate current and the gain accordingly, as shown in Fig. 3. However, the shape of the response curve is remarkably independent of gain.

TABLE I
GAIN VS FREQUENCY PERFORMANCE

Transformer type	R-2	R-4	R-3
Millihenries primary inductance at 1 kc	0.308	0.63	2.16
Millihenries secondary inductance at 1 kc	0.535	1.76	3.80
Per cent coupling	84	91	97
Ohms primary resistance at dc	11.2	16.1	28.4
Ohms secondary resistance at dc	17.2	27.4	45.3

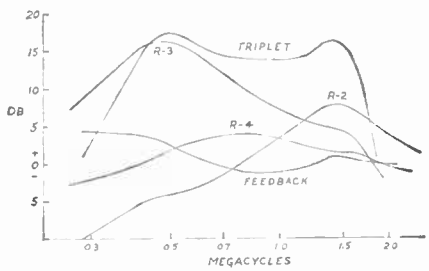

Fig. 1—First triplet and components.

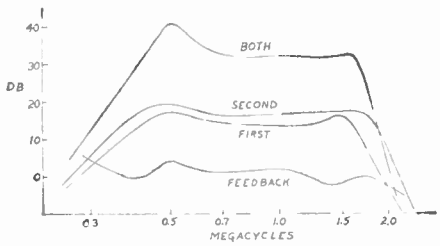

Fig. 2—Two triplets in series.

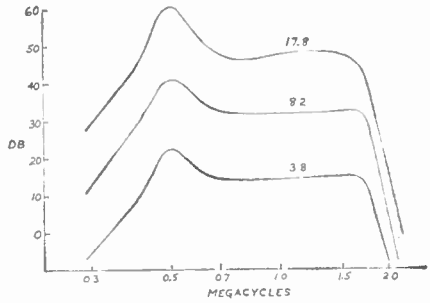

Fig. 3—Different total plate milliamperes for six tubes.

Apparently, the design was hit upon by empirical methods. The transformers were marketed by Acme Apparatus Company, Cambridge, Mass. Inspection tags give dates in November, 1922. Does anyone know the name of the engineer who was much ahead of his time and was responsible for this enlightened design? If any reader has other transformers of similar vintage and purpose, or UV201 and UV206 tubes, this author would be interested in entering into correspondence thereon.

GROTE REBER
Natl. Radio Astronomy Observatory
Green Bank, W. Va.

Simplification of Transistor Specifications*

Practical specifications of the small signal characteristics of transistors have been, and still are, of much concern to the user as well as the manufacturer of these devices. Current practices are not only inconsistent but, in most cases, inadequate for practical design work, since they fail to fully take into account the frequency dependency of the small signal parameters. These parameters generally vary widely with bias conditions. The picture would seem to become too involved if variations with frequency should also be considered—unless the frequency variations obey a simple law which makes it possible to describe it by means of, for example, a low-frequency value and a cutoff frequency.

Actually, the forward current transfer ratio, h_f, of most transistors has been found to follow closely such a function of frequency of the general form

$$\frac{1}{\sqrt{1+f^2/f_0^2}}.$$

At the cutoff frequency, f_0, the value of this expression becomes $1/\sqrt{2}$ (implying a 45° phase shift). Commercial transistor specifications normally include this cutoff frequency. However, explicit descriptions of the frequency characteristics of the remaining three parameters of the conventional hybrid matrix notation are rarely encountered. Sometimes the collector-to-base and collector-to-emitter capacities are listed, from which the frequency behavior of the reverse voltage transfer ratio (h_r) and the output admittance (h_0) may be deduced. The frequency characteristic of the very important input parameter h_i is not as easily defined.

Lacking this essential information, the expedient design of higher-frequency amplifiers, as well as the selection of a suitable transistor, is severely impeded. The cutoff frequency of h_f alone does not reveal enough of the high-frequency performance of a transistor to permit even a preliminary selection of a satisfactory device. Additional

* Received by the IRE, June 15, 1960.

* Received by the IRE, June 16, 1960.

high-frequency data have to be acquired by tests which, since they are oriented towards a very specific application, tend to be too special to make them useful for even a similar application. Inconvenient and costly special transistor specifications are the result.

This dilemma can be resolved by substituting a different parameter, the (forward) transconductance

$$g_m = \left.\frac{i_2}{V_1}\right|_{V_2=0\,(\text{output shorted})}$$

for the input characteristic.

This parameter, a classic in tube specifications, is extremely practical although it destroys, somewhat, the aesthetics of the hybrid parameters. In the common-emitter configuration, its frequency characteristic is very simple since, like h_f, it can also be defined in terms of a low-frequency value and a cutoff frequency.

The transconductance g_m is related to h_f and h_i by the simple expression

$$g_m = \frac{h_f}{h_i}.$$

since all three parameters are defined under shorted output conditions.

Martin and Schreiber[1] have shown how high-frequency amplifiers of the common-emitter configuration can be designed using only the parameters h_{fe} and g_{ie} and their respective cutoff frequencies, $f_{\alpha e}$ and f_{ie}. By neglecting h_{re}, the collector-to-base feedback, and h_{oe}, the output admittance, they arrive at very simple, practical design equations. These simplifications are quite realistic because

1) in a tuned amplifier, h_{re} is normally made ineffective by neutralization and the reactive component of h_{oe} is "tuned out," and
2) in a wide-band amplifier, the load impedance is low minimizing the influence of h_{re} and h_{oe}.

F. J. Potter
G. Sager
Advanced Dev. Lab.
Telecommun. Engrg. Dept.
Stromberg-Carlson Div.
General Dynamics Corp.
Rochester 3, N. Y.

[1] A. V. J. Martin and H. Schreiber, "Transistor External Parameters," AIEE Conference Paper No. CP 59-260, presented at AIEE Winter General Meeting, New York, N. Y.; February 1–6, 1959.

An Analysis of a Magnetoresistive Voltage Regulator*

The feasibility of employing magnetoresistive effects in InSb for voltage regulation has been established both analytically and experimentally. Voltage regulation of 1 per cent for 20 per cent variations in load and input voltage appears feasible without the use of added amplification in the feedback circuit. Magnetoresistive regulators using InSb are best suited to low voltage (less than 10 volts) and medium current (less than 10 amperes) applications.

* Received by the IRE, June 27, 1960. This research was sponsored by the Electronics Components Lab., Wright Air Dev. Division.

It has previously been shown that the magnitude of the Corbino magnetoresistive effect in high mobility InSb is such that the effective resistance of a sample at room temperature, in a field of 10,000 gauss, is about 15 times the resistance of the sample in the absence of a magnetic field.[1,2] This resistance change has been applied in a regulator using the circuit shown in Fig. 1.

The regulation action is accomplished in the following manner. An error signal, (E_0-E_R), is applied to the control coil. The resultant control magnetic field B_C either adds to or subtracts from the bias magnetic field, B_i, thereby increasing or decreasing the resistance of the magnetoresistance element, R, as required to regulate the output voltage, E_0. The change in R which results from this action has been shown to be

$$\Delta R = 2.1 R_0 B_i B_c, \qquad (1)$$

where A is a constant such that $\Delta R/R_0 = AB^2$ and R_0 is the resistance of the magnetoresistance element at zero magnetic field. This expression is valid over a limited range of field.

Let is define a control factor G in the following manner:

$$G = \Delta R/\Delta E_0. \qquad (2)$$

This factor, G, indicates the change in R, ΔR, which results from a change in output voltage, ΔE_0.

A dynamic solution to the control equation for the circuit shown in Fig. 1 can then be derived in terms of Laplace transforms to yield the following result:

$$\frac{\frac{\Delta E_0}{E_0}(s)}{} = \frac{\frac{\Delta E_i}{E_i}(s) + \left(\frac{R}{R+R_L}\right)\frac{\Delta R_L}{R_L}(s)}{1+\left(\frac{E_0 G}{R+R_L}\right)\left(\frac{1}{1+T_c s}\right)}, \qquad (3)$$

where

$\Delta E_0/E_0(s)$ is the Laplace transform of the relative change in output voltage,
$\Delta E_i/E_i(s)$ is the Laplace transform of the relative change in input voltage,
$\Delta R_L/R_L(s)$ is the Laplace transform of the relative change in load resistance,
T_c is the time constant, L_c/R_c in seconds, L_c is the inductance of the magnetizing coil, and R_c is its resistance,
s is the Laplace parameter.

Eq. (3) describes the control action of the magnetoresistive regulator. Performance curves are shown in Fig. 2 for the static case which indicate the regulation capabilities of this system for given changes in both input voltage and load when R_L is made equal to R. Also plotted are experimental points taken to provide a verification of the analysis. The experimental data were taken using a magnetoresistance element and associated magnetic coil and core originally designed for another purpose. For this reason, the experimental data could be obtained only over a limited range of circuit current, I. Over this limited range of $I\times G$, the correlation of experimental to predicted regulation is good.

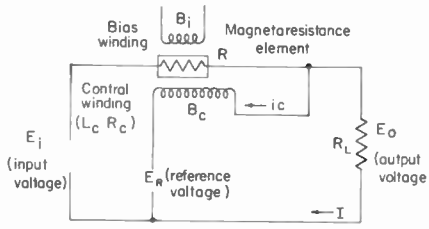

Fig. 1—Series magnetoresistive voltage regulator circuit.

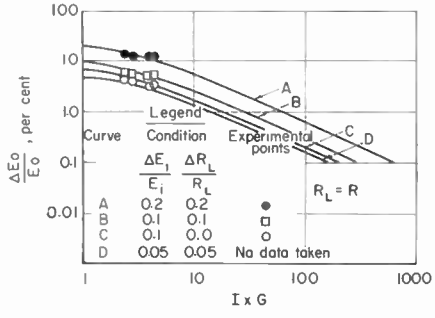

Fig. 2—Comparison of calculated and experimental performance of magnetoresistive regulator (for $R=R_L$).

[1] R. K. Willardson and A. C. Beer, "Magnetoresistance—a new tool for electrical control circuits," *Elec. Mfg.*, vol. 57, p. 79; January, 1956.
[2] R. K. Crooks, G. J. Falkenbach, and T. S. Shilliday, "Experimental Analysis of Performance of Galvanomagnetic Amplifiers," Battelle Memorial Inst., Columbus, Ohio. Final Rept. to Rome Air Dev. Center, RADC-TR-59-119, Contract No. AF 30(602)-1839; July 15, 1959.

The low resistivity of InSb and practical considerations involving the size of the semiconductor element and the associated magnetic devices indicate that InSb in a single element is most applicable for regulation at low voltages (less than 10 volts and medium currents (less than 10 amperes). Multiple elements could be used for higher ratings, however. Regulation of an output voltage to less than 1 per cent of its steady-state value appears achievable for values of IG of 60 and 20 per cent, or less, variations in load and voltage. Improved regulation could be achieved by the use of amplifiction in the feedback loop or by cascading several magnetoresistive regulators.

The performance of voltage regulation using magnetoresistance effects in InSb has been investigated analytically and verified under steady-state conditions experimentally. The regulation that can be achieved, in both the dynamic and static cases, can be predicted by applying the derived control equation to the specific situation being examined.

The authors are happy to acknowledge the assistance of Dr. H. S. Kirschbaum in the derivation of the dynamic control equation.

H. Berger
R. K. Crooks
Battelle Memorial Institute
Columbus, Ohio

Contributors

Malcolm R. Currie (S'52–A'55–SM'58) was born in Spokane, Wash., on March 13, 1927. He received the B.A. degree in physics from the University of California, Berkeley, in 1949, and the M.S. and Ph.D. degrees from the same institution in 1952 and 1954, respectively.

M. R. Currie

From 1944 to 1947, he served in the U. S. Navy Air Corps. He was associated with the Microwave Laboratory at the University of California from 1949 to 1951. From 1952 to 1954 he was a research assistant in the Electronics Research Laboratory. He was an instructor in the Department of Electrical Engineering during 1953–1954. Since 1954, he has been associated with the Research Laboratories of the Hughes Aircraft Company, Malibu, Calif., where he has been concerned primarily with problems in microwave electronics, plasma physics, and ion propulsion. From 1957 to 1959 he was head of the Electron Dynamics Department. At present he is director of the Physics Laboratory.

Dr. Currie received the Eta Kappa Nu Award (outstanding young electrical engineer) for 1958. He is a member of the American Physical Society, the American Rocket Society, Sigma Xi, RESA, and Phi Beta Kappa.

❖

Roy W. Gould (S'48–A'51–M'56) was born in Los Angeles, Calif., on April 25, 1927. He received the B.S.E.E. degree from the California Institute of Technology, Pasadena, in 1949, and the M.S. degree from Stanford University, Stanford, Calif., in 1950. He completed the requirements for the Ph.D. degree in physics at the California Institute of Technology in 1955. During his graduate study in physics he held a National Science Foundation Fellowship and a Howard Hughes Fellowship.

R. W. Gould

In 1951 and 1952, he was employed at the Caltech Jet Propulsion Laboratory as a research engineer and worked on the guidance system of the Corporal missile. Since 1955, he has been on the staff of the California Institute of Technology, where he is now an associate professor of electrical engineering and physics. He is teaching and conducting research in the field of physical electronics, and currently is concerned with microwave interaction with plasmas. He is also a consultant to the Electron Dynamics Department of the Hughes Research Laboratories, Malibu, Calif.

Dr Gould is a member of Tau Beta Pi, Sigma Xi, and the American Physical Society.

❖

Kenneth P. Grabowski (M'57) was born in Saginaw, Mich., on August 23, 1932. He received the B.S.E.E. and M.S.E.E. degrees in 1955 and 1956, respectively, from the University of Michigan, Ann Arbor.

K. P. Grabowski

From 1954 to 1956 he was employed by the Engineering Research Institute of the University of Michigan, where he worked on ferroelectric and ferrite devices. In 1956 he joined the Hughes Research Laboratories, Malibu, Calif., as a member of the Technical Staff. His work has included investigation of circuits for high-power traveling wave tubes and, more recently, investigation of parametric amplifiers and related devices.

Mr. Grabowski is a member of Tau Beta Pi, Eta Kappa Nu, Sigma Xi, and RESA.

❖

Ralph E. Hiatt (M'47–SM'59), for a photograph and biography please see page 1616 of the September, 1960, issue of Proceedings.

❖

Oscar J. Lumpkin, Jr. was born in Los Angeles, Calif., on September 13, 1937. He received the B.S. degree in physics magna cum laude in 1959 from St. Mary's College of California, where he held journalism and California State scholarships.

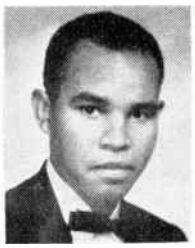

O. J. Lumpkin, Jr.

During the summer of 1959, he was employed in the Communications Section of Hoffman Electronics Corporation, analyzing electronic circuits. He is currently engaged in graduate studies in physics at Columbia University, New York, N. Y., where he holds an assistantship and was a National Science Foundation Fellow during the summer of 1960.

Sheldon Plotkin (S'53–M'57) was born in Denver, Colo., on September 3, 1926. He received the B.S.E.E. degree in 1946 and the B.S. degree in aeronautical engineering in 1949, both from the University of Colorado, Boulder. He received the Ph.D. degree in electrical engineering from the University of California, Berkeley, in 1956.

S. Plotkin

During 1946 he worked at the Los Alamos Scientific Laboratory developing electronic instrumentation. In 1949, he worked at the U.S.M.T.C., Point Mugu, Calif., evaluating and conducting missile tests. While in attendance at the University of California, he was a teaching assistant for three years and project engineer in charge of all electronic instrumentation in the Cosmic Ray Laboratory for two years. From 1956 to 1958, he was engaged in development of high-power electronic and magnetic pulse generators for Levinthal Electronic Products. Since 1958, he has been on the faculty of the University of Southern California, Los Angeles, and a part-time consultant for Hoffman Electronic Corporation engaged in various problems in electronics and communication systems.

Dr. Plotkin is a member of Eta Kappa Nu, Pi Mu Epsilon, and Sigma Xi.

❖

Edward G. Ramberg (M'53–SM'53–F'55) was born in Florence, Italy, on June 14, 1907. He received his undergraduate training at Reed College, Portland, Ore., and Cornell University, Ithaca, N. Y., receiving the B.A. degree from the latter in 1928. He continued his studies at Cornell, where he was Heckscher Research Assistant in the Physics Department. In 1930, he transferred to the University of Munich, where he received the Ph.D. degree in 1932.

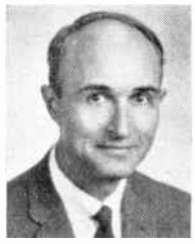

E. G. Ramberg

He interrupted his undergraduate study at Cornell for two years' employment as scientific aide in optical computation with the Bausch & Lomb Optical Company. After returning from Munich, he worked until 1935 as research assistant at Cornell University on the theory of X-ray satellites and line widths. In 1935, he joined the Electronic Research Laboratory of the RCA Manufacturing Company, Camden, N. J., as a junior engineer, and in 1942 he was

transferred as research physicist to the RCA Laboratories at the David Sarnoff Research Center in Princeton, N. J. From 1943 to 1945, he worked in Civilian Public Service, devoting part of this time to work on electronic aids for the blind under OSRD at Haskins Laboratory, New York, N. Y. After returning to the RCA Laboratories in 1946, he worked in the fields of electron microscopy, electron optics and optics relating to television, theory of thermoelectric refrigeration, and other problems in electron physics. In 1949, he interrupted this work to serve as visiting professor at the University of Munich, and for 1960–1961, he has received an appointment as Fulbright lecturer at the Technische Hochschule in Darmstadt, Germany.

Dr. Ramberg is a Fellow of the American Physical Society and a member of the Electron Microscope Society of America, the American Association of Physics Teachers, the AAAS, Sigma Xi, and Phi Kappa Phi. In 1959 he was named a Fellow of the technical staff of RCA Laboratories.

❖

Thomas B. A. Senior was born in England on June 26, 1928. He received the M.Sc. degree in mathematics research from Victoria University, Manchester, England, in 1950 and the Ph.D. degree in research from Cambridge University, Cambridge, England, in 1954.

T. B. A. Senior

In 1952, he was appointed an Established Scientific Officer and accepted a position with the Ministry of Supply at the Radar Research and Development Establishment (now the Royal Radar Establishment), Malvern, England. In 1955, he was promoted to Senior Scientific Officer. In 1957, he joined the Radiation Laboratory, University of Michigan, Ann Arbor, where his primary interests have been in the study of the diffraction and propagation of electromagnetic waves, with applications to physical problems.

John L. Stewart (S'48–A'50–M'53–SM'56) was born in Pasadena, Calif., on April 19, 1925. He received the B.S., M.S., and Ph.D. degrees in 1948, 1949, and 1952, respectively, from Stanford University, Stanford, Calif.

J. L. Stewart

He has worked on missile guidance at the Jet Propulsion Laboratory, on radar at Hughes Aircraft Company, on vacuum tubes at Stanford University, and on electronic countermeasures at the University of Michigan. Since 1952, he has taught at the University of Michigan, Ann Arbor, California Institute of Technology, Pasadena, and the University of Southern California, Los Angeles. He is now professor of electrical engineering at the University of Arizona, Tucson. His specific areas of interest include network theory, noise and statistics.

Dr. Stewart is a member of Sigma Xi, Tau Beta Pi and Eta Kappa Nu.

❖

Elmer Thomas (M'58) was born in Avalon, Pa., on September 6, 1926. After serving in the U. S. Navy, he attended the University of Pittsburgh from 1946 to 1949, where he received the B.S.E.E. degree.

E. Thomas

In 1949, he became associated with the Department of Defense, where he was engaged in developing circuits applicable to multiplex equipments. From 1951–1956, he was employed by the Applied Physics Laboratory of The Johns Hopkins University, where he assisted in the development of airborne control systems for guided missiles and designed new types of suppressed-carrier modulators and demodulators and servo control systems. Prior to joining Page in mid-1957, he was employed by the Department of Defense for two years, where he acted as head of the Time-Division Multiplex Section. He was responsible for the design and development of new types of multiplex equipment, many of which were classified.

He is presently manager of the Page Research and Development Laboratory, Washington, D. C. He is the inventor of the decision threshold computer, a recent Page development which permits increased orders of diversity in the presence of selectively fading signals by taking advantage of the lack of correlation between the mark and space frequencies. He is now working on signal detection and correlation problems on binary systems, studies of diversity and diversity-combining techniques, and the development of HF demodulation techniques. Other assignments at Page have included application of the decision threshold computer to HF circuits and HF propagation studies.

Mr. Thomas is a member of Sigma Tau and Eta Kappa Nu.

❖

R. D. Weglein, for a photograph and biography, please see page 1347 of the July, 1960, issue of PROCEEDINGS.

❖

Vaughan H. Weston was born in Terry Sound, Ont., Canada, on May 1, 1931. He received the Ph.D. degree in applied mathematics from the University of Toronto, Canada, in 1956.

V. H. Weston

He has since served as Research Assistant, Defense Research Board of Canada, University of Toronto, and as a Lecturer at the same institution. He has also consulted in numerical analysis for Atomic Energy of Canada, Ltd. He has developed a method of solving the Helmholtz equation for non-separable coordinates and has applied this method to the torus and the investigation of scattering from circular rings. He joined the Radiation Laboratory, University of Michigan, Ann Arbor, in 1958.

Dr. Weston is a member of the American Mathematical Society and the Mathematical Association of America.

Books

Servomechanism Fundamentals, 2nd ed., by Henri Lauer, Robert Lesnick, and Leslie E. Matson

Published (1960) by McGraw-Hill Book Co., Inc., 330 W. 42 St., N. Y. 36, N. Y. 485 pages+5 index pages+xiv pages. Illus. 6¼×9¼. $10.00.

Authors of modern undergraduate texts in the area of control systems generally respond rather strongly to a broad systems point of view which compels them to write either a monumental summary of the state of the art or a survey with a rather standard list of topics, each of which must be dispatched swiftly and somewhat superficially. This book is unique among books in the control field in that it takes an opposite point of view and makes no effort to generalize, but instead singles out a small, but important segment and deals with it thoroughly using classical methods of analysis based principally on the use of differential equations and to a lesser extent on the transfer function. First published in 1947, it achieved a reputation for its excellence in handling the analysis and design of simple position-control systems employing viscous damping, error-rate damping and integral control in various combinations. The authors assume very little preparation on the part of the reader and supply him with the essential background pertinent to the physics of mechanical and electrical systems as well as to the methods of solution of linear second-order differential equations.

In the new edition, the authors have wisely decided to stay with their original philosophy and have resisted the temptation to include the Laplace transform and the root-locus technique. Having selected as their vehicle systems which are usually not more complicated than second order, the authors largely avoid the competition among methods of analysis and are able to devote their whole attention to putting together an excellent primer for further study in the control field. They have added about 200 pages of new material, roughly half of which is devoted to further development of the transfer-function approach and half to a new chapter on nonlinear servosystems. Much of the earlier material has been rewritten and brought up to date, and a new format and many new figures give the book a pleasingly modern appearance. The original edition was distinguished for its excellent illustrative examples, many of which were worked out in complete numerical detail, and with observations that served to consolidate the ideas developed in the text. The new edition has added to the collection many new and interesting examples which give the reader a very useful background on which to base his own design ventures. The problems alone represent a valuable contribution to the control-system literature.

In the new material developed around the transfer-function viewpoint, several topics of current interest have been added or augmented. In a discussion of stability, the Nyquist test is presented in greater detail than previously and the Routh-Hurwitz test has been added. Here also the complex frequency is introduced briefly and the use of the poles and zeros in graphical descriptions of systems is sketched. A brief mention is also made at this point of the handling of disturbance inputs.

The chapter on nonlinear systems rounds out the earlier material by including for the basic group of position-control systems such commonly encountered nonlinearities as on-off operation with and without dead zone, backlash and nonlinear friction. The nonlinear systems are introduced via the unifying description of the differential equation, and solutions are effected through the use of phase-plane representations and describing-function techniques.

Because of its somewhat specialized subject matter, this book will probably not find a place in modern engineering curricula. It will continue, however, to have a strong appeal to engineers in industry and to any who wish a sound, nontrivial introduction to the design of position-control systems for industrial applications. In spite of its somewhat limited field of applications, its thoroughness and its outstanding clarity of presentation will continue to make it a valued addition to the library of anyone connected with the control-system field.

W. A. Lynch
Brooklyn Polytech. Inst.
Brooklyn, N. Y.

Operations Research and Systems Engineering, Charles D. Flagle, William H. Huggins, and Robert H. Roy, Eds.

Published (1960) by the John Hopkins Press, Homewood, Baltimore 18, Md., 879 pages+0 index pages+x pages+bibliography by chapter. Illus. 6¼×9¼. $14.50.

The foreword in this account of the growing involvement of a university in the day-to-day affairs of government and industry offers a fine review of the book itself and because of its excellence is repeated in part.

The chapters of the book are a set of lectures delivered by the authors in the Johns Hopkins University's annual two-week course for management in Operations Research and Systems Engineering. The assembled lectures came from many academic departments of the Johns Hopkins University and from its affiliated research branches, the Applied Physics Laboratory and Operations Research Office.

Many diverse disciplines are represented—physics, economics, statistics, psychology, several branches of engineering, and mathematics. Despite this range of backgrounds, the authors appear to share a common interest that unites them in the concern for the operation of total systems—human organizations, man-machine systems such as factories or military units, or complex physical systems.

The initial chapters are devoted to the philosophical and historical aspects of systems engineering and operations research. These are followed by chapters on specific methodologies that have developed or have been adapted for the field. A set of case histories concludes the volume.

The expanding application of new knowledge promotes rapid obsolescence, not only in physical equipment but also in the adequacy and capability of humans. In the case of physical equipment, little can be done but to replace it. Humans, on the other hand, can forestall their own obsolescense by continuous new learning. Each author offers a central interest in his professional life presenting it in brief form for a reader who is assumed to be mature and interested, but not a specialist in the field. The editors have accomplished an excellent job in bringing this material together.

The book is a fine technical and interesting presentation of the subjects of Operations Research and Systems Engineering and will hold the attention of the reader interested in this field.

Christian L. Engleman
C-F-I-R
Washington, D. C.

Digital Computer Principles, by Wayne C. Irwin

Published (1960) by D. Van Nostrand Co., Inc., 120 Alexander St., Princeton, N. J. 314 pages+3 index pages+iv pages+3 bibliography pages. Illus. 6¼×9¼. $8.00.

As stated in its preface, this book is for the beginner. It is for the person who wishes to become acquainted with digital computers, but who has a nontechnical background. As such, it fills an important need. A wide range of topics is treated, so the reader is introduced to almost all the elements of computers, the synthesis of these elements into a computer, and programming. Since these topics are surveyed rather than developed to any significant depth, it is not a book for someone who wishes to learn how to design computers or how to program.

Boolean algebra is introduced in the book in order to treat the binary elements of which digital computers are composed. The discussion is clear and, in general, is easy to follow; however, the representation of the binary elements first as logical propositions and only then interpreting them in terms of binary digits and algebraic operations seems to the reviewer to be an artificial complication. It would seem to be simpler to represent the computer signals and circuit elements directly as algebraic variables and operations. Concepts such as "the clock is false" and "the flip-flop A is to be turned true" do not seem to assist in the understanding of circuit performance or of the use of algebra as a tool in computer design.

Eldred C. Nelson
Ramo-Wooldridge
Canoga Park, Calif.

Physics of the Upper Atmosphere, J. A. Ratcliffe, Ed.

Published (1960) by Academic Press, Inc., 111 Fifth Ave., N. Y. 3, N. Y. 563 pages+21 index pages +xi pages+bibliography by chapter. Illus. 6¼×9¼. $14.50.

The IRE's new overseas vice-president, J. A. Ratcliffe,[1] is known to all ionospheric radio workers as a pre-eminent authority in their field and as a master of clear exposition. These qualities are plainly manifest in the editing of this new book on the upper atmosphere, and it is the first to rank with S. K. Mitra's "The Upper Atmosphere"[2] which has stood without a peer for thirteen years. As a monumental personal work, Mitra's book will probably never be challenged, for this burgeoning subject has reached the point where even editing a comprehensive work is a very great task. However, the plan of the chapters, the selection of the authors, and the continuity of the independent contributions in the new book have been skillfully achieved by Mr. Ratcliffe to produce a well-organized text written by eleven authors. As coauthor of the longest chapter, Mr. Ratcliffe shares the plaudits due the authors.

The authors and chapters are:

S. Chapman:	The thermosphere—the Earth's outermost atmosphere(16 pages)
M. Nicolet:	The properties and constitution of the upper atmosphere (56 pages)
H. E. Newell, Jr.:	The upper atmosphere studied by rockets and satellites (60 pages)
H. Friedman:	The sun's ionizing radiations (86 pages)
D. R. Bates:	The airglow (50 pages)
D. R. Bates:	General character of auroras (29 pages)
D. R. Bates:	The auroral spectrum and its interpretation (57 pages)
H. G. Booker:	Radar studies of the aurora (23 pages)
J. A. Ratcliffe and K. Weekes	The ionosphere (93 pages)
E. H. Vestine	The upper atmosphere and geomagnetism (42 pages)
J. S. Greenhow and A. C. B. Lovell	The upper atmosphere and meteors (38 pages).

Several of the authors have also contributed to a final chapter describing relevant advances achieved in the recent International Geophysical Year.

The individual monographs contain complete bibliographies so that, like Mitra's, this book has great value as a key to the voluminous literature of this field. The method of handling the bibliography, the indexing, and other matters of format are well arranged. Whereas the preface is very brief and is devoted to remarks concerning the manner of compilation of the work, an extensive interpretive preface would have been of much value to many readers.

Examining the book in the area of one of his own specialties, this reviewer has found no mention of the important natural phenomenon of audio-frequency ionospheric emissions (dawn chorus, etc.); and has noted the statement on page 401 that it is the *ordinary* magneto-ionic component which is guided by the Earth's magnetic field in whistler-mode propagation whereas it is, of course, generally believed to the *extraordinary* component.

Such examples notwithstanding, the book is unquestionably of wide scope and high quality. By good organization, and with benefit of new knowledge and insight, it places this vast field in new and sharper perspective.

M. G. Morgan
Thayer School of Engrg.
Dartmouth College
Hanover, N. H.

[1] See Proc. IRE, vol. 48, p. 434; April, 1960.
[2] Published by the Asiatic Society, Calcutta, India, 713 pp., 1947; 2nd ed., 1952.

The Mobile Manual for Radio Amateurs, 2nd Ed., Headquarters Staff of the American Radio Relay League, Eds.

Published (1960) by The American Radio Relay League, West Hartford 7, Conn. 279 pages+3 index pages. Illus. 6¼×9¼. $2.50.

This second edition of the "Mobile Manual" continues the ARRL tradition of comprehensive, practical publications for the "working" radio amateur. It is a collection of articles from the pages of *QST*, covering just about every aspect of amateur mobile operation.

Two introductory articles serve to orient the newcomer. These are followed by sections on conventional receiving and transmitting equipment and on single sideband equipment. The receiving equipment section leans heavily toward converters for use ahead of the car broadcast receiver, since this is the predominant technique in amateur mobile reception; but one complete receiver is described. Both high frequency and VHF types of converters are described, using conventional tubes, the new low voltage types, and transistors.

The transmitter section, like that on receiving equipment, covers both HF and VHF equipment. However, its primary function seems to be the presentation of a number of different ways of mechanically treating essentially the same low power transmitter. Several articles on SSB equipment show that this mode has dared invade even the mobile field.

The really significant differences between mobile and fixed station equipments lie in the antenna and the power supply. The "Mobile Manual" recognizes this point with an impressive collection of antenna and power supply articles. Noise suppression is covered adequately, and space is even given to a couple of pieces of test equipment. Eleven pages are devoted to transmitter hunting, leaving the somewhat disconcerting implication that this is about all a mobile installation is good for, once one has one.

A section on portable and emergency equipment and a section on FCC rules round out the fare for the mobile enthusiast.

In the "Mobile Manual," the ARRL staff has presented a reasonably thorough survey of the field, which, although being of little use to those who would slavishly follow instructions, will serve as an excellent source of information and ideas for those who wish to custom-design their own mobile amateur stations.

Kenneth K. Bay
GE Co.
Lynchburg, Va.

Direct Conversion of Heat to Electricity, Joseph Kaye and John Welsh, Eds.

Published (1960) by John Wiley and Sons, Inc., 440 Fourth Ave., N. Y. 16, N. Y. 354 pages+3 index pages+ix pages+bibliography by chapter. Illus. 6×9¼. $8.75

This book provides a group of edited papers in four different fields of direct conversion. The articles cover the operation and some theory of thermionic energy converters both of the high vacuum and low cesium pressure types, magnetohydrodynamic energy converters, thermoelectric devices, and fuel cells. Although most of these articles have been published before in several of the technical journals, the book offers the beginner in the field of direct conversion easy access to some well-selected papers in these new fields.

The articles on high vacuum type thermionic converters give a comprehensive treatment of the subject and enable a designer of these devices to predict their performance.

The articles on low cesium pressure type thermionic converters acquaint the beginner in the field with the problems involved and point out clearly the advantages of vapor-filled thermionic devices over the vacuum close-spaced ones, from the point of view of feasibility of higher power densities and efficiencies, particularly where high temperature heat sources can be utilized.

Although the greater portion of the book is devoted to thermionic converters, some fundamental articles have been included on magnetohydrodynamic converters and thermoelectric devices.

The two articles on magnetohydrodynamic converters expose the principles involved and give briefly a method for evaluating some aspects of the performance of one arrangement of the MHD generator using mercury vapor.

On thermoelectricity, the articles are divided between basic thermodynamic consideration of the thermoelectric phenomena, basic procedures for measurement of thermoelectric properties, and device design consideration. A very valuable bibliography is added to help those who seek more details on the subject.

The one article on fuel cells acquaints the reader with an important area of direct conversion other than heat to electricity conversion.

On the whole, the book makes a useful addition to the library of investigators in the field of direct energy conversion.

M. E. Talaat
The Martin Co.
Baltimore, Md.

Basic Ultrasonics, by Cyrus Glickstein

Published (1960) by John F. Rider, Publisher, Inc., 116 W. 14 St., N. Y. 11, N. Y. 131 pages+4 index pages+2 glossary pages. Illus. 6×9. $3.50.

The author states in the preface that while there are "excellent engineering texts on ultrasonics, no simple but authoritative introduction to the subject has as yet appeared." Accordingly, this book (which, incidentally, is a paper-bound pocket book) was designed to cover the ultrasonics fields in a qualitative manner. The author assumes that the reader has a very limited physics and electronics background.

The text is divided into three parts. The first section is devoted to "general theory." Actually, this section describes a brief history of ultrasonics, the nature of sound waves, how they are generated, and why ultrasonics is utilized in certain applications rather than audible sound waves. The concept of directional transmission of sound, acoustic impedance and types of wave motion (*i.e.*, shear, etc.) are explained quite well. Finally, the major groups of ultrasonic applications are classified according to industry, frequency and nature of application.

The second section of the book summarizes the basic types of ultrasonic equipment and transducers, starting with a description of ultrasonic generators. For those readers not too well grounded in electronics, the author digresses a bit to discuss the nature of electrical resonance, tank circuits, vacuum tube and transistor oscillators and amplifiers.

The principal part of this section is devoted to ultrasonic transducers. Considering that the book is essentially an introduction to ultrasonics, this subject is covered fairly well. Thus, the nature of quartz, ADP, barium titanate, and magnetostriction is discussed along with how they are utilized in transducers. Electromagnetic and sandwich type transducers are also included. A qualitative transducer analysis describes such items as equivalent circuit, matching to the medium, Curie temperature concept, and efficiency. Transducer shape, typical mounting arrangements and a discussion of tapered stubs are considered in a brief but concise manner. Finally, a summary table showing the various transducer materials with a few of their characteristics and typical applications is included.

The second section concludes with a description of the associated equipment generally required in ultrasonics. This includes indicating units, receivers, and various controls and control circuits.

The third section, dealing with ultrasonic applications, covers almost fifty per cent of the test. The most commonly used applications are treated first, with the discussion classified under one of the two important headings, low power and cavitation (high power). The author then describes the applications by specific industries or subjects.

The low power category involves typical echo-ranging applications such as those found in sonar, fathometer devices, nondestructive testing, continuous liquid-level gaging and various other devices such as ultrasonic delay lines utilized in computers and radar. The high power or cavitation technique opens up a large variety of other types of applications. At the top of the list is ultrasonic cleaning, which is finding increasing use in almost every major industry, and ultrasonic drilling, soldering, and welding. The author devotes a great deal of space to why cavitation enables cleaning action, consideration in the choice of cleaner transducers, tanks, cleaning holders, and detergents.

The ultrasonic applications in the concluding part of the third section are classified by industry. Some of the more interesting medical, biological and chemical effects are considered. Finally, the author gives a quick but adequate summary of the applications of ultrasonics to food processing, textiles, geology, optics, missiles, and flow monitoring. As the author points out, some of the above applications are still in the experimental field.

This book is an excellent introduction to ultrasonics. It is written in an easily readable style. Its illustrations are simple, concise, lively, and yet tell a story very well. Although the subheadings in the table of contents could have been arranged in a more coherent manner, the book, in general, is well organized.

In this reviewer's opinion, the book is suitable for the high school senior or college freshman. (The book might even serve as a stimulus for such students to consider ultrasonics as a field in which to specialize!) Questions and problems are included together with a fairly useful glossary of terms. The treatment of a few simplified electronic circuits (including transistors) is obviously inserted to plug some holes in the background of the young student. This book is also useful for any engineer or scientist not specializing in the field of ultrasonics. The discussions on barium titanate, transducers, and certain applications such as nondestructive testing, cleaning and drilling were handled more thoroughly than some of the other topics, probably because of the author's closer personal affiliation with these subjects.

In conclusion, the book is heartily recommended for its role in filling a gap in the literature on an "introduction to ultrasonics."

A. L. Lane
RCA
Camden, N. J.

Basic Data of Plasma Physics, by Sanborn C. Brown

Published (1959) by Technology Press, Mass. Inst. Tech., Cambridge and John Wiley and Sons, Inc., 440 Fourth Ave., N. Y. 16, N. Y. 325 pages+9 index pages+viii pages. Illus. 6×9¼. $6.50.

With the rapid growth of research in the fields of high speed aerodynamics, controlled fusion, and magnetohydrodynamics, there arises a need for a book which provides an over-all survey of the physics of gaseous discharges as well as a guide to the now voluminous literature on the subject. Such an introduction is provided by Professor Brown's book. Roughly two-thirds of the book is devoted to the fundamental processes occurring in plasmas: scattering, ionization, recombination, etc. Each chapter consists of a brief summary of relevant definitions and theory followed by numerous graphs and tables with references, covering enormous amounts of data which would otherwise have to be laboriously hunted through the literature. The latter part of the book contains a more detailed but still condensed treatment of the various standard types of gaseous discharges.

This book provides a concise but readable introduction to gas discharge physics. Perhaps its greatest utility, however, resides in the great wealth of experimental results presented, for which it will no doubt become a standard reference work. Unfortunately, experiments in this field are often exceedingly difficult and the clean experiment which succeeds in disentangling one effect from a host of others is indeed a rarity. Similarly, our theoretical understanding of the basic processes is far from satisfactory; so-called calculations often being no more than sophisticated guesses. In this situation it is somewhat regrettable that much of the data are presented with no assessment of their accuracy or reliability. While it may be too much to ask for a critical evaluation of all the experiments in a book of this kind, since the selection of the "best" number from a host of conflicting results often becomes a major project, some guidance of this nature would be most useful.

Stephen Tamor
GE Res. Lab.
Schenectady, N. Y.

Control Systems Engineering, William W. Seifert and Carl W. Steeg, Eds.

Published (1960) by McGraw-Hill Book Co., Inc., 330 W. 42 St., N. Y. 36, N. Y. 944 pages+8 index pages+xiv pages+bibliography by chapter+11 appendix pages. Illus. 7½×10. $15.00.

In the preface the authors state that this book is "intended both as a textbook for a graduate-level course in control and as a source of reference material for practicing control-systems engineers." The book is based on a set of notes prepared for a two-week program in Control-System Engineering offered at M.I.T. during the summer of 1956.

The first part of the book (Chapters 1–2) discusses in very broad terms the concepts of systems analysis and the formulation of models. This is followed by (Chapters 3–6) a presentation of differential equations, linear analysis, feedback theory and matrices. The subject matter of these chapters is presented mainly in survey form, which makes it well suited for the purposes of review and reference. The next two chapters (Chapters 7–8) give the basic numerical analysis and analog computation techniques as applied to the solution of differential and algebraic equations.

In preparation for some of the later chapters, linear integral equations are presented in Chapter 9 and basic statistical theory in Chapters 10 and 11. Chapter 12 is entitled "Optimization of Linear Systems." This chapter deals in general with linear time-variable system analysis and optimization. For the time invariant case the Wiener-Hopf equation is obtained, as well as Phillips' optimization with configuration constraints, and Newton's optimization with dynamic constraints.

The following two chapters consider the analysis of nonlinear systems. Chapter 13 gives the principles of phase space analysis. The chapter on describing functions (Chapter 14) gives methods of using the sinusoidal describing function for stability and frequency response analysis of closed loop systems. Also, two types of describing functions for Gaussian inputs are presented with an example of the calculation of the resulting response statistics.

Chapter 15 treats the time-domain synthesis for control systems; the problem of the design of a terminal value controller is discussed. In Chapter 16 the analysis of sampled data systems is presented. Particular attention is given to the analysis required to determine the complete output as a function of time. Also, two methods are presented for the determination of the response of a sample-data system to random signals. Chapter 17, entitled "Elements of Game Theory," consists of a short description and the terminology of a two-person, zero-sum game. An example is worked out. No mention is made of the equivalence of the two-person, zero sum game to a linear programming problem. This equivalence makes available a variety of hand computation and digital machine methods for the solution of game theoretic problems. The Appendix gives a table of integrals useful in evaluating the mean square value of a power spectrum expressed in rational function form. Copious references are given at the end of each chapter.

This book is much more suitable as a reference book than as a graduate-level text. It contains a large amount of material previously unavailable in book form. However, due to the large range of topics covered, many of the results are just stated or developed only superficially; also, there are, no exercise problems. Both of these omissions detract from the book's value as a text.

J. A. Norton
Bell Telephone Labs.
Whippany, N. J.

Advances in Computers, Vol. 1, Franz L. Alt, Ed.

Published (1960) by Academic Press, Inc., 111 Fifth Ave., N. Y. 3, N. Y. 308 pages+7 index pages +x pages+bibliography by chapter. Illus. 6¼×9¼. $10.00.

The stated intention of this text is to bridge the gap between scientific or technical journals and textbooks, and to do this in a manner suitable for a wide audience including computer mathematicians, computer engineers, and computer users. By and large this text does a fairly good job of meeting these goals for the topics selected.

The topics selected include general purpose programming for business applications, numerical weather prediction, the present status of automatic translation of languages, programming computers to play games, machine recognition of spoken words, and binary arithmetic. As an example, the chapter on numerical weather prediction begins with a rather good self-contained exposition of the bases of some of the mathematical models presently used in weather forecasting. Following this, computational techniques are briefly but to a certain extent adequately treated. The chapter then concludes with some of the results of predictions for the various models. All chapters have for the most part adequate bibliographies, and the reader interested in following a particular area in greater detail should have little difficulty. There is also material of value and interest to the specialist in each of the subjects covered in the text. Specifically, it is always of interest and significance to note how an expert feels regarding the status of his field of interest, and this is certainly found in this text for most of the subjects covered.

On the whole, in the opinion of this reviewer, this text constitutes a rather fine addition to the literature, and subsequent volumes in this series should likewise be fine contributions. As things now stand, the advances in a particular field will be reviewed and brought up to date every several years, hopefully, for publication in this series. Actually, to many individuals an annual review in a rapidly moving field such as computer circuits and devices, for example, would undoubtedly be most valuable in view of the rate of contributions in this field. Somewhere in the literature such an annual review in adequate detail for several specific areas would be most valuable. The question is whether it should be found in a textbook such as this or whether the Transactions of the Professional Group on Electronic Computers can and should devote an annual issue to meet this need.

Cornelius T. Leondes
Univ. of Calif.
Los Angeles

Electromagnetic Wave Propagation, M. Desirant and J. L. Michiels, Eds.

Published (1960) by Academic Press, Inc., 111 Fifth Ave., N. Y. 3, N. Y. 730 pages+xiii pages +bibliography by chapter. Illus. 6¼×9¼. $22.00.

This book consists of the fifty-four papers which were accepted for presentation at the International Conference sponsored by the Postal and Telecommunications Group of the Brussels Universal Exhibition in 1958. The authors came from eleven different countries and the papers are in English except for four papers in French and five in German. Approximately one-half of the contributors came from the United States, a point which may indicate only the relative ease of obtaining travel funds, but the important laboratories in this country and in European countries are well represented. The book is thus the printed Proceedings of an important conference and deals with a range of topics in wave propagation that is currently of primary research and technological interest. As a result, it has both the virtues and the shortcomings of a conference Proceedings. In the language of its editors, "no attempt has been made to standardize notations, and so on, the papers having been prepared according to the customs prevailing in the country of origin." There is no index. In a number of papers, no references to prior work are given, while in others the bibliography may comprise 5 or perhaps 25 titles, depending on the author. The book abounds in reproductions of graphical records and calculated curves, and this graphical material is well reproduced.

As regards subject matter, the greatest single emphasis in the book is on ionospheric and tropospheric scatter. A wealth of experimental data is presented; other papers deal with the statistical and other methods used in interpreting the results. It would be futile for a reviewer to list either authors or title of papers. There are papers that deal with low frequency propagation, and others with propagation at VHF, or UHF, or microwave frequencies. There are no expository papers that attempt to give an overview of fundamental theory, or of currently held views of the ionosphere or troposphere.

The book will be useful, not to the beginner, but rather to a research worker in propagation and will be useful also as a reference in graduate courses in propagation. Its principal value lies in the variety of field results that are presented and in the discussion and development of the methods used in analyzing and interpreting these results.

It would be presumptuous to attempt to criticize the papers for soundness of content, especially in view of the fact that in a research area that is important in its own right and in which rapid advances are being made, interpretations are subject to change and techniques are subject to improvement. The papers are not uniform in quality but the book fills a current need and therein lies its virtue.

W. D. Hershberger
Univ. of Calif.
Los Angeles

Advances in Space Science, Vol. 2, Frederick I. Ordway, III, Ed.

Published (1960) by Academic Press, Inc., 111 Fifth Ave., N. Y. 3, N. Y. 436 pages+13 index pages +xiii pages+bibliography by chapter. Illus. 6¼×9¼. $13.00.

The book will be of interest to physicists and engineers engaged in the conquest of space. Its six chapters are:

I. Experimental Physics Using Space Vehicles
II. Tracking Artificial Satellites and Space Vehicles
III. Materials in Space
IV. Plasma Propulsion Devices
V. Electrostatic Propulsion Systems for Space Vehicles
VI. Attitude Control of Satellites and Space Vehicles

Written by seven competent scientists, the book presents a balance of measurement methods, test results, and underlying principles of phenomena and vehicles in space. It presents basic mathematical treatment of the several subjects to become a reference text for students and designers. It is written clearly and concisely with many tables of applicable physical constants.

The book fills a need for reference material in the new field of space science and will be a welcome addition to scientific libraries.

Conrad H. Hoeppner
Radiation, Inc.
Melbourne, Fla.

Recent Books

Brenner, Egon and Javid, Mansour, *Analysis of Electric Circuits*. McGraw-Hill Book Co., Inc., 330 W. 42 St., N. Y. 36, N. Y. $9.50. Introduction to linear electrical circuit analysis on the sophomore-junior level which utilizes a background in calculus but does not require an introduction to advanced mathematics.

Geiger, Darrell L., *Successful Preparation for F. C. C. Radio Operator License Examinations*. Prentice-Hall, Inc., Englewood Cliffs, N. J. $9.25 Answers to many questions on F.C.C. examinations, as well as discussions of these answers.

Hamilton, J. J., *Reflex Klystrons*. The Macmillan Co., 60 Fifth Ave., N. Y. 11, N. Y. $9.00.

High Altitude and Satellite Rockets: A Symposium. The Philosophical Library, Inc., 15 E. 40 St., N. Y. 16, N. Y. $15.00. The Proceedings of the first symposium on high altitude and satellite rockets to be held in Great Britain. Convened jointly by the Royal Aeronautical Society, the British Interplanetary Society, and the College of Aeronautics, July 18–20, 1957. Twelve papers by British and American authors dealing with the problems of design and propulsion, recovery after re-entry, high temperature materials, instrumentation, telemetry, guidance and human flight beyond the atmosphere.

Mason, Warren P., *Physical Acoustics and the Properties of Solids*. D. Van Nostrand Co., Inc., 257 Fourth Ave., N. Y 10, N. Y. $9.00.

Neeteson, P. A., *Junction Transistors in Pulse Circuits*. The Macmillan Co., 60 Fifth Ave., N. Y. 11, N. Y. $6.00. Gives methods which may be used to analyze the fundamental pulse circuits containing transistors and hence to simplify their design.

Nixon, Floyd E., *Handbook of Laplace Transformations*. Prentice-Hall, Inc., Englewood Cliffs, N. J. $6.00. Gives examples of practical physical problems solved by the Laplace transform method, and contains a table of transform pairs available, number-coded for reference.

Pettit, Joseph M., *Electronic Switching, Timing, and Pulse Circuits*. McGraw-Hill Book Co., Inc., 330 W. 42 St., N. Y. 36, N. Y. $7.50. To promote both physical understanding and analytical techniques for dealing with several important classes of electronic circuits.

Seifert, Howard S., Ed., *Space Technology*. John Wiley and Sons, Inc., 440 Fourth Ave., N. Y. 16, N. Y. $22.50.

Watson-Watt, Sir Robert, *The Pulse of Radar* (Autobiography). The Dial Press, Inc., 461 Fourth Ave., N. Y. 16, N. Y. $6.00. Story of the development of radar and the role it played, as the major factor in the winning of the battle of Britain against the Luftwaffe.

Zucker, A., E. C. Halbert, and F. T. Howard, Eds., *Proceedings of the Second Conference on Reactions Between Complex Nuclei*, Gatlinburg, Tenn., May 2–4, 1960. John Wiley and Sons, Inc., 440 Fourth Ave., N. Y. 16, N. Y. $7.00. Contains all forty research papers presented at the conference and transcripts of the discussions which followed them.

Scanning the Transactions

What next? Neuristors! This novel device has been proposed as a universal element for digital systems of the future. The Neuristor acts somewhat like a burning spot on a very special dynamite fuse that repairs itself and is ready for use again a short time after the burn-spot (the signal) passes. There is evidence that such a scheme (without the dynamite, usually) is similar to the way in which pulses are transmitted by neurons through the human nervous system. Logic and dynamic storage are readily possible with the Neuristor. Nobody has ever seen one or tried to build one, but there seems to be little doubt that the Neuristor is physically realizable. (H. D. Crane, "The Neuristor," IRE Trans. on Electronic Computers, September, 1960.)

By using light as a feedback element, an interesting amplitude-limiting device has been developed. The device makes use of the photoconductive properties of cadmium sulfide, a material whose conductivity increases markedly upon exposure to light. The feedback circuit consists of a neon lamp attached to the output of a power amplifier. When the output exceeds a desired voltage, the neon lamp ignites and illuminates a cadmium sulfide photoresistor at the input, causing its resistance—and the amplifier output—to drop rapidly. Thus we have an electronic device in which light controls sound. (J. E. de Miranda, "Photo-sensitive resistor in an overload-preventing arrangement," IRE Trans. on Audio, July–August, 1960.)

Thin Films, but not the Hollywood variety, are currently a most vigorous frontier of computer technology. Beginning about 1954, a surge of research activity in magnetic thin films has catapulted them into a predominant position as the high-speed digital memory element of the future. As memory elements, typically an anisotropic round dot of 80 per cent Ni—20 per cent Fe permalloy with 0.040″ diameter and 1000 A thickness will store one bit. Access time to a stored bit may be of the order of 0.1 to 0.2 μsec. (A working thin-film memory in the TX-2 computer at Lincoln Laboratory of MIT has an access time of 0.8 μsec, and is loafing along at half speed to be compatible.) Memory isn't all! The little film dots may be used effectively as parametric oscillators, and hence as logic amplifiers, and register cells. Uniformity of performance is just now becoming a widely established fact; with the perfection of thin-film technology extensive use of the devices can be predicted (at least until some newer and better device is invented!). Three papers in the September 1960 issue of IRE Transactions on Electronic Computers discusses three aspects of the thin-film story: 1) A. V. Pohm and E. N. Mitchell, "Magnetic film memories, a survey"; 2) R. F. Schauer, *et al.*, "Some applications of magnetic film parametrons as logical devices"; and 3) K. D. Broadbent, "A thin magnetic film shift register."

Is the stereophonic effect dependent on frequency? There has been considerable discussion of this point in the last two years, with the result that a number of different upper and lower frequency limits have been mentioned beyond which the stereo effect is said to become less perceptible. These frequency limits are of substantial practical interest, for their existence could lead to reduced RF bandwidth requirements for stereo broadcasting systems and to more efficient and ecomical designs of tape and phonograph equipment. To shed more light on this question an extensive literature study and listening tests were recently conducted. Although the literature search uncovered 88 references dealing with work dating as far back as 1921, no experimental evidence could be found to indicate that a lack of stereophonic perception existed over any particular frequency range. This was confirmed by tests with actual program material, which showed that the extreme lower frequencies had equal or superior directional content to the higher frequencies. It, therefore, appears that good stereophonic systems require reproduction of the stereophonic effect over the entire audible band. (W. N. Beaubien and H. B.

Moore, "Perception of stereophonic effect as a function of frequency," IRE TRANS. ON AUDIO, September–October, 1960.)

What's in a name? The answer sometimes may depend on whether you are an optimist or a pessimist. For the benefit of those readers of the latter persuasion, we have listed below a few definitions pertaining to the audio field.

Audio Amplifier—A device for adding distortion to an audio signal.

Compliance—The result of weak resistance.

FM—A system for listening to a phonograph played at a remote location.

High Fidelity—What the sales department recently discovered in equipment you had been making all these years.

High-Fi—A phonograph; also see FM

Stereo—A more expensive phonograph for playing more expensive stereo records through more loudspeakers.

Super-Fi—Your system, as compared to the one your friends own.

Ultra-Fi—What your friend thinks of his system, compared to yours.

High Fi Record—Any phonograph record pressed later than the year 1926.

Loudspeaker—A transducer for converting electrical energy into noise energy.

Program Equalizer—Means for modifying a program according to judgment of the music director.

Tone Control—Means for neutralizing the judgment of the music director.

Flat Response—Characteristic of an audio component which tends to flatten the pocketbook.

(Marvin Camras, "The Editor's Corner," IRE TRANS. ON AUDIO, September–October, 1960.)

That tunnel diode circuit, the morning after, must work. Tolerances and such mundane matters must be considered when today's dream elements are translated into work-a-day circuits. Tolerance considerations for the Goto-pair and for other modes of tunnel-diode operation have been investigated and the various modes of tunnel-diode operation have been compared in a most timely paper that also presents a new tunnel-diode flip-flop configuration. (W. F. Chow, "Tunnel diode digital circuitry," IRE TRANS. ON ELECTRONIC COMPUTERS, September, 1960.)

Abstracts of IRE Transactions

The following issues of TRANSACTIONS have recently been published, and are now available from the Institute of Radio Engineers, Inc., 1 East 79th Street, New York 21, N. Y. at the following prices. The contents of each issue and, where available, abstracts of technical papers are given below.

Publication	Group Members	IRE Members	Libraries and Colleges	Non Members
Vol. AU-8, No. 4	$ .80	$1.20	$1.20	$2.40
Vol. AU-8, No. 5	2.25	2.25	3.25	4.50
Vol. AC-5, No. 3	1.75	2.60	2.60	5.25
Vol. E-3, No. 4	2.25	2.25	3.25	4.50
Vol. EC-9, No. 3	1.55	2.30	2.30	4.65
Vol. IE-7, No. 2	1.40	2.10	2.10	4.20
Vol. MTT-8, No. 5	2.25	2.25	3.25	4.50
Vol. RQC-9, No. 2	1.15	1.70	1.70	3.45

Audio

VOL. AU-8, NO. 4, JULY–AUGUST, 1960

A Message from the Chairman—Hugh S. Knowles (p. t05)

The Editor's Corner—Marvin Camras (p. t06)

The New WLM AGC Amplifier—R. J. Rockwell (p. t07)

Since the inception of radiobroadcasting, the control of audio level has been a constant problem. This paper discusses some of the shortcomings of presently-used circuitry in limiting and automatic gain control amplifiers and describes a new approach to the problem of level control, which provides both slow gain increase and decrease along with fast limiting action while maintaining wide frequency response and extremely low distortion under all operating conditions.

The Distortion Resulting from the Use of Center-Tapped Transformers in a Class B Power Amplifier—R. G. De Buda (p. t12)

The transformer-coupled Class B amplifier is investigated with regard to harmonic distortion caused indirectly by the self-resonance of the transformer primary. For undistorted Class B operation, the short-circuited flow of even harmonic unbalanced mode currents is essential. When these harmonics are at a frequency at which the transformer primary is close to self-resonance, the flow is impeded and harmonic plate voltages will appear. A slight circuit asymmetry or nonlinearity will permit the harmonic voltages to couple into the load, as harmonic distortion. By a similar effect negative feedback circuits can increase distortion by an amount for which formulas are given.

A Speaker System with Bass Back-Loading of Unusual Parameter Values—Paul W. Klipsch (p. 118)

Work with corner horn speakers has led to a philosophy that there is a narrow range of optimum size limited by performance on the one hand and cohesion of bass and treble events on the other. In the design of a new speaker system of size smaller than these limits, the horn principle was abandoned for the bass section but continued to be used for the midrange-tweeter functions in the interest of lowest distortion. The bass section is of the enclosure type with a tubular back exhaust, corresponding in principle to the Bass Reflex but differing in the high inertance of the port. Adjusted empirically, the response of the new speaker resembles that of a three-way corner-horn reference system. The new speaker may be used against a wall, but as in all speakers affords best performance in a corner. It may be used for any of the two or three positions of a stereo array, including the bridged or derived center output.

A Plotter of Intermodulation Distortion—E. F. Feldman and B. Ranky (p. 122)

For use mainly in audio systems, the instrument plots on a CRT screen or chart recorder the amplitude of the difference-frequency tone vs the lower excitation frequency in CCIF intermodulation distortion measurements. The unit furnishes two swept equal-amplitude tones with a selected audio difference frequency to excite the tested system. Readout is on a modified audio-frequency spectrum analyzer which remains tuned to the difference frequency. The automatic excursion provides considerable test time economy in quality measurements of such devices as loud-speakers which exhibit wide variation in intermodulation with excitation frequency. Point-by-point techniques, in addition to being tedious, run the risk of missing critical conditions.

With slight modification, the unit is also capable of plotting the lower third-order distortion component as $(2f_1-f_2)$ vs excitation frequency.

A swept spectrum analyzer and means for single-line plots of frequency response curves are also integral components of the equipment. Switching facilities permit alternate displays on successive scans of any two of the modes of operation. Four example, acoustic output and IM distortion vs frequency of loud-speakers may be plotted alternately for rapid comparisons.

Calculation of the Gain-Frequency Characteristics of an Audio Amplifier Using a Digital Computer—Donald E. Brinkerhoff (p. 130)

Electronic circuit designs are most commonly made by "analog" (or "breadboard") methods. This is particularly true in arriving at the desired gain-frequency response characteristics. The mathematical approach to circuit analysis has suffered from the distinct disadvantage of involving the solution of large systems of simultaneous equations with complex, frequency-dependent coefficients often requiring days to solve by hand calculations.

The ability of digital computers to solve large systems of simultaneous equations at high speed and without mistakes allows the audio engineer to solve many problems faster by using classical methods than by use of the breadboard technique.

Photo-Sensitive Resistor in an Overload-Preventing Arrangement—J. Rodrigues De Miranda (p. 135)

The signal from a pre-amplifier or tuner is supplied to the input terminals of the power amplifier by means of a voltage-dividing network, the element in parallel to these input terminals being a photo-sensitive resitor of new design. Facing this photoresistor in a lightproof enclosure is a neon lamp connected to the output voltage of the amplifier. Because a neon lamp ignites at a fixed voltage, the value of the photo-resistor resistance will be decreased as soon as this voltage is reached. Consequently, the input signal to the amplifier will be decreased as well, making overload substantially impossible.

Audio

Vol. AU-8, No. 5, September–October, 1960

Perception of Stereophonic Effect as a Function of Frequency—W. H. Beaubien and H. B. Moore (p. 142)

A literature study and listening tests have been conducted to contribute to an understanding of the stereophonic effect as a function of frequency. The literature study failed to reveal tests showing loss of stereophonic direction for any part of the audio spectrum and pointed to arrival time difference of the transient portion of sound waves as the significant contributor to stereophonic perception.

Tests employing actual program material with a specially developed Stereo Spectrum Selector showed the extreme lower frequencies to have equal or superior directional content to the higher frequencies. The perception loss at any frequency may be of a quantitative nature rather than strictly related to certain wavelengths. Test results and consideration for future developments suggest adoption of full frequency stereophonic systems.

Listener Rating of Stereophonic Systems—Harwood B. Moore (p. 151)

Subjective listening tests have been completed which indicate that stereo in any of the forms compared is preferred over monaural, but normal stereo from two full range speakers well physically separated is, in all probability, the most preferred.

A 1 7/8-IPS Magnetic Recording System for Stereophonic Music—P. C. Goldmark, C. D. Mee, J. D. Goodell, and W. P. Guckenburg (p. 159)

The primary aim of this work has been to develop a stereophonic system for recorded music, using a small, inexpensive and practical cartridge with magnetic tape as the information carrier. In order to make the cost of the recorded cartridge comparable with a disk containing an equivalent amount of music, it was realized that basic developments in magnetic recording such as efficiency of recording and reproducing techniques were necessary to meet the packing density requirements.

This paper describes developments which have led to a recorded cartridge one fifth of the volume of a disk and capable of playing more than one hour of stereophonic sound uninterrupted. In order to obtain the desired signal-to-noise ratio and frequency response to 15 kc, radical improvements have been made to tape, recording system and playback head.

In conjunction with this work, a fully automated tape machine has been developed. The machine is equipped with a changer-type mechanism and accommodates a number of cartridges which are played and rewound completely automatically, one after another, furnishing music for several hours. The machine requires no manual threading and has a rewind cycle of less than twenty seconds for an hour-long tape.

Signal Mutuality in Stereo Systems—Paul W. Klipsch (p. 166)

Four stereo systems are compared:

1) 3 microphones, 3 independent transmission means or "tracks," and 3 speaker output or "channels," designated 3-3-3.
2) 3 microphones, 2 sound tracks and 3 outputs using a bridging or "derived" center channel, designated 3-2-3.
3) 2 microphones, 2 tracks, 3 outputs with derived center, designated 2-2-3.
4) A stereo microphone pair in a single housing with stereo separation derived by directional response of the 2 microphones, using 2 sound tracks and 3 play back speakers with derived center, designated SD-2-3 (SD for "stereo-directional" applied to the microphone).

Each of the 4 systems is shown to contain mixtures of all signals in each channel.

Crosstalk may be defined as the inadvertent transfer of a signal from one channel to another. Signal mutuality is the natural consequence of one microphone in a stereo array detecting signals pertinent to other microphones.

The magnitude of differences between the 4 types of stereo studied is found to be small—of the order of less than 4 decibels.

Delay effects are similar in the first 3 types, but where a single microphone location is used and dependence is on directional pattern for stereo separation, the delay effects are different. A separate study of the combined effects of sound delay and quality was made to corrobrate the suspected delay effects of the so-called "stereo microphone."

Stereophonic Localization: An Analysis of Listener Reactions to Current Techniques—John M. Eargle (p. 172)

Playback localization plots, similar to the technique employed by Steinberg and Snow in the Bell Laboratory experiments of 1933, afford perhaps the only means of evaluating quantitatively the performance of representative stereophonic systems. In the present tests, which deal with two-channel systems comprising a center bridged loudspeaker in addition to the two flanking loudspeakers, it is seen that the performance of wide-angle loudspeaker arrays can be optimized to give accurate localization over a large listening area. As an aid to the evaluation of test data, brief discussions of loudness and time-delay effects—the essential factors providing localization—are included.

Compatible Cartridges for Magnetic Tapes—Marvin Camras (p. 176)

Magnetic tape may be offered in cartridge form at a price competitive with phonograph disks. Cartridges of different sizes are designed either for high quality or for maximum tape economy. All of these will operate on present-day machines, as well as on automatic designs. A cartridge changer allows records to be played in sequence. The erase feature offers interesting possibilities for sale of pure music separate from the sale of cartridges.

Automatic Control

Vol. AC-5, No. 3, September, 1960

Stability of Systems with Randomly Time-Varying Parameters—A. R. Bergen (p. 159)

The stability of a system which alternates between stable and unstable configurations at random times may be investigated conveniently using Kronecker products. The system is stable with probability one if, and only if, all the eigenvalues of a specified matrix lie within the unit circle. If stability in the presence of a parameter adjustment is to be investigated, a root-locus plot of the eigen-values is convenient.

Dynamic Programming Approach to a Final-Value Control System with a Random Variable Having an Unknown Distribution Function—Masanao Aoki (p. 164)

As described in the introduction of this paper, the state vector x_n, representing the present state of a sampling control system, is assumed to satisfy a difference equation

$$x_{n+1} = T(x_n, r_n, v_n),$$

where v_n is the control vector of the system subject to random disturbances r_n. The random variables r_n are assumed to be independent of each other and to be defined in a parameter space in the following manner: Nature is assumed to be in one of a finite number, q, of possible states and each state has its own parameter value, thus specifying uniquely and unequivocally the distribution function of r_n. It is further assumed that we are given the *a priori* probability $z=(z_1, \cdots, z_q)$ of each possible state of nature,

$$i = 1, 2, \cdots, q, \quad \sum_{i=1}^{q} z_i = 1, \qquad z_i \geq 0.$$

Given a criterion of performance, the duration of the process and the domain of the control variable, a sequence of control variables, $\{v_n\}$ is to be determined as a function of the state vector of the system and time, so as to optimize the performance.

The sequential nature of the determination of v_n is evident here, since the stochastic nature of the problem prevents specification of such a sequence of v's as a function of the initial state and time. By means of the functional equation technique of dynamic programming, a recurrence relation of the criterion function of the process, $k_n(x, z)$, is derived, where x is the state variable of the system when there remain n control stages.

When q is taken to be two and the criterion of performance to be $x_N{}^2$ with the constraint on the control variables

$$\sum_{i=0}^{N-1} v_i{}^2 \geq K,$$

where x_N is the final state vector of the system, is is shown that $k_n(x, z)$ is the form $w_n(z)x^2$ and the optimal $v_n(x, z)$ is linear in x, as might be expected. The dependence of $k_n(x, z)$ and $v_n(x, z)$ on z is investigated further, and $w_n(z)$ is found to be concave in z. Explicit quadratic forms for $w_n(z)$ are obtained in the neighborhood of $z=0$ and 1. The optimal $v_n(x, z)$ is found to be monotonically decreasing in z.

When the domain of v_n is restricted to a finite set of values, as in contactor servo systems, no explicit expressions for $k_n(x, z)$ and $v_n(x, z)$ are available. However, $k_n(x, z)$ is still concave in z and approximately given by

$$zk_n(x, 1) + (1 - z)k_n(x, 0).$$

By solving the recurrence relation numerically, this approximation is found to be very good for moderately large n, say 10. This means that if one has explicit solutions for $p = p_1$ and $p = p_2$, then one can approximate the criterion function for the adaptive case where $Pr(p = p_1) = z$ by a linear function in z as shown above.

This provides fairly good lower bound on $k_n(x, z)$, and in turn serves to determine an initial approximate policy.

A concept of suboptimal policy is introduced and numerial experiments are performed to test suboptimal policy suggested from numerical solution. The system behavior under the suboptimal policy is also discussed.

Mathematical Aspects of the Synthesis of Linear Minimum Response-Time Controllers—E. Bruce Lee (p. 177)

A procedure is presented for finding, in a systematic matter, the forcing function to be applied to a process to give time-optimal control. The results are limited to the case where the process to be controlled has dynamics which are completely known and are adequately described by a system of linear differential equations. It has also been assumed that the process is not subject to unknown disturbances.

The implication of the method presented is that any process as limited above can be time-optimally controlled, in those cases where a time-optimal controller exists, provided an underlying system of transcendental equations can be solved. This system of transcendental equations can be quite easily solved for systems of order less than three, even with two forcing functions, and for various other special cases of higher order. The results of a study which indicate that the method can be applied in quite general situations are being presented elsewhere.

Statistical Design of Digital Control Systems—Julius T. Tou (p. 184)

This paper is concerned with the problem of statistical design of digital control systems. A simplified design procedure is introduced. The minimum mean-square error is adopted as the performance criterion; and the system design is based upon the Wiener-Kolmogoroff theory of optimum filtering and prediction. The treatment of this optimization problem makes use of the modified z-transform technique, and is presented in close parallel with the procedure for the statistical design of linear continuous-data control systems. By making use of some important properties of the auto-correlation sequence, the cross-correlation sequence, the pulse spectral density and the pulse cross-spectral density, the statistical design of digital control systems can be carried out in a simple and systematic manner.

Determination of Periodic Modes in Relay Servomechanisms Employing Sampled Data—H. C. Torng and W. E. Meserve (p. 192)

A difference equation approach is presented to determine the periodic modes in relay servomechanisms employing sampled data. In using the method, together with Izawa and Weaver's method, the investigator can have all the information concerning possible periodic modes of a system.

This new technique is based on expressing periodic sequences in terms of orthogonal functions in the discrete sense and balancing the harmonics.

Analysis of Pulse Duration Sampled-Data Systems with Linear Elements—R. E. Andeen (p. 200)

This paper deals with the application of z-transform techniques to the analysis of sampled-data systems in which signals appear in *pulse duration* modulated form. The characteristics of pulse duration sampled data are first briefly described. An analytical means for studying the transient response and stability of systems which use this kind of data is then presented. Finally, a comparison is shown of analytical results with tests on several representative experimental systems. A short discussion of the relative advantages and disadvantages of pulse duration modulation in control systems is also included.

The Analysis of Cross-Coupling Effects on the Stability of Two-Dimensional, Orthogonal, Feedback Control Systems—David Bruce Newman (p. 208)

The analysis of two-dimensional cross-coupled feedback control systems is studied because many such systems are in existence, and methods for their analysis and criteria for measuring their performance have had only limited attention in the technical literature. Previous literature has generally been in the area of matrix analysis of multidimensional or multiloop systems, and has not treated the handling of poles and zeroes in the complex s-plane or cross-coupling, as they are treated in this paper.

An algebraic model is developed for a generalized system, using the assumption that all components of the system, including the cross-coupling transfer function, may be represented by expressions in the complex frequency domain which have real-time domain equivalents describable by linear differential equations.

The stability of the two-dimensional, cross-coupled, feedback control system is studied by complex-plane methods, and a method is developed for determining whether a system is stable or not. A technique is also indicated to show how an unstable system may be made stable by the introduction of appropriate cross-coupling.

Stabilization of Linear Multivariable Feedback Control Systems—E. V. Bohn (p. 215)

Stabilization techniques for single variable feedback control systems are well known. For multivariable feedback control systems, comparable methods are still in the initial stage of development. A method of system stabilization is discussed, which reduces the problem to essentially that of a single variable system. This method uses a compensating matrix which is either the inverse system- or transposed system-matrix. An example of this method of system stabilization is given and its usefulness discussed.

Education

Vol. E-3, No. 4, December, 1960

Characteristics of Electrons in Solids—John N. Shive (p. 106)

The origin of the familiar valence band-forbidden gap-conduction band features of the electronic energy level scheme of a crystalline solid is developed according to 1) the extension of the atomic energy level scheme for individual atoms, 2) examination of the quantized momentum spectrum of a valence electron gas in a periodic potential enclosure, and 3) analogy with the pass-band and stop-band features in the frequency characteristic of a periodically-loaded mechanical transmission line. Since the first two approaches are amply treated in the conventional literature, this paper dwells particularly on the third approach which may be preferred over the other two by readers having more extensive backgrounds in mechanical or electrical engineering than in theoretical physics. A simple mechanical wave transmission apparatus is described, with which the frequency characteristic can be observed and plotted. This characteristic is then related to the energy band picture of a solid by recognizing that a crystal can be regarded as a "loaded" transmission line for electron waves.

Semiconductors—Roy H. Mattson (p. 111)

The principal aim of this paper is to present the concepts associated with the electrical properties of semiconductors. Simplified ways of envisioning holes, electrons, and diode and transistor action are presented. Intrinsic or pure semiconductor material is discussed first, followed by discussions of n- and p-type material, p-n junction diodes, photodiodes, and transistors. This paper is aimed at educators who are not directly involved with semiconductor devices.

Physical Electrons Underlying Junction Transistor Characteristics—William G. Dow (p. 116)

In most transistors which are useful to engineering, densities of electrons and holes are low enough so that random energies have the classical Maxwell-Boltzmann distribution. Also, the customary large ratios of majority-to-minority carrier densities result in majority-carrier flow occurring in response to electric gradients, and minority-carrier flow by diffusion due to concentration gradients. Steps using these principles to derive junction transistor volt-ampere characteristic equations are: 1) interface contact potential determination, 2) expression of emitter and collector currents in terms of random-motion interface penetration, 3) boundary-value solution of the diffusion-flow differential equation, to give minority-carrier density distributions, 4) expression of currents in terms of at-interface density distribution gradients, 5) elimination of at-interface minority-carrier densities between 2) and 4), giving the Ebers and Moll volt-ampere equations.

These equations show how base thickness, diffusion lengths, and relative majority carrier densities in emitter, base, and collector affect the characteristics. The residual collector current is found to be a measure of electron-hole pair generation. The relation of this current to surface energy states, and to the associated double layer of charge at and near the surface, is discussed.

Diodes—Marlin O. Thurston (p. 128)

Semiconductor diodes have achieved great prominence in the electronic industry because of their outstanding performance and great versatility. They are consequently of increasing importance in the education of electrical engineers. Since new diodes are being continually developed, it is essential that the edu-

cational emphasis be placed on underlying principles rather than on the devices themselves. In this paper a brief descriptive outline is presented of some of the p-n junction phenomena that are important in understanding diode performance. Among these phenomena are nonlinear resistance, conductivity modulation, avalanche breakdown, carrier storage, junction capacitance, and carrier tunneling. As illustrations of these effects, the characteristics of several types of diodes are discussed.

Solid-State Energy Conversion Devices—Stephen J. Angello (p. 134)

Conversions of energy in general are considered first, with emphasis on schemes appropriate for energy conversion devices. For the purposes of this paper, the vast numbers of conversion possibilities are restricted to solid-state devices. The direct coupling between heat and electricity is singled out for more detailed discussion of a useful figure of merit. The present state of the thermoelectric generator art is reviewed briefly, with some predictions of future developments.

Low-Temperature Devices—Alan L. McWhorter (p. 137)

The basic operating principles of three low-temperature devices—the maser, the cryotron, and the cryosar—are discussed. In masers the process of stimulated emission of radiation is used to produce an extremely low noise amplifier, with all practical solid state masers thus far employing the electron spins in paramagnetic salts. The cryotron and the cryosar are both primarily intended for computer applications. The former utilizes the phenomenon of superconductivity and its quenching in magnetic fields; the latter uses impact ionization of impurities in semiconductors.

Integrated Circuits and Microminiaturization—John L. Moll (p. 141)

The meanings of the words microcircuits, molecular electronics, integrated circuits, and functional devices are examined with the conclusions that, as generally used, the only sensible definitions are as follows: a microcircuit is one in which connections are made between circuit elements on a microscopic scale. Molecular electronics, integrated circuits, and functional devices all have essentially the same meaning, which is that connections are made between circuit elements inside a single block of material without bringing leads out.

The next order of miniaturization that is required for space vehicles and large-scale computers will use a microelectronic or molecular electronic technology in combination with conventional miniature techniques. The feasibility of very large components of systems being made by a molecular or microelectronic technique depends on the combination of many orders of magnitude reduction in manufacturing shrinkage combined with the design of circuits to tolerate unreliable or defective elements.

Electronic Computers

VOL. EC-9, NO. 3, SEPTEMBER, 1960

Tunnel Diode Digital Circuitry—W. F. Chow (p. 295)

This paper is divided into two parts. In the first part, the basic tunnel diode logic circuits are discussed. These include the monostable and the bistable analog-threshold gates and the "Goto-pair," which uses the principle of majority decision. These circuits are studied to determine the requirement on tunnel diodes and other component tolerances. Relations between the "fan-in" and the "fan-out" numbers and the component tolerances are derived. The results indicate that the "Goto-pair" is somewhat superior to the analog-threshold gates with respect to circuit reliability.

In the second part, a tunnel diode flip-flop stage which has advantages with respect to speed, ease, of operation and component tolerances is described. Combination of these flip-flops in counter and shift-register configurations have been successfully operated. Several potential advantages over conventional transistor circuits are discussed.

Transistor Current Switching and Routing Techniques—D. B. Jarvis, L. P. Morgan, and J. A. Weaver (p. 302)

A system of circuit logic is described in which transistors, particularly diffused base transistors, are operated well out of saturation in order to make the most of their speed. Logical information is contained in the presence or absence of a current which can be switched or routed by the gates described. Also described is the application of this system of logic to certain specific computer problems, namely, a parallel adder with a carry propagation time of 40 mμsec over 6 stages, a shifting register capable of operating at 10 mc and a binary decoder with a maximum delay of 40 mμsec.

Magnetic Film Memories, A Survey—A. V. Pohm and E. N. Mitchell (p. 308)

An analysis is made of the modes of magnetization reversal and rotation in thin ferromagnetic films. The ways in which the various modes can be employed for destructive and nondestructive memories are discussed and their performance limitations considered. Existing film memory efforts are partially surveyed and the material and system problems are examined. Possible future developments are also discussed.

Some Applications of Magnetic Film Parametrons as Logical Devices—R. F. Schauer, R. M. Stewart, Jr., A. V. Pohm, and A. A. Read (p. 315)

High-frequency magnetic film parametrons have been made and observed to exhibit two- or three-state operation for a single bias condition. As a two-stable-state device, the magnetic film parametron can be used as a majority decision element in much the same way as the ferrite core parametron. Another useful logical two-state device is a threshold element, in which the input excitation must reach a minimum level to sustain oscillations. The magnetic film inductor, when suitably clocked, can be used as a gate to permit unilateral flow of information in a system. The gating action, controlled by the bias field, can result from the rectified output of a parametron. Proposed logical designs for a two-element binary adder, a binary shift counter, and a shift register are presented. The possibilities of three-state operation are also explored in the logical design of a seven-element ternary full adder.

A Thin Magnetic Film Shift Register—Kent D. Broadbent (p. 321)

An initial application of the dynamics and and interactions of domains within continuous magnetic thin film structures is made to a shift register in which binary information is stored and translated in and along a continuous evaporated thin magnetic film. These thin magnetic film shift registers are capable of storing information having a density of several hundred bits per square inch of vacuum evaporated structure and of translating this amount of information at bit rates in excess of a megacycle with powers of less than 10 watts.

Fluxlox—A Nondestructive, Random-Access Electrically Alterable, High-Speed Memory Technique Using Standard Ferrite Memory Cores—Robert M. Tillman (p. 323)

The Fluxlok memory technique uses the principle of cross-field magnetization to achieve the nondestructive sensing of the information state of standard, readily available, ferrite memory cores in a simply wired memory plane. Bipolar output (ONE and ZERO) signals are obtained at the rate of rise of the READ pulse. The signals are unaffected by test temperatures of from $-65°C$ to $+100°C$. Coincident current WRITE operation or an inherent orthogonal field WRITE may be used. A 2-mc 64-word Fluxlok memory test vehicle is described.

Magnetostrictive Ultrasonic Delay Lines for a PCM Communication System—D. A. Aaronson and D. B. James (p. 329)

A servo-operated delay-line pad and a temperature-compensated delay-line memory, both magnetostrictively driven at 1.5 mc, have been used in an experimental PCM communication system.

The delay-line pad automatically compensates for external delay changes as small as plus or minus 8 mμsec at a rate of 75 mμsec/second. The delay-line memory stores 192 bits which are available serially with an access time of 125 μsec. Both applications use the same basic delay lines which consist of a length of 0.003-inch diameter supermendur wire, two tiny solenoids, and a supporting structure.

Error Detecting and Correcting Binary Codes for Arithmetic Operations—David T. Brown (p. 333)

The most important property of the codes derived in this paper is that two numbers, i and j, have coded forms, $C(i)$ and $C(j)$ that when added in a conventional binary adder, give a sum $C(i)+C(j)$ that differs from $C(i+j)$, the code for the sum, by (at most) an additive constant. This makes possible the detection and/or correction of errors committed by the arithmetic element of a computer. In addition, messages can be coded and decoded and errors can be detected and corrected by arithmetic procedures, making it possible to eliminate some or all of the special-purpose equipment usually associated with error-detecting or correcting codes. This property may make these codes useful for data transmission as well as for computation.

A Theorem for Deriving Majority-Logic Networks Within an Augmented Boolean Algebra—R. Lindaman (p. 338)

Recent developments in computer technology have produced devices (parametrons, Esaki diodes) that act logically as binary majority-decision elements. Conventional design techniques fail to utilize fully the logical properties of these devices. The resulting designs are extravagant with respect to the number of components used and the operating time required. This paper reviews the conventional technique briefly and proposes an alternative method that produces more nearly minimal designs.

The Use of Parenthesis-Free Notation for the Automatic Design of Switching Circuits—E. L. Lawler and G. A. Salton (p. 342)

A parenthesis-free notation is introduced for the representation of series-parallel switching networks. The notation facilitates the calculation of circuit parameters and permits an unambiguous characterization of the circuit topology.

Given certain criteria for feasibility of a switching network related to the circuit parameter values, it is shown how an infeasible series-parallel network can be transformed into an equivalent feasible network by "cascading" operations applied to the two-terminal subnetworks of the original network. A systematic method is developed, resulting in an optimum choice of cascading operations such that the number of switching elements required to implement the transformed circuit is minimized relative to cascading.

DC Amplifier Misalignment in Computing Systems—R. L. Konigsberg (p. 352)

The equivalent input circuit representation for dc misalignment (offset) has appeared in the literature for the special case of a vacuum tube voltage amplifier with infinite input impedance.

This paper will generalize the concept of the equivalent input circuit representation for dc offset for the four amplifier types with finite input impedances, and will give the conditions under which the use of each equivalent circuit is justified. In each case, two offset generators which are characteristic of the amplifier alone —independent of driving source impedance and load impedance termination—are defined. Because of this independence, the offset generators are referred to herein as "characteristic misalignment generators." When the amplifier is connected into a system, a knowledge of these generators permits calculation of the effect of amplifier offset on system performance.

Treated in some detail is the finite input impedance voltage amplifier case. It is shown how the characteristic generators are evaluated in general for this case, and how these generators may be used in determining the effects of amplifier offset in computing systems employing dc operational amplifiers. In addition, the characteristic generators are derived for a transistorized dc-voltage-type amplifier containing a grounded emitter input stage.

By analogy it is seen that "characteristic noise generators," similar to the characteristic misalignment generators, may completely represent the internal noise of an amplifier.

A Feedback Method for Obtaining a Synchro Output Signal Proportional to Input Angle θ for Large θ—M. B. Broughton (p. 359)

If the ac signal at the "cosine" terminal of a sine-cosine resolver (or synchro transmitter connected to a transformer so as to perform the function of a sine-cosine resolver) is fed back to the rotor through an amplifier of suitable gain, the signal at the "sine" terminal can be made proportional to rotor rotation for angles up to 90° or greater. A theoretical analysis of the relationship

$$\theta \doteq \frac{\sin \theta}{a + b \cos \theta}$$

is given, along with a method for deriving its analog. The theoretical development is supported by experiment.

A Solution to the Euler Angle Transformation Equations—Gilbert R. Grado (p. 362)

As simulation studies grow more elaborate and complex, the computer operator is confronted with an ever increasing number of problems not directly associated with the study at hand. This paper describes a specially designed computer for solving the coordinate transformation equations normally encountered in a six degree of freedom simulation study. This computer expands the capabilities of present analog computer consoles and eliminates the tedious task of patching the solution to these equations, while eliminating a source of human error. Besides incorporating several unique features for changing sequences and scales, this machine has accuracies and responses compatible with those found in linear equipment.

Industrial Electronics

Vol. IE-7, No. 2, July, 1960

A New Digital Computer System for Commercial Data Processing—J. A. Brustman (p. 2)

A computer system, the RCA 501, has been designed to meet the needs of commercial data processing. The equipment utilizes transistors as active elements, ferrite cores for high-speed memory, magnetic tape as primary bulk and working store, and built-in and programmable accuracy control. Input-output equipment includes paper tape (in), card (in and out), and line printer (out).

The language of the computer system exploits variable-word and variable-message-length for efficiency. The instruction complement is designed to facilitate the programming of data-processing tasks, taking advantage of the variable word and message and of built-in simultaneous operation provisions.

The system is adaptable in size to small and large applications.

The Operational Information System and Automation of Sterlington Steam Electric Station—Joseph A. Reine, Jr. (p. 14)

The system for scanning and logging operational data at Sterlington Electric Station is described. This advanced system includes the sensors, scanning equipment, analog-to-digital converters, data storage, computer, and various output presentations. Operating experience and problems associated with incorporation of the system into normal plant operation are described.

Production-Line Testing Programmed by Punched Cards—Richard E. Wendt, Jr. (p. 20)

Automatic equipment for production-line testing of power capacitors provides advantages in speed and accuracy over previous manual testing. The equipment described provides means for automatic part handling, test selection, data collection and interpretation, and test results recording.

The Universal Elements of Multipurpose Automatic Test Systems—Ibrahim H. Rubaii (p. 24)

To assure the continuing satisfactory operation of a complex bombing-navigation and missile guidance system, extensive efforts must be extended in the testing process, which depends heavily upon the test system. In this paper, the testing process and test systems are treated in analytical fashion. The test system is divided into basic functional elements that are universal to all test systems. These functional elements, or subsystems, are then integrated into a theoretical automatic multipurpose test system; boundary conditions imposed on this general system would lead to any special-purpose test system.

The theoretical model created is useful:

1) in designing any test system where boundary conditions are imposed;
2) in evaluating and standardizing existing and proposed test systems for a specific application; and
3) in extending available techniques of analysis in the fields of communication, computing, and control systems to the important, integrated system testing and test systems.

A New High-Power Electron Accelerator—M. R. Cleland and K. H. Morganstern (p. 36)

An electron accelerator for industrial use has been developed which provides improved efficiency and reduced cost of operation. The design incorporates a unique dc accelerating voltage supply consisting of cascaded rectifiers driven in parallel from an RF oscillator. Data are given for equipment rated up to 3 mev, 30 kw.

Microwave Theory and Techniques

Vol. MTT-8, No. 5, September, 1960

Noise Studies on Two-Cavity CW Klystrons—George A. Espersen (p. 474)

The noise properties of a two-cavity CW 3-cm klystron oscillator are discussed with the purpose of studying the noise contribution located close to the center frequency in the audiofrequency range. A system permitting measurements to be made of the mean square frequency deviation is described. Comparisons are made indicating the noise performance of the klystron oscillator when operated under air-cooled and water-cooled conditions.

Optimum Quarter-Wave Transformers—Leo Young (p. 478)

The design of uniformly dispersive quarter-wave transformers is a well explored subject. Common examples are rectangular waveguide E-plane transformers, in which the a dimension is kept constant.

In this paper, it is shown that the performance of conventional quarter-wave transformers of a single section can always be improved by making the middle section less dispersive than the input and output waveguides, and a formula for the optimum a dimension is given.

The theory was verified experimentally. In this instance, the improved transformer measured 50 per cent more bandwidth than did the conventional one, and was 25 per cent shorter besides.

The Quarter-Wave Transformer Prototype Circuit—Leo Young (p. 483)

A quarter-wave transformer not only changes impedance levels, but will also behave as a band-pass filter. In practice, however, band-pass filters are usually required to terminate in equal input and output impedances. They often consist of several direct-coupled cavities, which are similar to transformers whose impedance steps have been replaced by reactive obstacles.

It is demonstrated how one can synthesize a quarter-wave transformer, and then "distort" it to obtain a direct coupled cavity filter with a predictable performance. This is illustrated and confirmed by numerical examples.

The method is particularly convenient to use in reverse. The quarter-wave transformer prototype is easily derived for a direct-coupled cavity filter which has already been designed by another approximate method, and thus gives an independent evaluation of its performance. If necessary, the filter can then be redesigned, as illustrated in this paper.

Broad-Band Ridge Waveguide Ferrite Devices—E. S. Grimes, Jr., D. D. Bartholomew, D. C. Scott, and S. C. Sloan (p. 489)

The design and development of a medium CW power level, 1.57:1 bandwidth, quadruply-ridged circular waveguide Faraday rotator and two high CW power, 2:1 bandwidth, double ridge rectangular waveguide isolators are discussed.

The rotator is designed in quadruply-ridged circular waveguide with a ferrite configuration somewhat different from that proposed by other investigators. It can be made to exhibit broadband rotation and large rotation per unit length of ferrite section, and may be used in most medium CW power level applications. Forty-five degree rotation is achieved over the 7.0-kMc to 11.0-kMc band.

The isolators operate from 2.0 kMc to 4.0 kMc in DR-37 waveguide and from 3.8 kMc to 7.6 kMc in D-34 waveguide respectively. The reverse to forward wave attenuation ratio exceeds 10.0 db to 1.0 db for both isolators.

Radiation Patterns of a Noise-Excited Thin Slot—Nicholas George (p. 493)

Theoretical and experimental radiation patterns are given in spectral form for the thermal radiation from a cylindrical discharge column which is adjacent to a long thin slot in a metallic plane. A spatial distribution is predicted which exhibits interference minima and maxima when the length of the slot and the wavelength of the emission are the same order of magnitude. The analysis is based on Maxwell's equations and the Leontovich-Rytov

distributed source generalization of Nyquist's noise formula.

Fraunhofer pattern measurements are presented in which an argon source is used to excite slots of 7.3π and 9.5π radians in length. Data are also presented to show the effects of variations in the pressure and the dc current of the discharge. The pattern measuring apparatus is a Dicke radiometer, having the following characteristics: frequency 9200 Mc, bandwidth to the detector 16 Mc, modulation frequency 1000 cps, and residual noise level 0.3 rms°K.

An interference phenomenon is predicted by the theory and demonstrated by an experiment, even though the source excitation is spatially distributed and essentially uncorrelated in time and in space. The patterns are not even approximately Lambertian, *e.g.*, a thin slot of 9.5π radians exhibits a pattern having nine relative maxima in 180°, with the maximum emission at 63° from the normal.

Variational Principles and Mode Coupling Periodic Structures—T. J. Goblick, Jr. and R. M. Bevensee (p. 500)

Variational techniques are used in analyzing periodic "cold" microwave structures for the angular frequency, ω, as a function of assumed phase shift per periodic cell. Two variational expressions are given: one for ω in terms of the E- and H-fields, and one for $k^2=\omega^2\mu\epsilon$ in terms of the E-field. For structures with relatively light coupling between cells, the trial fields to be used with the variational expressions are composed of closed cavity modes, phase shifted by ϕ radians from cell to cell. Both variational expressions yield determinantal equations for $k^2(\phi)$ which agree with equations previously derived from a mode coupling point of view. One form of an equivalent lumped circuit is given to represent the structure within one of its pass bands.

Curves compare the variational-mode coupling expression for $k^2(\phi)$ of a periodically lumped loaded transmission line with exact expressions.

Determination of the Capacitance, Inductance, and Characteristic Impedance of Rectangular Lines—Tsung-Shan Chen (p. 510)

This paper determines the capacitance, inductance, and characteristic impedance of rectangular lines by the method of conformal transformation. In practical applications, such lines may be used as transmission links of RF energy as impedance-transforming sections, or as components in electron tubes.

Formulas are given for the calculation of the parameters of rectangular lines having the following characteristics: 1) The inner conductor may have varying thickness compared with the depth of the outer conductor. 2) The axes of the conductors may coincide or may be displaced with respect to each other. 3) the edges of the inner conductor may be rounded to lessen the electrical stress occurring at sharp corners.

Excellent agreement has been obtained between the calculated results and those found by use of the relaxation method, by direct measurement of models, and by electrolytic tank measurement.

The Analysis of a Broad-Band Circular Polarizer Including Interface Reflections—S. Adachi and E. M. Kennaugh (p. 520)

Transmission characteristics of a broad-band circular polarizer consisting of anisotropic dielectric plates are rigorously analyzed. The transmitted wave is formulated in terms of the incident wave including interface reflections. The influence of the interface reflections on the axial ratio of the polarization is numerically shown vs frequency. Frequency dependence of the power transmission ratio is also obtained. From the above analysis, it can be concluded that a circular polarizer of this type is promising as a new broad-band circular polarizer.

Large Signal Analysis of a Parametric Harmonic Generator—K. M. Johnson (p. 525)

Large signal analysis of a harmonic generator using a semiconductor diode reveals a larger possible efficiency than a similar small signal analysis. As higher harmonic numbers are reached, large signal analysis becomes increasingly more important in predicting the maximum conversion efficiency. It is shown that there exists an optimum value for the diode bias voltage and an optimum coupling of the load and generator to the diode, and that the diode operating voltage should almost drive the diode into conduction. An expression is derived for the maximum conversion efficiency for any harmonic, and it is shown that the conversion loss increases with increasing harmonic number, approximately 2.9 db per n for large harmonic numbers in a typical case.

A Waveguide Switch Employing the Offset Ring-Switch Junction—R. C. Johnson, A. L. Holliman, and J. S. Hollis (p. 532)

This paper describes an X-band microwave ring switch employing a junction of new design. The insertion loss is less than $\frac{1}{4}$ db over the design of 9.0–9.6 kmc; this low loss was obtained through the use of a coupling junction which is designated the offset ring-switch junction. A physical description, the electrical characteristics of the switch, and a qualitative theoretical discussion of the junction are included.

Some Limitations on Parametric Amplifier Noise Performance—R. D. Weglein (p. 538)

Now that the precursory period following the solid-state parametric amplifier invention has given way to an era of determined effort to reduce to practice some of the early, optimistic predictions, practical limitations setting an upper bound to the performance of this ingenious communications device have become apparent. In this paper, two such limitations are discussed: First, for a given diode Q and junction geometry, there exists a noninfinite idler frequency, which determines the lowest radar noise temperature. Second, because of its extreme noisiness the reverse-breakdown current limits the maximum capacitance swing at both extremes and consequently the minimum noise performance. It is suggested that in certain cases refrigeration may be a partial remedy to both limitations.

TE Mode Excitation on Dielectric Loaded Parallel Plane and Trough Waveguides—M. Cohn, E. S. Cassedy, and M. A. Kott (p. 545)

A theoretical and experimental study of the launching of TE surface wave modes on dielectric loaded parallel plane and trough waveguides has been performed. The source is a linear transverse current filament perpendicular to and extending across the space between the parallel side walls. Families of curves are presented, which show the bidirectional launching efficiencies for the dominant TE modes of these two transmission lines as a function of dielectric constant, dielectric slab thickness, and current filament location. Measured bidirectional efficiencies are compared to the theoretically predicted values. Measured unidirectional launching efficiencies as high as 97 per cent were obtained for the case where a short circuit is located on one side of the current filament.

A New Semiconductor Microwave Modulator—H. Jacobs, F. A. Brand, M. Bananti, R. Benjamin, and J. Meindl (p. 553)

A new semiconductor device is proposed for use as an amplitude modulator for microwave transmission. The principle of action depends upon the increase of absorption with an increase of conductivity caused by the injection of excess minority carriers. Experiments conducted at 9600 Mc indicate little or no phase and frequency modulation. The mechanism of the modulation action and the device design are discussed here.

Theory and Measurement of Q in Resonant Ring Circuits—Hellmut Golde (p. 560)

The loaded and unloaded Q of a resonant ring circuit are derived on the basis of the fundamental definition. Simple experiments are described to measure Q_0, Q_L, and the ring power gain without additional coupling to the ring. A number of graphs are given which are useful for these measurements.

Reliability and Quality Control

VOL. RQC-9, NO. 2, SEPTEMBER, 1960

Automation for Quality Control Testing of Electron Tubes—Roy A. McNaughton (p. 16)

Prior to the mid Forties most electron tubes were production- and quality-tested on an attributes (go-no-go) basis only. Quality-sampled sizes were moderate and statistical paper work was at a minimum. Since that time quality-control testing has increased by leaps and bounds under the pressure for high reliability, performance, and uniformity. These factors have increased the quality-control work load to the point where an appreciable portion of the tube manufacturing cost is involved in the quality-control testing and statistical evaluation procedures.

In an effort to hold down the rapidly mounting costs of quality testing and data evaluation, to improve operator accuracy, and to reduce the number of tests, a test set has been developed which performs many of the tests automatically. The set provides digital data output for each test on each tube in punched tape, reads out the tape, and prints a copy of the punched data. The punched tape is then fed to a computer which analyzes the data for the entire sample and prints out the answers for those statistical factors such as lot means, standard deviations, per cent deltas, etc., required for the attributes-variables acceptance criteria for lot acceptance. The test set is designed to perform those static and dynamic tests normally performed on a Vacuum-Tube-Bridge test console. It has twenty test positions and will measure and record ten different characteristics on dual section tubes. Provisions are included for manually feeding test data from other equipments into the punched tape for analysis by the computer as desired.

The use of precision components and test circuitry has provided a high-accuracy, one-operator test set capable of supplanting four or five manually operated test sets and of reducing the time lag and labor force required for statistical reduction of the test data obtained.

Abstracts and References

Compiled by the Radio Research Organization of the Department of Scientific and Industrial Research, London, England, and Published by Arrangement with that Department and the *Electronic Technology* (incorporating *Wireless Engineer* and *Electronic and Radio Engineer*) London, England

NOTE: The Institute of Radio Engineers does not have available copies of the publications mentioned in these pages, nor does it have reprints of the articles abstracted. Correspondence regarding these articles and requests for their procurement should be addressed to the individual publications, not to the IRE.

The number in heavy type at the upper left of each Abstract is its Universal Decimal Classification number. The number in heavy type at the top right is the serial number of the Abstract. DC numbers marked with a dagger (†) must be regarded as provisional.

UDC NUMBERS

Certain changes and extensions in UDC numbers, as published in PE Notes up to and including PE 666, will be introduced in this and subsequent issues. The main changes are:

Artificial satellites:	551.507.362.2	(PE 657)
Semiconductor devices:	621.382	(PE 657)
Velocity-control tubes, klystrons, etc.:	621.385.6	(PE 634)
Quality of received signal, propagation conditions, etc.:	621.391.8	(PE 651)
Color television:	621.397.132	(PE 650)

The "Extensions and Corrections to the UDC," Ser. 3, No. 6, August, 1959, contains details of PE Notes 598–658. This and other UDC publications, including individual PE Notes, are obtainable from The International Federation for Documentation, Willem Witsenplein 6, The Hague, Netherlands, or from The British Standards Institution, 2 Park Street, London, W.1, England.

ACOUSTICS AND AUDIO FREQUENCIES

534.2–14:534.88 3704

A Moiré Fringe Analogue of Sound Propagation in Shallow Water—D. E. Weston. (*J. Acoust. Soc. Amer.*, vol. 32, pp. 647–654; June, 1960.) The pattern obtained with moiré fringes, or in Wood's model experiments (1086 of April), may be predicted in detail when there are only two modes present. In a simple medium, large spatial fluctuations in level due entirely to wave interference effects may be obtained.

A list of organizations which have available English translations of Russian journals in the electronics and allied fields appears at the end of the Abstracts and References section.

The Index to the Abstracts and References published in the PROC. IRE from February, 1959 through January, 1960 is published by the PROC. IRE, June, 1960, Part II. It is also published by *Electronic Technology* (incorporating *Wireless Engineer* and *Electronic and Radio Engineer*) and included in the April, 1960 issue of that Journal. Included with the Index is a selected list of journals scanned for abstracting with publishers' addresses.

534.2–14:534.88 3705

A Numerical Solution for the Problem of Long-Range Sound Propagation in Continuously Stratified Media, with Applications to the Deep Ocean—I. Tolstoy and J. May. (*J. Acoust. Soc. Amer.*, vol. 32, pp. 655–660; June, 1960.)

534.2–6–14:534.88 3706

Propagation of Low-Frequency Sound Signals in the Deep Ocean—C. W. Guthrie, A. N. Tolstoy and J. Shaffer. (*J. Acoust. Soc. Amer.*, vol. 32, pp. 645–647; June, 1960.) The acoustic field of a 10-cps CW source towed at slow speeds at a depth of 24 meters was measured by a stationary hydrophone to ranges of about 70 km. The depth of the hydrophone was approximately 450 meters. Results obtained are found to be in fair agreement with theoretical calculations.

534.22–14:534.88 3707

Speed of Sound in Sea Water as a Function of Temperature, Pressure and Salinity—W. D. Wilson. (*J. Acoust. Soc. Amer.*, vol. 32, pp. 641–644; June, 1960.) Tables have been prepared from an empirical formula which was derived to fit measured sound-speed data obtained over the temperature range −3°C to +30°C, the pressure range 1,033–1000 kg per cm² and the salinity range 33–37 per cent.

534.611 3708

Meaning and Interpretation of Acoustic Momentum and Acoustic Radiation Stress—E. J. Post. (*Phys. Rev.*, vol. 118, pp. 1113–1118; June 1, 1960.) A survey of viewpoints and available procedures of analysis of acoustic radiation stress and the concept of acoustic momentum is given.

534.839 3709

The Evaluation of Noise—E. Lübcke. (*Frequenz.*, vol. 13, pp. 287–289; September, 1959.) Simplified sound-pressure/frequency curves consisting of straight-line sections which are based on octave-band spectra and intended for the objective assessment of noise effects are given. See also 3914 of 1959.

534.84 3710

Audience and Seat Absorption in Large Halls—L. L. Beranek. (*J. Acoust. Soc. Amer.*, vol. 32, pp. 661–670; June, 1960.) It is postulated that the absorbing power of a seated audience in a large hall is proportional to the floor area occupied, provided that the audience density is between 4.5 and 8.5 feet² per person including aisles, and that the hall has a volume between 250,000 and 1,500,000 feet.³

621.395.623.7 3711

A Compact Loudspeaker Enclosure with Extended Low-Frequency Response—J. E. Benson. (*AWA Tech. Rev.*, vol. 11, pp. 37–48; August, 1959.) An analysis is made of a reflex enclosure having two tandem-coupled cavities behind the loudspeaker cone.

ANTENNAS AND TRANSMISSION LINES

621.372.2 3712

The Goubau Line—R. Hübner. (*Tech. Mitt. PTT.*, vol. 37, pp. 453–458; October, 1959.) The properties of the line are summarized and data of some commercial versions of the "G-line" and of existing or projected installations are given. 14 references.

621.372.2:621.396.67 3713

Wave Propagation in a Coaxial System—V. M. Papadopoulos. (*Quart. Appl. Math.*, vol. 17, pp. 423–436; January, 1960.) A solution is obtained for the problem of the propagation of em waves in a semi-infinite flanged coaxial line with an infinite center conductor, in terms of an infinite set of coefficients which are determined by an infinite set of linear equations. The solution is discussed for limiting cases corresponding to a thin vertical antenna on a plane earth and a thick vertical antenna with a low-impedance line feed.

621.372.823:621.372.83 3714

Short Junctions for H_{01} Waves—M. G. Andreasen. (*Acta. Polyt. Scand.*, No. 253, El 3, pp. 22; 1959. In German.) A theoretical investigation is made of the possibility of reducing the length of junctions in cylindrical waveguide while keeping the energy losses caused by transformation to the H_{02} mode at a low value over a wide frequency band. This can be done by modifying the shape of the conical junction. See also 3715 below.

621.372.823:621.372.83 3715

Smooth Junctions for H_{01} Waves with Particular Reference to the Conical Junction—M. G. Andreasen. (*Acta. Polyt. Scand.*, No. 254, El 4, pp. 25; 1959. In German.) The energy losses due to reflections and to transformation into other modes are calculated.

621.372.823:621.372.85 3716

Cavity Measurements of the TE_{11} Propagation Constants of a Circular Waveguide containing a Magnetized Ferrite Rod—E. V. Sorensen. (*Acta. Polyt. Scand.*, No. 282, El 7, pp. 30; 1960.) A tunable cavity method, based on that described by van Trier (2890 of 1953) has been used to measure propagation constants at 4600 Mc. The measured figures of

merit were found to be one or two orders of magnitude higher than theoretical values derived on the assumption of a Lorentzian resonance-line shape [203 of 1957 (Lax)].

621.372.823:621.372.853 3717
New Calculations on the Faraday Effect in Waveguides—A. P. van Gelder, A. M. de Graaf and R. Kronig. (*Appl. Sci. Res.*, vol. B7, no. 6, pp. 441–448; 1959.) The propagation of em waves for a circular waveguide containing a nonconducting ferromagnetic material in the form of a thin cylindrical shell adjacent to the wall of the waveguide is investigated theoretically.

621.372.837.3 3718
A New Ferrite Short-Circuit Device—B. Chiron. (*Cables & Trans.*, vol. 14, pp. 170–171; April, 1960.) The device is a ferrite rod which is placed symmetrically across a rectangular waveguide propagating the TE_{10} mode; switching properties are controlled by a dc magnetic field perpendicular to the axis of the rod and inclined 45° to the major faces of the guide. Almost all the incident power is reflected.

621.372.85 3719
Determination of the Dispersion Relation for a Waveguide with a Helix—A. K. Berezin, P. M. Zeĭdlits, A. M. Nekrashevich and G. A. Silenok. (*Zh. Tekh. Fiz.*, vol. 29, pp. 808–814; July, 1959.) An investigation is made of dispersion as a function of helix thickness, describing measurements carried out in the range 150–800 Mc with relative error of 4.5–1.5 per cent.

621.372.85 3720
Experimental Investigation of the Dispersion Relation for a Waveguide with a Modified Double Helix—A. K. Berezin, P. M. Zeĭdlits, A. M. Nekrashevich and I. P. Skoblik. (*Zh. Tekh. Fiz.*, vol. 29, pp. 815–818; July, 1959.) A modified contrawound helix cut from precision copper tubing is described. Experiments show that in such a system four waves are propagated with different phase velocities. Measurements have been made of the dispersion of three of these waves as a function of the structure geometry and of frequency in the range of 150–800 Mc. [See 1247 of 1955 (Sensiper).]

621.396.674.1 3721
Impedance Characteristics of a Uniform Current Loop having a Spherical Core—S. Adachi. (*J. Res. NBS*, vol. 64D, pp. 295–299; May/June, 1960.) An analysis of the radiation impedance of a loop with a resonant core of dielectric or magnetic material is given.

621.396.674.3 3722
Response of a Loaded Electric Dipole in an Imperfectly Conducting Cylinder of Finite Length—C. W. Harrison, Jr., and R. W. P. King. (*J. Res. NBS*, vol. 64D, pp. 289–293; May/June, 1960.) An analysis is made of the response of a short-terminated dipole placed along the axis of a partially-conducting closed cylindrical shield.

621.396.674.3 3723
The Resistance of Dipoles of Finite Length and Thickness—K. Fränz and E. Henze. (*Arch. elekt. Übertragung*, vol. 13, pp. 429–434; October, 1959.) The resistance of a family of dipoles $2h$ of length is calculated between the limits $\lambda < 2h < 3\lambda/2$. For calculations of dipole conductance, see 1870 of June (Fränz and Mann).

621.396.677:523.164 3724
The Synthesis of Large Radio Telescopes—M. Ryle and A. Hewish. (*Mon. Not. R. Astr. Soc.*, vol. 120, no. 3, pp. 220–230; 1960.) Two antennas are arranged so that their relative position may be altered successively over the area of a much larger equivalent antenna. By combining mathematically the information derived from these different positions, it is possible to obtain a resolving power equal to that of the large equivalent antenna. Two practical systems have been designed using this principle: (*a*) an interferometer, and (*b*) a pencil-beam antenna. [See also 3691 of 1958 (Blythe).]

621.396.677:621.396.96 3725
Investigation of the Technical Application of Cylindrical Surface-Wave Aerials as Radar Aerials—R. Jähn. (*Nachrtech.*, vol. 9, pp. 418–426; September, 1959.) The type of antenna investigated consists of a metal rod with parallel circumferential corrugations. Two different radiation patterns can be obtained depending on the feed arrangements. The usefulness of an antenna system comprising antennas with different radiation and polarization characteristics is outlined.

621.396.677.32:621.372.826 3726
Systems for Guiding Waves on End-Fire Radiators—G. V. Trentini. (*Nachrichtentech. Z.*, vol. 12, pp. 501–508; October, 1959.) The theory of surface-wave transmission and practical forms of waveguide systems such as disk, ring and dipole assemblies, are reviewed. Design data and radiation characteristics of these systems are given. 24 references.

621.396.677.71 3727
Calculated Patterns of Slotted Elliptic-Cylinder Antennae—J. R. Wait and W. E. Mientka. (*Appl. Sci. Res.*, vol. B7, no. 6, pp. 449–462; 1959.)

621.396.677.73 3728
The Dielectric Horn Aerial—M. Procházka. (*Hochfrequenz. u. Elektroak.*, vol. 68, pp. 93–104; September, 1959.) The development and methods of the design of dielectric antennas are reviewed. Design theory is developed for the dielectric horn antenna by investigating the effect of the dimensions and the material of the horn on antenna characteristics; comparison is also made with experimental results, and the mechanism of horn-antenna operation is determined.

AUTOMATIC COMPUTERS

681.142:537.311.33:538.632 3729
Hall-Effect Multipliers.—W. A. Scanga, A. R. Gilbinger and C. M. Barrack. (*Electronics*, vol. 33, pp. 64–67; July 15, 1960.) An experimental multiplier with an accuracy within 1 per cent is described. The design of the Hall generator comprising an InAs element between ferrite plates is given, together with details of suitable transistor amplifier circuits. Curves showing the performance of the unit for frequencies up to 4 kc are included.

681.142:537.312.62 3730
An Improved Film Cryotron and its Application to Digital Computers.—V. L. Newhouse, J. W. Bremer and H. H. Edwards. (PROC. IRE vol. 48, pp. 1395–1404; August, 1960.) A crossed-film cryotron formed by deposition on an insulated superconductor is described and its operation is analyzed. It has a time constant of 0.38 μ sec, and the dc dissipation is less than 5 μW. A cryotron storage circuit and a shift register are described.

681.142:538.221:539.23 3731
Electrical Read-Out from Thin Ferromagnetic Films—S. Feinstein and H. J. Weber. (*Electronics*, vol. 33, pp. 100–102; July 29, 1960.) A method of astatic coupling and amplification which gives a read-out with good signal-to-noise ratio is described.

681.142:621.317.7 3732
Electronic Digitizing Techniques—(*J. Brit. IRE*, vol. 20, pp. 513–522; July, 1960.) The text is given of papers presented at a symposium held in London, November 18, 1959.

a) Electronic Digitizing Techniques—G. J. Herring (pp. 513–517).
b) A Simple Analogue-to-Digital Converter with Nonlinearity Compensation—W. N. Jenkins (pp. 518–522).
c) The Step-by-Step Potentiometer as a Digitizer—G. P. Tonkin (pp. 523–528).
d) An Analogue-Digital Converter with Long Life—R. L. G. Gilbert (pp. 529–535).
e) A Wide-Range Fully Automatic Digital Voltmeter—J. A. Irvine and D. A. Pucknell (pp. 536–540).
f) An All-Electronic Four-Digit Digital Voltmeter—H. Fuchs and D. Wheable (pp. 541–547).

Discussion (pp. 548–552).

681.142:621.318.57 3733
Three-Hole Cores for Coincident-Flux Memory—H. F. Priebe, Jr. (*Electronics*, vol. 33, pp. 94–97; July 29, 1960.) Coincident-flux operation permits pulse currents that are not limited by coercive-force threshold. Shorter read-write times and greater tolerance to temperature and pulse-current variations are obtained.

CIRCUITS AND CIRCUIT ELEMENTS

621.319.43 3734
Conical Coaxial Capacitors and their Advantages—M. C. Selby. (*J. Res. NBS*, vol. 63C, pp. 87–89; October–December, 1959.) In an example cited, the ratios of maximum-to-minimum capacitance for disk, cylindrical and conical capacitors are 10, 40, and 168 to 1, respectively. An approximate equation is derived for the conical capacitor, and close agreement is shown between computed and measured values of capacitance.

621.319.43.089.6 3735
Capacitor Calibration by Step-Up Methods—T. L. Zapf. (*J. Res. NBS*, vol. 64C, pp. 75–79; January–March, 1960.) A procedure for calibrating variable capacitors in the range 100–1100 pF is described.

621.372.5 3736
Active-Power Transfer by Linear Quadripoles—E. Klausmann. (*Arch. elekt. Übertragung*, vol. 13, pp. 435–442; October, 1959.) The transfer of power through an arbitrary linear quadripole is considered as a function of matching conditions, source impedance, input and output impedances and gain of the quadripole.

621.372.5:681.142 3737
Connection and Measurement of Transfer Functions on an Analogue Computer—W. Schüssler. (*Arch. elekt. Übertragung*, vol. 13, pp. 405–419; October, 1959.) The transfer function of linear systems is split into products of partial transfer functions which facilitates the solution of network problems by analogue computer. Circuits representing the partial functions are given, and methods of measuring the frequency and time characteristics of filter networks are described.

621.372.54 3738
Three-Branch Reactive Sections for Ladder Filters with One or Two Cut-Off Frequencies—J. Bimont. (*Cables & Trans.*, vol. 14, pp. 86–112; April, 1960.) A graphical method for the synthesis of three-branch networks consisting of reactances which have no mutual inductive coupling is proposed.

621.372.54 3739
Dissipative Networks with Third-Order Maximally Flat Amplitude Characteristics—J. B. Rudd. (*AIWA Tech. Rev.*, vol. 11, pp.

1–36; August, 1959.) An analysis is made of dissipative lowpass networks; a simple change of the frequency variable allows the results to be applied to bandpass networks. For the case of narrow-band operation, the concept of quarter-wave coupling is developed and the equivalent triple-tuned circuit configuration is derived.

621.372.54 3740
Zig-Zag Filters—T. Laurent. (*Kungl. tek. Högsk. Handl., Stockholm*, no. 133., p. 58; 1959. In English.) A systematic method of calculating zig-zag sections for bandpass ladder filters is described. See 2363 of 1957.

621.372.54 3741
Filter Calculations using the Template Method—T. Laurent. (*Kungl. tek. Högsk. Handl., Stockholm*, no. 135, pp. 30; 1959. In English.) A part-graphical method for calculating filter characteristics which has been developed using frequency transformations is described. (See, *e.g.*, 2154 of 1950.)

621.372.54 3742
"Echostant" Matching. Systematic Matching of Filter Ladders Calculated Section by Section—T. Laurent. (*Ericsson Tech.*, vol. 15, no. 1, pp. 109–132; 1959.) See 1902 of June.

621.372.54 3743
Recurrence Formulae for the Calculation of the Characteristic Function of Filters with Tchebycheff Pass-Band Behaviour—A. Fettweis. (*Rev. HF. Brussels*, vol. 4, no. 10, pp. 230–239; 1960. In English.)

621.372.54 3744
Matching of Image-Parameter Filters and Associated Problems—V. Peterson. (*Ericcson Tech.*, vol. 15, no. 1, pp. 133–218; 1959.)

621.372.553 3745
The Physical Realizability and Realization of Linear Phase-Shift Networks—P. M. Chirlian. (*Quart. Appl. Math.*, vol. 18, pp. 31–35; April, 1960.)

621.372.553 3746
Restrictions Imposed upon the Unit Step Response of Linear Phase-Shift Networks—P. M. Chirlian. (*Quart. Appl. Math.*, vol. 17, pp. 225–230; October, 1959.) Limits for the 10–90 per cent rise time and overshoot of the unit step response of networks free from phase distortion are defined.

621.372.553:621.397 3747
The Design of Delay Equalizers using the Analogue Method—K. Bernath, B. Binz and E. Salvetti. (*Tech. Mitt. Ptt.*, vol. 37, pp. 445–452; October 1, 1959.) A resistance-network analogue and its application to the design of a television circuit delay equalizer are described.

621.372.63 3748
A Circuit for the Electrical Integration and Differentiation of Periodic Phenomena—W. Berger, F. Hövelmann and H. J. Kössler. (*Elektronische Rundschau*, vol. 13, pp. 336–338; September, 1959.) Integration or differentiation is carried out by means of two independent *RC* or *RL* sections separated by a tube stage.

621.372.63 3749
Synthesis of Driving-Point Impedances with Active *RC* Networks—I. W. Sandberg. (*Bell Sys. Tech. J.*, vol. 39, pp. 947–962; July, 1960.) A general method is presented for realizing any real rational driving-point function using *RC* networks and one type of active element, leading to a simple structure. Biquadratic impedance functions are considered in detail.

621.373:621.391.822 3750
Noise in Oscillators—W. A. Edson. (Proc. IRE, vol. 48, pp. 1454–1466; August, 1960.) Effects of white noise of thermal or electronic origin on the initiation of oscillations and on perturbations in amplitude and phase of sustained oscillations are analyzed.

621.373:621.391.822 3751
Background Noise in Nonlinear Oscillators—J. A. Mullen. (Proc. IRE, vol. 48, pp. 1467–1473; August, 1960.) An examination is made of the effects of wideband noise at or near the frequency of oscillation on self-excited oscillators.

621.373:621.391.822 3752
The Behaviour of Nonlinear Oscillating Systems in the Presence of Noise—C. L. Tang. (Proc. IRE, vol. 48, p. 1493; August, 1960.) Comment on 1996 of 1956 (Rytos); see also 3751 above.

621.373.1 621.318.57:537.312.8 3753
On the Resolving Time and Flipping Time of Magnetoresistive Flip-Flops—A. Aharoni and E. H. Frei. (Proc. IRE, vol. 48, pp. 1436–1448; August, 1960.) The time constant τ of the exponential approach to the stable states is shown to be a fair approximation for the flipping item of a bridge-type magnetoresistive flip-flop; τ is of the order of 10^{-3} seconds for materials available at present. The method of calculating flipping time is extended to more general networks, and the dependence of the flipping time on the incoming pulse is considered.

621.373.4.072.9 3754
Impulse-Governed Oscillator Techniques: Part I—C. J. de Lussanet de la Sablonière. (*Phillips Telecommun. Rev.*, vol. 21, pp. 78–90 and 155–165; October, 1959 and April, 1960. The general principles of IGO techniques are discussed; special circuits and theoretical data will be given in subsequent issues.

621.373.421:621.391.822 3755
Monochromaticity and Noise in a Regenerative Electrical Oscillator—M. J. E. Golay. (Proc. IRE, vol. 48, pp. 1473–1477; August, 1960.) Expressions are derived for the departure from monochromaticity of a regenerative oscillator represented by an equivalent *RLC* circuit having a negative resistance in parallel with *R*. The intensity and bandwidth of the thermal noise generated in the oscillator by resistance *R* are also considered.

621.373.431.1:621.382.3 3756
Frequency Stability of Astable Multivibrators using Transistors—E. Brückner. (*Nachrichtentech. Z.*, vol. 12, pp. 509–513; October, 1959.) The dependence of multivibrator frequency on transistor characteristics and operating conditions is investigated and rules for an optimum design are derived.

621.373.444.1:621.397.621 3757
Synthesis of a Circuit for Flywheel Synchronization—J. Vlach. (*Hochfrequenz. u. Elektroak.*, vol. 68, pp. 86–93; September, 1959.

621.374 3758
A Special Effect in Some Pulse Systems—J. Tschauner. (*Nachrichtentech. Z.*, vol. 12, pp. 456–458; September, 1959.) The order of the transfer function of pulse-driven closed-circuit systems can, under certain conditions, be increased by one degree relative to the corresponding steady-state system. The reasons for this effect are given with experimental confirmation.

621.374.4:621.372.44 3759
Parametric Excitation of Harmonic Oscillations in a Linear Oscillating Circuit with Nonperiodic Variation of its Parameters with Time—P. G. Gorodetskiĭ. (*Zh. Tekh. Fiz.*, vol. 29, pp. 580–583; May, 1959.) Conditions for harmonic generation by nonperiodic variation of *R*, *L* and *C* are established.

621.374.4:621.387 3760
Harmonics from a Microwave Gas Discharge—N. R. Bierrum and D. Walsh. (*J. Electronics Control*, vol. 8, pp. 81–90; February, 1960.) The conversion loss can be reduced to 3–4 db per harmonic after an initial drop of 35 db to the third harmonic. A typical loss from 10 cm λ to 8 mm λ is 63 db. See 2652 of August (Bierrum, *et al.*).

621.375.226 3761
Amplifier with Stagger-Tuned Circuits with Maximum Linearity of the Phase and Attenuation Characteristics—G. Cartianu. (*Hochfrequenz. u. Elektroak.*, vol. 68, pp. 75–86; September, 1959.) The design of wideband amplifiers for FM signals is detailed with tabulated data on various types of stagger-tuned circuit whose group-delay and attenuation characteristics are also given.

621.375.232.3 3762
Transient Analysis of the White Cathode Follower—M. Brown. (*Rev. Sci. Instr.*, vol. 31, pp. 403–409; April, 1960.) The circuit provides an output impedance of about 5Ω and transmits pulses of either polarity with minimum distortion. A dc and transient analysis is made and the effect of varying circuit parameters is discussed.

621.375.4:621.396.665 3763
Amplifier Compensates for Speech-Level Variations—L. E. Getgen. (*Electronics*, vol. 33, pp. 103–106; July 29, 1960.) An automatic gain-adjusting amplifier produces constant output, without peak-clipping, for input variations of 40 db.

621.375.9:538.569.4 3764
Influence of Fluctuations of the Number of Molecules on the Frequency of a Molecular-Beam Maser Oscillator—Wang. (See 3802.)

621.375.9:621.372.44:621.372.832.8 3765
A Parametric Device as a Nonreciprocal Element—A. K. Kamal. (Proc. IRE, vol. 48, pp. 1424–1430; August, 1960.) An arrangement for combining an up-converter with a down-converter to obtain a nonreciprocal phase-shifting device is proposed. Measurements made at a signal frequency of 500 Mc on both a circulator and an isolator are discussed.

621.375.9:621.372.44:621.385.6 3766
Parametric Amplification, Power Control, and Frequency Multiplication at Microwave Frequencies using Cyclotron-Frequency Devices—Cuccia. (See 4076.)

621.375.9:621.372.44:621.385.6 3767
An Electrostatically Focused Electron-Beam Parametric Amplifier—Udelson (See 4077.)

621.375.9:621.372.44:621.385.6 3768
Lower-Frequency-Pumping Electron-Beam Parametric Amplifier—Chakraborti. (See 4075.)

621.376:621.374 3769
Phase-Sensitive Demodulation with Interpolation—J. S. Johnston. (*Elec. Engr.*, vol. 32, pp. 488–490; August, 1960.) Details of a pulse-sampling system for demodulation of a low-frequency carrier are given. Errors may be reduced by interpolation if the general form of the modulation envelope is known in advance.

621.376.3 3770
The Calculation of Static and Dynamic Amplitude and Frequency Distortion of Fre-

quency-Modulated Oscillations with the Transmission Factor given in Series Form—E. G. Wosthni. (*Hochfrequenz. u. Elektroak.*, vol. 68, pp. 104–110; September, 1959.) The cases of frequency, amplitude and "limiting" distortion, *i.e.*, distortion due to nonideal limiting conditions, are investigated to derive general expressions for the treatment of FM signal distortion. See also 4190 of 1959.

GENERAL PHYSICS

534.283–8 3771

Theory of Ultrasonic Attenuation in Metals and Magneto-Acoustic Oscillations—A. B. Pippard. [*Proc. Roy. Soc.* (London) *A.*, vol. 257, pp. 165–193; September 6, 1960.]

537.311.33:539.23:539.61 3772

The Possible Role of the Electrical Double Layer in the Contact of Solids and in Adhesion Phenomena—V. B. Sandomirskii and V. P. Smilga. (*Fiz. Tverdogo Tela*, vol. 1, pp. 307–314; February, 1959.) Calculations are made of the surface charge density and the electrostatic component of adhesive force for the case of (*a*) contact between a metal and a semiconductor film, and (*b*) a semiconductor film between two metals.

537.311.5 3773

Evidence for a Configurational E.M.F. in a Conducting Medium—M. Chester. (*Phys. Rev. Lett.*, vol. 5, pp. 91–93; August, 1960.) By analogy with hydrodynamic effects, an EMF is expected to be associated with a current constriction. Experimental evidence for such an effect is given.

537.312.62:537.311.4 3774

Theory of Superconducting Contacts—R. H. Parmenter. (*Phys. Rev.*, vol. 118, pp. 1173–1182; June 1, 1960.) A generalization of the Bardeen-Cooper-Schrieffer theory of superconductivity for the case of a position-dependent energy gap, and application to several problems involving superconducting contacts is given. (*Ibid.*, vol. 108, pp. 1175–1204; December 1, 1957.)

537.324 3775

Diagrams Representing States of Operation of a General Thermocouple—A. H. Boerdijk. (*J. Appl. Phys.*, vol. 31, pp. 1141–1144; July, 1960.) For a wide range of possible thermocouples, the operating characteristics depend on the current and the junction temperatures; as an example, the calculation of a cooling region of a diagram for a general couple is given.

537.523 3776

Pre-breakdown Phenomena in Uniform Fields—D. T. A. Blair, F. M. Bruce, J. E. Matthews and D. J. Tedford. (*Proc. Phys. Soc.*, vol. 75, pp. 729–732; May 1, 1960.) Observations were made of prebreakdown phenomena in uniform field gaps under ambient atmospheric conditions and measured irradiation intensities, in which current and light pulses were recorded. From measurements of the current pulse duration, a value for the mobility of positive ions of 2.6 $cm^2 sec^{-1}V^{-1}$ was obtained at field strengths approaching the breakdown value."

537.523 3777

Some Sparkover Phenomena with Enclosed Gaps—A. Aked, F. M. Bruce and C. Gordon. (*Proc. Phys. Soc.*, vol. 75, pp. 733–738; May 1, 1960.) Breakdown characteristics of an unventilated and nonirradiated uniform gap are examined and compared with those obtained under a variety of conditions of ventilation.

537.525 3778

Experimental Determination of the Individual Secondary Ionization Coefficients in Hydrogen and their Dependence on Cathode Work Functions—F. L. Jones and E. Jones. (*Proc. Phys. Soc.*, vol. 75, pp. 762–771; May 1, 1960.)

537.525.6 3779

The Space-Charge Retardation of Electron Avalanches—K. J. Schmidt-Tiedemann. (*Z. Naturforsch.* vol. 14a, pp. 989–994; November, 1959.) The electric field generated by the positive and negative space charge of a single electron avalanche moving in a homogeneous electric field is calculated. A growth formula which differs from the Townsend formula is derived. Good agreement between the theoretical results and statistical data given by other authors is obtained.

537.527 3780

Negative Current-Voltage Characteristics in Hydrogen at High Pressure using Plane Parallel Electrodes—D. J. DeBitetto, L. H. Fisher and A. L. Ward. (*Phys. Rev.*, vol. 118, pp. 920–923; May 15, 1960.) Measurements of the characteristics are described and studied theoretically.

537.533 3781

Comments on Necessary and Sufficient Trajectory Conditions for Dense Electron Beams—W. M. Mueller. (*J. Electronics Control*, vol. 8, pp. 111–112; February, 1960.) Addendum to 448 of Feburary.

537.533:537.525.5 3782

High-Voltage Electron Extraction from an Arc-Discharge Plasma—K. G. Hernqvist. (*RCA Rev.*, vol. 21, pp. 170–183; June, 1960.) A method is described for obtaining stable electron beams of current densities to 30a/cm^2 using a magnetically confined mercury-pool arc.

537.533:538.3 3783

Shift of an Electron Interference Pattern by Enclosed Magnetic Flux—R. G. Chambers. (*Phys. Rev. Lett.*, vol. 5, pp. 3–5; July, 1960.) Experiments to confirm the shift are described and the results discussed. See 821 of March (Aharonov and Bohm).

537.533:538.56 3784

The Propagation of Oscillations in Electron Beams with Uncompensated Space Charge—B. N. Rutkevich and Ya. B. Faĭnberg. (*Zh. Tekh. Fiz.*, vol. 29, pp. 280–286; March, 1959.) A mathematical treatment of an electron cloud rotating in a uniform magnetic field is given.

537.533:538.56 3785

Theory of Longitudinal Oscillations of an Electron-Ion Beam—R. V. Polovin and N. L. Tsintsadze. (*Zh. Tekh. Fiz.*, vol. 29, pp. 831–832; July, 1959.) A generalization of results of earlier analysis (1835 of 1959) to the case of arbitrary deformation of the beam is given.

537.533:538.63 3786

A Paraxial Formulation of the Equations for Space-Charge Flow in a Magnetic Field—P. T. Kierstein. (*J. Electronics Control*, vol. 8, pp. 207–225; March, 1960.)

537.56 3787

Stability of Uniform Plasmas with Respect to Longitudinal Oscillations—P. D. Noerdlinger. (*Phys. Rev.*, vol. 118, pp. 879–885; May 15, 1960.)

537.56:538.63 3788

Excitation of Waves in Plasma—A. G. Sitenko and Yu. A. Kirochkin. (*Zh. Tekh. Fiz.*, vol. 29, pp. 801–807; July, 1959.) A mathematical analysis is made of plasma excitation by external currents, based on two-component plasma theory applicable to wave excitation at any frequency.

538.221 3789

Statistical Mechanical Theory of Ferromagnetism. High-Density Behaviour—R. Brout. (*Phys. Rev.*, vol. 118, pp. 1009–1019; May 15, 1960.) The partition function of the Ising model of ferromagnetism is examined in the limit of high density. See also 817 of March.

538.221:539.2 3790

Surface Magnetostatic Modes and Surface Spin Waves—J. R. Eshbach and R. W. Damon. (*Phys. Rev.*, vol. 118, pp. 1208–1210; June 1, 1960.) The general existence of surface-wave modes in the frequency region above the spin waveband is shown. See also Damon and Eshbach, (*J. Appl. Phys.*, vol. 31, suppl., pp. 1045–1055; May, 1960.)

538.566 3791

On the Propagation of a Discontinuous Electromagnetic Wave—B. van der Pol and A. H. M. Levelt. (*Proc. Koninkl. Ned. Akad. Wetenschap. A*, vol. 53, no. 3, pp. 254–265; 1960.) A treatment of a variant of Sommerfeld's problem is made in which the oscillating dipole is replaced by a dipole whose moment jumps from zero to one. A solution for the general case in terms of complete elliptic integrals is given.

538.566:531.51 3792

Electromagnetic Waves in Gravitational Fields—J. Plebanski. (*Phys. Rev.*, vol. 118, pp. 1396–1408; June 1, 1960.) A study is made of the scattering of plane em waves by the gravitational field of an isolated physical system.

538.566:535.42 3793

Boundary-Layer Problems in Diffraction Theory—R. N. Buchal and J. B. Keller. (*Commun. Pure Appl. Math.*, vol. 13, pp. 85–114; Feburary, 1960.)

538.566:535.42 3794

Planar Problem of Diffraction of Electromagnetic Waves by an Ideally Conducting Strip of Finite Width—Yu. V. Pimenov. (*Zh. Tekh. Fiz.*, vol. 29, pp. 597–603; May, 1959.) An application is given of the method of solution proposed earlier [1515 of 1959 (Grindberg and Pimenov)] to the case of small values of ka, where k is the wave number and a the half-width of the strip.

538.566:535.42 3795

Distribution of Current Densities on the Edges of an Ideally Conducting Rectangular Wedge Placed in the Field of a Plane Electromagnetic Wave—N. N. Lebedev and I. P. Skal'skaya. (*Zh. Tekh. Fiz.*, vol. 29, pp. 928–931; July, 1959.) Simplified formulas for calculating current densities are derived which, in their final form, contain only well-known tabulated functions.

538.566:535.42 3796

High-Frequency Diffraction of Plane Waves by an Infinite Slit: Parts 1 & 2—S. R. Seshadri. (*Proc. Nat. Inst. Sci. India*, pt. A, vol. 25, pp. 301–336; November 26, 1959.)

538.566:535.43]+534.26 3797

On the Plane-Wave Extinction Cross-Section of an Obstacle—A. T. de Hoop. (*Appl. Sci. Res.*, vol. B7, no. 6, pp. 463–469; 1959). The relation between the extinction cross section of an obstacle, which both absorbs and scatters power, and the amplitude and phase of a scattered time-harmonic plane em wave is proved using an explicit representation of the scattered field. The result is valid for a plane wave with arbitrary elliptic polarization.

538.566.2:537.56 3798

Electromagnetic Waves in a Plasma Located in a Magnetic Field—Ya. B. Faĭnberg and M. F. Gorbatenko. (*Zh. Tekh. Fiz.*, vol. 29,

pp. 549–562; May, 1959.) A mathematical analysis is made for the case of a cylindrical plasma rod located in a uniform external field and isolated from the metallic walls of a waveguide. A dispersion equation is derived and the em field configuration is determined. It is shown that em waves can be propagated in the system at frequencies significantly lower than the Langmuir and Larmor frequencies.

538.569:537.56 3799
The Absorption Coefficient of a Plasma at Radio Frequencies—P. A. G. Scheuer. (*Mon. Not. R. Astr. Soc.*, vol. 120, no. 3, pp. 231–241; 1960.)

538.569.4:538.222 3800
Passage Effects in Paramagnetic Resonance Experiments—M. Weger. (*Bell Sys. Tech. J.*, vol. 39, pp. 1013–1112; July, 1960.) Paramagnetic-resonance signals under various experimental conditions are classified theoretically and some experimental checks are carried out.

538.569.4:621.375.9 3801
Study of Damping by Coherent Radiation in Nuclear Magnetic Resonance—H. Benoit. (*J. Phys. Radium*, vol. 21, pp. 212–216; April, 1960.) The general equations derived are applied to a calculation of the range of oscillation and frequency pulling in a maser-type oscillator.

538.569.4:621.375.9 3802
Influence of Fluctuations of the Number of Molecules on the Frequency of a Molecular-Beam Maser Oscillator—T. C. Wang. (*J. Phys. Radium*, vol. 21, pp. 261–263; April, 1960.) Extension of earlier work [3710 of 1956 (Shimoda, *et al.*)].

538.691 3803
Charged-Particle Orbits in Varying Magnetic Fields—E. I. Gordon. (*J. Appl. Phys.*, vol. 31, pp. 1187–1190; July, 1960.) A magnetic field with time variation but with azimuthal symmetry about an axis is considered. The movement of the charged particle is found by considering it to move nearly in a circle about a guiding center whose motion can also be calculated.

538.691 3804
Drift of a Charged Particle in a Magnetic Field of Constant Gradient—P. W. Seymour. (*Aust. J. Phys.*, vol. 12, pp. 309–314; December, 1959.)

539.2 3805
Giant Fluctuations in a Degenerate Fermi Gas—W. Kohn and S. J. Nettel. (*Phys. Rev. Lett.*, vol. 5, pp. 8–9; July 1, 1960.) Arguments are presented that for sufficiently weak interactions the Hartree (and Hartree-Fock) ground states in two or more dimensions are the familiar plane-wave states. See also 3068 of September (Overhauser).

GEOPHYSICAL AND EXTRATERRESTRIAL PHENOMENA

523+55+57+61]:621.38 3806
Electronics Probes Nature—W. E. Bushor and M. F. Wolff. (*Electronics*, vol. 33, pp. 53–86; July 29, 1960.) A general review of present investigations into space, our atmosphere, the earth, the oceans and living matter is given. The instrumentation of satellites and probes successfully launched by the United States and U.S.S.R. is tabulated.

523.16 3807
Measurement of the Neutron Flux in Space—W. N. Hess and A. J. Starnes. (*Phys. Rev. Lett.*, vol. 5, pp. 48–50; July 15, 1960.) The experimentally determined count rate agrees well with that calculated from multigroup diffusion theory if allowance is made for a background flux.

523.164:621.396.677 3808
The Synthesis of Large Radio Telescopes—Ryle and Hewish. (See 3724.)

523.164.3 3809
The Spectrum of the Galactic Radio Emission—C. H. Costain. (*Mon. Not. R. Astr. Soc.*, vol. 120, no. 3, pp. 248–255; 1960.) Absolute measurements of the cosmic background radiation have been made at wavelengths of 1.7 and 7.9mλ.

523.164.3 3810
An Experimental Investigation of the Effects of Confusion in a Survey of Localized Radio Sources—C. Hazard and D. Walsh. (*Mon. Not. R. Astr. Soc.*, vol. 119, no. 6, pp. 648–656; 1959.) Surveys of RF sources have been made using (*a*) total-power equipment, and (*b*) an interferometer; the results are compared.

523.164.3 3811
Radio Emission from the Cygnus Loop—J. E. Baldwin and P. R. R. Leslie. (*Mon. Not. R. Astr. Soc.*, vol. 120, no. 1, pp. 72–78; 1960.) Good positional agreement has been obtained between several of the radio and optical features, but an intense extended source lying one degree south of the center of the Loop is not correlated with any outstanding optical feature.

523.164.3 3812
A Spectral Analysis of the Radio Sources in Cygnus X at 1390 Mc/s and 408 Mc/s—D. S. Mathewson, M. T. Large and C. G. T. Haslam. (*Mon. Not. R. Astr. Soc.*, vol. 120, no. 3, pp. 242–247; 1960.) The results support the conclusion of other workers, showing that the emission is from optically thin HII regions except for the strongest source in the region, the γ-Cygni source, which was found to have a nonthermal component.

523.164.3:523.4 3813
The Ionosphere of Jupiter—H. Rishbeth. (*Aust. J. Phys.*, vol. 12, pp. 466–468; December, 1959.) An approximate analysis based on Chapman theory suggests that Jupiter may possess an ionosphere, of critical frequency about 20 Mc, existing a few hundred kilometers above the visible clouds. See also 3426 of 1958 (Gardner and Shain).

523.164.3:523.4 3814
Radio Emission from Jupiter at 408 Mc/s—R. J. Long and B. Elsmore. (*Observatory*, vol. 80, pp. 112–114; June, 1960.) A report is given on measurements made by the four-element interferometer at Cambridge of the relation between flux density and the diameter of the Jupiter RF source at 408 Mc. Comparison is made with flux density observations of other authors.

523.164.32 3815
The Planning and Results of the Program of Observations of the Department for Ionospheric Research and Radio Astronomy of the P.T.T.—L. D. de Feiter. (*Tijdschr. ned. Radiogenoot.*, vol. 24, no. 4, pp. 189–198; 1959.) Radio observations of the sun made at 200 and 545 Mc during the recent period of maximum solar activity at the observatories Nera (Netherlands), Paramaribo (Surinam) and Hollandia (New Guinea) are discussed.

523.164.32 3816
Solar Radio Bursts of Spectral Type II—J. A. Roberts. (*Aust. J. Phys.*, vol. 12, pp. 327–356; December, 1959. Plates.) An analysis of 65 spectral type-II bursts is used to review the properties of such bursts. In addition to features already well recognized, a "herringbone" structure is described. Statistical methods are used to study the association of type-II bursts with solar flares and geomagnetic storms.

523.164.32 3817
Location of the Sources of 19-Mc/s Solar Bursts—C. A. Shain and C. S. Higgins. (*Aust. J. Phys.*, vol. 12, pp. 357–368; December, 1959.) An improved method of observing source positions is described. From correlations with optical data the radial distances of the radio sources from the center of the sun have been deduced.

523.164.32 3818
An Association between Solar Radio Bursts at Metre and Centimetre Wavelengths—A. A. Neylan. (*Aust. J. Phys.*, vol. 12, pp. 399–403; December, 1959.) It appears that type-III events which coincide with cm-λ bursts are frequently followed by a wideband emission, termed type V. Mechanisms for generating the cm-λ and type-V radiation are considered.

523.164.32:523.75 3819
An Investigation of the Speed of the Solar Disturbances Responsible for Type III Radio Bursts—J. P. Wild, K. V. Sheridan and A. A. Neylan. (*Aust. J. Phys.*, vol. 12, pp. 369–398; December, 1959.) Simultaneous directional observations at a number of frequencies between 40 and 70 Mc are described. The results support the hypothesis that type-III bursts are due to plasma oscillations excited in the coronal gas.

523.164.32:550.385.4 3820
Solar Radio Events and Geomagnetic Storms—L. D. de Feiter, A. D. Fokker, H. P. T. Van Lohuizen and J. Roosen. (*Planet. Space Sci.*, vol. 2, pp. 223–227; August, 1960.) An attempt is made to identify solar RF bursts of importance 3+ with subsequent sudden commencements of geomagnetic storms for the period April 1957–August 1959. See also 121 of January (de Feiter, *et al.*).

523.164.32:550.385.4 3821
Solar Radio Emission of Spectral Type IV and its Association with Geomagnetic Storms—D. J. McLean. (*Aust. J. Phys.*, vol. 12, pp. 404–417; December, 1959.) A study of spectral records has been used to distinguish between type-I and type-IV storms. The association of type-IV storms with solar flares and geomagnetic storms is described.

523.164.4 3822
The Eta Carinae Nebula and Centaurus A near 1400 Mc/s: Part 2—Physical Discussion of the Eta Carinae Nebula—C. M. Wade. (*Aust. J. Phys.*, vol. 12, pp. 418–429; December, 1959.) The temperature, density and mass of the object are inferred from observations at 1400 Mc and other radio data [Part 1: 2706 of August (Hindman and Wade)].

523.164.4 3823
The Extended Component of Centaurus A—C. M. Wade. (*Aust. J. Phys.*, vol. 12, pp. 471–476; December, 1959.) Observations at 85.5 Mc and 1400 Mc are used to distinguish between the two components of Centauras A. A comparison between Centauras A and Cygnus A is made.

523.165 3824
Physical State of Outer Atmosphere and the Origin of Radiation Belts—T. Obayashi. (*J. Geomag. Geoelect.*, vol. 11, no. 3, pp. 80–84; 1960.) The trapping of high-energy particles is explained by the interaction of hot plasmas with the geomagnetic field.

523.165:523.164.32 3825
Cosmic-Ray Storms and Solar Radio Outbursts—Y. Kamiya and M. Wada. (*Rep.*

Ionos. Space Res. Japan, vol. 13, pp. 105–111; June, 1959.) An analysis has been made of type-IV RF bursts. Results suggest that a large corpuscular cloud with an associated strong magnetic field is emitted simultaneously with the RF bursts. The cloud has a small core and when this core covers the earth, cosmic-ray and magnetic storms occur.

523.3:621.396.96 3826

A Theory of Radar Scattering by the Moon—T. B. A. Senior and K. M. Siegel. (*J. Res. NBS*, vol. 64D, pp. 217–229; May/June, 1960.) A detailed discussion of available experimental evidence leads to the theory that the scattering is composed of a number of individual returns from 20–30 single scattering areas, with those nearest to the earth providing a specular return. Information about the material of which this area is composed can then be obtained.

523.5:621.396.96 3827

Radio Echo Observations of the Geminid Meteor Stream—A. A. Weiss. (*Aust. J. Phys.*, vol. 12, pp. 315–319; December, 1959.) A summary is given of radiant-coordinate and echo rate measurements from 1952 to 1957; these agree with northern hemisphere observations between 1949 and 1954. See also 112 of 1958.

523.75:551.510.535 3828

On the Current System of Solar-Flare Effects—J. Veldkamp and D. van Sabben. (*J. Atmos. Terr. Phys.*, vol. 18, pp. 192–202; June, 1960.) The current system associated with large solar flares is symmetric about the magnetic equator. It is shown that the current must flow in a region where electron decay is caused by attachment. The D region is suggested, and the loss coefficient β is estimated to be 5×10^{-4} sec^{-1}.

523.755:550.38 3829

Coupling of the Solar Wind and the Exosphere—C. P. Sonett. (*Phys. Rev. Lett.*, vol. 5, pp. 46–48; July 15, 1960.) Possible physical processes at the geomagnetic boundary are considered in order to resolve the different estimates of its position obtained from rocket magnetometer experiments (see 3822 below) and from the study of cometary tails of type I.

550.38:523.75 3830

Interaction of the Solar Plasma with the Earth's Magnetic Field—D. B. Beard. (*Phys. Rev. Lett.*, vol. 5, pp. 89–91; August 1, 1960.) A calculation is made of the reshaping and termination of the earth's magnetic field by the solar flux of protons and electrons.

550.38:551.594.5 3831

The Geomagnetic Field in Space, Ring Currents, and Auroral Isochasms—E. H. Vestine and W. L. Sibley. (*J. Geophys. Res.*, vol. 65, pp. 1967–1979; July, 1960.) The relations between positions of maximum auroral frequency and the geomagnetic field lines were studied by using a spherical harmonic representation of the field.

551.507.362.1:550.380.8 3832

Steady Component of the Interplanetary Magnetic Field: Pioneer V—P. J. Coleman, Jr., L. Davis and C. P. Sonett. (*Phys. Rev. Lett.*, vol. 5, pp. 43–46; July 15, 1960.) Satellite magnetometer measurements suggest the existence of a galactic interstellar field which is uniform over the solar system. See 3490 of October (Coleman, *et al.*).

551.507.362.2 3833

On the Magnetic Damping of Rotation of Artificial Satellites of the Earth—L. LaPas. (*J. Geophys. Res.*, vol. 65, pp. 2201–2202; July, 1960.) Previous theoretical work is criticized, and suggestions are made for removing some of the analytical limitations.

551.507.362.2 3834

Some Simple Formulas for Latitude Effects and Lifetimes of Satellites—A. Lundbak. (*Planet. Space Sci.*, vol. 2, pp. 212–213; August, 1960.) Empirical equations are presented and their validity checked by considering the air drag expected.

551.507.362.2 3835

New Method of Solution for Unretarded Satellite Orbits—J. P. Vinti. (*J. Res. NBS*, vol. 63B, pp. 105–116; October–December, 1959.) "An axially symmetric solution of Laplace's equation in oblate spheroidal coordinates is found, which may be used as the gravitational potential about an oblate planet. This potential, which makes the Hamilton-Jacobie equation for a satellite orbit separable, has an expansion in zonal harmonics in which the amplitudes of the zeroth and second harmonics can be adjusted to agree exactly with the values for any axially symmetric planet and a fourth harmonic which then agrees approximately with the latest value for that of the earth."

551.507.362.2 3836

The Sudden Discontinuity in the Orbital Period of Sputnik 4 Satellite—B. R. May and D. E. Smith. (*Nature*, vol. 187, pp. 866–867; September 3, 1960.) Radio observations show that a discontinuity in the orbital period occurred at 2357 UT on May 18, 1960, as a result of an unsuccessful attempt to bring the "space capsule" out of orbit.

551.507.362.2:551.510.535 3837

Ionospheric Information from Satellite Signals—G. H. Munro. (*Nature*, vol. 187, pp. 1017–1018, September 17, 1960). Results of observations made over a two-year period of the fading rate of satellite signals are briefly described and compared with ionization profiles for the same period. The fading rate changed abruptly from winter to summer values within two days during September, 1958. This effect was preceded by a change in the direction of travelling disturbances.

551.507.362.2:551.510.535 3838

The Determination of Ionospheric Electron Content by Observation of Faraday Fading—W. T. Blackband. (*J. Geophys. Res.*, vol. 65, pp. 1987–1992; July, 1960.) Fading was observed on satellite signals at 20 and 40 Mc. Derived electron densities agreed with those deduced from vertical-incidence soundings, up to the maximum of the F_2 layer, and decreased to 0.45 of the maximum value 250 km above this layer.

551.507.362.2:551.510.535 3839

The Use of Geostationary Satellites for the Study of Ionospheric Electron Content and Ionospheric Radio-Wave Propagation—O. K. Garriott and C. G. Little. (*J. Geophys. Res.*, vol. 65, pp. 2025–2027; July, 1960.) A proposed experiment for measuring the total electron content of the ionosphere and for propagation studies is given.

551.510.52:551.508.8 3840

An Analysis of Radiosonde Effects on the Measured Frequency of Occurrence of Ducting Layers—N. K. Wagner. (*J. Geophys. Res.*, vol. 65, pp. 2077–2085; July, 1960.) 51 per cent of the ducting layers present over the Southern California coast are not observed owing to a 10-second time lag in the sensing elements. Data transmission loses only another 3 per cent.

551.510.535 3841

Artificial Electron Clouds: Part 6—Low-Altitude Study, Release of Cesium at 69, 82 and 91 km—J. Pressman, F. F. Marmo and L. M. Aschenbrand. (*Planet. Space Sci.*, vol. 2, pp. 228–237; August, 1960.) The electron clouds were detected by radar at several frequencies and the measured duration was in reasonable agreement with theory. Effective artificial clouds below 70 km could not be produced. Part 5: 3095 of September (Marmo, *et al.*).

551.510.535 3842

On the Determination of the True Height of Ionization at High Latitudes—D. Lepechinsky and C. Taieb. (*J. Atmos. Terr. Phys.*, vol. 18, pp. 152–159; June, 1960. In French.) The matrix method of Budden (755 of 1956) for determining true-height/electron-density profiles from ionograms is modified to allow the use of the third magneto-ionic (z) component when the ordinary component is unsuitable.

551.510.535 3843

The General Methods of the Station Lindau/Harz for the Determination of the True Electron-Density Distribution in the Ionosphere—W. Becker. (*Arch. elekt. Übertragung*, vol. 13, pp. 373–382; September, 1959.) Three methods are described: a "general method," assuming longitudinal propagation for the extraordinary ray, and two correction methods for the reduction of the ordinary – and extraordinary—ray traces. These two methods are used to determine the corrections to be applied to the profile of the reference layer, previously obtained by a comparison method (2000 of June), to obtain the true profile. See also 1217 of April.

551.510.535 3844

Performance of an R.F. Impedance Probe in the Ionosphere—J. E. Jackson and J. A. Kane. (*J. Geophys. Res.*, vol. 65, pp. 2209–2210; July, 1960.) New values of electron density agree with those from other techniques. Earlier data (156 of January) were found to be too low, owing to distortion of the environment by the potentials applied to the probe.

551.510.535 3845

Diurnal Variation of the Electron Distribution in the Ionospheric E Layer—B. J. Robinson. (*J. Atmos. Terr. Phys.*, vol. 18, pp. 215–233; June, 1960.) An analysis of the results of measurements made using a high-resolution sounder shows (*a*) a variation of scale height of approximately 0.2 scale heights per km; (*b*) a mean value of the recombination coefficient of $(2.0\pm0.5)\times10^{-8}$ cm^3 sec^{-1} during spring and summer; (*c*) vertical drift effects comparable to the effects of recombination.

551.510.535 3846

Some Aspects of Sporadic E at Mid-Latitudes—G. G. Bowman. (*Planet. Space Sci.*, vol. 2, pp. 195–211; August, 1960.) It is found that E_s ionization often occurs where the trough and crest slope lines of F_2-layer irregularities meet the E_s-layer level. This suggests that E_s and spread-F are caused by the same mechanism. A possible structure of E_s is proposed, and its relation to the occurrence of the green line of the airglow is discussed.

551.510.535 3847

The Equatorial F Region of the Ionosphere—R. A. Duncan. (*J. Atmos. Terr. Phys.*, vol. 18, pp. 89–100; June, 1960.) Critical frequencies in the F region at Panama and Chimbote are negatively correlated in the afternoon. This phenomenon, together with the diurnal variation in height, thickness and electron density of the equatorial F region, is consistent with the theory of ionization transportation from the equator to the subtropics, suggested by Martyn (755 of 1956).

551.510.535 3848
Electron Distribution in the F Layer of the Ionosphere over Haringhata (Calcutta) on Quiet and Disturbed Days—P. Bandyopadhyay. (*J. Atmos. Terr. Phys.*, vol. 18, pp. 127–134; June, 1960.) Electrondensity height profiles have been reduced for 1955 and compared with similar results for Slough and Maui. It was found that the scale height in the model given by Ratcliffe, *et al.*, (2724 of 1956) is 30 km for Calcutta.

551.510.535 3849
The Geographical Distribution of Ionization in the F_2 Layer—C. M. Minnis and G. H. Bazzard. (*J. Atmos. Terr. Phys.*, vol. 18, pp. 181–183; June, 1960.) Existing data are not sufficient to prove conclusively that the equatorial trough in f_0F_2 exists in the western hemisphere at certain times of the year.

551.510.535 3850
Equilibrium Electron Distributions in the Ionospheric F_2 Layer—H. Rishbeth and D. W. Barron. (*J. Atmos. Terr. Phys.*, vol. 18, pp. 234–252; June, 1960.) The equilibrium equation has been solved numerically for the daytime F region using isothermal and actual ionospheric models. At the F-layer peak, the effects of production, loss and plasma diffusion are approximately equal. Below the peak, diffusion is unimportant but becomes dominant above it where the electron distribution takes on an exponential form.

551.510.535 3851
The Temperature of the F_2 Region of the Upper Atmosphere as deduced from Ionospheric Measurements—M. W. McElhinny. (*Proc. Trans. Rhod. Sci. Assoc.*, vol. 47; pp. 37–46; March 1, 1960.) Chapman's theory has been extended to include the variation of an attachment-like loss coefficient with height in the F_2 region. Application of the theory to data obtained in the form of Kelso distributions shows that the region may be regarded as isothermal with a lower limit of 700°K.

551.510.535 3852
Triple Splitting with the F_2 Region of the Ionosphere at High- and Mid-Latitudes—G. G. Bowman. (*Planet. Space Sci.*, vol. 2, pp. 214–222; August, 1960.) Occurrence of the third (z-ray) component is investigated at various times of day, season and sunspot cycle and at different magnetic inclinations. A connection with the occurrence of spread-F is suggested.

551.510.535 3853
Possibility of Detecting Ionospheric Drifts from the Occurrence of Spread-F Echoes at Low Latitudes—R. W. Knecht. (*Nature*, vol. 187, p. 927; September 10, 1960.) Observations of the times of occurrence of spread-F echoes have been made at four stations in Peru. Results suggest that ionospheric drifts may play an important part in the occurrence of spread-F echoes at low latitudes.

551.510.535:523.5:621.396.96 3854
Diurnal Variations of Density and Scale Height in the Upper Atmosphere—J. S. Greenhow and J. E. Hall. (*J. Atmos. Terr. Phys.*, vol. 18, ppl 203–214; June, 1960.) The radio-echo meteor technique has been used to calculate the neutral-particle densities between 85 and 105 km. Diurnal oscillations in density are found with amplitudes of 6, 13 and 17 per cent at heights of 85, 95 and 100 km, respectively. Semidiurnal oscillations are also present, having approximately half these amplitudes.

551.510.535:523.78 3855
Photochemical Rates in the Equatorial F_2 Region from the 1958 Eclipse—T. E. Van Zandt, R. B. Norton and G. H. Stonehocker. (*J. Geophys. Res.*, vol. 65, pp. 2003–2009; July, 1960.) It is deduced that temperature changes and transport of electrons were probably negligible during the eclipse. Formulas are given for the rate of photoionization and the linear recombination coefficient as a function of height, and the total rate of absorption of energy in the F region is deduced.

551.510.535:539.16 3856
Geophysical Effects associated with the High-Altitude Nuclear Explosion—H. Uyeda, H. Maeda, A. Kimpara, T. Obayashi, S. Ishikawa and Y. Kawabata. (*J. Geomag. Geoelect.*, vol. 11, no. 2, pp. 39–63; 1959.) Collected papers are given on observations of atmospheric and geomagnetic disturbances associated with the explosions at Johnston Island on August 1, and 12, 1958.

551.510.535:550.385 3857
Hydromagnetic Wave Propagation in the Ionosphere—J. A. Fejer. (*J. Atmos. Terr. Phys.*, vol. 18, pp. 135–146; June, 1960.) General equations governing hydromagnetic wave propagation are obtained, assuming approximations valid for the ionosphere. For wave periods of less than 1h, the equations are very similar to those for the propagation of radio waves in the ionosphere.

551.510.535:550.385.37 3858
On the Ionospheric Heating by Hydromagnetic Waves Connected with Geomagnetic Micropulsations—S. I. Akasofu. (*J. Atmos. Terr. Phys.*, vol. 18, pp. 160–173; June, 1960.) Heat production and consequent temperature increase are negligible.

551.510.535:621.391.812.63 3859
The Size of the Moving Irregularities in the F Region and the Spread Angle of the Radio Waves Scattered from Them.—S. R. Khastgir and R. N. Singh. (*J. Atmos. Terr. Phys.*, vol. 18, pp. 123–126; June, 1960.) An analysis of fading patterns, obtained by a three-receiver method, discloses an average length of irregularity of 270 m with an average spread angle of 6°.

551.510.535:621.391.812.63 3860
Incoherency of Pulse Echoes and the Measurement of Ionospheric Absorption—J. Taubenheim. (*J. Atmos. Terr. Phys.*, vol. 18, pp. 147–151; June, 1960.) Incoherently scattered energy gives rise to errors in absorption measured by the pulse echo method. Calculations of the magnitude of the error are confirmed by experimental observations.

551.510.535(98):550.354.4 3861
Polar Ionospheric Disturbances associated with a Severe Magnetic Storm—T. Obayashi. (*J. Geomag. Geoelect.*, vol. 10, no. 1, pp. 28–35; 1958.) A detailed investigation of the storm on October 28, 1951, is made, using world-wide geomagnetic and ionospheric data.

551.510.535(98):550.585.4 3862
Morphology of the Ionospheric F_2 Disturbances in the Polar Region—T. Sato. (*Rep. Ionos. Space Res. Japan*, vol. 13, pp. 91–104; June, 1959.) An analysis is made of IGY data for July, 1957–February, 1958.

551.510.535(99) 3863
Anomalous f_0F_2 Variations in the Antarctic—G. E. Hill. (*J. Geophys. Res.*, vol. 65, pp. 2011–2023; July, 1960). "The daytime minimum in the F_2-layer critical frequency which is often observed in the Antarctic is explained on the basis of a vertical shear in the horizontal wind and the resulting movement of charged particles in the presence of the earth's magnetic field."

551.510.62:621.391.812.621 3864
Models of the Atmospheric Radio Refractive Index—Misme, Bean and Thayer. (See 4010.)

551.594.2:551.508.76 3865
Lightning Counter and Results Obtained in Sweden during the Thunderstorm Period 1958—D. Müller-Hillebrand. (*TVF, Stockholm*, vol. 30, no. 6, pp. 217–233; 1959. In English.) Tests performed on a Pierce-Gode cold-triode counter show that it records both strokes to earth and discharges between clouds.

551.594.21 3866
The Electrical Structure of Thunderstorms—Y. Tamura, T. Ogawa and A. Okawati. (*J. Geomag. Geolect.*, vol. 10, no. 1, pp. 20 27; 1958.) A model representing the structure of thunderstorm electricity has been developed from an analysis of simultaneous observations of thunderstorms in the vicinity of Kyoto, Japan.

551.594.5:621.391.812.63 3867
The Scattering of 36-Mc/s Radio Waves by Weak Auroral Ionization—Greenhow, Neufeld and Watkins. (See 4016.)

551.594.5:621.391.812.63.029.62 3868
The Distribution of Radio Aurora in Central Canada—P. A. Forsyth, F. D. Green and W. Mah. (*Canad. J. Phys.*, vol. 38, pp. 770–778; June, 1960.) The results of five months' observations using bistatic VHF radio systems are described. Nighttime and daytime events are detected and their distributions compared. See also 2001 of 1959 (Collins and Forsyth).

551.594.6 3869
Association between Aurorae and Very-Low-Frequency Hiss Observed at Byrd Station, Antarctica—L. H. Martin, R. A. Helliwell and K. R. Marks. (*Nature*, vol. 187, pp. 751–753; August 27, 1960.)

551.594.6 3870
Observations of "Whistlers" and "Chorus" at the South Pole—L. H. Martin. (*Nature*, vol. 187, pp. 1018–1019; September 17, 1960.)

551.594.6 3871
A Study of "Chorus" Observed at Australian Stations—J. Crouchley and N. M. Brice. (*Planet. Space Sci.*, vol. 2, pp. 238–245; August, 1960.) The variation of occurrence with geomagnetic latitude, time of day and K-index has been studied. Possible movements of the generating region are deduced.

551.594.6 3872
The Current-Jet Hypothesis of Whistler Generation—W. C. Hoffman. (*J. Geophys. Res.*, vol. 65, pp. 2047–2054; July, 1960.) The suggested mechanism involves the interaction between an electron stream traveling upwards, as the result of a lightning discharge, and the em radiation from a second discharge.

551.594.6 3873
Some Comments on the Penetration of Whistlers through Ionospheric Layers—H. Norinder. (*Planet. Space Sci.*, vol. 2, pp. 261–262; August, 1960.) Ionospheric irregularities, smaller than the whistler wavelength, may prevent penetration of the layer and lead to the cessation of whistlers at certain times. See, *e.g.*, 149 of January (Budden).

551.594.6 3874
Hyperbolic Direction Finding with Sferics of Transatlantic Origin—E. A. Lewis, R. B. Harvey and J. E. Rasmussen. (*J. Geophys. Res.*, vol. 65, pp. 1879–1905; July, 1960.) A description is given of a system for locating thunderstorms by measurement of the time difference of arrival of atmospherics at several

stations. Position lines for sources in the Atlantic were established from a network in the U. S. and compared with fixes from a UK DF network.

551.594.6 3875
Some Measurements of Atmospheric Noise Levels at Low and Very Low Frequencies in Canada—C. A. McKerrow. (*J. Geophys. Res.*, vol. 65, pp. 1911–1926; July, 1960.) Values are expressed in terms of mean noise power and are compared with predictions. Effects of location of source and propagation conditions are discussed. Amplitude/frequency curves are studied in detail.

551.594.6:621.391.812.6.029.45 3876
V.L.F. Attenuation for East-West and West-East Daytime Propagation using Atmospherics—Taylor. (See 4004.)

LOCATION AND AIDS TO NAVIGATION

621.396.9:621.391.812.63 3877
Recording-Type Direction Finder—K. Miya ank S. Matsushita. (*Rep. Ionos. Space Res. Japan*, vol. 13, pp. 120–122; June, 1959.) A brief description is given of a pen-recorder system for use with the direct-vision direction finder [465 of 1958 (Miya, *et al.*)].

621.396.93 3878
An All-Wave Cathode-Ray Direction Finder using the Two-Channel Principle—M. Wachtler. (*Nachrichtentech. Z.*, vol. 12, pp. 449–451; September, 1959.) The equipment described incorporates interchangeable units to cover various frequency bands.

621.396.933:621.396.969.11 3879
Direction-Finding Experience and the Performance of Transmitting Navigational Aids—H. G. Hopkins. (PROC. IRE, vol. 48, pp. 1481–1482; August, 1960.)

621.396.934:621.398 3880
The Construction of Missile Guidance Codes Resistant to Random Interference—A. R. Eckler. (*Bell Sys. Tech. J.*, vol. 39, pp. 973–994; July, 1960). The problem of selection of codes which satisfy the restrictions necessary to prevent formation of false commands by random interference is considered.

621.396.96 3881
Application to Radar of the Phenomenon of the Reflection of Electromagnetic Waves by the Ground—R. Richter, J. Bessis and P. Catella. (*Onde élect.*, vol. 40, pp. 392–410; May, 1960.) Factors influencing the range of coverage of a radar signal propagated over irregular ground are analyzed.

621.396.96:551.51 3882
Radar Echoes from Atmospheric Inhomogeneities—R. F. Jones. (*Quart. J. R. Met. Soc.*, vol. 86, pp. 116–118; January, 1960.) Discussion of 819 of 1959.

621.396.96:621.398 3883
Remote Transmission of the Angular Position of a Shaft Rotating at a Uniform Average Speed—K. Dinter. (*Nachrichtentech. Z.*, vol. 12, pp. 491–496; October, 1959.) The transmission of the information relating to the fluctuations in rotational speed of radar antennas to a distant point where the speed is to be accurately reproduced is considered. Calculations are based on a series of measurements carried out on a surveillance radar installation, and a practical transmission system is described.

621.396.962.3 3884
An Adjustable Polarizer for the Suppression of Rain Echoes in Pulse Radar—M. H. Bodmer. (*Tijdschr. ned. Radiogenoot*, vol. 24, nos. 2/3, pp. 63–70; 1959.) Using left-hand circularly polarized waves for the transmission, the receiver is made sensitive to left-hand polarized echoes only, thus eliminating the right-hand polarized echoes from rain drops which are assumed to be spherical. Rain echo suppression of better than 20 db can be achieved.

621.396.962.3 3885
The Theory and Design of Chirp Radars—J. R. Klauder, A. C. Price, S. Darlington and W. J. Albersheim. (*Bell Sys. Tech. J.*, vol. 39, pp. 745–808; July, 1960.) A new radar technique which provides simultaneous long-range and high-resolution performance is described. A long high-duty-factor pulse is used with linear frequency modulation, giving a greatly increased signal bandwidth of which optimum use is made. Details adopted of the analytical methods and circuit techniques and of the effect of distortion are given.

621.396.969.181.4 3886
The Design of Radar Signals having both High Range Resolution and High Velocity Resolution—J. R. Klauder. (*Bell Sys. Tech. J.*, vol. 39, pp. 809–820; July, 1960.) The fundamental limitations of simultaneous range and velocity determinations are discussed in terms of ambiguity diagrams. Signals having the desired properties can be found, but their waveforms are not suitable for maximum efficiency. See also 3885 above.

MATERIALS AND SUBSIDIARY TECHNIQUES

533.58 3887
Use of the Omegatron in the Determination of Parameters Affecting Limiting Pressures in Vacuum Devices—D. Lichtman. (*J. Appl. Phys.*, vol. 31, pp. 1123–1221; July, 1960.) The omegatron mass spectrometer is used to determine the residual gases in vacuum systems difficult to outgas.

535.215 3888
Analysis of Composite Spectral-Sensitivity Functions—J. S. Anderson, E. A. Faulkner and D. F. Klemperer. (*Aust. J. Phys.*, vol. 12, pp. 469–470; December, 1959). The two parts of the spectral sensitivity curve obtained from measurements of photoemission on certain semiconductors are interpreted in terms of two emitting mechanisms which act independently.

535.215:546.48'221 3889
Frequency Factor and Energy Distribution of Shallow Traps in Cadmium Sulphide—J. J. Brophy and R. J. Robinson. (*Phys. Rev.*, vol. 118, pp. 959–966; May 15, 1960.) Current-noise and photoconductivity measurements on CdS single crystals under uniform 5200 Å illumination are used to derive the energy distribution and frequency factor of shallow traps.

535.215:546.48'221 3890
Saturation of Photocurrent with Light Intensity—R. H. Bube. (*J. Appl. Phys.*, vol. 31, pp. 1301–1302; July, 1960.) Specially prepared pure crystals of CdS were used. The sensitivity of the crystal fell with increasing light intensity but complete saturation was not reached. A discussion of the possible mechanism is given.

535.37:546.48'221 3891
Measurement of the Temperature Dependence of the Luminescence of CdS—K. Albers. (*Z. Naturforsch*, vol. 14a, pp. 1002–1002; November, 1959.) A preliminary discussion of some observations of luminescence changes with temperature in CdS crystals is presented.

535.37:546.48'221 3892
Mechanically-Excited Emission in Cadmium Sulphide—D. M. Warschauer and D. C. Reynolds. (*J. Phys. Chem. Solids*, vol. 13, pp. 251–256; June, 1960.)

535.376 3893
Investigations of Cathodothermoluminescence: Part 1—D. Hahn and K. Lertes. (*Z. Phys.*, vol. 156, pp. 425–435; September 23, 1959.) Measurements were made on $CaWO_4$, Zn_2S, Zn_2O, Zn_2SiO_4Mn, and other phosphors to investigate the variation of cathodoluminescence as a function of temperature, in view of the results obtained by Bril, *et al.*, (2624 of 1959). The effects observed are attributed to pressure fluctuations in the CRT used for the experiment.

535.376.546.47'221 3894
The Enhancement and Quenching of Luminescence in Manganese-Activated Zinc Sulphides by Electric Fields—H. Gobrecht and H. E. Gumlich. (*Z. Phys.*, vol. 156, pp. 436–445; September 23, 1959.) A continuation of earlier experimental investigations (1462 of 1957) of luminescence characteristics as a function of field strength, frequency, excitation, and activator content is made.

537.226:621.396.677.85 3895
Artificial Anisotropic Dielectrics formed of Two-Dimensional Lattices of Infinite Strips and Rods—N. A. Khizhnak. (*Zh. Tekh. Fiz.*, vol. 29, pp. 604–614; May, 1959.) Expressions for effective permittivity are derived, and permeability and dispersive properties are examined with reference to rod cross section and lattice geometry.

537.227 3896
On the Isotopic Effects in the Ferroelectric Behaviour of Crystals with Short Hydrogen Bonds—R. Blinc. (*J. Phys. Chem. Solids*, vol. 13, pp. 204–211; June, 1960.)

537.227 3897
Ferroelectric Properties of Lead Metatantalate—V. A. Isupov. (*Fiz. Tverdogo Tela*, vol. 1, pp. 242–245; February, 1959.)

537.227:546.431'824-31 3898
180° Domain Wall Motions in $BaTiO_3$ Crystal—K. Husimi. (*J. Phys. Soc. Japan*, vol. 15, p. 731; April, 1960.) Wall motion for high-field switching has been studied.

537.227:546.431'824-31:537.312.9 3899
Piezoresistivity in Semiconductive Barium Titanates—O. Saburi. (*J. Phys. Soc. Japan*, vol. 15, pp. 733–734; April, 1960.) A note is made on temperature dependence of the piezoresistivity observed in the system of semiconducting $(Ba, Sr)TiO_3$ doped with Ce, which has an anomalous positive temperature characteristic of resistivity.

537.228.1 3900
Response of a Loaded Idealized Piezoelectric Plate to an Electric Signal—L. Levi. (*J. Appl. Phys.*, vol. 31, pp. 1237–1242; July, 1960.) The response is derived on the basis of close approximations to practical systems. The solution is applicable to other electromechanical transducers.

537.228.1:546.48'221 3901
Measurement of Piezoelectric Constants of a CdS Crystal—T. Tanaka and S. Tanaka. (*J. Phys. Soc. Japan*, vol. 15, p. 726; April, 1960.) Experimental values are given.

537.228.1:549.514.51 3902
Topography and Etch Patterns of Synthetic Quartz—F. Augustine and D. R. Hale. (*J. Phys. Chem. Solids*, vol. 13, pp. 344–346; June, 1960.)

537.228.1:549.514.51 3903
The Effect of Impurities on the Growth of Synthetic Quartz—C. S. Brown and L. A. Thomas. (*J. Phys. Chem. Solids*, vol. 13, pp. 337–343; June, 1960.)

537.228.1:549.514.51 3904
Defects in Natural and Synthetic Quartz—G. W. Arnold, Jr. (*J. Phys. Chem. Solids*, vol. 13, pp. 306–320; June, 1960.) 76 references.

537.311.33 3905
Semiconducting Mixed Crystals of the Type $(A^{I}_{x/2}|B^{IV}_{1-x}|C^{V}_{x/2}|)D^{VI}$—H. Fleischmann, O. G. Folberth and H. Pfister. (*Z. Naturforsch.*, vol. 142, pp. 999–1000; November, 1959). The mixed crystals investigated, *e.g.*, those of the system $(Ag_{x/2}Pb_{1-x}\ Bi_{x/2})$ Te, have a very low thermal conductivity combined with a relatively high electrical conductivity. See also 2413 of July (Folberth).

537.311.33 3906
Carrier Recombination in Semiconductors after High Excitation—M. Zerbst, G. Winstel and W. Heywang. (*Z. Naturforsch.*, vol. 14a, pp. 958–962; November, 1959.) Calculated values of the decay of carrier concentration are compared with experimental results obtained on Si [2798 of August (Zerbst and Heywang)].

537.311.33 3907
The Problem of Exo-electron Emission—R. Seidl. (*Naturwiss.*, vol. 46, pp. 573–574; October, 1959.) An interpretation of exo-electron emission effects on the basis of lattice-defect interactions is given. See also 1686 of May (Menold).

537.311.33 3908
Analysis of the Effects of Multiply Charged Impurities in Semiconductors by the Mass Action Law—N. H. Saunders. (*J. Electronics Control*, vol. 8, pp. 91–96; February, 1960.)

537.311.33 3909
Surface Transport in Semiconductors—R. F. Greene, D. R. Frankl and J. Zemel. (*Phys. Rev.*, vol. 118, pp. 967–975; May 15, 1960.) For diffuse, surface scattering, the effective surface mobilities may differ significantly from the bulk mobility for any strength of space-charge layer. Agreement with Schrieffer's formulas (2322 of 1955) is found only for strong space-charge layers.

537.311.33 3910
Rectification without Injection at Metal-to-Semiconductor Contacts—N. J. Harrick. (*Phys. Rev.*, vol. 118, pp. 986–987; May 15, 1960.) Extraction in the semiconductor bulk may occur for either direction of current flow through the same metal-to-semiconductor contact when an insulating layer separates the metal and the semiconductor. Strong rectification without injection may occur for such contacts to extrinsic, but not intrinsic, semiconductors. See also 927 of March.

537.311.33:535.215:538.63 3911
The Application of the Photomagnetoelectric Effect to the Measurement of Surface Recombination Velocity—T. I. Galkina. (*Fiz. Tverdogo Tela*, vol. 1, pp. 216–217; February, 1959.) A formula for calculating the surface recombination velocity from the effective lifetime in thin Ge specimens is given. An increased PME voltage is observed as the illuminated strip approaches the ends of the specimen. The application of this for estimating the recombination velocity at the contacts is suggested.

537.311.33:535.5 3912
Double Refraction of Uniaxial Semiconductor Crystals—A. V. Sokolov, G. I. Kharus and V. P. Shirokovskiĭ. (*Fiz. Tverdogo Tela*, vol. 1, pp. 354–356; February, 1959.) Equations are derived showing that the refractive indexes for radiation polarized parallel and perpendicular to the z axis have quite different values, and indicating applications for infrared polarization filters.

537.311.33:537.312.9 3913
Effects of Hydrostatic Pressure on the Piezoresistance of Semiconductors: $i-$InSb, $p-$Ge, $p-$InSb, and $n-$GaSb—R. W. Keyes and M. Pollak. (*Phys. Rev.*, vol. 118, pp. 1001–1007; May 15, 1960.) A method of measuring the piezoresistance of a sample under high hydrostatic pressure by comparison with intrinsic InSb is described. Measurement of the piezoresistance of n-GaSb as a function of pressure up to 12000 kg/cm² provides confirmation of the correctness of Sagar's conduction-band model (2448 of July).

537.311.33:538.63 3914
Magnetoelectric and Thermomagnetoelectric Effects in Semiconductors—L. Godefroy and J. Tavernier. (*J. Phys. Radium*, vol. 21, pp. 249–260; April, 1960.) The electrical conductivity of a crystal in the presence of a magnetic field is investigated by the method of average energy gain. Results are applied to Ge and Si models.

537.311.33:538.632 3915
Hall Effect in Semiconductors with p-n Junctions—O. Madelung. (*Z. Naturforsch.*, vol. 14a, pp. 951–958; November, 1959.) The existence of floating potentials in p-n junctions is investigated for the case of ambipolar currents caused by the Lorentz field. The theory developed is used to provide a partial explanation of the anomalous temperature characteristics of the Hall coefficient, discussed, *e.g.*, by Rupprecht (3385 of 1959.)

537.311.33:546.23 3916
The Electrical Properties of Polycrystalline Selenium with Halogen Impurities (Br_2, Cl_2, I_2)—D. S. Gel'khman, V. N. Romankevich and V. G. Sidyakin. (*Fiz. Tverdogo Tela*, vol. 1, pp. 218–226; February, 1959.)

537.311.33:546.28 3917
Gamma-Irradiation of Silicon: Part 1—Levels in n-Type Material Containing Oxygen—E. Sonder and L. C. Templeton. (*J. Appl. Phys.*, vol. 31, pp. 1279–1286; July, 1960.)

537.311.33:546.28 3918
Shallow Impurity Traps and Electron Transfer Dynamics in n-Type Silicon at Liquid Helium Temperatures—A. Honig and R. Levitt. (*Phys. Rev. Lett.*, vol. 5, pp. 93–96; August 1, 1960.) Experiments which give data on electron transfer concentrations and trapping cross sections for P and B impurities are described.

537.311.33:546.28 3919
Vacancy Interactions in Silicon—H. H. Woodbury and G. W. Ludwig. (*Phys. Rev. Lett.*, vol. 5, pp. 96–97; August 1, 1960.) Vacancies were introduced into Si by the precipitation of Cu, or by electron irradiation, and their interactions with Mn or Cr impurities were studied by spin resonance techniques.

537.311.33:546.28 3920
Electronic Structure of Transition Metal Ions in a Tetrahedral Lattice—G. W. Ludwig and H. H. Woodbury. (*Phys. Rev. Lett.*, vol. 5, pp. 98–100; August 1, 1960.) A model is deduced from electron spin resonance measurements on Si.

537.311.33:546.28 3921
Impurity Redistribution and Junction Formation in Silicon by Thermal Oxidation—M. M. Atalla and E. Tannenbaum. (*Bell Sys. Tech. J.*, vol. 39, pp. 933–946; July, 1960.) Impurities redistribute themselves between a growing oxide film and the parent Si in a manner depending on the diffusion and distribution coefficients. The phenomenon is analyzed and the formation of single- or two-junction material is predicted. Experimental confirmation is given.

537.311.33:546.28 3922
Uniform Silicon p-n Junctions: Part 1—Broad Area Breakdown—R. L. Batdorf, A. G. Chynoweth, G. C. Davey and P. W. Foy. (*J. Appl. Phys.*, vol. 31, pp. 1153–1160; July, 1960.) Small area junctions have been made free from exposed edges and dislocations passing through the space-charge region. The avalanche breakdown phenomena in these uniform junctions are shown to be drastically different from those occurring in junctions containing many dislocations.

537.311.33:546.28 3923
Uniform Silicon p-n Junctions: Part 2—Ionization Rates for Electrons—A. G. Chynoweth. (*J. Appl. Phys.*, vol. 31, pp. 1161–1165; July, 1960.) Charge multiplication as a function of reverse bias has been studied in a number of junctions free from defects which promote local avalanche breakdown sites. From the multiplication characteristics, new data have been derived for the field dependence of the ionization rate for electrons. Part 1: 3922 above.

537.311.33:546.28 3924
Two-Phonon Indirect Transitions and Lattice Scattering in Si—W. P. Dumke. (*Phys. Rev.*, vol. 118, pp. 938–939; May 15, 1960.) Several of the intensity maxima in the intrinsic low-temperature emission spectrum of Si can be explained in terms of these indirect transitions.

537.311.33:546.28 3925
Reactions of Group III Acceptors with Oxygen in Silicon Crystals—C. S. Fuller, F. H. Doleiden and K. Wolfstirn. (*J. Phys. Chem. Solids*, vol. 13, pp. 187–203; June, 1960.) Conductivity and Hall measurements show that specific structures are formed. The mechanisms and precise structures have not been determined. Certain assumptions can explain most of the observations.

537.311.33:546.28 3926
Impact Ionization in Silicon. Saturation of the Phenomenon—A. Zylbersztejn. (*J. Electronics Control*, vol. 8, pp. 97–101; February, 1960. In French.) Experiments on three Si samples of different length cut from the same bar showed that the presence of contacts does not sensibly affect the saturation phenomenon. This was observed in conductivity measurements under pulse conditions at 20.75°K.

537.311.33:546.28 3927
Zeeman Effect of Impurity Levels in Silicon—S. Zwerdling, K. J. Button and B. Lax. (*Phys. Rev.*, vol. 118, pp. 975–986; May 15, 1960.) Zeeman spectra for the Bi donor and Al acceptor in Si are presented and used to study the energy band structure and the effective mass parameters.

537.311.33:546.28 3928
The Thermal Expansion of a Silicon Single Crystal—R. R. Bires and R. J. Horne. (*Proc. Phys. Soc. London*, vol. 75, pp. 793–795; May 1, 1960.)

537.311.33:546.28 3929
Crystal Potential and Energy Bands of Semiconductors: Part 3—Self-Consistent Calculations for Silicon—L. Kleinman and J. C. Phillips. (*Phys. Rev.*, vol. 118, pp. 1153–1167;

June 1, 1960.) A calculation of crystal potential from a superposition of free-atom core and a sampling of crystal valenceband charge densities are given. Part 2: 2424 of July.

537.311.33:546.28:541.135 3930
Electrode Phenomena in the System Single-Crystal Silicon/Caustic Soda—M. Seipt. (*Z. Naturforsch.*, vol. 14a, pp. 926–928; October, 1959.) The *I/V* characteristics and voltage distribution are investigated for current-carrying *n*- or *p*-type Si electrodes with or without illumination, and the photo-EMF is measured on current-free Si electrodes as a function of NaOH concentration. The results are discussed with reference to theoretical considerations of a semiconductor/electrolyte system.

537.311.33:546.28:669.046.54/.55 3931
Zone Melting of Silicon with an Electron Beam—V. Gusa, I. Krzhizh and I. Ladnar. (*Fiz. Tverdogo Tela*, vol. 1, pp. 290–293; February, 1959.) Application of the method to Si is based on focusing the electron beam by means of a specially shaped cathode and deflecting the beam by an electric field to shield the filament from sputtering.

537.311.33:546.289 3932
Investigation of the Lifetime of Minority Carriers in Germanium—T. Stubb. (*Acta. Polyt. Scand.*, no. 269, ph. 3, 17 pp.; 1960. In German.) The specimen is illuminated by light from sparks of variable intensity and repetition frequency. Various light filters and etching solutions are used to differentiate between bulk and surface recombination effects.

537.311.33:546.289 3933
Contribution to the Study of the Recombination of Excess Carriers in Germanium—C. Benoit à la Guillaume. [*Ann. Phys.* (*Paris*), vol. 4, pp. 1187–1237; September/October, 1959.] An analysis is made of recombination at dislocations and from band to band in Ge at low temperatures by measurement of the infrared emission spectra.

537.311.33:546.289 3934
Relation between Electrical Conductivity and Electron Density Distribution in Germanium Crystals—Yu. N. Shuvalov. (*Fiz. Tverdogo Tela*, vol. 1, pp. 208–215; February, 1959.) Variation of X-ray reflection intensities associated with increased conductivity caused by doping or heating is attributed to a redistribution of electron density leading to the formation of electron 'bridges' between nearest-neighbour atoms.

537.311.33:546.289 3935
Propagation Mechanism of Germanium Dendrites—D. R. Hamilton and R. G. Seidensticker. (*J. Appl. Phys.*, vol. 31, pp. 1165–1168; July, 1960.)

537.311.33:546.289 3936
Growth of Atomically Flat Surfaces on Germanium Dendrites—R. L. Longini, A. I. Bennett and W. J. Smith. (*J. Appl. Phys.*, vol. 31, pp. 1204–1207; July, 1960.)

537.311.33:546.289 3937
On the Kinetics and Mechanism of the Precipitation of Lithium from Germanium—J. R. Carter, Jr., and R. A. Swalin. (*J. Appl. Phys.*, vol. 31, pp. 1191–1200; July, 1960.)

537.311.33:546.289 3938
Measurement of Lifetime in Ge from Noise—S. Okazaki and H. Oki. (*Phys. Rev.*, vol. 118, pp. 1023–1024; May 15, 1960.) Experimental results of noise power measurements in which hole electron pairs are liberated by light are given.

537.311.33:546.289 3939
Measurement of Dielectric Constant of Germanium at Microwave Frequencies—T. Fukuroi and K. Yamagata. (*Sci. Rep. Res. Inst. Tohoku Univ., Ser. A*, vol. 11, pp. 285–295; August, 1959.)

537.311.33:546.289 3940
Effect of High Pressure on some Hot-Electron Phenomena in *n*-Type Germanium—S. H. Koenig, M. I. Nathan, W. Paul and A. C. Smith. (*Phys. Rev.*, vol. 118, pp. 1217–1221; June, 1960.) Measurements of pressure dependence of the current-density/electric-field characteristic at 297°K, and of the angle between current and field at 77°K, are discussed.

537.311.33:546.289 3941
Tunnelling Probability in Germanium *p-n* Junctions—Y. Furukawa. (*J. Phys. Soc. Japan*, vol. 15, p. 730; April, 1960.) A study of the density of the maximum tunneling current as a function of carrier concentration shows dependence on specific donor impurities.

537.311.33:546.289:538.569.4 3942
Power-Induced Shifts of Cyclotron Resonances in the Valence Band of Germanium—B. Levinger and D. R. Frankl. (*Phys. Rev. Lett.*, vol. 5, pp. 12–13; July, 1960.) Absorption measurements at 4.2°K and 1.4°K over a range of power levels at 24 kMc showed that the light-hole absorption and, in some orientations, the heavy-hole absorption shifted to slightly higher magnetic field strengths with increasing power.

537.311.33:546.3–31 3943
Electrical Properties and Structure of Compound Oxide Semiconductors: Part I—MnO-CuO-CoO-O_2 System—I. T. Sheftel', A. I. Zaslavskiĭ, E. V. Kurlina and G. N. Tekster-Proskuryakova. (*Fiz. Tverdogo Tela*, vol. 1, pp. 227–241; February, 1959.)

537.311.33:[546.68'18+546.68'19 3944
Preparation of Crystals of InAs, InP, GaAs and GaP by a Vapour-Phase Reaction—G. R. Antell and D. Effer. (*J. Electrochem. Soc.*, vol. 106, pp. 509–511; June, 1959.)

537.311.33:546.681'19 3945
Diffusion of Cadmium and Zinc in Gallium Arsenide—B. Goldstein. (*Phys. Rev.*, vol. 118, pp. 1024–1027; May 15, 1960.)

537.311.33:[546.682.19+546.682.86 3946
The Variation with Temperature of the Magnetic Susceptibility of InAs and InSb—G. Römelt, D. Geist and W. Schlabitz. (*Z. Naturforsch.*, vol. 14a, pp. 923–924; October, 1959.) The results of measurements of magnetic susceptibility at 90° and 300°K of *n*-type InAs and InSb as a function of electron density are discussed, together with the results of other authors.

537.311.33:546.682'19 3947
Heat Treatment Effects in Indium Arsenide—J. T. Edmond and C. Hilsum. (*J. Appl. Phys.*, vol. 31, pp. 1300–1301; July, 1960.) Experiments are described which indicate that heat treatment of InAs in ordinary silica causes a permanent change which reduces the electron concentration, and a temporary change which increases it. The temporary change is due to copper contamination from the container.

537.311.33:[546.682:19+546.682'18 3948
Infrared Faraday Rotation in InAs and InP—I. G. Austin. (*J. Electronics Control*, vol. 8, pp. 167–169; March, 1960.) Measurements have been made at room temperature over the range 2–17μ.

537.311.33:546.682'86 3949
Observation of Stark Splitting of Energy Bands by means of Tunnelling Transitions—A. G. Chynoweth, G. H. Wannier, R. A. Logan and D. E. Thomas. (*Phys. Rev. Lett.*, vol. 5, pp. 57–58; July 15, 1960.) The conductance of narrow *p-n* junctions of InSb immersed in liquid He shows an oscillation with variation of bias. This is attributed to the available energy states forming a series of Stark ladders.

537.311.33:546.682'86 3950
Magneto-tunnelling in InSb—A. R. Calawa, R. H. Rediker, B. Lax and A. L. McWhorter. (*Phys. Rev. Lett.*, vol. 5, pp. 55–57; July 15, 1960.) *I/V* characteristics at 77°K are shown for magnetic fields, parallel and perpendicular to the current flow, up to 88 kG. A marked decrease in the tunneling current with increased magnetic field is attributed to the creation of magnetic sub-bands and their shift in energy with magnetic field.

537.311.33:546.682'86:338.63 3951
Galvanomagnetic Phenomena in n-Type InSb in Pulsed Magnetic Fields—Kh. I. Amirkhanov, R. I. Bashirov and Yu. É. Zakiev. (*Dokl. Akad. Nauk SSSR*, vol. 132, pp. 793–796; June 1, 1960.) Results are given of experimental investigation of the Hall effect and the transverse and longitudinal magnetoresistance as a function of temperature and field strengths up to 900 kilo-oersteds.

537.311.33:546.723–31 3952
Electrical Conductivity of $\alpha-Fe_2O_3$—T. Nakau. (*J. Phys. Soc. Japan*, vol. 15, p. 727; April, 1960.) Measurements were made to examine any anisotropy and conductivity anomalies.

537.312.62:539.234 3953
Superconductivity of Iron Films—Yu. G. Mikhaĭlov, E. I. Nikulin, N. M. Revlnov and A. P. Smirnov. (*Zh. Tekh. Fiz.*, vol. 29, pp. 931–932; July, 1959.) Films of 10^{-5} cm thickness, freshly deposited at the rate of a few ångströms per minute, become superconducting at 4.2°K. At higher temperatures, the film returns to its normal state.

537.32:537.311.33 3954
Thermoelectric Investigations of $Zn_xCd_{1-x}Sb$—E. Justi, G. Neumann and G. Schneider. (*Z. Phys.*, vol. 156, pp. 217–234; September 23, 1959.) Discrepancies in the values of thermo-emf of ZnSb obtained by various authors are attributed to the presence of Zn_4Sb_3, Zn_3Sb_2 and Sb in the ZnSb specimens tested. With special heat treatment, a repeatable and higher value of the thermo-emf α is obtained, and an increase of α almost proportional to T is found for the temperature range 86°–365°K. Results of measurements of thermoelectric parameters of $Zn_xCd_{1-x}Sb$ as a function of Cd content are given; thermoelectric properties better than those of Bi_2Te_3 materials may be obtainable.

537.58 3955
Thermionic Properties of UC—G. A. Haas and J. T. Jensen, Jr. (*J. Appl. Phys.*, vol. 31, pp. 1231–1233; July, 1960.) Thermionic emission measurements using pulse techniques have been made on UC-coated W filaments in the temperature range 1200–2100°K.

537.58:621.385.032.212 3956
Cold-Emitting Cathode Materials—Y. Mizushima, Y. Igarashi and T. Imai. (*J. Phys. Soc. Japan*, vol. 15, p. 729; April, 1960.) Various materials have been studied for the possibility of cold emission. Results are noted.

538.221 3957
Ferromagnetic Anisotropy and Its Quantum-Theoretical Treatment by a Single-Electron Model.—K. Merkle. (*Z. Naturforsch.*, vol. 14a, pp. 938–951; November, 1959.) The investigations are based on a consideration of spin-orbit coupling.

538.221 3958
Thermomagnetic Behaviour of Ferromagnetic Domain Nuclei—P. F. Davis. [*Proc. Phys. Soc. (London)*, vol. 75, pp. 739–744; May 1, 1960.]

538.221 3959
Magnetization of a Dilute Suspension of a Multidomain Ferromagnetic—C. P. Bean and I. S. Jacobs. (*J. Appl. Phys.*, vol. 31, pp. 1223–1230; July, 1960.) The observed magnetization curve of a dilute suspension of carbonyl iron conforms to that derived from consideration of a dilute assembly of randomly oriented, single-crystal multidomain spheres.

538.221:538.569.4 3960
Theory of Magnetic Resonance in α-Fe_2O_3—P. Pincus. (*Phys. Rev. Lett.*, vol. 5, pp. 13–15; July 1, 1960.)

538.221:538.65 3961
Theory of the Temperature Dependence of the Magnetoelastic Constants of Cubic Crystals—C. Kittell and J. H. Van Vleck. (*Phys. Rev.*, vol. 118, pp. 1231–1232; June 1, 1960.)

538.221:538.65 3962
The Vibrations of a Ferromagnetic Material in an Alternating Magnetic Field—L. G. Ipatov. (*Zh. Tekh Fiz.*, vol. 29, pp. 662–667; May, 1959.) A formula is derived for the dynamic magnetostrictive force. Factors controlling the frequency of vibrations are discussed. For Permendur with a resonance frequency of 43.8 kc, magnetization-to-saturation causes a frequency shift of 520 cps.

538.221:538.652 3963
The Temperature Dependence of Magnetostriction in Polycrystalline Gadolinium—W. D. Corner and F. Hutchinson. [*Proc. Phys. Soc. (London)*, vol. 75, pp. 781–788; May 1, 1960.] The magnetostriction and magnetization have been measured between 78°K and 365°K. Results show that Gd has a large volume magnetostriction which is proportional to the square of the paramagnetic magnetization above the Curie point.

538.221:539.23 3964
Electron-Microscope Reproduction of Weiss Domains in Ferromagnetic Thin Films—H. Boersch and H. Raith. (*Naturwiss.*, vol. 46, p. 574; October, 1959.) Weiss domains can be reproduced with high resolution using a schlieren method particularly suitable for electrostatic electron microscopes.

538.221:621.318.134 3965
The Dependence of the Measured Physical Properties of Ferrites on the Sintering Temperature—H. Hultschig. (*Nachrtech.*, vol. 9, pp. 390–391; September, 1959.) The importance of physical measurements in assessing ferrite quality is briefly discussed.

538.221:621.318.134 3966
Electrical Measurements on Magnetically Soft Ferrites—H. Henninger, H. Rudloff and G. Engelhardt. (*Nachrtech.*, vol. 9, pp. 392–395; September, 1959.) Methods of measurement and typical results obtained for various types of ferrite are reviewed.

538.221:621.318.134:537.311.33 3967
On the Spin Mechanism of Recombination of Current Carriers in Ferromagnetic Semiconductors—V. L. Bonch-Bruevich. (*Fiz. Tverdogo Tela*, vol. 1, pp. 186–191; February, 1959.) The process of carrier recombination in ferrites in which liberated energy is transferred to spin waves is discussed. The dependence of the recombination coefficients on temperature and saturation magnetization is determined.

538.221:621.318.134:538.569.4 3968
Interaction of Phonons and Spin Waves in Yttrium Iron Garnet—E. H. Turner. (*Phys. Rev. Lett.*, vol. 5, pp. 100–101; August 1, 1960.) Measurements of spinwave resonance linewidth on a Y-Fe garnet sphere show evidence of the coupling of spinwaves to phonons of the same frequency and wave number.

538.221:621.318.134:538.569.4 3969
Microwave Properties of Nonstoichiometric Polycrystalline Yttrium Iron Garnet—P. E. Seiden, C. F. Kooi and J. M. Katz. (*J. Appl. Phys.*, vol. 31, pp. 1291–1296; July, 1960.) A systematic investigation as a function of Y/Fe ratio is made.

538.221:621.318.134:538.69 3970
Piezomagnetic Ferrites—C. M. van der Burgt. (*Electronic Tech.*, vol. 37, pp. 330–341; September, 1960.) The properties of Ni-Cu-Co ferrites and their applications as transducers in bandpass filters and high-power ultrasonics are described in detail.

538.632 3971
Hall Effect and Intrinsic Hall Effect in Normal Conductors and Superconductors—R. Jaggi and R. Sommerhalder. (*Helv. Phys. Acta*, vol. 32, pp. 167–196; June 30, 1959. In German.) Suitable specimen shapes, probe arrangements for plate-shaped and cylindrical specimens, and methods for the measurement of Hall-effect, with or without external magnetic field, are discussed. The results of measurements on cylindrical specimens of single-crystal *p*-type InSb are given. The problem of Hall effect in superconductors is also investigated on the basis of experimental work.

539.23:546.883–31:621.319.45 3972
***p-i-n* Junction in the Anodic Oxide Film of Tantalum**—Y. Sasaki. (*J. Phys. Chem. Solids*, vol. 13, pp. 177–186; June, 1960.) To clarify the structure of the film, photoeffects and variation of capacitance with applied bias potential were studied for relatively thin films. Results indicate the formation of a *p-i-n* junction in the oxide film.

548.0 3973
A Method of Evaluating Diffusion Coefficients in Crystals—O. P. Manley. (*J. Phys. Chem. Solids*, vol. 13, pp. 244–250; June, 1960.) The mechanism of diffusion proposed by Rice (*Phys. Rev.*, vol. 112, pp. 804–811; November 1, 1958) is reconsidered.

MATHEMATICS

513.83:621.318.57 3974
Topological Methods and Applications—L. Sideriades. (*Ann. Télécommun.*, vol. 14, pp. 185–207; July/August, 1959.) A study is made of electronic switching systems.

517.512.2:621.372.44 3975
Function Transforms for the Study of Nonlinear Systems—R. Codelupi. (*Note Recensioni Notiz.*, vol. 8, pp. 478–495; September, October 1959.) A calculation of the Fourier transform of the output voltage from a nonlinear circuit element using a distortion function and a function expressing the input voltage variation with time is presented.

MEASUREMENTS AND TEST GEAR

621.3.018.41(083.74) 3976
The 'GBR Experiment': a Transatlantic Frequency Comparison between Caesium-Controlled Oscillators—J. A. Pierce, G. M. R. Winkler and R. L. Corke. (*Nature*, vol. 187, pp. 914–916; September 10, 1960.) Fluctuations in transmission time are responsible for an error of about two parts in 10^{9} in transatlantic frequency measurements over a 24-hour period.

621.3.018.41(083.74) 3977
Technical Equipment of the Quartz Clock Installation for the Control of Standard-Frequency Transmissions of the Physikalisch-Technische Bundesanstalt over the Transmitter DCF 77—R. Süss. (*Nachrichtentech. Z.*, vol. 12, pp. 475–476; September, 1959.) See also 3610 of October (Ohl).

621.3.018.41(083.74):389.2 3978
Experimental Timing Code Added to WWV Broadcasts—(*Tech. News Bull. NBS*, vol. 44, pp. 114–115; July, 1960.) The code designates day, hour, minute and second (UT) and is broadcast for 1-minute intervals ten times per hour on 2.5, 5, 10, 15, 20 and 25 Mc.

621.317.3:621.391.822:519.24 3979
Approximate Distributions of Noise Power Measurements—W. Freiberger and U. Grenander. (*Quart. Appl. Math.*, vol. 17, pp. 271–283; October, 1959.) An analytical and numerical treatment is presented of the frequency functions of certain spectral estimates.

621.317.3.029.6 3980
Measurement of Small Voltages and Power at Hyper-Frequencies—N. Inage. (*Rep. elect. Commun. Lab., Japan*, vol. 7, pp. 448–466; December, 1959.) Voltages up to 1 mv have been measured at frequencies up to several Mc, to an accuracy within ± 2 per cent and powers up to 10–15 watts to within ± 5 per cent by reference to a standard level derived either from a barretter or a noise generator.

621.372.413 3981
Field Measurements in Resonant Cavities—D. K. Callebaut and M. C. Vanwormhoudt. (*Physica*, vol. 26, pp. 255–258; April, 1960.) The perturbation method of Maier and Slater (2265 of 1952) has been simplified using a cylinder as the perturbing body, with its axis parallel to the electric field. In this case, the shape of the cylinder will be a function of α, the ratio of the height to the radius of the cylinder, which allows the electric field to be determined from a single perturbation measurement. The function $f(\alpha)$ has been determined experimentally and found to be nearly linear when $\alpha < 2$.

621.317.335:537.227 3982
Nondestructive Measuring Method of Polarization for the Study of Ferroelectrics—K. Husimi and K. Kataoka. (*Rev. Sci. Instr.*, vol. 31, pp. 418–421; April, 1960.) A measurement of the piezoelectric output voltage of a ferroelectric crystal in an ultrasonic field is used to determine the state of polarization of the crystal.

621.317.335.3:621.372.413 3983
On an Absolute Method of Measurement of Dielectric Parameters of a Solid using a H-Shaped Resonator—O. V. Karpova. (*Fiz. Tverdogo Tela*, vol. 1, pp. 246–255; February, 1959.) Expressions are derived relating the permittivity of a cylindrical sample filling the space between the cavity arms to the resonance wavelength, and the loss tangent to the cavity Q. These expressions have been applied to measurements at dm λ on polystyrene, TiO_2, etc., and results are given. See also 2657 of 1956 (Patrushev).

621.317.335.3.029.6:621.372.826 3984
Application of Slow Surface Waves for the Measurement of Dielectric Constants of Substance at Ultra High Frequencies: Part 1—V. P. Shestopalov and K. P. Yatsuk. (*Zh. Tekh. Fiz.*, vol. 29, pp. 819–830; July, 1959.) See 3614 of October.

621.317.432:620.19 3985
An Eddy-Current Flaw Detector—E. Ruff. (*Elec. Engrg.*, vol. 32, pp. 480–483; August,

1960.) A search coil probe energized at a frequency of 6 kc placed in airframe bolt holes provides eddy current penetration of the surrounding metal to a depth of 1 mm. Changes of path length caused by cracks are detected by a bridge comparison network.

621.317.7:621.373.078 3986
Feedback Stabilizes Signal Generator—A. Fong. (*Electronics*, vol. 33, pp. 71–73; July 15, 1960.) Details of the performance and circuit of a 50-kc–65-Mc signal generator with output signal levels stabilized by negative feedback to within ±1 db are given.

621.317.7:621.396.934 3987
Automatic Test Equipment Checks Missile Systems—D. B. Dobson and L. L. Wolff. (*Electronics*, vol. 33, pp. 74–78; July 15, 1960.) A description is given of digital evaluation equipment (DEE) for checking electronic subassemblies of missiles and the associated ground equipment. Punched tapes are used to select the tests.

621.317.763.029.6 3988
Accurate Microwave Wavemeters with Convenient Calibration Tables—N. E. Bussey and A. J. Estin. (*Rev. Sci. Instr.*, vol. 31, pp. 410–413; April, 1960.) Principles of design of cavity-type wavemeters giving an accuracy within 0.02 Mc at 9 kMc are discussed, and a procedure for constructing a calibration table containing 10^4 entries is described.

621.317.794 3989
Criteria for the Choice of a Superconducting Bolometer—B. Lalevic. (*J. Appl. Phys.*, vol. 31, pp. 1234–1236; July, 1960.) The correlation between the noise and the value of the surface boundary energy (interface between normal and superconducting laminas) is used as the basis for the choice of a superconducting bolometer and its minimum dimensions.

621.317.794:621.391.822 3990
A Low-Frequency Noise Generator—N. T. Slater. (*Elec. Engrg.*, vol. 32, pp. 473–475; August, 1960.) The construction of a 10-volt noise generator for the range 0.01 20 cps is described. Use of high-grain dc amplifiers is avoided by amplifying the noise in a frequency band of 2–8 kcs and using a sampling technique for conversion to LF noise.

OTHER APPLICATIONS OF RADIO AND ELECTRONICS

535.376:681.6 3991
A Review of Panel-Type Display Devices—J. J. Josephs. (PROC. IRE, vol. 48, pp. 1380–1395; August, 1960.) 67 references.

537.533:621.7 3992
Electron-Beam Processes—T. Maguire. (*Electronics*, vol. 33, pp. 59 63; July 15, 1960.) The applications of electron beams as heat sources in microminiature machining, melting, evaporation-welding and sintering are discussed. Suggested basic designs with a graph of process times and power requirements are given.

621.38:523+55+57+61 3993
Electronics Probes Nature—Bushor and Wolff. (See 3806.)

621.384.622 3994
Variable-Phase Focusing in Linear Accelerators—Ya. B. Fainberg. (*Zh. Tekh. Fiz.*, vol. 29, pp. 568–579; May, 1959.) A mathematical analysis is made of the relation of radial and phase instability with reference to focusing methods.

621.384.7:621.372.8 3995
On the Possibility of Mass Separation of Relativistic Charged Particles by Means of Travelling-Wave Waveguides—D. V. Volkov. (*Zh. Tekh. Fiz.*, vol. 29, pp. 414–416; March, 1959.) A note on the conditions necessary for particle separation in a high-energy bunched electron beam is given. Separation is effected by virtue of the transverse component of the Lorentz force caused by the traveling em field in the waveguide.

621.385.833 3996
On the Effect of the Thickness of the Focusing Electrode on the Optical Properties of an Electrostatic Immersion Objective—A. M. Rozenfel'd. (*Zh. Tekh. Fiz.*, vol. 29, pp. 584–588; May, 1959.) An investigation shows that refracting power does not depend on electrode thickness h. For practical use, the focal length must not be less than $3h$.

621.385.833 3997
Image Defects of Cathode Electron Lenses with Deviations from Axial Field Symmetry—Yu. V. Vorob'ev. (*Zh. Tekh. Fiz.*, vol. 29, pp. 589–596; May, 1959.)

621.385.833 3998
Theoretical Investigations of Image Distortion in Electron Diffraction Images—H. Noven and F. Lenz. (*Z. angew. Phys.*, vol. 11, pp. 375–380; October, 1959.) The distortion due to magnetic electron lenses interposed between object and image is investigated.

621.385.833 3999
An Extension of the Field of Application of the Focal Length Formula for Simple Aperture Lenses—J. Hoeft. (*Z. angew. Phys.*, vol. 11, pp. 380–382; October, 1959.) The conventional formula is modified to cover the case of large-aperture diaphragms. Experimental results for three different electrode systems are compared with calculated values.

621.387.464(083.7) 4000
I.R.E. Standards on Nuclear Techniques: Definitions for the Scintillation Counter Field, 1960—(PROC. IRE, vol. 48, pp. 1449–1453; August, 1960.)

621.398:536.5:538.569 4001
Using Nuclear Resonance to Sense Temperature—C. Dean. (*Electronics*, vol. 33, pp. 52–54; July 8, 1960.) Circuit details are given of a telemetry modulation system in which signals specifying the nuclear quadrupole resonance frequency of $KClO_3$ are transmitted. The resonant frequency is ~28 Mc and falls smoothly with temperature at a rate of 4.8 kc/°C.

621.398:621.384.8 4002
Electronic Equipment for In-Flight Processing of Rocket-Borne Mass-Spectrometer Data—J. H. Wager. (*J. Electronics Control*, vol. 8, pp. 227–240; March, 1960.) High-frequency signals from the spectrometer are converted by a sampling process to a form suitable for transmission over a narrowband telemetry link.

PROPAGATION OF WAVES

621.391.812.6.029.45 4003
On the mode Theory of Very-Low-Frequency Propagation in the Presence of a Transverse Magnetic Field—D. D. Crombie. (*J. Res. NBS*, vol. 64D, pp. 265–267; May/June, 1960.) "The effect of a purely transverse horizontal magnetic field on the propagation of VLF waves is considered. It is shown that the magnetic field introduces nonreciprocity, and that for propagation along the magnetic equator, the rate of attenuation is less for west-to-east propagation than for east-to-west propagation." See also 2523 of 1958.

621.391.812.6.029.45:551.594.6 4004
V.L.F. Attenuation for East-West and West-East Daytime Propagation using Atmospherics—W. L. Taylor. (*J. Geophys. Res.*, vol. 65, pp. 1933–1938; July, 1960.) An analysis of the spectra of atmospherics recorded simultaneously at four widely-separated stations has shown that there is greater attenuation in an east-west direction. This supports conclusions from the waveguide mode theory of propagation. For a more detailed account, see *J. Res. NBS*, vol. 64D, pp. 349–355; July/August, 1960.

621.391.812.62 4005
Focusing, Defocusing, and Refraction in a Circularly Stratified Atmosphere—K. Toman. (*J. Res. NBS*, vol. 64D, pp. 287–288; May/June, 1960.) An analysis is made of propagation through a medium of constant refractive index which is circularly bounded.

621.391.812.62 4006
An Analysis of Propagation Measurements made at 418 Megacycles per Second will beyond the Radio Horizon (a Digest)—H. B. Janes, J. C. Stroud and M. T. Decker. (*J. Res. NBS*, vol. 64D, pp. 255–257; May/June, 1960.) A summary is given of field strength, diversity, and height-gain measurements made over a 134-mile path, and a comparison with predictions.

621.391.812.62.029.63 4007
A Preliminary Study of Radiometeorological Effects on Beyond-Horizon Propagation—F. Ikegami. (*J. Res. NBS*, vol. 64D, pp. 239–246; May/June, 1960.) Diurnal variation of field strength seems to occur when the path crossover height is under 500 m. The laminar structure of the atmosphere is considered to be the dominant cause of variations in field occurring within a month.

621.391.812.62.029.63 4008
A Theory of Wavelength Dependence in Ultra-High-Frequency Transhorizon Propagation based on Meterological Considerations—R. Bolgiano, Jr. (*J. Res. NBS*, vol. 64D, pp. 231–237; May/June, 1960.) A theory of homogeneous turbulence in a stably stratified atmosphere provides an explanation for the observed distribution of wavelength dependence in a scaled-frequency experiment. It suggests that when the mean potential temperature of the air within the common volume is independent of height, the received power is nearly independent of radio wavelength, but with a dynamically stable atmosphere it should be proportional to the square or a higher power of wavelength.

621.391.812.621 4009
On the Calculation of the Departures of Radio Wave Bending from Normal—B. R. Bean and E. J. Dutton. (*J. Res. NBS*, vol. 64D, pp. 259–263; May/June, 1960.) The effect of local "perturbations" from an exponential atmosphere is estimated by a graphical process.

621.391.812.621:551.510.62 4010
Models of the Atmospheric Radio Refractive Index—P. Misme, B. R. Bean and G. D. Thayer. (PROC. IRE, vol. 48, pp. 1498–1501; August, 1960.) A comment on 2725 of 1959 and the authors' reply are given.

621.391.812.622 4011
The Trade-Wind Inversion as a Transoceanic Duct—M. Katzin, H. Pezzner, B. Y. C. Koo, J. V. Larson and J. C. Katzin. (*J. Res. NBS*, vol. 64D, pp. 247–253; May/June, 1960.) An analysis of radiosonde and airborne-refractometer soundings indicates the presence of a semipermanent elevated tradewind inversion duct in the South Atlantic. An experiment involving transmissions at about 200 Mc between two aircraft flying within the duct is suggested.

621.391.812.624 4012

Transport Equation for the Spectral Density of a Multiple-Scattered Electromagnetic Field—D. S. Bugnolo. (*J. Appl. Phys.*, vol. 31, pp. 1176–1182; July, 1960.) A theory for multiple scattering by dielectric noise is given, and a method of solution for forward scattering is developed. The particular case of a monochromatic planewave incident on a halfspace is discussed in detail, and its relevance to tropospheric scattering is pointed out.

621.391.812.624 4013

Carrier-Frequency Dependence of the Basic Transmission Loss in Tropospheric Forward Scatter Propagation—K. A. Norton. (*J. Geophys. Res.*, vol. 65, pp. 2029–2045; July, 1960.) An interpretation of Lincoln Laboratory scaled-antenna propagation data [1666 of 1959 (Bolgiano)] is given. It is pointed out that the antennas used did not illuminate the same positions of the atmosphere, and conclusions about the apparent hourly variation of wavelength dependence are therefore considered suspect. An alternative theory is advanced.

621.391.812.63 4014

Direct H. F. Back-Scatter from the F Region—H. F. Bates. (*J. Geophys. Res.*, vol. 65, pp. 1993–2002; July, 1960.) Scatter from field-aligned irregularities in the F region is a common occurrence in winter daytime in Alaska. The irregularities appear to be widespread at night, but concentrated in small areas by day.

621.391.812.63 4015

Focusing of Electromagnetic Waves by E_s Clouds—G. Umlauft. (*J. Atmos. terr. Phys.*, vol. 18, pp. 253–255; June, 1960.) A note is made on the occurrence of enhanced F-layer echoes when strong E_s echoes are present.

621.391.812.63:551.594.5 4016

The Scattering of 36-Mc Radio Waves by Weak Auroral Ionization—J. S. Greenhow, E. L. Neufeld and C. D. Watkins. (*J. Atmos. Terr. Phys.*, vol. 18, pp. 174–180; June, 1960.) Echoes were obtained for up to 30 per cent of the observing time. Ionization irregularities are aligned along the earth's magnetic field and have lengths of about 500 km and a scattering polar diagram with a width of $\pm 3°$.

621.391.812.63.029.45/.53 4017

On the Theory of Reflection of Low-and Very-Low-Radiofrequency Waves from the Ionosphere—J. R. Johler and L. C. Walters. (*J. Res. NBS*, vol. 64D, pp. 269–285; May/June, 1960.) A rigorous application of magneto-ionic theory to calculating reflection coefficients for a sharply bounded ionosphere is evaluated by an electronic computer, and is compared with the "quasi-longitudinal" approximation in certain cases.

621.391.812.63.029.45 4018

The 'Waveguide Mode' Theory of Radio Wave Propagation when the Ionosphere is Not Sharply Bounded—D. W. Barron. (*Phil. Mag.*, vol. 4, pp. 1068–1081; September, 1959.) A method is described for calculating the mode characteristics for any horizontally stratified ionosphere in which the electron density and collision frequency vary with height in some arbitrary prescribed manner. Results are given of calculations of the effect on the waveguide modes of (*a*) changing from a sharp to a gradual boundary and an otherwise homogeneous ionosphere, and (*b*) changes in the parameters of an exponential ionosphere.

621.391.812.63.029.51/.53 4019

Review of the State of the Work of the Union Européenne de Radiodiffusion (U.E.R.) on Ionospheric Propagation of Long and Medium Waves—W. Ebert, H. Ehlers and R. Dobiasch. (*Rundfunktech. Mitt.*, vol. 3, pp. 205–218; October, 1959.) Methods of measurement and evaluation are described [see also 585 of 1958 (Ehlers and Dobiasch)]. Results of statistical analyses of field-strength recordings are given, including some taken during the series of all-night runs initiated early in 1959. For English translation see *EBU Rev.*, no. 57A, pp. 2–16; October, 1959.

621.391.812.63.029.62 4020

Extraordinary Propagation Conditions for Ultra Short Waves—J. Ortner and A. Egeland. (*Arch. elekt. Übertragung*, vol. 13, pp. 420–428; October, 1959.) The reception at Kiruna Sweden, of 90-Mc transmissions from Central European and Scandinavian VHF transmitters on a few occasions between February, 1958, and August, 1959, is discussed. The possible causes of such unusual propagation conditions are examined; the presence of an exceptional E_s layer provides the best explanation of the phenomenon.

621.391.814.029.64 4021

The Group Velocity of Plane Surface Waves—A. G. Mungall and D. Morris. (*Canad. J. Phys.*, vol. 38, pp. 779–786; June, 1960.) The group velocity for both *TM* and *TE* surface-wave modes is treated theoretically. Measurements of signal velocities show good agreement with the theoretically predicted value for the first-order *TM* mode.

621.391.814.2 4022

Group-Wave Propagation (Mixed Path)—J. Houtsmuller. (*Tijdschr. ned. Radiogenoot*, vol. 24, no. 1, pp. 1–10; 1959.) Calculations of attenuation and phase, based on a method developed by Bremmer (531 of 1955) have been made at frequencies of 1.764 and 2.824 Mc over a model surface consisting of two homogeneous sections, one sea water and the other dry sand, separated by a number of different transition zones.

RECEPTION

621.391.812.029.45/.51:523.75 4023

The Frequency Dependence of Solar Flare Effects in the V.L.F. Region—H. Volland. (*Arch. elekt. Übertragung*, vol. 13, pp. 443–448; October, 1959.) Results are analyzed of field-strength measurements made in Berlin of transmissions from British stations operating at 16, 19.6 and 51.95 kc during solar flares. The anomalies observed are interpreted as caused by interference between the ground wave and rays reflected from the ionosphere, with the height of reflection decreasing during a solar flare. This model also provides an explanation for the change of the frequency spectrum of atmospherics under such conditions.

621.391.821:621.3.087.4 4024

Recording Atmospheric Radio Noise—C. Clarke. (*Electronic Tech.*, vol. 37, pp. 346–349; September, 1960.) The method described involves recording on magnetic tape that IF noise envelope obtained from a receiver with a bandwidth of 300 cps centered on 10 kc. It is possible to obtain an undistorted amplitude range of 60 db with unwanted amplitude variations limited to a standard deviation of 5–10 per cent.

621.391.823:621.397.62 4025

Radio Interference in the V.H.F. Range—E. V. Jensen. (*Teleteknik, Copenhagen*, vol. 10, pp. 1–15; April, 1959.) Methods of measuring and suppressing television interference caused by car ignition systems and electrical appliances are described.

621.396.666 4026

Experimental Comparison of Equal-Gain and Maximal-Ratio Diversity Combiners—R. V. Locke, Jr. (PROC. IRE, vol. 48, pp. 1488–1489; August, 1960.) The relative simplicity of the equal-gain system outweighs the 1-db improvement in signal-to-noise ratio obtained with the maximal-ratio system.

STATIONS AND COMMUNICATION SYSTEMS

621.391 4027

Method of Determining an Original Message to any Required Accuracy from a Finite Number of Observations behind a Square-Cut-Off Band-Pass Filter—H. Wolter. (*Arch. elekt. Übertragung*, vol. 13, pp. 393–404; September, 1959.) A theorem is derived of particular application to the determination of the information content of short messages, where the sampling theorem and Küpfmüller's condition fail to provide a solution. See also 3252 of September and back references.

621.396.4 4028

The Compatibility Problem on Single-Sideband Transmission—K. H. Powers. (PROC. IRE, vol. 48, pp. 1431–1435; August, 1960.) Results of an analysis of SSB signals show that conventional SSB transmissions cannot be made fully compatible with standard AM receivers. A square-law SSB system is proposed in which the signal generated has a spectral width equal to that of a conventional SSB system. Distortionless reception could only be achieved with a square-law detector, but there would be some measure of compatibility with a conventional AM receiver. For comment by Kahn, see *ibid.*, p. 1504.

621.396.4:551.507.362.2 4029

How Courier Satellite's Ground System Works—(*Electronics*, vol. 33, pp. 38–39; July 22, 1960.) A description is given with block diagrams of (*a*) the VHF receiving system used for locating and tracking the relay satellite, and (*b*) the UHF receiving system for communication; this is a quadruple-diversity system in which parametric converters are used. The information capacity of the satellite is equivalent to 40 telegraphy channels operating at 100 words per minute. See also *ibid.*, vol. 33, p. 44; July 15, 1960.

621.396.4:621.397 4030

The Combined Transmission of Multiplex Telephone and Television Signals—Y. Shigei. (*Rep. elect. Commun. Lab., Japan*, vol. 7, pp. 444–447; December, 1959.) A short analysis is made of requirements relating to modulation index and distortion caused by nonlinearity of repeaters.

621.396.41:621.376.55 4031

Microminiature Multichannel Pulse-Position-Modulation System incorporating Transistor/Magnetic-Core Circuitry—H. Kihn, R. J. Klensch and A. H. Simon. (*RCA Rev.*, vol. 21, pp. 199–227; June, 1960.) An experimental five-channel time-division multiplex system, based on variable time triggering of a transistor/magnetic-core pulse generator by the variation of either the transistor input-voltage or ferrite-core coercive-force threshold, is described.

621.396.65 4032

Automatic Stand-By Circuits for Radio Links—E. Rempt. (*Nachrtech.* vol. 9, pp. 411–414; September, 1959.) Automatic switching systems for stand-by equipment are described and compared. The use of reserve sections operating at different frequencies to overcome the effects of selective fading is discussed.

621.396.65 4033

The TJ Radio Relay System—J. Gammie and S. D. Hathaway. (*Bell Sys. Tech. J.*, vol. 39, pp. 821–877; July, 1960.) A detailed de-

scription, with circuit details and performance data, of the system designed for short-haul transmission of either multichannel telephone or television circuits is given. See 3106 of 1959 (Hathaway and Haas).

621.396.944.029.45 4034
New V.L.F. to Reach all Polaris Subs—(*Electronics*, vol. 33, pp. 34–35; July 15, 1960.) Radiated power will be 1 mw in the frequency range 14–30 kc.

621.396.946 4035
Providing Communication and Navigation for Space Probes—R. C. Hansen and E. R. Spangler. (*Electronics*, vol. 33, pp. 43–47; July 8, 1960.) Some features of the modulation systems and receiver equipment used in the Able Space Navigation Network are described. Field-strength calculations indicate that a 10-kw ground transmitter with a 250-foot parabolic antenna can provide control to a range of 70 million miles.

621.396.97:534.76 4036
A Summary of the Present Position of Stereophonic Broadcasting—D. E. L. Shorter and G. J. Phillips. (*BBC Engrg. Div. Monographs*, no. 29, 27 pp.; April, 1960.) The various methods by which stereophonic programs can be produced for sound recording or broadcasting are discussed.

SUBSIDIARY APPARATUS

621.314.5 4037
Static Inverter Delivers Regulated 3-Phase Power—M. Lilienstein. (*Electronics*, vol. 33, pp. 55–59; July 8, 1960.) Silicon controlled rectifiers in conjunction with magnetic amplifiers are used to provide a 115-volt, 400-cps output from a 30-volt dc input.

621.314.63:621.382.2:621.316.91 4038
The Characteristics and Protection of Semiconductor Rectifiers—D. B. Corbyn and N. L. Potter. (*Proc. IEE, pt. A*, vol. 107, pp. 255–268; June, 1960. Discussion, pp. 269–272.)

621.318.57:621.382 4039
Design of Static Relays for Signalling and Control—R. Langfelder. (*Electronics*, vol. 33, pp. 64–68; July 22, 1960.) The advantages of static relays and the replacement of mechanical relays by semidonductor devices are discussed. Circuit diagrams are given.

TELEVISION AND PHOTOTELEGRAPHY

621.397:621.396.97 4040
The Present State of Television at Home and Abroad—H. Rindfleisch. (*Rundfunktech. Mitt.*, vol. 3, pp. 219–227; October, 1959.) Details are given of the world-wide distribution of television standards and of viewers, and maps are included showing the location and power of television transmitters in Europe and the German Federal Republic. The international and intercontinental exchange of television programs is also discussed.

621.397.132 4041
Adaptation of the N.T.S.C. Signal to Sequential Systems of Colour Television—K. Wirth. (*Onde élect.*, vol. 40, pp. 411–414; May, 1960.) An analysis of the NTSC signal shows that, with slight modification to the standards, a compatible chrominance signal in which the primary colour components are equal in amplitude and balanced in phase may be derived.

621.397.132 4042
Colour-Subcarrier Attenuation for Colour Television by the N.T.S.C. Method—H. Schönfelder. (*Arch. elekt. Übertragung*, vol. 13, pp. 383–392; September, 1959.) Attenuation of the chrominance signal in the luminance channel of the receiver is required to reduce interference effects in color and monochrome television images. Suitable attenuator circuits are given and their effect on picture quality is investigated.

621.397.331.24 4043
The Reflected-Beam Kinescope—H. B. Law and E. G. Ramberg. (*Proc. IRE*, vol. 48, pp. 1409–1417; August, 1960.) A short television picture tube which retains the conventional gun and external deflection arrangements and is axially symmetric is described. The electron beam passes through a perforated phosphor screen and is then reflected back to the screen by a spherically curved tube face having an inner coating of a transparent conductive material at cathode potential. The brightness for television display is reduced four times due to attenuation of the beam at the perforated screen; tubes designed for radial scanning would not be subject to this loss.

621.397.331.3 4044
Automatic White- and Black-Level Regulation in Vidicon Film Scanners—E. Sennhenn. (*Elektron. Rundschau*, vol. 13, pp. 319–323; September, 1959.) A description of a magnetic-amplifier circuit for controlling the projector lamp current to stablize the white level is given. The black-level control circuit given holds the signal voltage corresponding to the darkest picture spot at a constant level which is related to the gradation characteristics.

621.397.61:621.3.018.78 4045
Study of Linear Distortion in a Television Transmission System—K. Kinoshita and T. Yasuhiro. (*Onde élect.*, vol. 40, pp. 415–420; May, 1960.) In a system of limited bandwidth, minimal distortion occurs with a square-law characteristic.

621.397.61:681.42.08 4046
New Measurements for the Determination of the Transmission Characteristics of Objectives from the Point of View of Television Engineering—D. Frenzel. (*Rundfunktech. Mitt.*, vol. 3, pp. 235–241; October, 1959.) The oscillographic method described takes account only of the over-all effect of the aberrations of the objective on the quality of the television image. See also 3286 of September (Grabke and Below).

621.397.61–182.3 4047
A Mobile Television Camera and Recording Vehicle—A. Harris. (*J. Brit. IRE*, vol. 20, pp. 553–559; July, 1960.) A description of a complete television system with two cameras, a video tape recorder and auxiliary equipment is given.

621.397.62:621.375.2 4048
Improvements in Television Receivers: Part 7—I.F. Video Amplifiers Equipped with Frame-Grid Tubes—B. G. Dammers, A. G. W. Uitjens, A. J. Alferink, J. G. W. Bom, K. Hoefnagel, J. G. Versteeg and L. W. Loeffen. (*Electronic Applic.*, vol. 19, pp. 93–114; August, 1959.) Part 6: 3124 of 1959 (Dammers, *et al.*).

621.397.712.3 4049
A New Television Studio of the N.W.R.V. Hamburg—G. Schadwinkel, F. Naupert and E. Struss. (*Rundfunktech. Mitt.*, vol. 3, pp. 228–234; October, 1959.)

621.397.74.001.4:621.374 4050
Sine-squared Pulses in Television System Analysis—R. Kennedy. (*RCA Rev.*, vol. 21, pp. 253–265; June, 1960.) A comprehensive comparison of sine-squared pulses and Heaviside step function as used in television system analysis is given, together with methods of producing the waveforms.

621.397.743:621.315.212 4051
Operational Experiences with New Coaxial-Cable Television Links—R. Rasch. (*Nachrichtentech. Z.*, pp. 452–456; September, 1959.) A report is made on tests made on the German carrier-frequency cable link system TV1 which uses pilot frequencies for level control. The effects, such as "ringing" due to the presence of pilot-frequency bandstop filters and to deviation from the nominal linescan frequency, are investigated.

621.397.743:621.372 4052
A Common-Carrier Multichannel Television Wire Broadcasting System—K. A. Russell and F. Sanchez. (*J. Brit. IRE*, vol. 20, pp. 497–512; July, 1960.) A survey of television wire relay systems and a technical description of a system carrying four television and four radio programs are given, with details of station and repeater equipment.

621.397.9 4053
The Possibility of Applying Television Camera Tubes in the Detection of Faint Optical Images—I. L. Valik and L. I. Khromov. (*Zh. Tekh. Fiz.*, vol. 29, pp. 881–884; July, 1959.) Experimental data on the sensitivity of image-orthicon and image-iconoscope tubes for a range of exposure times is given, together with a short discussion of the storage process.

621.397.9:522.2 4054
The Stratoscope I Television System—L. E. Flory, G. W. Gray, J. M. Morgan and W. S. Pike. (*RCA Rev.*, vol. 21, pp. 151–169; June, 1960.) See 3667 of October.

TRANSMISSION

621.396.61:621.395.665.1 4055
Investigations of the Noise Reduction by means of Pre-emphasis and De-emphasis in Broadcast Transmission—W. von Guttenberg and H. Hochrath. (*Nachrichtentech. Z.*, vol. 12, pp. 467–474; September, 1959.) The use of pre-emphasis for noise reduction in carrier-frequency systems is discussed with reference to experimental investigations and CCITT recommendations. The necessity of peakpower compression calls for modification of the pre-emphasis characteristic, which results in less effective noise suppression and other disadvantages.

621.396.61.029.45 4056
Sea-Going Lightning Generator—M. M. Newman, J. R. Stahmann, J. D. Robb and E. A. Lewis. (*Electronics*, vol. 33, pp. 53–55; July 22, 1960.) A million-volt generator and a 10,000-foot antenna supported by a helicopter have been used to generate VLF transients similar to lightning discharges.

TUBES AND THERMIONICS

621.382 4057
Space-Charge-Limited Currents in Cylindrical and Spherical Insulator Diodes—B. Meltzer. (*J. Electronics Control*, vol. 8, pp. 171–176; March, 1960.) Formulas for the current in cylindrical and spherical diodes have been derived by the Mott-Gurney approximations previously applied to planer diodes. Numerical results are compared.

621.382.23 4058
Gallium Arsenide Tunnel Diodes—N. Holonyak, Jr., and I. A. Lesk. (*Proc. IRE*, vol. 48, pp. 1405–1409; August, 1960.) The preparation, consutrction and properties of GaAs diodes are described. Peak-to-alley current ratios $>15:1$ have been consistently observed, with voltage swings in the range 0.9 to 1.2 volts and current densities from 2000–10,000 a/cm.^{2}

621.382.23:621.317.3 4059
Determination of the Impurity Distribution in Junction Diodes from Capacitance-Voltage Measurements—J. Hilibrand and R. D. Gold. (*RCA Rev.*, vol. 21, pp. 245–252; June, 1960.) A method is described for measuring impurity distributions in semiconductor devices within the accuracy required to understand and control their operation.

621.382.23:621.375.9 4060
Noise Performance of Tunnel-Diode Amplifiers—P. Penfield, Jr. (*Proc. IRE*, vol. 48, pp. 1478–1479; August, 1960.) Expressions for the noise figure at low- and high-frequency limits are derived.

621.382.23:621.375.9:621.372.44 4061
Parametric Diode Figure of Merit and Optimization—K. E. Mortenson. (*J. Appl. Phys.*, vol. 31, pp. 1207–1212; July, 1960.) A new figure of merit is defined which is directly applicable in comparing diodes of different types, as well as in obtaining the optimum design. The figure can also be employed to predict the noise figure of an amplifier using a parametric diode. An evaluation of the figure of merit is given for the case of the abrupt junction diode.

621.382.23:621.375.9:621.372.44 4062
Capacitance and Charge Coefficients for Parametric Diode Devices—S. Sensiper and R. D. Weglein. (PROC. IRE, vol. 48, pp. 1482–1483; August, 1960.)

621.382.23:621.391.822.3 4063
Shot Noise in Tunnel-Diode Amplifiers—J. J. Tiemann. (PROC. IRE, vol. 48, pp. 1418–1423; August, 1960.) The contributions of Johnson noise and shot noise to the noise in a tunnel diode are analyzed according to a simple theoretical model.

621.382.33:621.318.57 4064
A Double-Diffused Silicon High-Frequency Switching Transistor produced by Oxide Masking Techniques—J. F. Aschner, C. A. Bittmann, W. F. J. Hare and J. J. Kleimack. (*J. Electrochem. Soc.*, vol. 106, pp. 415–422; May, 1959.) A process is described for producing a localized emitter structure in *n-p-n* transistors, using the masking property of SiO_2 against subsequent diffusion by phosphorus; electrical characteristics are given.

621.383:535.371.07 4065
On the Signal/Noise Ratio of Light Amplifiers—P. V. Makovetskii. (*Zh. Tekh. Fiz.*, vol. 29, pp. 406–413; March, 1959.) The frequency response and noise properties of a photocathode/phosphor system are discussed with reference to phosphor inertia and the basic requirements for noise suppression.

621.383.032.217.2 4066
Absolute Spectral Response Characteristics of Photosensitive Devices—R. W. Engstrom (*RCA Rev.*, vol. 21, pp. 189–190; June, 1960.) Data for comparison of response characteristics of commercial photocathodes are tabulated.

621.385.004.6 4067
The Reliability of Thermionic Values in Practical Applications—W. Chladek. (*Nachrichtentech. Z.*, vol. 12, pp. 443–449; September, 1959.) Reports on tube failure rate from various sources and formulas given by other author for predicting tube reliability are discussed and compared. Figures and curves, based on statistical analyses, of the mean rate of tube failure and of the effect of tube operating conditions are given. 13 references.

621.385.032.213.6 4068
A Low-Wattage Planar Cathode—T. N. Chin. (*RCA Rev.*, vol. 21, pp. 191–198; June, 1960.) A new cathode construction for use in electron-beam devices is described.

621.385.032.213.62 4069
The Origin of Nonstationary Processes in Alundum [Aluminum Oxide] Coatings of Radio Valve Heaters—Yu K. Shalabutov. (*Fiz. Tverdogo Tela*, vol. 1, pp. 296–306; February, 1959.) A systematic investigation is made of cathode-to-heater leakage currents under ac and pulsed conditions.

621.385.032.269.1 4070
Investigations on an Electron Gun for Flat Beams—G. Bolz. (*Nachrichtentech. Z.*, vol. 12, pp. 464–466; September, 1959.) The design and construction of an electron gun for producing flat beams are described. Experimental results are briefly discussed.

621.385.2.029.6 4071
Conductance Measurements on a Plane-Parallel Diode in the Transit-Time Region—K. Hennings. (*Nachrichtentech. Z.*, vol. 12, pp. 459–464; September, 1959.) Investigations were made on a special planar diode with a bimetal-strip system for varying the electrode spacing. Admittance characteristics were obtained for spacing between 40 μ and 1mm, with current densities up to 200 ma/cm^2 at 1.6, 2.4, and 4 kMc.

621.385.5.032.265 4072
A New Miniature Beam-Deflection Tube—M. B. Knight. (*RCA Rev.*, vol. 21, pp. 266–289; June, 1960.) A description of a new method of beam-deflection control of plate current is given, with its application to a new tube for use in modulators.

621.385:537.533 4073
Power Flow and Stored Energy in Thin Electron Beams—W. W. Rigrod. (*J. Appl. Phys.*, vol. 31, pp. 1147–1153; July, 1960.) The kinetic and em components of ac power and stored energy are evaluated for space-charge waves along thin drifting beams. It is found that, when fast and slow waves are excited by a common source, the real kinetic power varies periodically with distance. The energy transport velocity of a space-charge wave is shown to equal its group velocity. See 1736 of 1959.

621.385.6:537.533 4074
Beam Refrigeration by means of Large Magnetic Fields—R. Adler and G. Wade. (*J. Appl. Phys.*, vol. 31, pp. 1201–1203; July, 1960.) An electron beam can be made to have a very low noise temperature by applying a large magnetic field and using the fast cyclotron wave. The temperature is reduced in the ratio of signal frequency to cyclotron frequency. An experiment with a signal at 90 Mc gave a noise temperature of 186°K. The large magnetic field need not extend throughout the length of the beam.

621.385.6:621.375.9:621.372.44 4075
Lower-Frequency-Pumping Electron-Beam Parametric Amplifier—N. B. Chakraborti. (*J. Electronics Control*, vol. 8, pp. 161–165; March, 1960.) A theoretical analysis is given with particular reference to gain conditions.

621.385.6:621.375.9:621.372.44 4076
Parametric Amplification, Power Control, and Frequency Multiplication at Microwave Frequencies using Cyclotron-Frequency Devices—C. L. Cuccia. (*RCA Rev.*, vol. 21, pp. 228–244; June, 1960.) An explanation of the principles of operation of the electron-beam parametric amplifier, electron-coupler power-control tube, and electron-coupler frequency multiplier is given.

621.385.6:621.375.9:621.372.44 4077
An Electrostatically Focused Electron-Beam Parametric Amplifier—B. J. Udelson. (*Proc. IRE*, vol. 48, pp. 1485–1486; August, 1960.) The amplifier proposed has an electron sheet beam with electrostatic focusing. Gain is achieved by pumping the fast wave of the natural electron resonance frequency associated with the focusing fields.

Translations of Russian Technical Literature

Listed below is information on Russian technical literature in electronics and allied fields which is available in the U. S. in the English language. Further inquiries should be directed to the sources listed. In addition, general information on translation programs in the U. S. may be obtained from the Office of Science Information Service, National Science Foundation, Washington 25, D. C., and from the Office of Technical Services, U. S. Department of Commerce, Washington 25, D. C.

PUBLICATION	FREQUENCY	DESCRIPTION	SPONSOR	ORDER FROM:
Acoustics Journal (Akusticheskii Zhurnal)	Quarterly	Complete journal	National Science Foundation—AIP	American Institute of Physics 335 E. 45 St., New York 17, N. Y.
Automation and Remote Control (Avtomatika i Telemekhanika)	Monthly	Complete journal	National Science Foundation—MIT	Instrument Society of America 313 Sixth Ave., Pittsburgh 22, Pa.
	Monthly	Abstracts only		Office of Technical Services U. S. Dept. of Commerce Washington 25, D. C.
Journal of Abstracts, Electrical Engineering (Referativnyy Zhurnal: Electronika)	Monthly	Abstracts of Russian and non-Russian literature		Office of Technical Services U. S. Dept. of Commerce Washington 25, D. C.
Journal of Experimental and Theoretical Physics (Zhurnal Eksperimentalnoi i Teoreticheskoi Fiziki)	Monthly	Complete journal	National Science Foundation—AIP	American Institute of Physics 335 E. 45 St., New York 17, N. Y.
Journal of Technical Physics (Zhurnal Tekhnicheskoi Fiziki)	Monthly	Complete journal	National Science Foundation—AIP	American Institute of Physics 335 E. 45 St., New York 17, N. Y.
Proceedings of the USSR Academy of Sciences: Applied Physics Section (Doklady Akademii Nauk SSSR: Otdel Prikladnoi Fiziki)	Bimonthly	Complete journal		Consultants Bureau, Inc. 227 W. 17 St., New York 22, N. Y.
Radio Engineering (Radiotekhnika)	Monthly	Complete journal	National Science Foundation—MIT	Pergamon Institute 122 E. 55 St., New York 22, N. Y.
	Monthly	Abstracts only		Office of Technical Services U. S. Dept. of Commerce Washington 25, D. C.
Radio Engineering and Electronics (Radiotekhnika i Elektronika)	Monthly	Complete journal	National Science Foundation—MIT	Pergamon Institute 122 E. 55 St., New York 22, N. Y.
	Monthly	Abstracts only		Office of Technical Services U. S. Dept. of Commerce Washington 25, D. C.
Solid State Physics (Fizika Tverdogo Tela)	Monthly	Complete journal	National Science Foundation—AIP	American Institute of Physics 335 E. 45 St., New York 17, N. Y.
Telecommunications (Elekprosviaz')	Monthly	Complete journal	National Science Foundation—MIT	Pergamon Institute 122 E. 55 St., New York 22, N. Y.
	Monthly	Abstracts only		Office of Technical Services U. S. Dept. of Commerce Washington 25, D. C.
Automation Express	10/year	A digest: abstracts, summaries, annotations of various journals		International Physical Index, Inc. 1909 Park Ave., New York 35, N. Y.
Electronics Express	10/year	A digest: abstracts, summaries, annotations of various journals		International Physical Index, Inc. 1909 Park Ave., New York 35, N. Y.
Physics Express	10/year	A digest: abstracts, summaries, annotations of various journals		International Physical Index, Inc. 1909 Park Ave., New York 35, N. Y.
Express Contents of Soviet Journals Currently being Translated into English	Monthly	Advance tables of contents of translated journals		Consultants Bureau, Inc. 227 W. 17 St., New York 22, N. Y.
Technical Translations	Twice a month	Central directory in the U. S. of translations available from all major sources in the U. S.	OTS and Special Libraries Assoc.	Superintendent of Documents U. S. Gov't Printing Office Washington 25, D. C.

Index to

PROCEEDINGS OF THE IRE

Volume 48, 1960

The Institute of Radio Engineers, Inc.
1 East 79 Street, New York 321, N.Y.

TABLE OF CONTENTS

PROCEEDINGS OF THE IRE
CONTENTS OF VOLUME 48—1960

Volume 48, Number 1, January, 1960

Volume 48, Number 2, February, 1960

Volume 48, Number 3, March, 1960

Volume 48, Number 4, April, 1960

Volume 48, Number 5, May, 1960

Volume 48, Number 6, June, 1960

Volume 48, Number 7, July, 1960

Volume 48, Number 8, August, 1960

Volume 48, Number 9, September, 1960

Volume 48, Number 10, October, 1960

Volume 48, Number 11, November, 1960

Volume 48, Number 12, December, 1960

INDEX TO AUTHORS

Listings are by month and page, and include authors of papers, authors of correspondence items (C), and reviewers of books (B).

INDEX TO SUBJECTS

Listings are by month and page. Authors and paper titles may be determined from the tables of contents in the front part of this index.

G

H

I

J

K

L

M

N

O

P

NONTECHNICAL INDEX

Abstracts and References

Abstracts of TRANSACTIONS

Awards

Calendar of Coming Events

Committees

Front Covers

Frontispieces

IRE People

News and Notices

Obituaries

Photographs

Poles and Zeros

Professional Groups

Programs

Report of the Secretary

Scanning the Issue

Scanning the TRANSACTIONS

Sections and Subsections

Translations of Russian Technical Literature

INDEX TO BOOK REVIEWS

Index to

IRE INTERNATIONAL CONVENTION RECORD

Volume VIII, 1960

The Institute of Radio Engineers, Inc.
1 East 79 Street, New York 321, N.Y.

TABLE OF CONTENTS

IRE INTERNATIONAL CONVENTION RECORD

CONTENTS OF VOLUME VIII—1960

Part 1—Antennas and Propagation

Part 2—Circuit Theory; Electronic Computers

Part 3—Electron Devices; Microwave Theory and Techniques

Part 4—Automatic Control; Information Theory

Part 5—Communications Systems; Space Electronics and Telemetry

Part 6—Component Parts; Industrial Electronics; Production Techniques; Reliability and Quality Control; Ultrasonics Engineering

Part 7—Audio; Broadcast and Television Receivers; Broadcasting

Part 8—Aeronautical and Navigational Electronics; Military Electronics; Radio Frequency Interference; Vehicular Communications

Part 9—Instrumentation; Medical Electronics; Nuclear Science

Part 10—Engineering Management; Engineering Writing and Speech; Human Factors in Electronics

INDEX TO AUTHORS

Listings are by part number and page.

INDEX TO SUBJECTS

Listings are by part number and page. Authors and paper titles may be determined from the tables of contents in the front part of this index.

Index to

IRE WESCON CONVENTION RECORD

Volume 4, 1960

TABLE OF CONTENTS

The Institute of Radio Engineers, Inc.
1 East 79 Street, New York 321, N.Y.

IRE WESCON CONVENTION RECORD
CONTENTS OF VOLUME IV—1960

Part 1—Antennas; Microwave Theory and Techniques

Part 2—Circuit Theory; Pulse-Handling Techniques; Varactors and Tunnel Diode Applications

Part 3—Microminiaturization; Semiconductor Devices and Tubes

Part 4—Computers; Man-Machine Systems

Part 5—Information Theory; Instrumentation; Magnetic Data Recording; Pioneer V Experiments; Telemetry

Part 6—Air Traffic Control; Military Electronics; Reliability

Part 7—Communications; Stereo Broadcasting; Vehicular Communications

Part 8—Engineering Proposals; The Technical Symposium; Working with Engineers

INDEX TO AUTHORS

Listings are by part number and page.

INDEX TO SUBJECTS

Listings are by part number and page. Authors and paper titles may be determined from the tables of contents in the front part of this index.